Title
Steric Effects in the Reactivity and Bonding of Low Coordinate Germanium and Tin Species

Author
Lai, Ting Yi

Publication Date
2022

Peer reviewed|Thesis/dissertation

Steric Effects in the Reactivity and Bonding of Low Coordinate Germanium and Tin Species

By

TING YI LAI

DISSERTATION

Submitted in partial satisfaction of the requirements for the degree of

DOCTOR OF PHILOSOPHY

in

Chemistry

in the

OFFICE OF GRADUATE STUDIES

of the

UNIVERSITY OF CALIFORNIA

DAVIS

Approved:

_____

Philip P. Power, Chair

_____

Jesús M. Velázquez

_____

Louise A. Berben

Committee in Charge

2022

List of Symbols, Nomenclature, or Abbreviations

Å	Angstrom (10^{-10} m)
$Ar^{iPr}{}_4$	C_6H_3-2,6-(C_6H_3-2,6-$^{i}Pr_2$)$_2$
$Ar^{iPr}{}_6$	C_6H_3-2,6-(C_6H_2-2,4,6-$^{i}Pr_3$)$_2$
$Ar^{Me}{}_6$	C_6H_3-2,6-(C_6H_2-2,4,6-Me_3)$_2$
ca.	approximately
CW	Continuous-Wave
DFT	Density Functional Theory
Dipp	C_6H_3-2,6-$^{i}Pr_2$
DMAP	4-Dimethylaminopyridine
Ether	Diethyl Ether
ENDOR	Electron Nuclear Double Resonance
EPR	Electron Paramagnetic Resonance
IR	Infrared
^{i}Pr	isopropyl
Mes	C_6H_2-2,4,6-Me_3
NMR	Nuclear Magnetic Resonance
^{n}Bu	n-butyl
PhMe	Toluene

Trip	C_6H_2-2,4,6-$^{i}Pr_3$
THF	Tetrahydrofuran
^{t}Bu	t-butyl
UV-vis	Ultraviolet–visible
VMT	Variable mixing-time
VT	Variable Temperature
ΔG	Gibbs Free-Energy Change
ΔH	Enthalpy Change
ΔS	Entropy Change
δ	chemical shift
ε	molar absorption coefficient
ν	frequency

Acknowledgments

First and foremost, I would like to express my sincere gratitude to my advisor, Prof. Philip P. Power for his support and guidance during my time at Davis and throughout my Ph.D. I have learned an enormous amount of knowledge on main group organometallics chemistry from him and his passion for the topic had always inspired me. I will always remember his words such as "the longest way round is the shortest way home" and make sure to keep his words in mind throughout my career. Hopefully, I don't make him look bad!

I am grateful to Prof. Alexander T. Radosevich, my undergraduate advisor, who got me interested in organometallic chemistry and helped me a tremendous amount during my time in his lab. I would also like to thank Dr. Sean M. McCarthy, who helped train me and introduced me to Schlenk line chemistry at Penn State.

I would like to thank Prof. Ching-Wen Chiu and the lab members at the National Taiwan University. They made me feel welcomed during the difficult times of the COVID pandemic. I enjoyed every bit of my time in the Chiu lab. The lab members include: Nagarjuna Srungavruksham, Po-Han Chen, Ching-Pei Hsu, Hsi-Ching Tseng, Ding-Nan Shih, Jin-Tai Lin, Kun-Hao Chen, Wei-Fang Liu, Ching-An Chang, Yu-Chiang Lin, Yu-Chuan Hsu, Yu-Chen Lin, Min-Hsiung Wu, Chu-Chiao Wen, Hsuan-Wen Fu, Wei-En Yen and Chia-Hsuan Lin.

I would also like to thank Prof. Louise A. Berben and Prof. Jesús M. Velázquez for their time and support to be on my thesis committee.

My sincere thanks also to my collaborators. Dr. James C. Fettinger and Dr. Marylin Olmstead for helping me with X-ray crystallography. Dr. Lizhi Tao for EPR spectroscopy. Dr. Guo Jing-Dong at the University of Kyoto and Prof. Petra Vasko at the University of

Jyväskylä for their computational work in my several projects. Jeffrey Walton and Ping Yu for NMR spectroscopy. Their input has largely deepened our understanding of our chemistry and allowed us to design further experiments.

Many thanks to the current and former Power group members for providing a cooperative atmosphere in the lab and for their useful feedback on my work. The lab members include Prof. David Manke (UMass-Dartmouth), Prof. David Liptrot, Prof. Paul Lummis, Prof. Chun-Yi Lin, Jade Pratt, Dr, Madison McCrea-Hendrick, Dr. Jeremy Erickson, Prof. Clifton Wagner, Joshua Queen, Dr. Shuai Wang Dr. Cary Stennett, Robert Tureski, Alice Phung, Qihao Zhu, Wenxing Zou, Connor Mc Loughlin, Chia-Yuan Chen, and Dr. Kristian Mears.

I would like to acknowledge Joshua Queen for proofreading some of my manuscripts and giving me advice on this thesis.

Last but not least, I would like to express my deep gratitude to my parents and family, Lai Shui Mu, Lin Hui Ching, Lai Yang-Lin, and Lai Wen-Ling for their continuous support, love and encouragement. I would not have done this without them.

Abstract

This dissertation describes the reactivity a series of terphenyl-supported heavier group 14 germylenes and stannylenes toward fundamentally important small molecules. The germylenes and stannylenes that are used in this thesis are $Ge(Ar^{Me6})_2$, $Ge(Ar^{iPr4})_2$, $Ge(Ar^{iPr6})_2$, $Sn(Ar^{Me6})_2$, $Sn(Ar^{iPr4})_2$, and $Ge(Ar^{iPr6})_2$ (Ar^{Me6} = C_6H_3-2,6(C_6H_2-2,4,6-Me_3)$_2$, Ar^{iPr4} = C_6H_3-2,6(C_6H_3-2,6-*i*Pr_2)$_2$ and Ar^{iPr6} = C_6H_3-2,6(C_6H_2-2,4,6-*i*Pr_3)$_2$). The solid-state structures of their reaction procuts were determined by single X-ray spectroscopy. Other characterization method includes nuclear magnetic resonance spectroscopy, UV-visible spectroscopy, infrared spectroscopy, melting point analysis, and electron paramagnetic spectroscopy. All operations were carried out under anaerobic and anhydrous conditions using modified Schlenk techniques. All solvents were dried over alumina columns, stored over a sodium or potassium mirror, and degassed before use. A summary of the previous investigations of the synthesis and reactivity of tetrylenes is described in **Chapter 1**.

Chapter 2: The diarylstannylene, $:Sn(Ar^{iPr4})_2$ (Ar^{iPr4} = C_6H_3-2,6-(C_6H_3-2,6-$^{i}Pr_2$)$_2$), undergoes C-H metathesis with toluene, *m*-xylene or mesitylene in solutions of these solvents at 80 °C. The products afforded $[Ar^{iPr4}Sn(CH_2Ar)]_2$ (Aryl= C_6H_5 (**1a**), C_6H_4-3-Me (**1b**), C_6H_3-3,5-Me_2(**1c**)) were characterized via ^{1}H , ^{13}C and ^{119}Sn NMR, UV-vis and IR spectroscopy, and by X-ray crystallography for **1a** and **1b**. A stoichiometric amount of the arene, $Ar^{iPr4}H$, was also produced in these reactions. The use of EPR spectroscopy indicated the presence of a new type of one-coordinate, tin-centered radical, $\cdot SnAr^{iPr4}$, resulting from Sn-C bond cleavage in $:Sn(Ar^{iPr4})_2$.

Chapter 3: It is shown that the tin-tin triple bond in the distannyne $Ar^{iPr4}SnSnAr^{iPr4}$ (Ar^{iPr4} = C_6H_3-2,6-(C_6H_3-2,6-$^{i}Pr_2$)$_2$), undergoes reversible cleavage in deuterated toluene to afford two

·$SnAr^{iPr4}$ radicals as shown by ^{1}H NMR and EPR spectroscopy. Variable temperature ^{1}H NMR data afforded an enthalpy of dissociation of ΔH_{diss}=17.2±1.7 kcal mol-1 via van't Hoff analysis. The EPR and ^{1}H NMR data indicated that the Sn-Sn bond in $Ar^{iPr4}SnSnAr^{ipr4}$ is weak and is consistent with the Sn-Sn bond being a charge-shift bond.

Chapter 4: In this Chapter, the detection of tin and germanium radicals during the photolysis/thermolysis of diarylstannylene SnR_2 and diarylgermylene GeR_2 (R = Ar^{iPr4} = C_6H_3-2,6-(C_6H_3-2,6-$^{i}Pr_2$)$_2$ or Ar^{iPr6} = C_6H_3-2,6-(C_6H_2-2,4,6-$^{i}Pr_3$)$_2$), by using EPR spectroscopy complemented with theoretical calculations are described. The trapped tin radical is a one-coordinated *S* = 1/2 Sn(I) radical, i.e., : $\dot{S}nR$ (R = Ar^{iPr4} or Ar^{iPr6}), with **g** tensor values of [2.031, 1.980, 1.940] ($\mathbf{g_{iso}}$ = 1.984). In contrast, the trapped germanium radical is a pseudo-planar *S* = 1/2 Ge(III)-hydride species, i.e., ·GeHRR' (R = Ar^{iPr4} or Ar^{iPr6}, R' is a quaternary carbon), with **g** tensor values of [2.029, 2.003, 1.989] ($\mathbf{g_{iso}}$ = 2.007) and a strong ^{1}H-hyperfine tensor [-23.0, -20.5, -31.5] MHz for the hydride. The generation of this Ge(III)-hydride could be due to the greater reactivity Ge(I) radical intermediate (: $\dot{G}eR$) and the greater strength of a Ge-H bond. The Ge(III)-hydride species arise from the insertion of the active Ge(I) radical intermediate in a C-H bond. This chapter provides insights into the radical mechanistic understanding of the heavier group 14 element tetrylenes chemistry.

Chapter 5: It is shown that the diarylstannylenes, $Sn(Ar^{iPr4})_2$ and $Sn(Ar^{iPr6})_2$, (Ar^{iPr4} = C_6H_3-2,6-(C_6H_3-2,6-$^{i}Pr_2$)$_2$, Ar^{iPr6} = C_6H_3-2,6-(C_6H_2-2,4,6-$^{i}Pr_3$)$_2$), undergo a facile migratory insertion reaction with ethylene at 60 °C to afford the alkyl aryl stannylenes $Ar^{iPr4}SnCH_2CH_2Ar^{iPr4}$ and $Ar^{iPr6}SnCH_2CH_2Ar^{iPr6}$ these products were characterized via ^{1}H , ^{13}C and ^{119}Sn NMR, UV-vis and IR spectroscopy, as well as by X-ray crystallography. Quantum mechanical calculations were performed by our collaborator Dr. Guo, and two potential mechanisms were identified.

Chapter 6: The diarylgermylenes $Ge(Ar^{Me6})_2$ and $Ge(Ar^{iPr4})_2$ (Ar^{Me6}=C_6H_3-2,6-(C_6H_3-2,4,6-Me_3)$_2$), Ar^{iPr4}=C_6H_3-2,6-(C_6H_3-2,6-iPr_2)$_2$) were shown to react reversibly with ethylene. It is shown that the more sterically crowded $Ge(Ar^{iPr4})_2$ also reversibly binds propylene. The germirane products $Ar_2\overline{GeCH_2CHR}$) (Ar,R = Ar^{Me6}, H **(1a)**, Ar^{iPr4}, H (**1b**) and Ar^{iPr4}, Me (**1c**) were characterized via ^1H and ^{13}C NMR spectroscopy and by X-ray crystallography in the case of **1b.** Thermolysis of $Ge(Ar^{iPr4})_2$ under ethylene resulted in Ge-C bond homolysis and the formation of the digermene $[(Ar^{iPr4})Ge(Et)]_2$(**1d**). The thermodynamic parameters of the reactions were determined by variable temperature ^1H NMR spectroscopy.

Chapter 7: The diarylgermylene, $Ge(Ar^{Me6})_2$ (Ar^{Me6} = C_6H_3-2,6-(C_6H_2-2,4,6-Me_3)$_2$), were shown to react reversibly with the four unstrained alkynes: 3-hexyne, diphenylacetylene, trimethylsilylacetylene and phenylacetylene at ambient temperature in toluene. The germirene products, $(Ar^{Me6})_2\overline{GeC(R)=C(R')}$ (R, R' = Et, Et (**1a**), Ph,Ph (**1b**), H, $SiMe_3$ (**1c**) and H, Ph (**1d**) were characterized via ^1H and ^{13}C NMR spectroscopy and by X-ray crystallography in the case of **1a** and **1d**. The thermodynamic parameters of the reactions were determined by variable temperature ^1H NMR spectroscopy and the experimental Gibbs free energies indicated their near thermoneutrality.

Chapter 8: The facile heterodehydrocoupling of a range of primary or secondary amines and even ammonia with pinacolborane (HBPin) was accomplished using $\{Ar^{Me6}Sn(\mu\text{-}OMe)\}_2$ (**1**, Ar^{Me6} = C_6H_3-2,6-(C_6H_2-2,4,6-Me_3)$_2$) as a pre-catalyst for a catalytically active tin(II) hydride. The more sterically hindered pre-catalyst {**2**, $Ar^{iPr4}Sn(\mu\text{-}OMe)\}_2$ (Ar^{iPr4} = C_6H_3-2,6-(C_6H_3-2,6-iPr_2)$_2$) facilitated the dehydrocoupling only of primary amines with HBPin, but at an increased rate relative to the less crowded $\{Ar^{Me6}Sn(\mu\text{-}OMe)\}_2$. Also presented is $\{Ar^{Me6}Sn(\mu\text{-}NEt_2)$ (**3**), which can be converted into the structurally characterizable $\{Ar^{Me6}Sn(\mu\text{-}NEt_2)(\mu\text{-}H)SnAr^{Me6}\}$

(**4**) via the addition of pinacol borane. This, alongside stoichiometric studies, gives insight into the mechanism of the catalysis.

Chapter 9: The diarylgermylene $Ge(Ar^{Me6})_2$ (Ar^{Me6}=C_6H_3-2,6-(C_6H_2-2,4,6-Me_3)$_2$) was shown to react with azobenzene at room temperature to yield the Ge(IV) diamido products, $(Ar^{Me6})_2Ge\{N(H)(Ph)$-o$(Ph)(H)N\}$ **(1a)** and $(Ar^{Me6})_2Ge\{N(H)$-o-$C_6H_4N(Ph)\}$ (**1b**) which were characterized via ^1H and ^{13}C NMR spectroscopy and by X-ray crystallography**.** Treatment of $Ge(Ar^{Me6})_2$ with bulkier diazenes,1,2-bis(2,6-diethylphenl)diazene or 1,2-bis(1,3,5-trimetylphenyl)diazene, even at elevated temperature did not afford N-N bond cleavage and only C-H activation of the germylene was observed. Use of the analogous tin species $Sn(Ar^{Me6})_2$ under the same condition afforded no reactions.

Table of Contents

Chapter 1: The Synthesis and Reactivity of Heavier Element Tetrylenes

1.1: General Introduction

Main group chemistry has undergone very rapid growth since the mid-1970s that has largely followed from numerous reports investigating the "double bond rule" and the recognition that sterically encumbering bulky substituents could stabilize many reactive low coordinate main group molecules featuring multiple bonds.

From the early to mid-20th century, several experimental failures[1] in attempts to synthesize double bonds between main group elements having a principal quantum number greater than 2 and the seminal theoretical calculation by Pitzer[2] and Mulliken[3] had led to the formulation of the "double bond rule".[4] The theory was debunked upon the synthesis and single X-ray analysis of a distannene R_2SnSnR_2 by Lapper et. al. in 1976,[5] a double-bonded disilene, $Mes_2Si{=}SiMes_2$ (Mes = C_6H_2- 2,4,6-Me_3) in 1981,[6] by West et. al. and diphosphene, ArP=PAr (Ar = C_6H_2-2,4,6-$^tBu_3$),[7] by Yoshifuji et. al. in 1981.

The isolation of an Sn analog of an alkene, R_2SnSnR_2 (R=$CH(SiMe_3)_2$)[5a] by Lappert et. al. in 1973 showed that a large substituent can be employed to prevent association and oligomerization of a multiple bonded derivatives of a low coordinate heavier main group element. These species were once thought to be unstable.[1] The X-ray analysis results[5b] were highly unusual where the structure features a trans-pyramidalized tetrel coordination illustrating the fundamental difference between carbon and its heavier group 14 analogs in their bonding properties.

1.2: Carbon and its Heavier Congeners

The remarkable chemical differences between carbon and its heavier congeners arise from the difference in the average radii of their valence *n*s and *n*p atomic orbitals. The atomic radii of the maximum radial density of *n*s and *n*p orbitals are shown in **Figure 1**.[8] Going from C to Si, both the sizes of the *n*s and *n*p orbitals increase as the principal quantum number increases. For carbon, however, there are core 1s electrons but no core (1p) electrons. This the core 1s electron renders the 2s electrons to have an R_{max} value near to that of the 2p electron such that the 2s and 2p orbitals have similar radii which facilitates their hybridization.[9] Moving forward, the slight decrease in the R_{max} of the 4s orbitals of germanium is due to the filling of the 3d shell electrons which do not shield the 3s or 4p electron efficiently. This causes the 4s electron R_{max} to contract. This is also known as the d-block contraction or scandide contraction.[10] The contraction of the 6s orbital compared to the 5s is due to the combined influence of the lanthanide contraction and relativistic effects.[11]

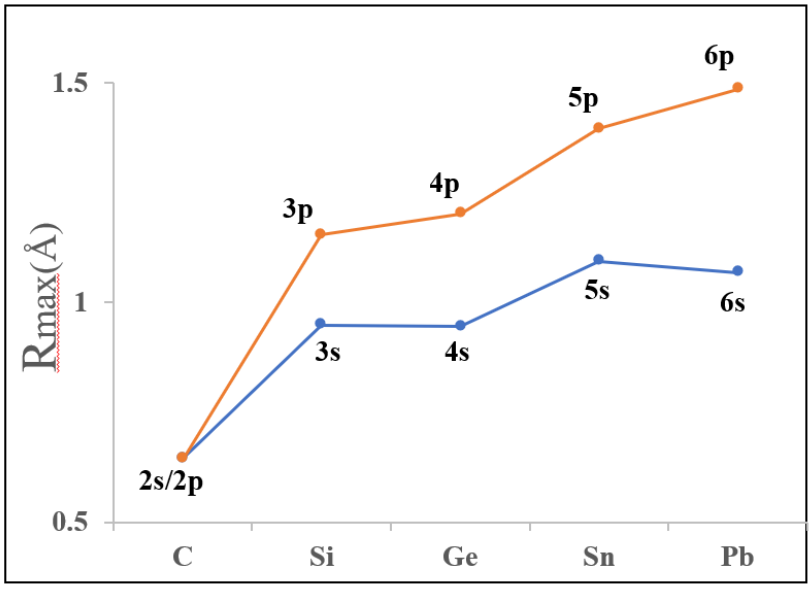

Figure 1. The atomic radius of *n*s and *n*p orbitals of group 14 atoms in angstrom.

In respect of the bonding, the assumptions of valence orbital hybridization are only valid when orbitals to be hybridized have comparable radial radii.[9,12] In contrast to carbon, the difference in the R_{max} values of the heavier tetrels Si-Pb causes them to have a lower tendency to hybridize and preserves the distinction between the valence s and p orbitals. The orbital binding energy of *n*s and *n*p orbitals are shown in **Figure 2**.[8]

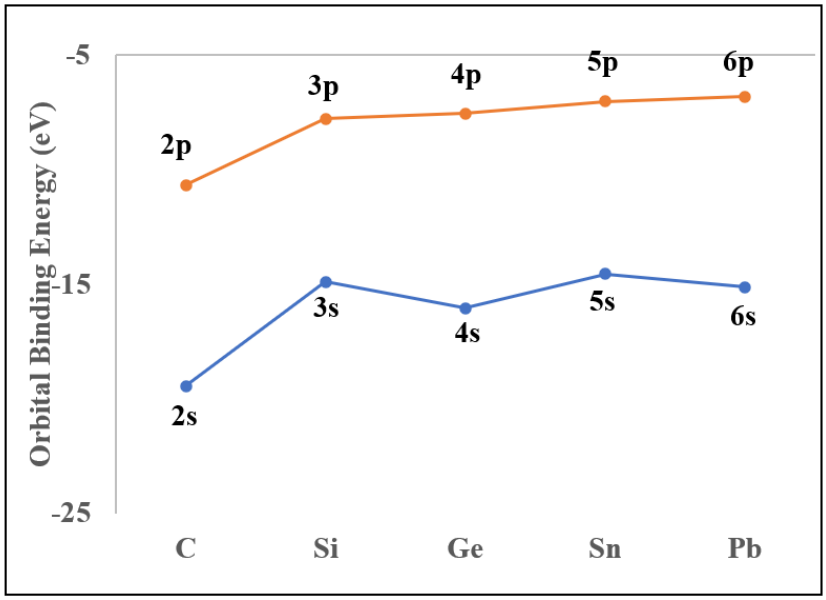

Figure 2. The orbital binding energy of *n*s and *n*p orbitals of group 14 atoms in eV.

1.3: Synthesis of Tetrylenes

The challenges in synthesizing heavier tetrylene can be explained by the increasingly preferred ground states of these species. In contrast to carbenes ($:CH_2$), which have a triplet ground state($^3B_1$) with the singlet($^1A_1$) lying 14.0 kcal/mol higher in energy, the heavier analogs ($:EH_2$; E= Si, Ge, Sn, and Pb) prefer to have in ground state singlets. Thus the lower valency of the group 14 elements becomes more preferred on descending the group.[13] The

calculated singlet-triplet energy separation (ΔE_{ST}) steadily increases going down the group shown in **Table 1.**[13]

EH_2	H-E-H(°)	ΔEst(Triplet-Singlet) kcal/mol
C	134.0	-14.0
Si	92.7	16.7
Ge	91.5	21.8
Sn	91.1	24.8
Pb	90.5	34.8

Table 1. Singlet-triplet energy separation and bond angles of H_2C and H_2E.

Tetrylenes are thus characterized by a relatively inert lone pair with high s-character and a vacant p orbital. Isolation of stable tetrylenes is often effected via thermodynamic stabilization or kinetic stabilization of the reactive vacant p orbitals to prevent dimerization, oligomerization, or decomposition. Thermodynamic stabilizations are usually accomplished by π-electron donating ligands or by intramolecular or intermolecular coordinating ligands, whereas kinetic stabilization is effected by incorporating bulky ligands as shown in **Figure 3**.[14]

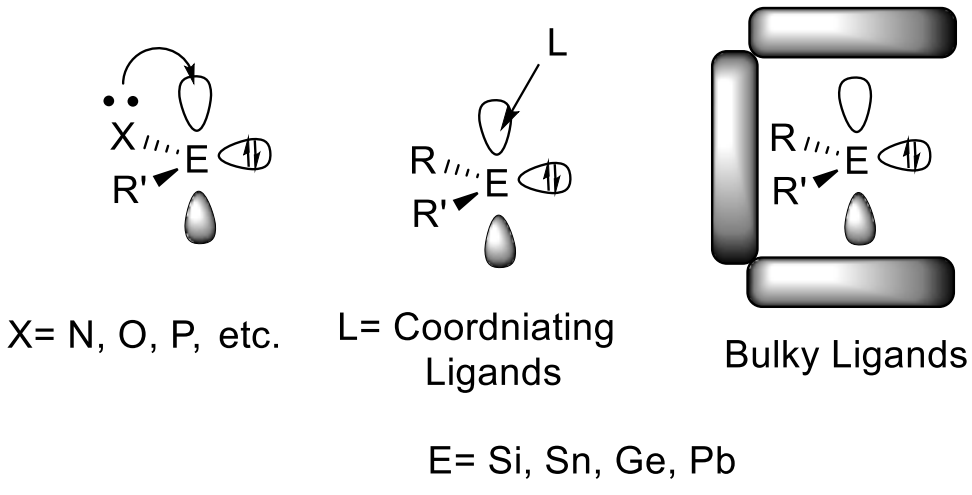

Figure 3. Kinetic and thermodynamic stabilization of tetrylenes.

1.3.1: Silylenes

In 1986, Jutzi and coworkers isolated a decamethylsilicocene, Si(η^5-C_5Me_5)$_2$ (**Figure 4, I-1**),[15] which was the first divalent monomeric silicon (II) compound that was stable at room temperature. The silicon atom is coordinated by ten carbon atoms of the Cp* rings.

The first stable two coordinate silylene, Si(N(^{t}Bu)CH)$_2$ (**Figure 4, I-2**)[16] was reported by West and coworkers in 1994. The silylene was synthesized from the reduction of the corresponding dichlorosilane with potassium at 65°C in THF. The first dialkyl silylene (**Figure 4, I-3**) was isolated as a cyclic species [17] by Kira et. al. in 1999. It was synthesized from the reduction of the corresponding dibromosilane with KC_8 at -50°C in THF. The silylene was stable at 0°C but it slowly isomerized into the corresponding silaethene in solution via a 1,2-migration of the trimethylsilyl group. In 1998 the same group reported a acyclic bisamidosilyene, {Si(N^{i}Pr$_2$)$_2$}$_2$,[18] which exist in a monomer/dimer equilibrium with the corresponding disilene. The silylene was generated photochemically by the irradiation of 3,3-bis(diisopropylamino)-1,2-bis(trimethylsilyl)-3-silacyclopropene.

The first stable acyclic silylene was reported simultaneously by Aldridge/Jones and our group in 2012. Aldridge and Jones synthesized the acyclic heteroleptic silylene, Si{B(NDippCH)$_2$}{N-(SiMe3)Dipp}(**Figure 4, I-4**),[19] via the reaction of the silicon(IV) tribromide, Si{N(SiMe$_3$)Dipp}Br$_3$, with 2 equivalents of the boryl lithium reagent, (thf)$_2$Li{B(NDippCH)$_2$}. The silylene is stable in the solid state up to 130°C but slowly decomposes at 50°C in benzene. On the other hand, Brian Rekken of our group synthesized the first stable homoleptic two-coordinate silylene, Si(SAr^{Me6})$_2$ (ArMe6 = C_6H_3-2,6(C_6H_2-2,4,6-Me$_3$)$_2$ (**Figure 4, I-5**),[20] by the reduction of the corresponding dibromosilane, Br_2Si(SAr^{Me6})$_2$, with a Mg(I) reductant, (IMesMg)$_2$ (IMes = [(2,4,6-

trimethylphenyl)NC(CH_3)]$_2$CH).[21] The silylene is stable in the solid state up to 130°C and is indefinitely stable at 70°C in benzene.[22]

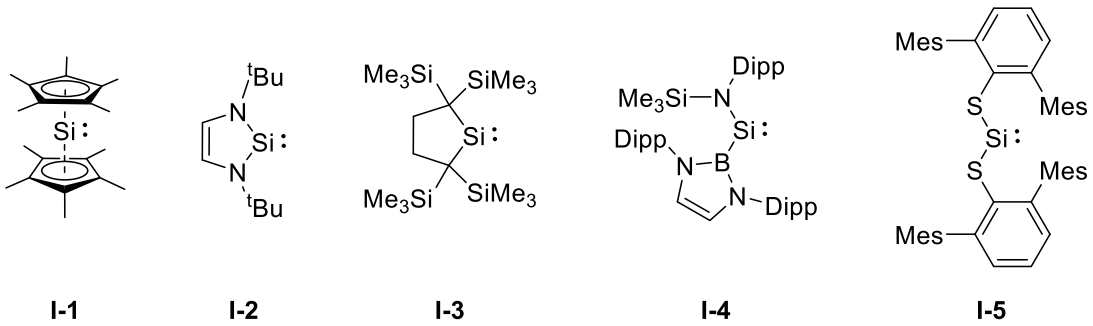

I-1 **I-2** **I-3** **I-4** **I-5**

Figure 4. Selected example of divalent silicon.[15,16,17,19,20]

1.3.2: Germylenes

The common germanium (II) halide precursors, $GeCl_2$(1,4- dioxane) and $GeCl_2$(benzothiazole), were prepared and characterized in the early 1960s.[23] The first stable amidogermylene, Ge[N($SiMe_3$)$_2$]$_2$ (**Figure 5, I-6**)[24] were prepared by Lappert and Harris in 1974[24a] and was structurally characterized by our group in 1992.[24b] The germylene was synthesized by salt metathesis of LiN($SiMe_3$)$_2$(OEt_2) and $GeCl_2$(1,4-dioxane) in ether at 0°C. The first stable dialkylgermylene (**Figure 5, I-7**)[5b] was reported by the same group in 1976. The germylene is known to equilibrate with its corresponding dimer in the solution and the X-ray analysis revealed that the dialkylgermylene exists as a dimer in the solid state.[5c]

In 1982, Veith and coworkers reported a cyclic four-membered ring N-heterocyclic germylene, Ge[(N^tBu)$_2$$SiMe_2$] (**Figure 5, I-8**),[25] whereas in 1992, Herrmann and coworkers reported a five-membered ring N-heterocyclic germylene Ge(N^tBuCH)$_2$ (**Figure 5, I-9**).[26] They are both isolated from the reaction of $GeCl_2$(1,4-dioxane) with the lithiated ligand. Jutzi et al. isolated an acyclic dialkylgermylene Ge[C($SiMe_3$)$_3$][CH($SiMe_3$)$_2$] (**Figure 5, I-10**)[27] that is shown to be monomeric in the solid states. The dialkylgermylene was synthesized

from a nucleophilic substitution of $(THF)_2LiC(SiMe_3)_3$ with $[C_5Me_5]Ge[CH(SiMe_3)_2]$. The first stable cyclic dialkylgermylene (**Figure 5, I-11**)[28] was presented by Kira and coworkers in 1999. The germylene was synthesized by the reduction of the corresponding cyclic dichlorogermane with sodium in toluene at room temperature.

In 1987 du Mont et al. reported a diarylgermylene, $Ge(C_6H_2\text{-}2,4,6\text{-}{}^tBu_3)_2$ (**Figure 5, I-12**),[29] which was prepared by reacting with two equivalents of the aryl lithium salt with $GeCl_2$(1,4-dioxane). The germylene was originally thought to be unstable at room temperature and it undergoes a C-H insertion into one of the *o*-^{t}butyl groups of the aryl substituent. However, a subsequent investigation by Jutzi et al.[30] showed that the germylene only C-H inserts when a Lewis acid is present in solution. Another aryl-substituted germylene was reported by Richard Simons of our group in 1997. The diarylgermylene $Ge(C_6H_3\text{-}2,6\text{-}Mes_2)_2$ (Mes = C_6H_2-2,4,6-Me_3) (**Figure 5, I-13**)[31] was prepared by the reaction of aryl lithium with $GeCl_2$(1,4-dioxane) in diethyl ether. The first germylene bearing an electropositive substituent $Ge(C_6H_3\text{-}2,6\text{-}Mes_2)(Ge{}^tBu_3)$ (**Figure 5, I-14**)[32] was synthesized by Kira in collaboration with our group via the reaction of $GeCl(C_6H_3\text{-}2,6\text{-}Mes_2)$ with $LiGe{}^tBu_3$.

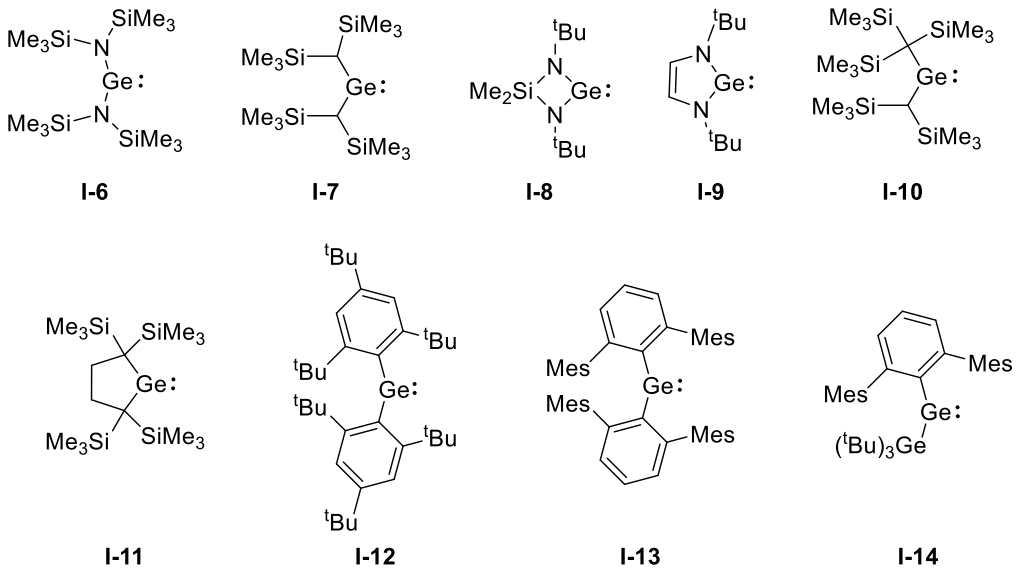

Figure 5. Selected example of germylenes.[24-32,5b]

1.3.3: Stannylenes

The first isolable amidostannylene, $Sn[N(SiMe_3)_2]_2$ (**Figure 6, I-15**), was reported by Lappert and Harris in 1974.[24] It was prepared by salt metathesis of $SnCl_2$ with $LiN(SiMe_3)_2(OEt_2)$ in ether. The first dialkylstannylene, $Sn[CH(SiMe)_2]_2$ (**Figure 6, I-16**), was first reported in 1973[5a] and structurally characterized as described in a subsequent manuscript in 1976.[5b] The dialkylstannylene is shown to be a monomer in solution and X-ray analysis revealed that it is a dimer in the solid state. The first cyclic dialkylstannylene (**Figure 6, I-17**)[33] was synthesized by Kira in 1999 by the reaction of $SnCl_2$ with the lithiated alkyl ligand. Klinkhammer and coworkers reported the first silyl stannylene, $Sn[Si(SiMe_3)_3]_2$,[34] featuring an electropositive silyl substituent. This hypersilylstannylene (**Figure 6, I-18**) was prepared by the reaction of $Sn[N(SiMe_3)_2]_2$ and $(Me_3Si)_3SiK$. The stannylene was found to be monomeric in solution and dimeric in the solid state.

The first monomeric diarylstannylene, $Sn(C_6H_2\text{-}2,4,6\text{-}(CF_3)_3)$ (**Figure 6, I-19**),[35] was published by Grutzmacher in 1991 where the stannylene is stabilized by a 2,6-bis(trifluoromethyl)phenyl ligand and features a stabilizing Sn--F interaction. The stannylene was synthesized from the reaction of two equivalent of the corresponding aryl lithium with $SnCl_2$. The solid-state structure revealed that it has a short (2.8Å) Sn-F contact demonstrating some degree of intramolecular donor stabilization. The first diarylstannylene, $Sn(C_6H_2\text{-}2,4,6\text{-}{}^tBu_3)_2$ (**Figure 6, I-20**)[36] without further ligand donor stabilization was demonstrated by Weidenbruch and coworkers in 1994. X-ray analysis confirms that the compound is monomeric in the solid state and no agostic interaction of the neighboring C-H bond with the Sn atom was observed. The molecule undergoes a thermo-isomerization at 50°C with the flanking *o*-tert-butyl group. Another aryl-substituted stannylene, $Sn(C_6H_3\text{-}2,6\text{-}Mes_2)_2$ (**Figure 6, I-21**),[31] was reported by our group in 1997.

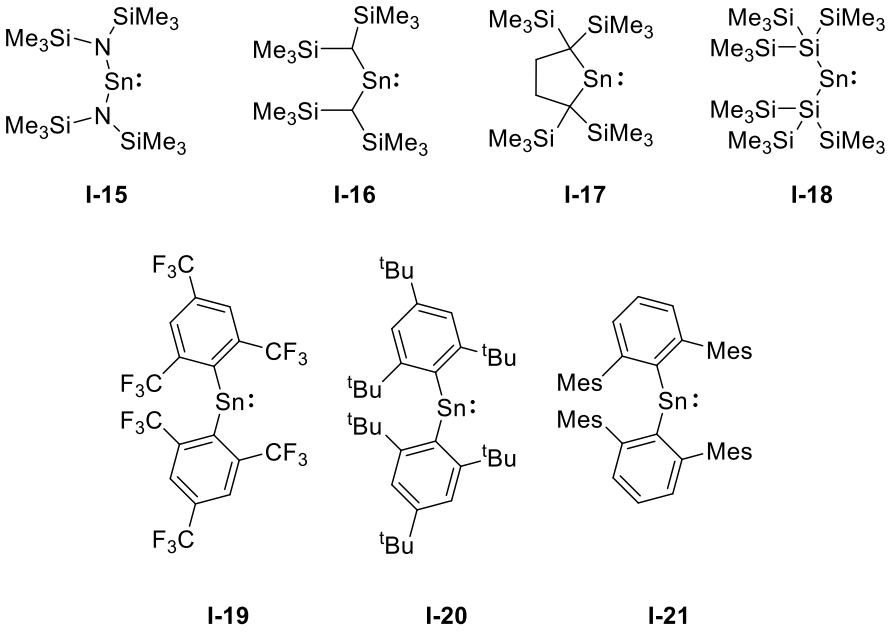

Figure 6. Selected example of stannylenes.[5,24,31,33-36]

1.3.4: Plumbylenes

The first isolable organoplumbylene, $Pb[CH(SiMe_3)_2]_2$ (**Figure 7, I-22**), was reported by Lappert and coworkers in 1973.[5a,5b] The plumbylene was synthesized by salt metathesis of $LiCH(SiMe_3)_2$ and $PbCl_2$. In a subsequent report in 1974, the same group synthesized the first amidoplumbylene $Pb[N(SiMe_3)_2]_2$ (**Figure 7, I-23**).[24] The plumbylenes was also synthesized via the salt metathesis of $LiN(SiMe_3)_2$ with $PbCl_2$.

The first structurally characterized diarylplumbylene, $Pb(C_6H_2\text{-}2,4,6\text{-}(CF_3)_3)$ (**Figure 7, I-24**),[37] was demonstrated by Edelmann et al. in 1990. Klinkhammer and coworkers reported the first plumbylene featuring an electropositive silyl substituent in 1995.[34] The hypersilylstannylene, $Pb[Si(SiMe_3)_3]_2$ (**Figure 7, I-25**), was prepared by transmetallation of $Pb[N(SiMe_3)_2]_2$ and $(Me_3Si)_3SiK$.

The first structurally characterized dialkylplumbylene, $Pb\{(Me_3Si)_2CSiMe_2CH_2\}_2$ (**Figure 7, I-26**),[38] was reported by Eaborn and coworkers in 1997, which was synthesized

via the reaction of $[Li(TMEDA)_2][CH_2SiMe_2C(SiMe_3)_2LiC\text{-}(SiMe_3)_2SiMe_2CH_2]$ with $PbCl_2$ in THF. In 1997 our group also reported another aryl-substituted plumbylene $Pb(C_6H_3\text{-}2,6\text{-}Mes_2)_2$ (**Figure 7, I-27**),[31] via the reaction of two equivalent of the corresponding aryl lithium with $PbCl_2$. Okazaki and coworkers describe a series of diarylplumbylene (**Figure 7, I-28**),[39] via transmetallation of $Pb[N(SiMe_3)_2]_2$ and two equivalents of the corresponding aryl lithium.

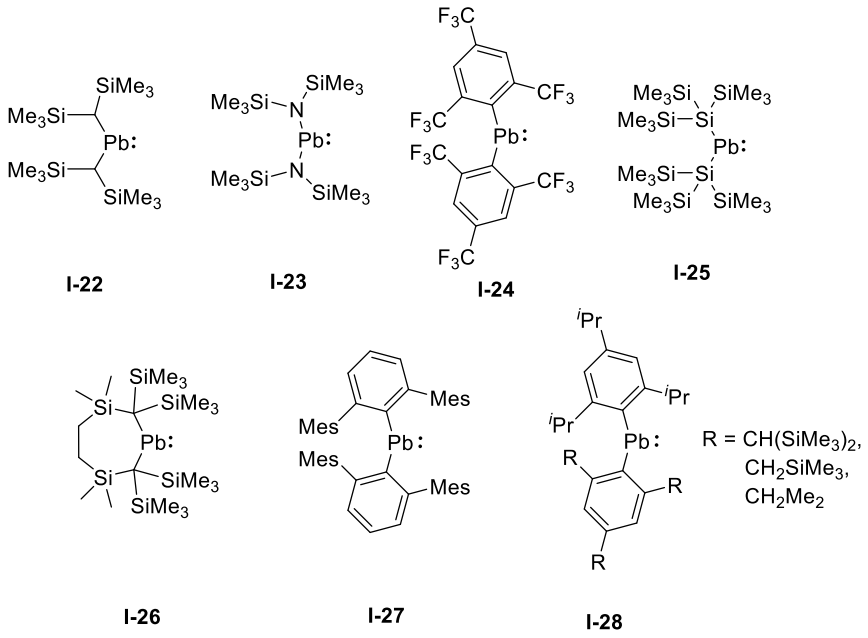

Figure 7. Selected example of plumbylenes.[5, 24, 31, 34, 37-39]

1.4: Reactivity of Tetrylenes

The reactivity of tetrylenes is strongly governed by the presence of a vacant p orbital and lone pair of electrons in their valence s shell.[14] However, as mentioned above, this lone pair is relatively inert, hence most tetrylene reactivity is initiated by the interaction of the reagents with the vacant p orbitals. Nonetheless, the small energy gaps (<4eV)[40] between the occupied s lone pair orbital (HOMO) and the vacant p orbital (LUMO) have allowed tetrylenes to activate classical small molecules such as H_2, NH_3, alkene, alkynes, CO_2, and CO.

1.4.1: Reactions with H_2

The activation of dihydrogen is important due to its industrial relevance in catalytic transformations, such as hydrogenation and hydrofuncationalization.[41] The challenges of the activation of dihydrogen originates from its high bond enthalpy (103 kcal mol^{-1}).[42] There have only been a handful of tetrylenes that have been shown to react with H_2 by overcoming a small HOMO-LUMO gap. The strategy can be summarized into 2 categories: **1.** Changing the symmetry of the molecular energy levels in the compounds via manipulating the electronic and steric properties of the substituents. or **2.** Utilizing a frustrated Lewis pair system to simultaneously have access to a high-lying HOMO and low-lying LUMO.

The reaction of tetrylene with hydrogen was first accomplished by our group in 2008.[43] This followed an earlier report of a reaction of hydrogen with the digermyne $Ar^{iPr4}GeGeAr^{iPr4}$ in 2005.[43b]The reaction of germylene $Ge(Ar^{Me6})_2$ **I-13** with H_2 afforded the tetravalent germanium dihydride $GeH_2(Ar^{Me6})_2$ **I-29**. Whereas the more sterically bulky $Ge(Ar^{iPr4})_2$ gave the trihydride, H_3GeAr^{iPr4}, with an aryl elimination (HAr^{iPr4}). In the same report, we demonstrated that the bulkier $Sn(Ar^{iPr4})_2$ **I-30** reacts with H_2 to give a tin hydride species, $HSnAr^{iPr4}$ **I-31,** along with the elimination of HAr^{iPr4} shown in **Scheme 1b**. The sterically less crowded $Sn(Ar^{Me6})_2$ displayed no reaction with H_2. This is likely due to the difference in higher energy gap between the $Sn(Ar^{iPr4})_2$(553nm; $\Delta E_{(HOMO\text{-}LUMO)}$=64.55 kcal mol^{-1})[44] and $Sn(Ar^{Me6})_2$ (600m; $\Delta E_{(HOMO\text{-}LUMO)}$= 61.57 kcal mol^{-1}).[31]

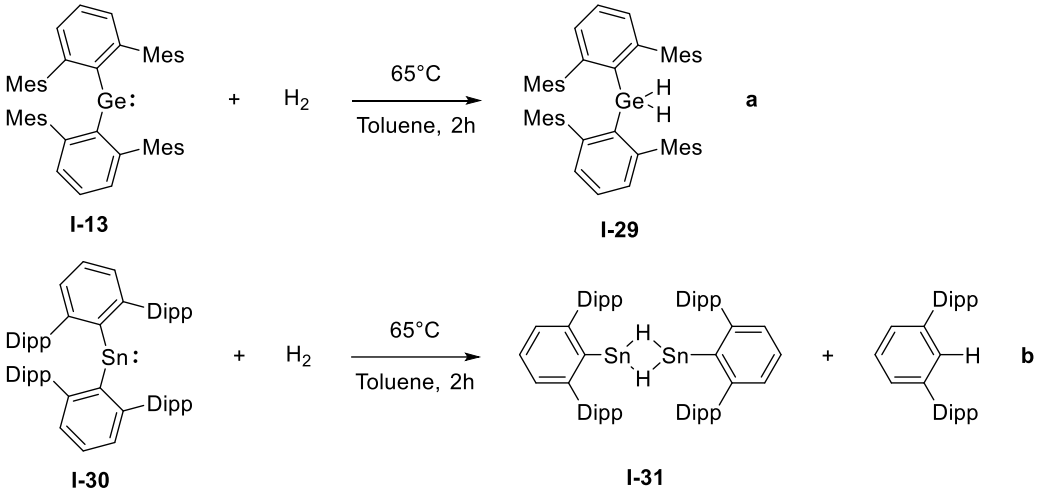

Scheme 1. Reaction of diarylgermylene and stannylene **I-13** and **I-30** with H_2.[43]

In 2012 and 2013, Aldridge reported the first activation of dihydrogen by a stable silylene. They demonstrated that a amido boryl silylene or boryl silyl silylene, $Si(B(N(Dipp)CH)_2)(N(SiMe_3)Dipp)$[19] **I-4** and $Si(B(N(Dipp)CH)_2)(Si(Si(SiMe_3)_3)$[45] **I-32** reacts with H_2 to give the corresponding dihydrosilane (**I-33** or **I-34**). The reaction is allowed by the relatively small HOMO-LUMO energy gap (1.96eV). The small energy gap is due to the strong σ-donor boryl ligand and a large bond angle around the silicon core. In 2016, the same group showed that a bis(boryl) stannylene, $Sn(B(N(Dipp)CH)_2)_2$, reacts with dihydrogen and gives the dihydrostannane $H_2Sn(B(N(Dipp)CH)_2)_2$.[46]

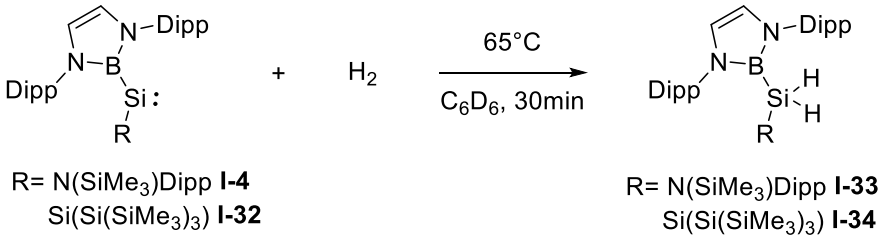

Scheme 2. Reaction of boryl silylene **I-4** and **I-32** with H_2.[19,45]

In 2017, Inoue and Rieger reported that an N-heterocyclic imino-ligated silepin **I-35**,[47] a masked silylene $Si(NC((Dipp)CH)_2(Si(SiMe_3)_3)$ **I-35T**, activates dihydrogen at 50°C to give the corresponding dihydrosilane **I-36**. In 2019, the same group demonstrated that a

disilene **I-37** which is in equilibrium with the silylene **I-37T** was also found to activate H_2 at -40°C shown in **Scheme 3b**.[48]

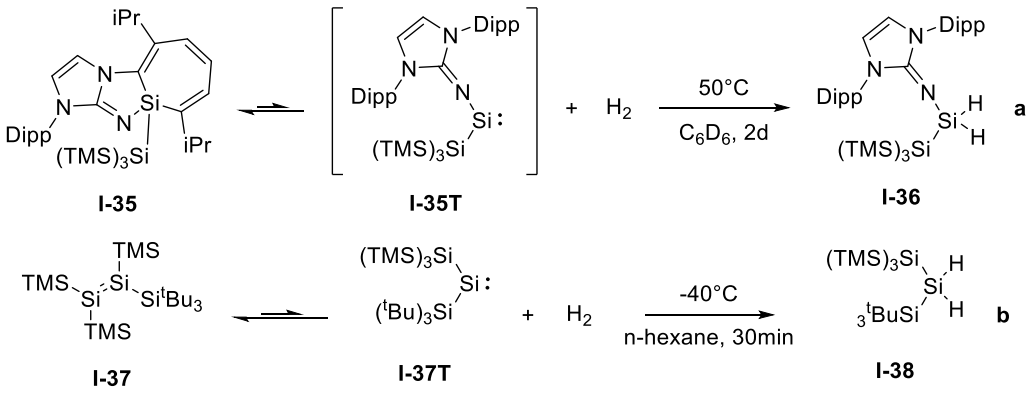

Scheme 3. Reaction of **I-35** and **I-37** with H_2.[47, 48]

Driess and coworkers reported that a FLP system of a N-heterocyclic silylene–borane complex, LSi-R-$BMes_2$ (L = $PhC(NtBu)_2$; R = 1,12-xanthendiyl-9,9-dimetyl),[49] **I-39** can split H_2 in a FLP manner affording a dihydrosilane **I-40**. It is interesting to note that the H_2 did not react with LSiPh or the combination of LSiPh and $BMes_2Ph$ in solution, indicating the necessity of a pre-organized Si-B system. In 2018, Ashley and coworkers reported an FLP system of Lappert's stannylene, $Sn[CH(SiMe_3)_2]_2$ **I-16**, and NEt_3 reacts with H_2 at 4 atm to yield the dihydrostanne $H_2Sn[CH(SiMe_3)_2]_2$ **I-41**.[50] Interestingly, the addition of a stronger base, DBU (1,8-diazabicyclo[5.4.0]undec-7-ene), enables an equilibrium of the stannylene with the corresponding dihydrostanne under H_2 atmosphere as shown in **Scheme 4b**.

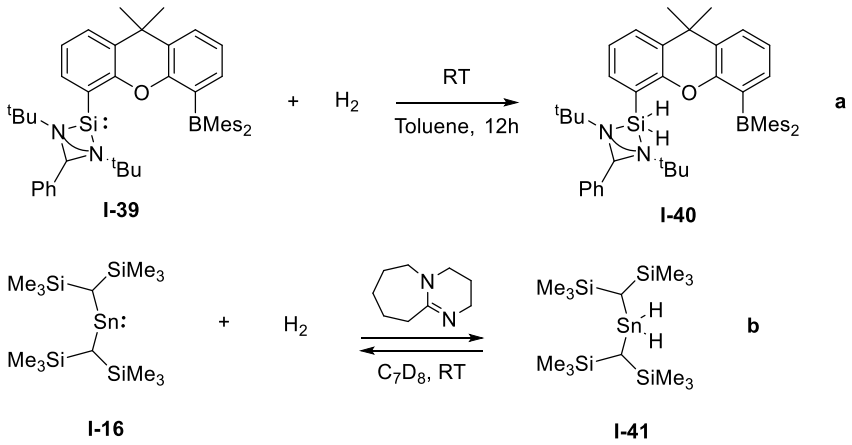

Scheme 4. Reaction of FLP system **I-39** and **I-16/DBU** with H_2.[49,50]

1.4.2: Reaction with NH_3

The activation of ammonia is similar to dihydrogen where the challenge arises from its high bond enthalpy (95 kcal mol^{-1})[42] and a similar activation strategy has been employed.

In 2008, our group reported that the diarylgermylenes and diarylstannylenes, $E(Ar^{Me6})_2$ and $E(Ar^{iPr4})_2$ (E= Ge or Sn)[43] activates NH_3 at room temperature. Both gremylenes gives the respective oxidative addition product, $(Ar^{Me6})_2GeH(NH_2)$**I-43** and $(Ar^{iPr4})_2GeH(NH_2)$**I-44**. DFT calculation showed that the reaction was initiated by the coordination of the ammonia to the empty 4p orbital on the germanium followed by the solvation of the complexed NH_3 via a second NH_3. The intermediate then goes on and form the facile oxidative addition product. In contrast, the stannylenes react with ammonia to give the bridge amido compounds, $Ar^{Me6}Sn(\mu\text{-}NH_2)_2SnAr^{Me6}$**I-45** and $Ar^{iPr4}Sn(\mu\text{-}NH_2)_2SnAr^{iPr4}$**I-46** with the elimination of HAr^{Me6} and HAr^{iPr4} respectively.

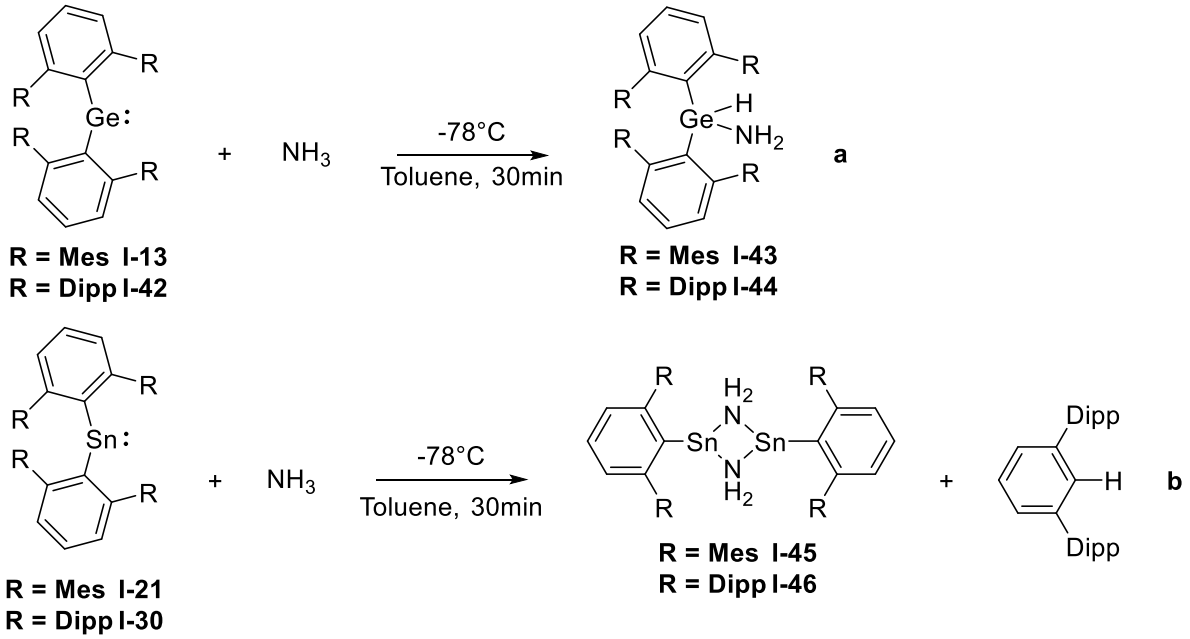

Scheme 5. Reaction of diarylgermylene and stannylene **I-13** and **I-30** reaction with NH_3.[43]

In 2009, Roesky reported that a NacNac derived silylene and germylene, E[CH(C=CH_2)(CMe)(2,6-$iPr_2C_6H_3N)_2$] (E= Si,[51]Ge[52]) **I-47**/**I-49** reacts with ammonia at room temperature. The silylene gave the 1,1, addition product **I-48**, whereas the germylene give the 1,4-addition product **I-50** as shown in **Scheme 6a** and **6b.** The selectivity is shown to be the difference in the bond strength of the Ge–H bond in the hypothetical 1,1-addition product versus the formation of the stronger C–H bond in the 1,4-addition product. In 2011, Driess also showed a NacNac germylene **I-51**,[53] reacts with ammonia and gave the similar 1,4 addition product **I-52** that was presented by Roesky (**Scheme 6c**).

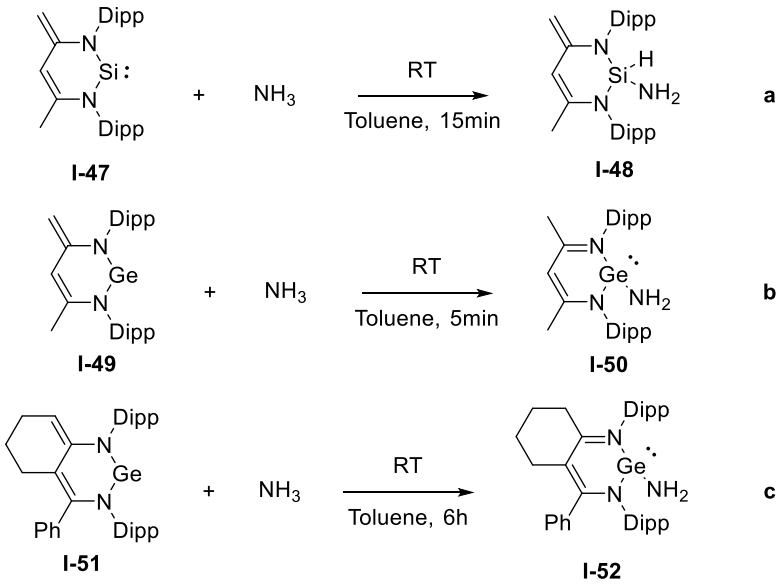

Scheme 6. Reaction of N-heterocyclic silylene and germylene with NH_3.[51-53]

In 2016, Aldridge and Jones demonstrated that an acyclic diamidosilylne, $Si[N(SiMe_3)(B(CHN\text{-}C_6H_3\text{-}2,6\text{-}iPr_2))]_2$ **I-53**,[54] reacts with excess ammonia in toluene and gives a triaminosilane $[N(SiMe_3)(B(CHN\text{-}C_6H_3\text{-}2,6\text{-}iPr_2))]SiH(NH_2)_2$ **I-55**. The authors proposed that the transient diamido silylene, $Si[N(SiMe_3)(B(CHN\text{-}C_6H_3\text{-}2,6\text{-}iPr_2))](NH_2)$ **I-54**, formed via a σ-bond metathesis between the starting silylene with NH_3, followed by oxidative addition of a second ammonia to give the final triaminosilane product **I-55**. In the same year, Aldridge demonstrated that a diborylstannylene, $Sn(B(N(Dipp)CH)_2)_2$ **I-56**,[46] reacts with NH_3 and give an oxidative addition product $(NH_2)(H)Sn(B(N(Dipp)CH)_2)_2$ **I-57**.

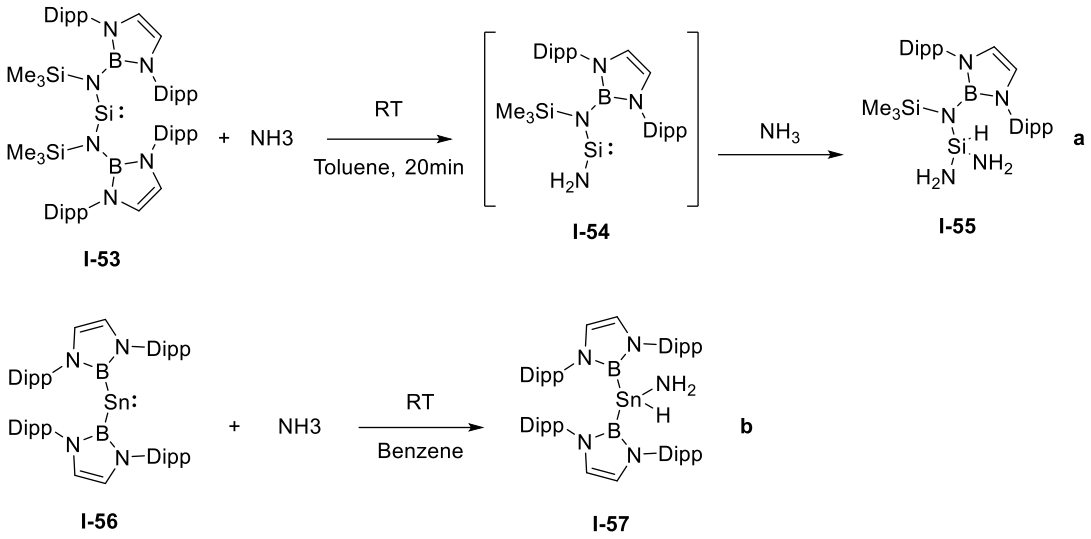

Scheme 7. Reaction of **I-53** and **I-56** with NH_3.[46, 54]

In 2020, Inoue reported amido(siloxy)silylene **I-58** that reacted with 1 equivalent of ammonia at -80°C to give the hydroamination product **I-59** identified by ^1H NMR spectroscopy.[55] **I-59** reacts further with an excess amount of ammonia afforded an as yet unidentified product.

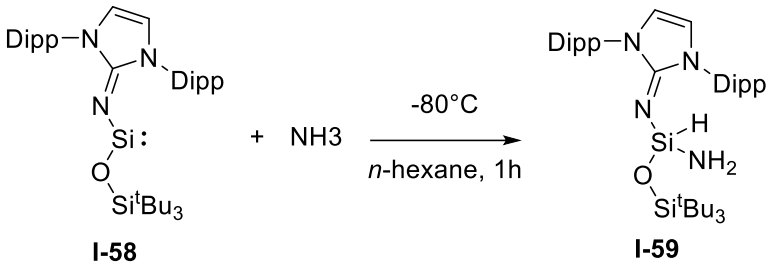

Scheme 7. Reaction of a amido(siloxy)silylene with NH_3.[55]

1.4.3: Reaction with Alkene and Alkynes

The relatively small HOMO-LUMO energy gap of tetrylenes has generated numerous reports of the reactions of heavier tetrylenes with alkenes and alkynes to afford either insertion or cycloaddition products.[56] However, examples of reversible reactions of alkenes

and alkynes with heavier tetrylenes remain extremely rare,[57] in part because the product metallocyclopropanes and propenes are relatively stable which hinders the reverse reaction. The background and reactivity of tetrylenes with unsaturated hydrocarbons will be discussed extensivity in Chapters 5, 6, and 7.

1.4.4: Reaction with CO_2

The activation and reduction of CO_2 have gained much attention over the last few decades due to growing environmental issues on global warming.[58] The reaction of CO_2 with lighter group 14 tetrylenes tend to result in facile deoxygenation with the reduction of CO_2 into CO and followed by the formation of an E=O moiety (E = Si, Ge). Ligand insertion is a more common reaction pattern for the heavier congeners.[59]

Driess and coworkers demonstrated that a siloxysilylene[60] **I-60** reacts with CO_2 to give a silanoic silyl ester **I-61** via deoxygenation as shown in **Scheme 8a**. Kato and Baceiredo demonstrated that a phosphine-stabilized silylene[61] **I-62** reduces CO_2 at room temperature affording a Si-O-P bridge product **I-63**. The mechanism was proposed to involve a phosphine-centered sila-Wittig reaction followed by the release of a CO molecule.

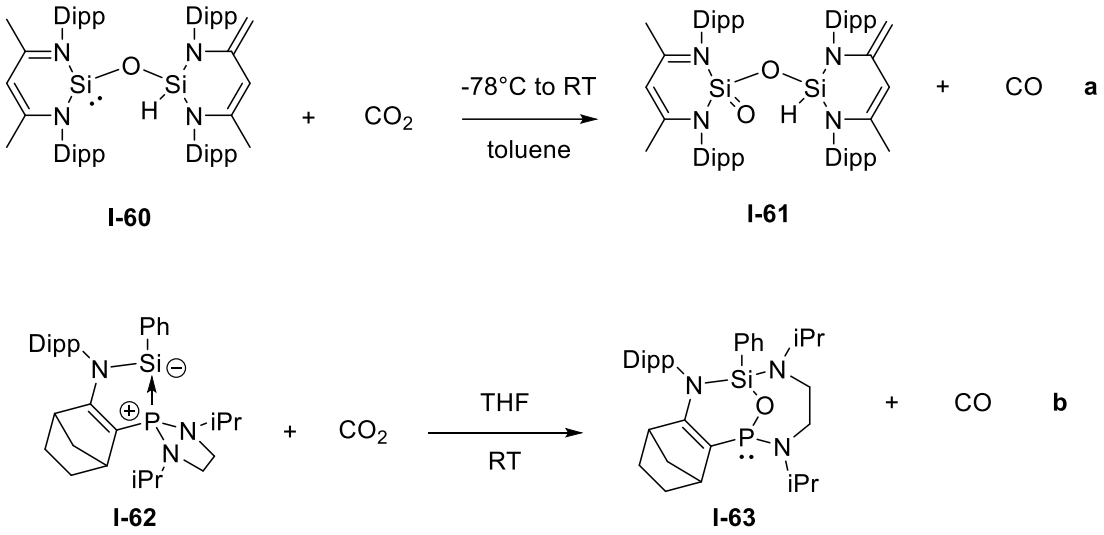

Scheme 8. Reaction of **I-60** and **I-62**with CO_2.[60, 61]

Kira and coworkers showed that a cyclic dialkylsilylene **I-3** reacts with CO_2 at room temperature.[62] After hydrolysis, the product was structurally characterized as a bis(silyl)carbonate **I-67**. DFT calculations showed that the reaction is initiated by the deoxygenation of CO_2 forming a silanone **I-64**, followed by an [2+2] addition with a second equivalent of CO_2 giving a cyclic carbonate **I-65**. The cyclic carbonate **I-65** then dimerizes with the silanone **I-64** to give the carbonate product **I-66**. A subsequent aqueous workup resulted in the bis(silyl)carbonate **I-67**.

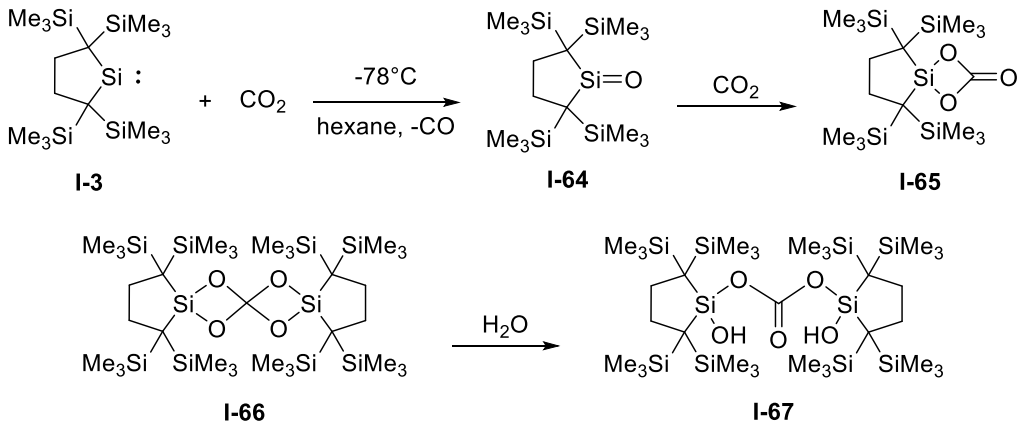

Scheme 9. Reaction of cyclic dialkylsilylene **I-3** with CO_2.[62]

Bickelhaupt and Tacke showed that a bis(amidinato)silylene **I-68** and the analogous bis(guanidinato)silylene **I-69** react with two equivalents of CO_2 to give a silicon carbonate product **I-72** and **I-73**.[63] Similar reactivity was also observed by Inoue et. al. with the N-heterocyclic imino-ligated silepin **I-35**.[48]

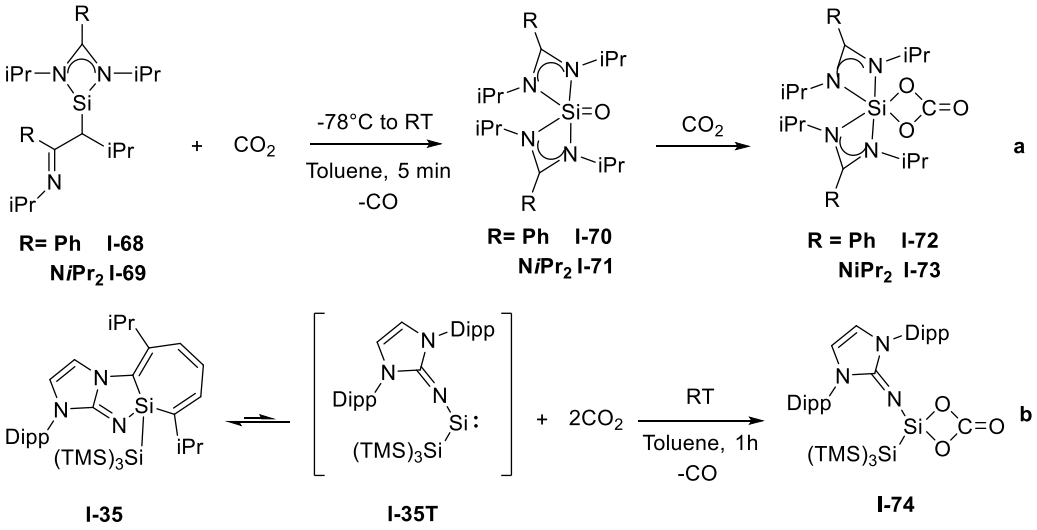

Scheme 10. Reaction of amido silylene with CO_2.[48, 63]

Kemp and coworkers showed that the reaction of diamido stannylene, $Sn(NMe_2)_2$ reacts with CO_2 to give an Sn-N insertion product, $[Sn(CO_2NMe_2)_2]_2$.[64] Similar insertion chemistry was observed by Fulton and coworkers for a reaction of CO_2 with N-heterocyclic stannylene, [CH(CMeNDipp)$_2$]SnNR (N(*i*Pr)$_2$ or NHDipp)[65] or [CH(CMeNDipp)$_2$]SnOR (R = *i*Pr, *s*Bu or ^{t}Bu)[66] leading to the formation of a tin(II) carbamate shown in **Scheme 11**.

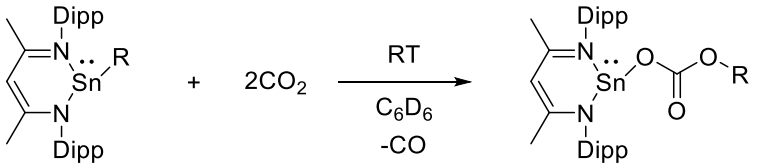

R = N(iPr)$_2$ **I-75**, NHDipp **I-76**,
O^{i}Pr **I-77**,O^{s}Bu **I-78**, O^{t}Bu **I-79**

R = N(iPr)$_2$ **I-80**, NHDipp **I-81**,
O^{i}Pr **I-82**,O^{s}Bu **I-83**, O^{t}Bu **I-84**

Scheme 11. Reaction of N-heterocyclic tin amide or alkoxide with CO_2.[65, 66]

Recently Aldridge and coworkers reported that a boryl substituted silylene **I-4** reacts with CO_2 at room temperature resulted in the formation of the(trimethylsiloxy)iminosilane **I-85**.[67] The proposed mechanism is that a silanone is generated in situ via deoxygenation of CO_2 followed by a silyl migration giving the carbonate product. The same group also reported a boryl substituted stannylene, $Sn(B(N(Dipp)CH)_2)_2$ **I-56**,[68] reacts with CO_2 forming an insertion product **I-86**. Storage of the insertion product under CO_2 for 10 days resulted in the insertion of the second equivalent of CO_2 to give $Sn[O_2CB(NDippCH)_2]_2$ **I-87**.

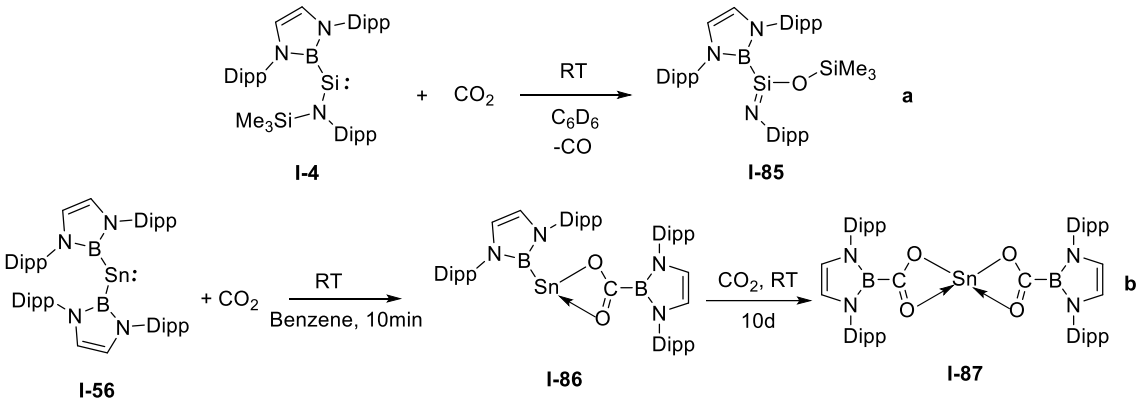

Scheme 12. Reaction of boryl silylene and stannylene with CO_2.[67, 68]

1.4.5: Reaction with CO

The activation of CO molecules has drawn significant interest in recent years due to the imminent shortage of fossil fuels.[69] CO has the potential to serve as a carbon feedstock to produce essential organic building blocks.[70] Due to the insufficient π back-bonding (lone pairs are fairly inert), the reaction of tetrylenes with carbon monoxide tends to result in the insertion of the ligand into the carbon monoxide moiety.[71]

The first CO activation by the stable germylene was reported by our group in 2009.[72] Stirring the diarylgermylene **I-88**/**I-90** under a CO atmosphere led to the isolation of a CO coupling product **I-89**/**I-91**. The product contains 2 coupled CO moieties which were inserted

into the C_{Aryl}-Ge bond followed by a migration of an isopropyl group to form a six-membered ring. In the case when a bulkier germylene, Ge(Ar^{Me6})(Ar^{iPr8}) **I-90** when exposed to CO, the two CO fragments were inserted into the less bulky Ar^{Me6} ligand.

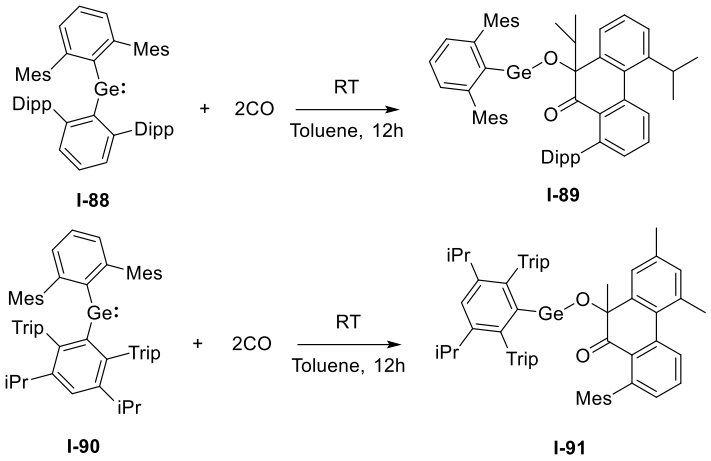

Scheme 13. Reaction of diarylgermylene with CO.[72]

In 2019, Driess and coworkers reported two chelated bis-silylene, Xant($SiL)_2$ [1,12-xanthendiyl-9,9-dimetyl; L= $PhC(NtBu)_2$][73] **I-92** and Fc($SiL)_2$ (Fc=1,1'-ferrocenyl)[73] **I-94** react and splits two equivalent of CO to give a ketene species **I-93** and **I-95** shown in **Scheme 14**. The same group reported another chelated bis-silylene, $[(SiL)C]_2B_{10}H_{10}$ **(**L= $(NtBu)_2CPh$)[74] **I-96** reacts with CO to give a dimeric C-O cleavage product **I-97** shown in **Scheme 14a**.

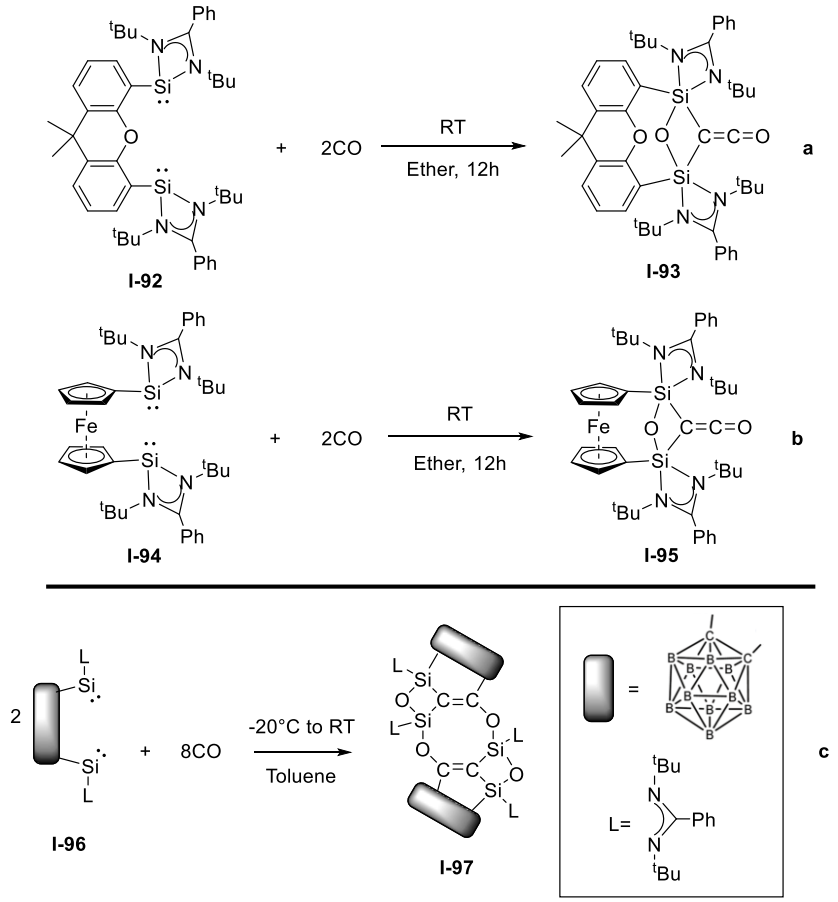

Scheme 14. Reaction of chelated silylenes with CO.[73,74]

In 2019, Aldridge and coworkers reported an amidoboryl silylene, Si{B(NDippCH)$_2$}{N(SiMe3)Dipp}[67] **I-4**, that reductively couples two CO molecules to afford a dimeric structure **I-98**. The product contains a six-membered ring with two bridging CO moieties.

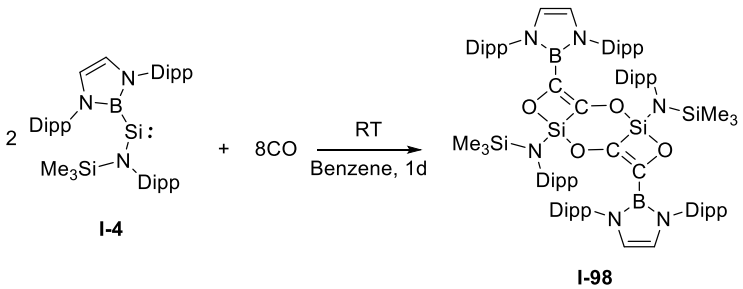

Scheme 15. Reaction of amido boryl silylene **I-4** with CO.[67]

Recently, Schulz and Inoue's group independently reported the isolation of two silylene-carbonyl complexes. Schulz group reported that stirring a silylene intermediate **I-101/I-102**, supported by a bulky and strongly electron-donating gallium based N-heterocyclic ligand (Ga(X)L, L = $HC[C(Me)NDipp]_2$/ X = Br,[75] I[76]), under CO atmosphere gives a silylene-carbonyl compound **I-103/I-104**. Inoue and coworkers reported a silylene **I-37T** with bulky silicon substituent $Si(SiMe_3)_3$ and Si^tBu_3 which also forms a silylene -carbonyl compound **I-106** when exposed to CO.[77] DFT computations[76-78] revealed that the presence of electron-rich L(X)Ga and Si^tBu_3 substituent increases the electron density at the silicon atom. This enables the π-back bonding into the π*-orbital of CO, resulting in a bonding model similar to the Dewar-Chatt Duncanson model for transition metals.[79] These examples show the importance of back bonding in tetrylenes for stabilizing multiple bonded small molecules such as CO, and reveal the potential for tetrylenes to activate N_2.

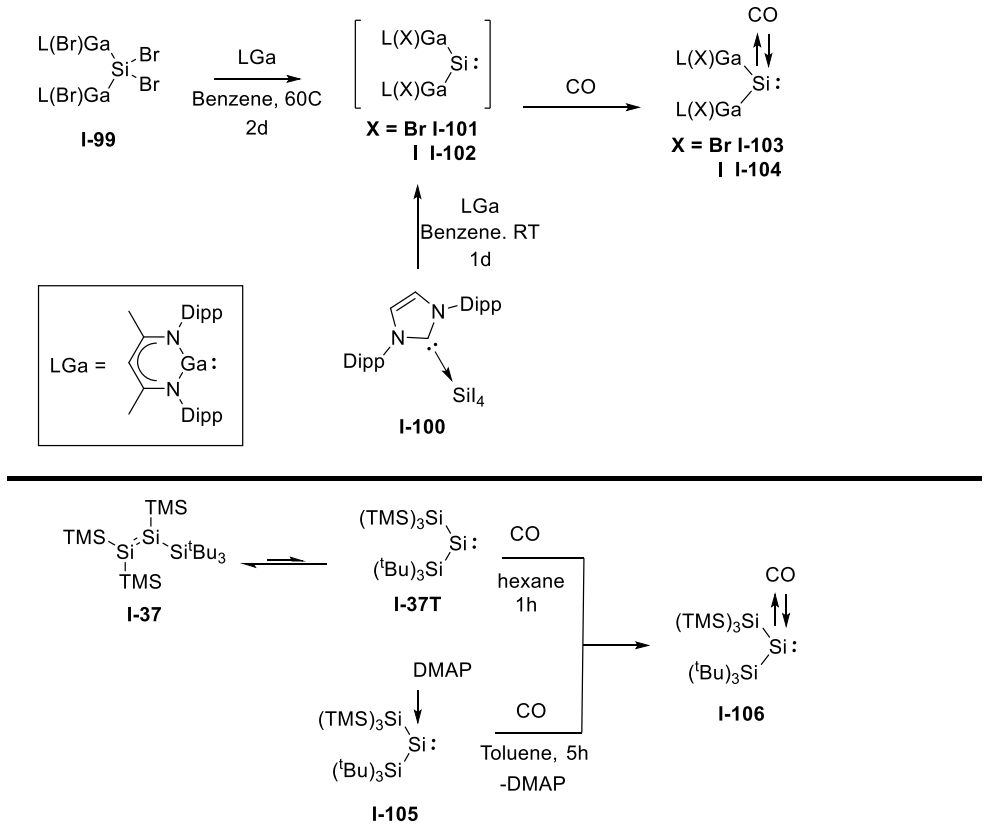

Scheme 16. Isolation of a silylene-carbonyl complex.[65-67]

1.5: References

1. Dasent, W. E. (1965). *Nonexistent Compounds and Compounds of Low Stability*. Marcel Dekker: New York, 1965.
2. Pitzer, K. S. The Thermodynamic and Physical Properties of the Elements. *J. Am. Chem. Soc.*, **1948,** *70*, 2140–2145.
3. Mulliken, R. S. Overlap Integrals and Chemical Binding. *J. Am. Chem. Soc.*, **1950**, *72*, 4493–4503.
4. a) Pettit, L. D. Multiple Bonding and Back-co-ordination in Inorganic Compounds. *Q. Rev. Chem. Soc.*, **1971**, *25*, 1-29. b) Jutzi, P. New Element-Carbon (p-p)n Bonds. *Angew. Chem. Int. Ed. Engl.*,**1975**,*14*, 232-245.
5. a) Davidson, P.J.; Lappert, M.F. Stabilisation of metals in a low co-ordinative environment using the bis(trimethylsilyl)methyl ligand; coloured Sn^{II} and Pb^{II} alkyls, $M[CH(SiMe_3)_2]_2$ *J. Chem. Soc., Chem. Commun.*, **1973**, 317a-317a b) Goldberg, D. E.; Harris, D. H.; Lappert, M. F.; Thomas, K. M. A New Synthesis of Divalent Group 4B Alkyls $M[CH(SiMe_2)_2]_2$ (M=Ge or Sn), and the Crystal and Molecular Structure of the Tin Compound *J. Chem. Soc., Chem. Commun.*, **1976**, 261-262. c) Goldberg, D.E.; Hitchcock, P.B.; Lappert, M.F.; Thomas, K.M.; Thorne, A.J. Subvalent Group 4B metal alkyls and amides. Part 9. Germanium and tin alkene analogues, the dimetallenes M_2R_4[M = Ge or Sn, R = $CH(SiMe_3)_2$]: X-ray structures, molecular orbital calculations for M_2H_4, and trends in the series $M_2R'_4$[M = C, Si, Ge, or Sn; R′ = R, Ph, $C_6H_2Me_3$-2,4,6, or $C_6H_3Et_2$-2,6] *J. Chem. Soc., Dalton Trans.*, **1986**, 2387-2394
6. West, R.; Fink M. J. ; Michl, J. Tetramesityldisilene, a Stable Compound Containing a Silicon-Silicon Double Bond. *Science*, **1981**, *214*, 1343– 1344

7. Yoshifuji, M. ; Shima, I. ; Inomoto, N. ; Hirotsu, K. ; Higuchi T. Synthesis and structure of bis(2,4,6-tri-tert-butylphenyl)diphosphene: isolation of a true phosphobenzene. *J. Am. Chem. Soc.*, **1981**, *103*, 4587− 4589.
8. Desclaux, J. P. Relativistic Dirac-Fock Expectation Values For Atoms With Z = 1 TO Z = 120 *At. Data Nucl. Data Tables*, **1973**, *12*, 311-406
9. Kutzelnigg, W. Chemical Bonding in Higher Main Group Elements. *Angew. Chem., Int. Ed. Engl.*,**1984**, *23*, 272−295.
10. Pyykko, P., & Desclaux, J.-P. Relativity and the Periodic System of Elements. *Acc. Chem. Res. 1979, 12*, 276–281. b) Pitzer, K. S. Relativistic Effects on Chemical Properties. *Acc. Chem. Res.* **1979**, *12*, 271–276.
11. a) Pyykkö, P. Relativistic Quantum Chemistry. *Advances in quantum chemistry*,**1978** *11*, 353-409. b) Pyykko, P. Relativistic Effects in Structural Chemistry *Chem. Rev.* **1988**, *88*, 563-594. c) Biron, E.V. *Zh. Russk. Fiz. Khim. Obsch.*, **1915**, *47*, 964–988.
12. Kutzelnigg, W. Orthogonal and non-Orthogonal Hybrids *Theochem*, **1988**, *169*, 403–419.
13. Trinquier, G. Double Bonds and Bridged Structures in the Heavier Analogues of Ethylene *J. Am. Chem. Soc.* **1990**, *112*, 2130-2137.
14. Mizuhata, Y.; Sasamori, T.; Tokitoh, N. Stable heavier carbene analogues. In *Chem. Rev.* **2009**, *109*, 3479–3511
15. Jutzi, P.; Holtmann, U.; Kannee, D.; Krugerb, C.; Blom, R.; Gleiterd, R.; Hyla-Kryspind, I. Decamethylsilicocene-The First Stable Silicon(II) Compound Synthesis, Structure, and Bonding. *Chemische Berichte*. **1986**, *122*,1629–1639.
16. a) Denk, M.; Lennon, R.; Hayashi, R.; West, R.; Belyakov, A.; Verne, H. P.; Haaland, A.; Wagner, M.; Metzler, N. Synthesis and Structure of a Stable Silylene. *J. Am. Chem. Soc*.**1994**, *116*, 2691-2692. b) Haaf, M.; Schmiedl, A.; A. Schmedake, T.; R.

Powell, D.; J. Millevolte, A.; Denk, M.; West, R. Synthesis and Reactivity of a Stable Silylene *J. Am. Chem. Soc*. **1998**, *120*, 12714–12719.

17. Kira, M.; Ishida, S.; Iwamoto, T.; Kabuto, C.The First Isolable Dialkylsilylene. *J. Am. Chem. Soc*. **1998**, *121*, 9722–9723.
18. Sakamoto, K.; Tsutsui, S.; Sakurai, H.; Kira, M. Generation and Trapping of Bis(dialkylamino)silylenes: Experimental Evidence for Bridged Structure of Diaminosilylene Dimers. *Bull. Chem. Soc. of Japan*, 1997, *70*, 253–260.
19. Protchenko, A.; Hassomal Birjkumar, K.; Dange, D.; D. Schwarz, A.; Vidovic, D.; Jones, C.; Kaltsoyannis, N.; Mountford, P.; Aldridge, S. A Stable Two-Coordinate Acyclic Silylene. . *J. Am. Chem. Soc*, **2012** *134*, 6500–6503.
20. Rekken, B. D.; Brown, T. M.; Fettinger, J. C., Tuononen, H. M.; Power, P. P. Isolation of a Stable, Acyclic, Two-Coordinate Silylene. *J. Am. Chem. Soc*. 2012, *134*, 6504–6507.
21. Green, S.P.; Jones, C.; Stasch, A Stable Magnesium(I) Compounds with Mg-Mg Bonds *Science* **2007**, *318*, 1754-1757.
22. Lips, F., Fettinger, J. C.; Mansikkamäki, A. J.; Tuononen, H. M.;Power, P. P. Reversible Complexation of Ethylene by a Silylene under Ambient Conditions. *J. Am. Chem. Soc.* 2014 *136*, 634–637.
23. a) S. P. Kolesnikov, V. I. Shiryaev, and O. M. Nefedov, *Izv. Akad. Nauk SSSR, Ser. Khim.*, 1966, 584. b) S. P. Kolesnikov, B. L. Perl'mutter, and O. M. Nefedov, *Dokl. Akad. Nauk SSSR*, 1971, *196*, 594
24. a) Harris, D. H.; Lappert, M. F. Monomeric, volatile bivalent amides of group IVB elements, $M(NR^1{}_2)_2$ and $M(NR^1R^2{}_2)_2$ (M=Ge, Sn, or Pb; R^1=Me_3Si, R^2=Me_3C). *J. Chem. Soc., Chem. Comm.* **2017,** *21*, 895–896. b) Chorley, R.W.; Hitchcock, P.B.; Lappert, M.F.; Leung, W.-P.; Power, P.P.; Olmstead, M.M. Subvalent Group 14 metal

compounds. XIV. The X-ray crystal structures of two monomeric Group 14 metal bisamides, Ge[N(SiMe3)2]2 and Sn[NC(Me)$_2$(CH$_2$)$_3$CMe$_2$]$_2$ *Inorganica Chimica Acta* **1992**, *198*, 203-209

25. a) M. Veith; M. Grosser, *Z. Naturforsch., B: J. Chem. Sci.*, **1982**, ***37***, 1375 b) Steiniger, P.; Bendt, G.; Bläser, D.; Wölper, C.; Schulz, S.Germane vs. Digermane formation. *Chemical Communications*, **2014**, 50, 15461–15463.
26. Herrmann, W.A.; Denk, M.; Behm, J.; Scherer, W.; Klingan, F.-R.; Bock, H.; Solouki, B.; Wagner, M; Stable Cyclic Germanediyls ("Cyclogermylenes"): Synthesis, Structure, Metal Complexes, and Thermolyses. *Angew. Chem. Int. Ed. Engl.* **1992**, *31*, 1485-1488
27. Jutzi, P.; Becker, A.; Stammler, H. G.; Neumann, B. Synthesis and solid-state structure of (Me$_3$Si)$_3$CGeCH(SiMe$_3$)$_2$, a monomeric dialkylgermylene. *Organometallics*, **2002**, *10*, 1647–1648.
28. Kira, M.; Ishida, S.; Iwamoto, T.; Ichinohe, M.; Kabuto, C.; Ignatovich, L.; Sakurai, H. Synthesis and Structure of a Stable Cyclic Dialkylgermylene. *Chem. Lett.* **1999** *28*, 263–264.
29. Lange, L.; Meyer, B.; du Mont, W.-W. Bis(2,4,6-tri-t-butylphenyl)germylene und Bis(2,4,6-tri-t-butylphenyl)germathion: Isomerisierung durch spontane C,H-Insertion *J. Organomet. Chem.* **1987**, *329*, C17-C20.
30. Jutzi, P.; Schmidt, H.; Neumann, B.; Stammler, H.-G.Bis(2,4,6-tri-tert-butylphenyl)germylene Reinvestigated: Crystal Structure, Lewis Acid Catalyzed C−H Insertion, and Oxidation to an Unstable Germanone. *Organometallics*, **1996**, *15*, 741–746
31. Simons, R.S.; Pu, L.; Olmstead, M. M.; Power, P. P. Synthesis and Characterization of the Monomeric Diaryls M{C$_6$H$_3$-2,6-Mes$_2$}$_2$ (M = Ge, Sn, or Pb; Mes = 2,4,6-

$Me_3C_6H_2$−) and Dimeric Aryl−Metal Chlorides [M(Cl){C=H_3-2,6-Mes_2}]$_2$ (M = Ge or Sn). *Organometallics*, **1997**, *16*, 1920–1925.

32. Setaka, W.; Sakamoto, K.; Kira, M.; Power, P. P. Synthesis and Structure of Stable Tri-tert-butylgermyl-Substituted Stannylene and Germylene. *Organometallics*, **2001**, *20*, 4460–4462.
33. Kira, M.; Yauchibara, R.; Hirano, R.; Kabuto, C.; Sakurai, H. Synthesis and x-ray structure of the first dicoordinate dialkylstannylene that is monomeric in the solid state. *J. Am. Chem. Soc.* **2002**, *113*, 7785–7787.
34. Klinkhammer, W. W.; Schwarz, W. Bis(hypersily1)tin and Bis(hypersilyl)lead, Two Electron-Rich Carbene Homolog. *Angew. Chem. Int. Ed. Engl.* 1995, **34**, 1334–1336
35. Grützmacher, H.; Pritzkow, H.;Edelmann, F.T. Synthesis and structure of a monomeric diarylstannylene. *Organometallics*, **1991**, *10*, 23–25.
36. Weidenbruch, M.; Schlaefke, J.; Schäfer, A.; Peters, K.; von Schnering, H. G.; Marsmann, H. Bis(2,4,6-tri-tert-butylphenyl)stannanediyl: A Diarylstannylene without Donor Stabilization. *Angew. Chem., Int. Ed. Engl.* **1994**, *33*, 1846– 1848.
37. Brooker, S.; Karel Buijink, J.; Edelmann, F. T. Synthesis, structure, and reactivity of the first stable diaryllead(II) compound. *Organometallics*, 1991, *10*, 25–26.
38. Eaborn, C.; Ganicz, T.; Hitchcock, P. B.; David Smith, J.; Sözerli, S. E. A Novel Organolead(II) Species, the Plumbacycloalkane Derivative [$CH_2SiMe_2C(SiMe_3)_2PbC(SiMe_3)_2SiMe_2CH_2$]. *Organometallics*, **1997**, *16*, 5621–5622.
39. Kano, N.; Shibata, K.; Tokitoh, N.; Okazaki, R. Synthesis, Structure, and Reactivity of Kinetically Stabilized Divalent Organolead Compounds (Plumbylenes). *Organometallics*, **1999**, *18*, 2999–3007.
40. Power, P. P. Main-group elements as transition metals. *Nature* **2010**, *463*, 171–177

41. a) Vries, J. G. In The Handbook of Homogeneous Hydrogenation; Elsevier, C. J., Ed.; Wiley-VCH: Weinheim, Germany, 2007 b) Girgis, M.J.; Gates, B.C. Reactivities, reaction networks, and kinetics in highpressure catalytic hydroprocessing, *Ind. Eng. Chem. Res.* **1991**, *30*, 2021–2058. b) Gates, B.C.; Katzer, J.R.; Schuit, G.C.A. Chemistry of Catalytic Processes, McGraw-Hill: New York, 1979, Ch. 5 c) Topsøe, H.; Clausen, B.S.; Massoth, F.E. Hydrotreating Catalysis, Science and Technology, Springer-Verlag: Berlin, 1996.
42. a) CRC Handbook of Chemistry and Physics, 75th ed.; Lide, D. R., Ed.; CRC Press: Boca Raton, FL, 1995. b) NIST Chemistry Webbook, February 2000 release; NIST Standard Reference Data Base; National Institute of Standards and Technology: Washington, DC, 2000
43. a) Peng, Y.; Guo, J.-D.; Ellis, B. D.; Zhu, Z.; Fettinger, J. C.; Nagase, S.; Power, P. P. Reaction of Hydrogen or Ammonia with Unsaturated Germanium or Tin Molecules under Ambient Conditions: Oxidative Addition versus Arene Elimination. *J. Am. Chem. Soc.* **2009** *131*, 16272–16282. b) Spikes, G.H.; Fettinger, J.C.; Power, P.P. "Facile Activation of Dihydrogen by an Unsaturated Heavier Main Group Compound" *J. Am. Chem. Soc.* **2005**, *127*, 12232-12233.
44. Spikes, G. H.; Peng, Y.; Fettinger, J. C.; Power, P. P. Synthesis and Characterization of the Monomeric Sterically Encumbered Diaryls E{C_6H_3-2,6-(C_6H_3-2,6-iPr_2)$_2$}$_2$ (E Ge, Sn, or Pb). *Z. Anorg. Allg. Chem.*, **2006**, *632*, 1005–1010.
45. Protchenko, A. V.; Schwarz, A. D.; Blake, M. P.; Mountford, P.; Aldridge, S.; Kaltsoyannis, N.; Jones, C. A Generic One-Pot Route to Acyclic Two-Coordinate Silylenes from Silicon(IV) Precursors: Synthesis and Structural Characterization of a Silylsilylene. *Angew. Chem. Int. Ed.*, **2013** *52*, 568–571.

46. Protchenko, A. V.; Bates, J. I.; Saleh, L.M.A., Blake, M. P., Schwarz, A. D., Kolychev, E. L.;Thompson, A. L.; Jones, C.; Mountford, P.; Aldridge, S. Enabling and Probing Oxidative Addition and Reductive Elimination at a Group 14 Metal Center: Cleavage and Functionalization of E–H Bonds by a Bis(boryl)stannylene. *J. Am. Chem. Soc.* **2016** *138*, 4555–4564.

47. Wendel, D.; Porzelt, A.; Herz, F. A.D.; Sarkar, D.; Jandl, C.; Inoue, S.; Rieger, B. From Si(II) to Si(IV) and Back: Reversible Intramolecular Carbon–Carbon Bond Activation by an Acyclic Iminosilylene. *J. Am. Chem. Soc.*, **2017**, *139*, 8134–8137.

48. Reiter, D.; Holzner, R.; Porzelt, A. J.; Altmann, P.; Frisch, P.; Inoue, S. Disilene–Silylene Interconversion: A Synthetically Accessible Acyclic Bis(silyl)silylene. *J. Am. Chem. Soc*. **2019** *141*, 13536–13546.

49. Mo, Z.; Szilvµsi, I.; Zhou, Y.-P.; Yao, S.; Driess, M. Small-Molecule Activation Hot Paper An Intramolecular Silylene Borane Capable of Facile Activation of Small Molecules, Including Metal-Free Dehydrogenation of Water. *Angew. Chem., Int. Ed*. **2017** *56*, 3699–3702.

50. Turnell-Ritson, R. C.; Sapsford, J. S.; Cooper, R. T.; Lee, S. S.; Földes, T.; Hunt, P. A.; Pápai, I.; & Ashley, A. E. Base-induced reversible H_2 addition to a single Sn(ii) centre. *Chem. Sci*. **2018** *9*, 8716–8722.

51. Jana, A.; Schulzke, C.; Roesky, H. W. Oxidative Addition of Ammonia at a Silicon(II) Center and an Unprecedented Hydrogenation Reaction of Compounds with Low-Valent Group 14 Elements Using Ammonia Borane. *J. Am. Chem. Soc*. **2009** *131*, 4600–4601.

52. Jana, A.; Objartel, I.; Roesky, H. W.; Stalke, D. Cleavage of a N−H Bond of Ammonia at Room Temperature by a Germylene. *Inorganic Chemistry*, **2009** *48*, 798–800.

53. Wang, W.; Inoue, S.; Yao, S.; Driess, M. Reactivity of N-Heterocyclic Germylene Toward Ammonia and Water. *Organometallics*, **2011** *30*, 6490–6494.

54. Hadlington, T. J.; Abdalla, J. A. B.; Tirfoin, R. M.; Aldridge, S.; Jones, C. Stabilization of a two-coordinate, acyclic diaminosilylene (ADASi): completion of the series of isolable diaminotetrylenes, :E(NR_2)$_2$ (E = group 14 element) *Chem. Commun*, **2016** *52*, 1717.

55. Reiter, D.; Frisch, P.; Wendel, D.; Hörmann, F. M.; Inoue, S. Oxidation reactions of a versatile, two-coordinate,acyclic iminosiloxysilylene. *Dalton Trans*. **2020** *49*, 7060.

56. a) Sita, L. R.; Bickerstaff, R. D. "Investigation of the Factors Influencing the Structure and Stability of Stannacyclopropenes: The Synthesis and Molecular Structure of Two Derivatives" *Phosphorus, Sulfur, Silicon Relat. Elem.* **1989**, *41*, 31−36. b) Krebs, A.; Berndt, J. "Synthese zweier germirene" *Tetrahedron Lett.* **1983**, *24*, 4083−4086. c) Ishida, S.; Iwamoto, T.; Kira, M. "Addition of a stable dialkylsilylene to carbon–carbon unsaturated bonds" *Heteroat. Chem.* **2011**, *22*, 432−437.

57. a) Peng,Y. ;Ellis, B.D. Wang, X.; Fettinger, J.C.; Power, P.P. Reversible Reactions of Ethylene with Distannynes Under Ambient Conditions *Science* **2009**, *325*, 1168-1670. b) Sugahara, T.; Guo, J.-D.; Sasamori, T.; Nagase, S.; Tokitoh, N. Reversible addition of terminal Alkenes to digermynes. *Chem. Commun.* **2018,** 54**,** 519-522. c)Rodriguez, R. C.; Gau, D,; Kato, T.; Saffon-Merceron, N.; de Cozar, A.; Cossio, F.P.; Baceiredo, A. Reversible Binding of Ethylene to Silylene–Phosphine Complexes at Room Temperature *Angew. Chem. Int. Ed.* **2011**, *50*, 10414-10416.

58. a) IPCC. Climate Change 2021: The Physical Science Basis. Contribution of Working Group I to the Sixth Assessment Report of the Intergovernmental Panel on Climate

Change; Masson-Delmotte, V.; Zhai, P.; Pirani, A., Connors, S. L.; Péan, C.; Berger, S.; Caud, N.; Chen, Y.; Goldfarb, L.; Gomis, M. I.; Huang, M.; Leitzell, K.; Lonnoy, E.; Matthews, J. B. R.; Maycock, T. K.; Waterfield, T.; Yelekci, O.; Yu, R.; ¸Zhou, B.; Cambridge University Press, in press, 2021. b) Bui, M.; Adjiman, C. S.; Bardow, A.; Anthony, E. J.; Boston, A.; Brown, S.; Fennell, P. S.; Fuss, S.; Galindo, A.; Hackett, L. A.; Hallett, J. P.; Herzog, H. J.; Jackson, G.; Kemper, J.; Krevor, S.; Maitland, G. C.; Matuszewski, M.; Metcalfe, I. S.; Petit, C.; Puxty, G.; Reimer, J.; Reiner, D. M.; Rubin, E. S.; Scott, S. A.; Shah, N.; Smit, B.; Trusler, J. P. M.; Webley, P.; Wilcox, J.; Mac Dowell, N. Carbon Capture and Storage (CCS): The Way Forward. Energy Environ. Sci. 2018, 11 (5), 1062− 1176.

59. a) Hanusch, F.; Groll, S.; Inoue, S. Recent advances of group 14 dimetallenes and dimetallynes in bond activation and catalysis *Chem. Sci.*, **2021**, *12*, 2001-2015. b) Fujimori, S.; Inoue, S. Small Molecule Activation by Two-Coordinate Acyclic Silylenes *Eur. J. Inorg. Chem.* **2020**, 3131-3142. c) Chu, T.; Nikonov, G. I. Oxidative Addition and Reductive Elimination at Main-Group Element Centers *Chem. Rev.* **2018**,*118*, 3608-3680. Yao, S.; Xiong, Y.; Driess, M. Zwitterionic and Donor-Stabilized N-Heterocyclic Silylenes (NHSis) for Metal-Free Activation of Small Molecules *Organometallics* **2011**, *30*, 1748-1767.
60. Yao, S.; Xiong, Y.; Brym, M.; Driess, M. An Isolable Silanoic Ester by Oxygenation of a Stable Silylene. *J. Am. Chem. Soc.* **2007** *129*, 7268–7269.
61. Gau, D.; Rodriguez, R.; Kato, T.; Saffon-Merceron, N.; de Cózar, A.; Cossío, F. P.; Baceiredo, A.; Saffon-Merceron, N.; de Cózar, A.; Cossío, F. P. Synthesis of a Stable Disilyne Bisphosphine Adduct and Its Non-Metal-Mediated CO 2 Reduction to CO. *Angew. Chem. Int. Ed*, **2011** *50*, 1092–1096.

62. Liu, X.; Xiao, X.-Q.; Xu, Z.; Yang, X.; Li, Z.; Dong, Z.; Yan, C.; Lai, G.; Kira, M. Reactions of an Isolable Dialkylsilylene with Carbon Dioxide and Related Heterocumulenes. *Organometallics*, **2014** *33*, 5434–5439.

63. Mück, F. M.; Baus, J. A.; Nutz, M.; Burschka, C.; Poater, J.; Bickelhaupt, F. M.; Tacke, R. Reactivity of the Donor-Stabilized Silylenes [iPrNC(Ph)NiPr]$_2$Si and [iPrNC(NiPr$_2$)NiPr]$_2$Si: Activation of CO_2 and CS_2. *Chem. – Eur. J.* **2015** *21*(46), 16665–16672.

64. Stewart, C. A.; Dickie, D. A.; Tang, Y.; Kemp, R. A. Insertion reactions of CO_2, OCS, and CS_2 into the Sn-N bonds of $(Me_2N)_2Sn$: NMR and X-ray structural characterization of the products. *Inorganica Chimica Acta*, **2011** *376*, 73–79.

65. Harris, L. A. M.; Coles, M. P.; Fulton, J. R. Synthesis and reactivity of tin amide complexes. *Inorganica Chimica Acta*, 2011 *369*, 97–102.

66. Ferro, L.; B. Hitchcock, P.; P. Coles, M.; Cox, H.; Robin Fulton, J. Activation of Carbon Dioxide by Divalent Tin Alkoxides Complexes. *Inorg. Chem.* **2011** *50*, 1879–1888.

67. Protchenko, A. V.; Vasko, P.; Do, D. C. H.; Hicks, J.; Fuentes, M. Á.; Jones, C.; Aldridge, S. Reduction of Carbon Oxides by an Acyclic Silylene: Reductive Coupling of CO. *Angew. Chem. Int. Ed.* **2019** *58*, 1808–1812.

68. Protchenko, A. V.; Fuentes, M. Á.; Hicks, J.; McManus, C.; Tirfoin, R.; Aldridge, S Reactions of a diborylstannylene with CO_2 and N_2O: diboration of carbon dioxide by a main groupbis(boryl) complex. *Dalton Trans.* **2021** *50*, 9059–9067.

69. a) Wood, J. H., G. Long, and D. Morehouse (2003), World conventional oil supply expected to peak in 21st century, Offshore, 63, 90 b) Kerr, R.A. Bumpy Road Ahead for World's Oil *Science* **2005**, *310*, 1106-1108 c) Kerr, R.A. The Looming Oil Crisis

Could Arrive Uncomfortably Soon *Science* **2007**, *316*, 351. c) Kerr, R.A. Are World Oil's Prospects Not Declining All That Fast? *Science* **2012**, *337*, 633.

70. a) Levi, P.G.; Cullen, J.M. Mapping Global Flows of Chemicals: From Fossil Fuel Feedstocks to Chemical Products *Environ. Sci. Technol*. **2018**, *52*, 1725-1734. b) Chaabouni, E.; Gassara, F.; Brar, S. K. Biopolymers Synthesis and Application. In Biotransformation Waste Biomass into High Value Biochemicals; Brar, S., Dhillon, G., Soccol, C., Eds.; Springer: New York, **2014**
71. Fujimori, S.; Inoue, S. Carbon Monoxide in Main-Group Chemistry *J. Am. Chem. Soc.* 2022, 144, 5, 2034–2050.
72. Wang, X.; Zhu, Z.; Peng, Y.; Lei, H.; Fettinger, J. C.; Power, P. P. Room-Temperature Reaction of Carbon Monoxide with a Stable Diarylgermylene. *J. Am. Chem. Soc*. **2009** *131*, 6912–6913.
73. Wang, Y.; Kostenko, A.; J. Hadlington, T.; Luecke, M.-P.; Yao, S.; Driess, M. Silicon-Mediated Selective Homo- and Heterocoupling of Carbon Monoxide. *J. Am. Chem. Soc.* **2018** *141*, 626–634.
74. Xiong, Y.; Yao, S.; Szilvá, T.; Ruzicka, A.; Driess, M. Homocoupling of CO and isocyanide mediated by a C,C'-bis(silylenyl)-substituted ortho-carborane. *Chem. Comm.* **2020** *56*, 747-750.
75. Ganesamoorthy, C.; Schoening, J.; Wölper, C.; Song, L.; Schreiner, P. R.; Schulz, S. A silicon-carbonyl complex stable at room temperature. *Nature Chem.* **2020** *12*, 608–614.
76. Schoening, J.; Ganesamoorthy, C.; Wölper, C.; Solel, E.; Schreiner, P. R.; Schulz, S. Synthesis, electronic nature, and reactivity of selected silylene carbonyl complexes. *Dalton Trans.* **2022** In press. DOI:10.1039/d2dt01335e

77. Reiter, D.; Holzner, R.; Porzelt, A.; Frisch, P.; Inoue, S. Silylated silicon-carbonyl complexes as mimics of ubiquitous transition-metal carbonyls. *Nature Chem.* 2020 *12*, 1131–1135.

78. Sergeieva, T.; Mandal, D.; Andrada, D. M. Chemical Bonding in Silicon Carbonyl Complexes. *Chem.— Euro. J.* **2021** *27*, 10601–10609.

79. a) Dewar, M. J. S. "A review of π Complex Theory", *Bull. Soc. Chim. Fr.*, **1951**, *18*, C79. b) Chatt, J.; Duncanson, L.A. 586. Olefin co-ordination compounds. Part III. Infra-red spectra and structure: attempted preparation of acetylene complexes *J. Chem. Soc.***, 1953**, 2939-2947

Chapter 2

Facile C-H Bond Metathesis Mediated by a Stannylene

This work is published in the Journal of the American Chemistry Society, DOI: 10.1021/jacs.8b01878

Lai, T. Y.; Fettinger J. C.; Power, P. P. *J. Am. Chem. Soc.* **2018**, *140*, 5674-5677.

2.1 Introduction

The chemistry of the heavier group 14 element tetrylenes (:ER_2, E = Si, Ge, Sn, or Pb; R = bulky substituent) has been the subject of widespread interest[1-4] since stable examples were first discovered in the mid 1970s.[1] They are characterized by a singlet ground state in which a non-bonding electron pair occupies one of the two remaining valence orbitals; thus they can function both as an electron pair donor and acceptor. The existence of an adjacent occupied orbital, mainly s in character, and an unoccupied p-orbital allows the tetrylenes to behave as ambiphilic species which facilitates synergistic reactivity with small molecules such as hydrogen,[5-9] olefins,[10-12] carbon monoxide,[13] ammonia,[8,9,14,15], carbon dioxide[16] and related species. In contrast C-H bond activation by main group compounds under ambient, or near ambient, conditions are much less studied. Nonetheless, several reactive group 14 element species, generated either at high temperature or as intermediates are known to react with C-H bonds.[17-21] For example the highly reactive silylene $SiN(1\text{-}Ad)CH_2CH_2C(SiMe_3)_2$ (1-Ad = 1-adamantyl) has been shown to react with toluene under pressurized reflux conditions at 150° C.[21] There are few instances of direct reaction of stable main group molecules with C-H bonds at ambient conditions. The known examples usually involve reactions with relatively acidic C-H bonds in phenylacetylene,[22] pentafluorobenzene[23] or cyclopentadiene.[24,25]

For stable group 14 metal species, reactions with relatively unreactive C-H bonds are rare. The first example was reported by Banaszak Holl and coworkers,[26] where a combination of a

stannylene/germylene/silylene and an aryl halide, i.e. an :EL_2/PhX (E = Si, Ge or Sn, L = $N(SiMe_3)_2$, $CH(SiMe_3)_2$) system, homolytically abstracts the most weakly bonded hydrogen from a substrate such as an alkane, alkene, alkyne, arene, or ether. However, the reaction has to be carried out in a high dilution due to the formation of an undesired aryl halide (ArX) oxidative addition product ($L_2E(Ar)X$).

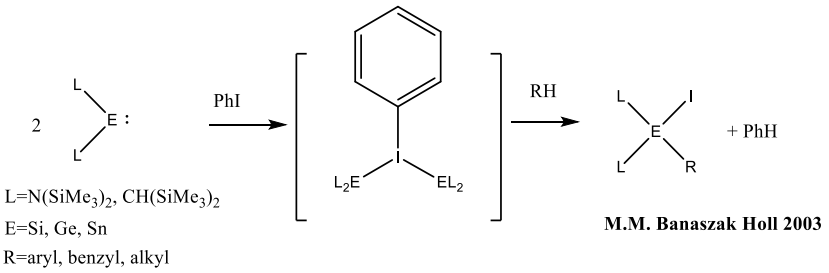

Scheme 1. C-H activation by an :EL_2/PhX complex[26f]

With use of iodobenzene, the reaction is believed to occur via the formation of an active intermediate involving two equivalents of the germylene/stannylene coordinated to one equivalent of an aryl iodide (Scheme 1). Electron transfer from the EL_2 donor to the phenyl ring initiates the breaking of the Ph-I bond and a simultaneous H radical abstraction from RH occurs at the ipso-carbon of the phenyl ring with formation of benzene while $L_2\dot{E}I$ and $R^{\bullet}$ recombine to form $L_2E(R)I$.

Despite the foregoing, the direct reaction of :EL_2 species with aliphatic hydrocarbons under ambient or near ambient conditions is unknown. In this chapter, we report the direct reaction of the diarylstannylene, :$Sn(Ar^{iPr4})_2$ (Ar^{iPr4} = C_6H_3-2,6-(C_6H_3-2,6-$^{i}Pr_2$)$_2$), with toluene, *m*-xylene or mesitylene at 80 °C. The isolated products did not result from the direct insertion of the stannylene, :$Sn(Ar^{iPr4})_2$, into a C-H bond however; instead the C-H metathesis products, the distannenes [$Ar^{iPr4}Sn(CH_2Ar)]_2$ (Aryl = C_6H_5, C_6H_4-3-Me, C_6H_3-3,5-Me_2), which dissociate into $Ar^{iPr4}Sn(CH_2Ar)$ monomers in solution, were obtained with elimination of $Ar^{iPr4}H$. (Scheme 2)

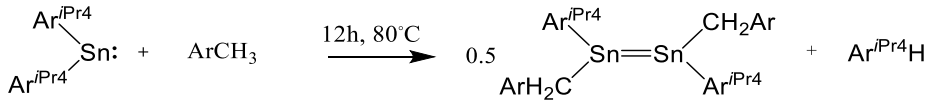

1a Ar= C_6H_5
1b Ar= C_6H_4-3-Me,
1c Ar= C_6H_3-3,5-Me_2

Scheme 2. The reaction of :$Sn(Ar^{iPr4})_2$ with arenes

2.2 Experimental Details

General Procedures. All operations were carried out under anaerobic and anhydrous conditions using modified Schlenk techniques. All solvents were dried over alumina columns, stored over an Na mirror and degassed prior to use. The ^{1}H, ^{13}C and ^{119}Sn NMR spectroscopic data were collected on a Bruker 400MHz spectrometer. ^{1}H chemical shifts are assigned by ^{13}C, ^{13}C-DEPT, ^{1}H-^{1}H COSY and ^{1}H-^{13}C HSQC NMR spectroscopic data. ^{119}Sn NMR data were referenced to $SnBu^{n}_4$ (−11.7 ppm). Infrared spectra were collected as a Nujol mull using a Bruker Tensor 27 IR spectrometer. UV−visible spectroscopy was carried out as dilute hexane solutions in 3.5 mL quartz cuvettes using an Olis 17 Modernized Cary 14 UV/vis/NIR spectrophotometer. $Sn(Ar^{iPr_4})_2$ was synthesized according to literature methods.

$[Ar^{iPr_4}Sn(CH_2C_6H_5)]_2$ (1a): A solution of $Sn(Ar^{iPr_4})_2$ (5.00 g, 5.47 mmol) in toluene (*ca.* 50 mL) was heated to 80 °C with stirring for 12 h. The solution was filtered using a filter-tipped cannula and concentrated to *ca.* 20 mL under reduced pressure. Storage of the solution at *ca.* -30°C for 12 h afforded **1a** as red crystals. Yield (2.09g, 62%) Mp: 140-145°C, ^{1}H NMR (600 MHz, C_6D_6, 298 K): δ =1.06 (d, 12H $CH(CH_3)_2$), 1.29(d, 12H $CH(CH_3)_2$) 2.12 (d, 2H, $SnCH_2Ar$), 3.23 (m, 4H, $CH(CH_3)_2$), 6-7.4(m, 14H, aromatic Hs) $^{13}C\{^{1}H\}$ NMR (126 MHz, C_6D_6, 298 K): δ = 22.65, 26.15, 30.62, 62.06, 123.65, 126.39, 126.65, 127.43, 127.68, 127.43, 127.68, 127.68, 127.92, 128.52, 128.84, 128.95, 128.95, 129.41, 146.79 $^{119}Sn\{^{1}H\}$ NMR (186.36 MHz, C_6D_6, 298 K): δ = 1660. UV-vis: λ_{max} (nm), ϵ

($M^{-1}\,cm^{-1}$) = 486nm, (2108). IR (CsI, nujol, mineral oil; selected, cm^{-1}) : 2900, 2700, 1450, 1350, 1250, 1100, 1050, 730

$[Ar^{iPr_4}Sn(CH_2C_6H_4\text{-}3\text{-}Me)]_2$ (1b): A solution of $Sn(Ar^{iPr_4})_2$ (2.00 g, 2.88mmol) in *m*-xylene (*ca.* 40 mL) was heated to 80 °C with stirring for 12 h. The solution was filtered using a filter-tipped cannula. The solvent was removed under reduced pressure and *ca.*10 mL of hexane was added. Storage of the solution at *ca.* -30°C for 12 h afforded **2a** as red crystals. Yield (0.775g, 43.32%) Mp: 155-160°C, ^1H NMR (600 MHz, C_6D_6, 298 K): δ = 1.06 (d, 12H, $CH(CH_3)_2$), 1.30 (d, 12H, $CH(CH_3)_2$), 2.07 (s, 3H, m-CH_3), 2.13 (d, 2H, $SnCH_2Ar$), 3.23 (m, 4H, $CH(CH_3)_2$), 6.2-7.4(m, 13H, aromatic Hs). $^{13}C\{^1H\}$ NMR (126 MHz, C_6D_6, 298 K): 21.25, 22.65, 26.16, 30.64, 57.64 123.64, 124.09, 127.44, 127.68, 127.92, 128.87, 129.42, 136.98, 137.79, 144.08, 146.83. $^{119}Sn\{^1H\}$ NMR (186.36 MHz, C_6D_6, 298 K): δ = 1670. UV-vis: λ_{max} (nm), ϵ ($M^{-1}\,cm^{-1}$) = 490nm, (2202). IR (CsI, nujol, mineral oil; selected, cm^{-1}) : 2900, 2700, 1450, 1350, 1250, 1100, 1050, 800, 730

$[Ar^{iPr_4}Sn(CH_2C_6H_3\text{-}3,5\text{-}Me_2)]_2$ (1c): A solution of $Sn(Ar^{iPr_4})_2$ (2.00 g, 2.88mmol) in mesitylene (*ca.* 40 mL) was heated to 80 °C with stirring for 12 h. The solution was filtered using a filter-tipped cannula and concentrated to *ca.* 10 mL under reduced pressure. The solvent was removed under reduced pressure, and 10mL of hexane was added. Storage of the solution at *ca.* -30°C afforded **3a** as red crystals. Yield (0.94g, 53.12%) Mp: 151-159 °C, ^1H NMR (600 MHz, C_6D_6, 298 K): δ = 1.06 (d, 12H, $CH(CH_3)_2$), 1.29 (d, 12H, $CH(CH_3)_2$), 2.03 (s, 6H, m-CH_3), 2.31 (d, 2H, $SnCH_2Ar$), 2.31 (m, 4H, $CH(CH_3)_2$), 6.2-7.4(m, 12H, aromatic Hs) $^{13}C\{^1H\}$ NMR (126 MHz, C_6D_6, 298 K): 21.15, 22.65, 24.09, 26.16, 30.63, 122.446, 123.56, 127.41, 127.64, 127.89, 128.87, 139.32, 140.71, 146.47, 146.62, 146.83, 147.26 $^{119}Sn\{^1H\}$ NMR (186.36 MHz, C_6D_6, 298 K): 1669 UV-vis: λ_{max} (nm), ϵ ($M^{-1}\,cm^{-1}$): 492nm, (2332). IR (CsI, nujol, mineral oil; selected, cm^{-1}) 2900, 2700, 1450, 1350, 1300, 1250, 1100 , 820, 730

2.3 Results and Discussion

The blue-purple diarylstannylene, :Sn(Ar^{iPr4})$_2$ (*ca.* 0.99 g, 1.09 mmol) was heated to *ca.* 80 °C for 12 h in either toluene, m-xylene, or mesitylene (*ca.* 40 mL) to yield red solutions. Concentration to *ca.* 10mL followed by storage at *ca.* -18 °C afforded red crystals of the distannenes **1a-c** in 43-62% yield (Scheme 2). The X-ray crystal structures of compound **1a** and **1b** are shown in Figure 1. Although the reaction of :Sn(Ar^{iPr4})$_2$ with mesitylene proceeded similarly to yield **1c**, no crystals suitable for X-ray crystallography have been isolated to date.

The crystal structures of **1a** and **1b** show that they crystallize as distannenes with pyramidalized tin coordination and a center of symmetry at the midpoint of the Sn-Sn bond. The inter-substituent angular sums at the tin atoms are $\sum_{Sn}^{o} = 330.71(3)°$**(1a)** and 338.31(2)° **(1b)** and the C-Sn-C angles are 101.55(5)° and 101.363(2)° respectively. These values are similar to those in the previously reported [Ar^{iPr4}Sn($CH_2C_6H_4$-4-Bu^t)]$_2$ ($\sum_{Sn}^{o}$ =329.574 and C-Sn-C angle, 101.47(2)°) which was synthesized by reacting one equiv Ar^{iPr4}SnCl with one equiv of $BrMgCH_2C_6H_4$-4-Bu^t.[27] The C-Sn-C bond lengths are 2.211(16) Å and 2.197(13) Å in **1a** and 2.8844(19) Å and 2.199(2) Å in **1b** and are similar to the 2.171(5)-2.184(6) Å values reported previously for [Ar^{iPr4}Sn($CH_2C_6H_4$-4-Bu^t)]$_2$. These distances are all close to the sum (2.17 Å) of the single bond radii of carbon (0.77 Å) and tin (1.40 Å).[28] The Sn1-Sn1' distances and the *trans*-bending out of the plane angles of 2.782(3) Å(**1a**), 2.787(1) Å(**1b**) and 41.2° (**1a**), 43.0° (**1b**) are near those of the earlier reported distannenes [Sn{$CH(SiMe_3)_2$}$_2$]$_2$ (2.764(2) Å and 41.6°),[29] [Ar^{iPr4}Sn(CH_2CH_3)]$_2$ (2.732(5) Å and 57.4°),[30] and [Ar^{iPr4}Sn($CH_2C_6H_4$-4-Bu^t)]$_2$ (2.7705(8) Å and 50.0°).[27]

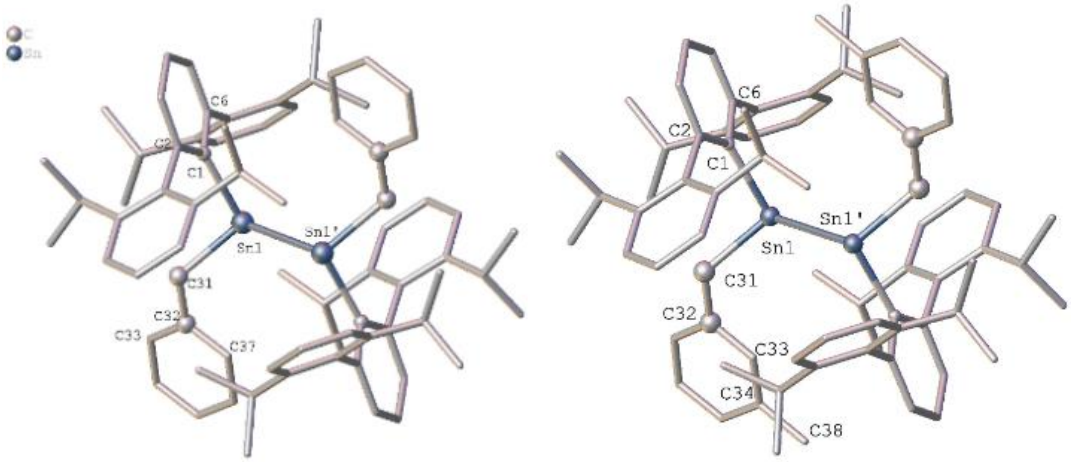

1a **1b**

Figure 1. X-ray Crystal structures of $[Ar^{iPr4}Sn(CH_2C_6H_5)]_2$ (**1a**, left) and $[Ar^{iPr4}Sn(CH_2C_6H_4\text{-}3\text{-}Me)]_2$ (**1b**, right). Hydrogen atoms and co-crystallized solvent molecules are not shown for clarity. Selected bond lengths [Å] and angles [°]: **1a**: Sn1-Sn1': 2.782(3), Sn1-C1: 2.211(16), Sn1-C31: 2.197(13), C1-Sn-C31: 101.55(5), C1-Sn1-Sn1': 116.32(2), C31-Sn1-Sn1': 112.84(6); **1b**: Sn1-Sn1': 2.750(2), Sn1-C1: 2.1844(19), Sn1-C31: 2.199(2), C1-Sn1-Sn1': 111.944(3), C31-Sn1-Sn1': 117.245(2), C1-Sn1-C31: 101.363(2).

The solution $^{119}Sn\{^1H\}$ NMR spectra of **1a-c** display a single downfield resonance at 1660 ppm (**1a**), 1671 ppm (**1b**) or 1669 ppm (**1c**). These chemical shifts fall well within the range (1200-2600 ppm) observed for two-coordinate diorganostannylenes and related species.[31] The similarly substituted distannene $Ar^{iPr4}SnCH_2C_6H_4\text{-}4\text{-}Bu^t$ was reported to have a ^{119}Sn NMR resonance further upfield at 1205.7 ppm and was initally assigned a dimeric structure in solution. However, since that publication in 2004,[27] several other related alkyl/aryl monomeric stannylenes have been characterized and their ^{119}Sn NMR chemical shifts determined.[30-32] These include $Ar^{iPr4}SnCH_2CH_2Bu^t$ and $Ar^{iPr6}SnCH_2CH_2Bu^t$ which have ^{119}Sn NMR chemical shifts of 1875 and 1832 ppm and $Ar^{iPr4}SnR$ (R = norbornyl, 1530 ppm; norbornenyl, 1709 ppm) and $Ar^{iPr4}Sn(norbornyl)SnAr^{iPr4}$ (1484 ppm). Thus, the majority of reported chemical shifts for stannylenes support monomeric structures for **1a-c** in solution.

The UV-vis spectra show one absorption at 486 nm(**1a**), 490 nm(**1b**) and 492 nm(**1c**), consistent with an n→p transition for a divalent organotin species having a monomeric sturcture in solution.[30-32] These absorption wavelengths are also consistent with those of the stannylenes mentioned above. These include $Ar^{iPr4}SnCH_2CH_2Bu^t$(486 nm),[30] $Ar^{iPr6}SnCH_2CH_2Bu^t$(484 nm), [30] and $Ar^{iPr4}SnR$ (R = norbornyl, 494 nm; norbornenyl, 502 nm)[32] and $Ar^{iPr4}Sn$(norbornyl)$SnAr^{iPr4}$ (496 nm).[32]

The reaction depicted in Scheme 2 shows direct cleavage of Sn-C and C-H bonds for which a radical mechanism is a possibility.[33] The observed ready cleavage of the Sn-C bond, apparently under steric pressure, receives support from the decomposition, under similar reaction conditions, [34,35] of the distannyne $Ar^{iPr4}SnSnAr^{iPr4}$ to form the cluster $Sn_7(Ar^{iPr4})_2$ in which five of the seven tins no longer carry an Ar^{iPr4} substituent.[34]

Attempts to trap a possible radical intermediate in the reaction sequence with organic spin-traps (TEMPO, AIBN) have so far been unsuccessful. However, EPR spectroscopy of a benzene solution of $:Sn(Ar^{iPr4})_2$ after *ca.* 1 h of photolysis or of thermolysis at 80 °C followed by flash freezing in liquid N_2 afforded the low-temperature (58.5 K) X-band spectrum shown in Figure 2. An intense signal centered at a magnetic field of 340 mT displays an average hyperfine coupling to $^{117/119}$Sn isotopes (^{119}Sn: I = 1/2, 8.59% abundance; ^{117}Sn: I = 1/2, 7.68% abundance) of 57.2 mT (1603 MHz) which suggests significant s-character[36] in the unpaired electron orbital. However, this coupling value is much lower than that typically observed in the $^{\bullet}SnR_3$ stannyl radicals which have $a(^{117}Sn)$ and $a(^{119}Sn)$ values in the range 130-340 mT.[33] In fact it is much closer to the $^{117/119}$Sn hyperfine coupling value of 59.8 mT (^{117}Sn) or 62.4 mT(^{119}Sn) observed for $^{\bullet}Sn(SiMe_3)_3$,[37] or the 32.9 mT, observed in $^{\bullet}Sn(SiMeBu^t_2)_3$, which have planar tin coordination where the unpaired electron resides in a 5p orbital.[38] Thus the EPR parameters suggests a unique one-coordinate[39] $:\dot{S}nAr^{iPr4}$ radical, generated by cleavage of one of the Sn-C bonds in $:Sn(Ar^{iPr4})_2$ in which the unpaired electron is in a valence 5p orbital.[40] This radical exhibits a rhombic g tensor with [g_1, g_2, g_3] = [2.033, 1.983, 1.947] and a g_{iso}=1.987.

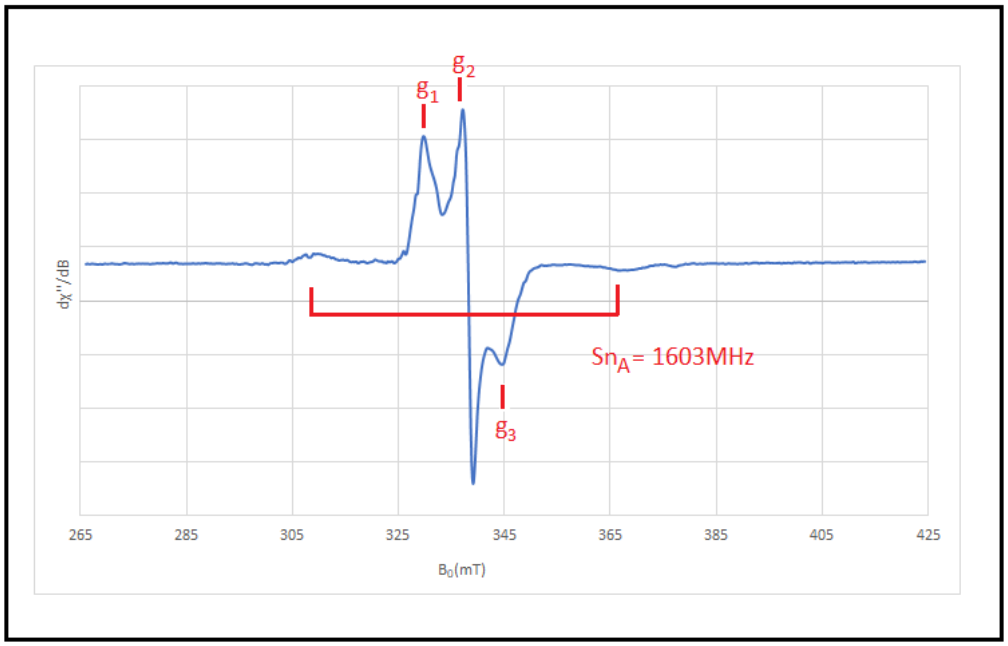

Figure 2. X-band CW EPR spectra of the radical intermediate trapped by UV photolysis of :Sn(Ar^{iPr4})$_2$ in benzene for 1 h at 58.5 K. The spectrometer settings were as follows: 0.02 mW power (no Saturation), microwave frequency, 9.38 GHz, conversion time 40.96 ms, modulation amplitude, 0.5 mT, modulation frequency, 100 kHz. The EPR parameters are as follow: g= [2.033, 1.983, 1.947] and a(^{119}Sn) =1603 MHz.

The generation of the :$\dot{\text{S}}$n(Ar^{iPr4}) radical by photolysis may be contrasted with the generation of the radical $^{\bullet}$Sn{CH(SiMe$_3$)$_2$}$_3$,[41] as well as an unidentified coproduct [Sn{CH(SiMe$_3$)}$_2$]$_n$ obtained via photolysis of the stannylene :Sn{CH(SiMe$_3$)$_2$}$_2$ (Scheme 3a). For :$\dot{\text{S}}$n(Ar^{iPr4}) however this course is likely prevented by the size of the Ar^{iPr4} substituent. Instead the proposed mechanism for the photolysis of :Sn(Ar^{iPr4})$_2$ is shown in Scheme 3b. In essence, the reaction of :Sn(Ar^{iPr4})$_2$ with toluene is initiated by thermal or photolytic cleavage of one of the Sn-C bonds to afford the radicals :$\dot{\text{S}}$n(Ar^{iPr4}) and $^{\bullet}$Ar^{iPr4}. This results in an abstraction of hydrogen from the weakest C-H bond available,[42] forming the C-H metathesis product (Scheme 3b).

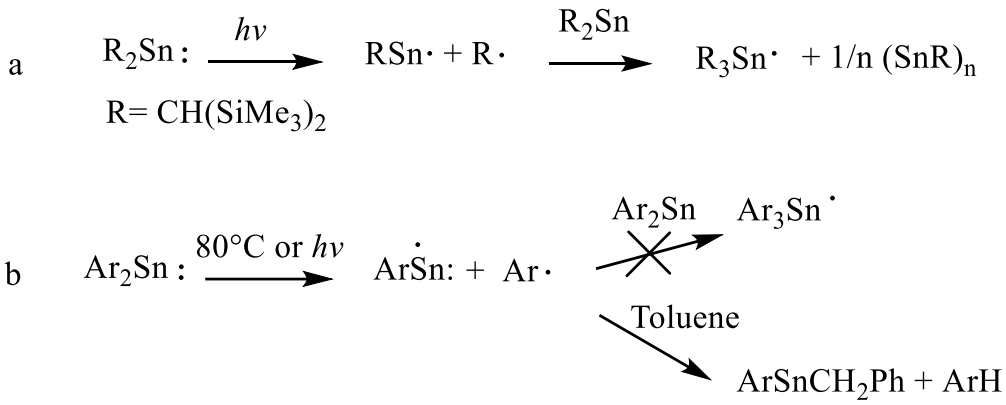

Scheme 3. Proposed Mechanism for the C-H metathesis.

2.4 Conclusions

In summary, the reaction of $:Sn(Ar^{iPr4})_2$ with toluene, xylene or mesitylene at 80 °C has afforded the distannene C-H metathesis products **1a**, **1b** or **1c** as red solids in good yields. The downfield ^{119}Sn NMR chemical shifts at 1660, 1671 and 1669 ppm and X-ray crystallography shows that the distannene products, $[Sn(CH_2Ar)Ar^{iPr4}]_2$, are dissociated to monomeric stannylenes in solution. A mechanism for the metathesis of $:Sn(Ar^{iPr4})_2$ with the arene solvents is proposed to occur via a new type of tin(I) radical intermediate which has been characterized by EPR spectroscopy. Further investigations on this new class of radicals and their reactions are underway.

2.5 References

1. Davidson, P. J.; Lappert, M. F. J. *Chem. Soc., Chem. Commun*. **1973**, 317a.
2. Mizuhata, Y.; Sasamori, T.; Tokitoh, N. *Chem. Rev.* **2009**, *109*, 3479-3511.
3. a) Ya. Lee, V.; Sekiguchi, A. *Organometallic Compounds of Low Coordinate Si, Ge, Sn, and Pb: From Phantom Species to Stable Compounds*; John Wiley & Sons: Chichester, 2010. b) Davis, A. G.; Gielen, M.; Pannell, K. H.; Tiekink, E. R. T. *Tin Chemistry-Fundamentals, Frontiers and Applications*; Wiley: United Kingdom, 2008
4. Asay, M.; Jones, C.; Driess, M. *Chem. Rev.* **2011**, *111*, 354-396

5. Inomata, K.; Watanabe, T.; Miyazaki, Y.; Tobita, H. *J. Am. Chem. Soc*. **2015**, *137*, 11935-11937.
6. Peng, Y.; Guo, J.-D.; Ellis, B. D.; Zhu, Z.; Fettinger, J. C.; Nagase, S.; Power, P. P. *J. Am. Chem. Soc.* **2009**, *131*, 16272-16282.
7. Wendel, D.; Porzelt, A.; Herz, F.A.D.; Sarkar, D.; Jandl, C.; Inoue, S.; Rieger, B. *J. Am. Chem. Soc*. **2017**, *139*, 8134-8137
8. Wang, W.; Inoue, S.; Yao, S.; Driess, M. *Organometallics* **2011**, *30*, 6490-6494.
9. Peng, Y.; Ellis, B. D.; Wang, X.; Power, P. P. *J. Am. Chem. Soc.* **2008**, *130*, 12268-12269.
10. Lips, F.; Fettinger, J. C.; Mansikkamaki, A.; Tuononen, H. M.; Power, P. P. *J. Am. Chem. Soc.* **2014**, *136*, 634-637.
11. Rodriguez, R.; Gau, D.; Kato, T.; Saffon-Merceron, N.; De Cozar, A.; Cossío, F. P.; Baceiredo, A.´ *Angew. Chem., Int. Ed.* **2011**, *50*, 10414-10416.
12. Wendel, D.; Eisenreich, W.; Jandl, C.; Pöthig, A.; Rieger, B. *Organometallics* **2016**, *35*, 1-4.
13. Wang, X.; Zhu, Z.; Peng, Y.; Lei, H.; Fettinger, J. C.; Power, P. P. *J. Am. Chem. Soc.* **2009**, 131, 6912-6913.
14. Ferro, L.; Hitchcock, P. B.; Coles, M. P.; Cox, H.; Fulton, J. R. *Inorg. Chem*. **2011**, *50*, 1879−1888
15. Jana, A.; Objartel, I.; Roesky, H. W.; Stalke, D. *Inorg. Chem*. **2009**, *48*, 798-800.
16. Jana, A.; Schulzke, C.; Roesky, H. W. *J. Am. Chem. Soc*. **2009**, *131*, 4600-4601.
17. a) Igau, A.; Grützmacher, H.; Baceiredo, A.; Bertrand, G. *J. Am. Chem. Soc***. 1988**, *110*, 6463-6466. b) Igau, A.; Baceiredo, A.; Trinquier, G.; Bertrand, G. *Angew. Chem., Int. Ed. Engl*. **1989**, *28*, 621-622.
18. Hino, S.; Olmstead, M. M.; Power, P. P. *Organometallics* **2005**, *24*, 5484-5486.
19. Huppmann, F.; Noltemeyer, M.; Meller, A. *J. Organomet. Chem,* **1994**, *1*, 217-228.
20. Waggoner, K.M; Power, P.P. *J. Am. Chem. Soc.* **1991**, *113*, 3385-3393.
21. Yao, S. L.; van Wullen, C.; Sun, X. Y.; Driess, M. Angew. Chem., Int. Ed. 2008, 47, 3250-3253.

22. Jana, A.; Samuel, P. P.; Tavcar, G.; Roesky, H. W.; Schulzke, C. *J. Am. Chem. Soc*. **2010**, *132*, 10164-10170.

23. Summerscales, O. T.; Fettinger, J. C.; Power, P. P. *J. Am. Chem. Soc*. **2011**, 133, 11960-11963.

24. Summerscales, O. T.; Caputo, C. A.; Knapp, C. E.; Fettinger, J. C.; Power, P. P. *J. Am. Chem. Soc*. **2012**, *134*, 14595-14603.

25. Kosai, T.; Ishida, S.; Iwamoto, T. *Angew. Chem., Int. Ed*. **2016**, *55*, 15554-15558.

26. a) Miller, K. A.; Bartolin, J. M.; O'Neill, R. M.; Sweeder, R. D.; Owens, T. M.; Kampf, J. W.; Banaszak Holl, M. M.; Wells, N. J. *J. Am. Chem. Soc.* **2003**, *125*, 8986-8987. b) Bartolin, J. M.; Kavara, A.; Kampf, J.; Banaszak Holl, M. M. *Organometallics* **2006**, *25*, 4738-4740. c) Kavara, A.; Cousineau, K. D.; Rohr, A. D.; Kampf, J. W.; Banaszak Holl, M. M. *Organometallics* **2008**, *27*, 1041-1043. d) Kavara, A.; Kampf, J. W.; Banaszak Holl, M. M. *Organometallics* **2008**, *27*, 2896-2897. e) Walker, R. H.; Miller, K. A.; Scott, S. L.; Cygan, Z. T.; Bartolin, J. M.; Kampf, J. W.; Banaszak Holl, M. M. *Organometallics* **2009**, *28*, 2744-2755. f) Kavara, A.; Boron III, T.T.; Ahsan, Z.S.; Banaszak Holl, M.M. *Oranometallics* **2010**, *29*, 5033-5039.

27. Stanciu, C.; Richards, A. F.; Power, P. P. *J. Am. Chem. Soc*. **2004**, *126*, 4106-4107.

28. Pyykko, P.; Atsumi, M. *Chem. - Eur. J.* **2009**, *15*, 186-197.

29. Goldberg, D. E.; Harris, D. H.; Lappert, M. F.; Thomas, K. M. *J. Chem. Soc., Chem. Commun.* **1976**, 261-262.

30. Wang, S.; McCrea-Hendrick, M. L.; Weinstein, C. M.; Caputo, C. A.; Hoppe, E.; Fettinger, J. C.; Olmstead, M. M.; Power, P. P. *J. Am. Chem. Soc*. **2017**, *139*, 6596-6604.

31. a) Wrackmeyer, B. *In Annual Reports on NMR Spectroscopy*; Academic Press: San Diego, CA, 1999; Vol. 38 b) Tokitoh, N.; Manmaru, K.; Okazaki, R. *Organometallics* **1994**, 13, 167-171 c) Weidenbruch, M.; Schlaefke, J.; Schafer, A.; Peters, K.; von Schnering, H. G.; Marsmann, H. *Angew. Chem., Int. Ed. Engl.* **1994**, *33*, 1846-1848.

32. Wang, S; McCrea-Hendrick, M. L.; Weinstein, C. M.; Caputo, C. A.; Hoppe, E.; Fettinger, J. C.; Olmstead, M. M.; Power, P. P. *J. Am. Chem. Soc*. **2017**, *139*, 6586-6595.

33. Davies, A.G. *Organotin Chemistry*; *WILEY*-VCH: Weinheim, 2004; Chapter 20

34. Rivard, E.; Steiner, J.; Fettinger, J.C.; Giuliani, J.R.; Augustine, M.P.; Power, P.P. *Chem Commun* **2007**, 4919-4921.

35. Wang, S.; Sherbow, T.J.; Berben, L.A.; Power, P.P. *J. Am. Chem. Soc.* **2018**, *140*, 590-593.

36. Morton, J.; Preston, K. *J. Magn. Reson.* **1978**, *30*, 577-582.

37. Becker, M.; Förster, C.; Franzen, C.; Hartrath, J.; Kirsten, E.; Knuth, J.; Klinkhammer, K.W.; Sharma, A.; Hinderberger, D. *Inorg. Chem.*, **2008**, *47*, 9965-9978

38. Sekiguchi, A.; Fukawa, T.; Lee, V.Y.; Nakamoto, M. *J. Am. Chem. Soc.* **2003**, *1225* 9250-9251.

39. One coordinate or quasi-one coordinate terphenyl derivatives of neighboring elements In, Pb have been described see: Haubrich S.T.; Power, P.P. *J. Am. Chem. Soc.* **1998**, *120*, 2202-2203 and Hino, S.; Brynda, M.; Philips, A.D.; Power, P.P. *Angew. Chem. Int. Ed.* **2004**, *43* 2655-2658.

40. a) Davidson, P.J.; Hudson, A.; Lappert, M.F.; Lednor, P.W.; *J. Chem. Soc., Chem. Commun.* **1973**, 829-830 b) Hudson, A.; Lappert, M.F.; Lednor, P.W.; *J. Chem. Soc., Dalton Trans.* **1976**, 2369-2375.

41. Blanksby, S.J.; Ellison G.B. *Acc. Chem. Res*. **2003**, *36*, 255-263.

Chapter 3

Reversible Sn-Sn Triple Bond Dissociation in a Distannyne: Support for Charge Shift Bonding Character

This work is published in the Journal of the American Chemistry Society, DOI: 10.1021/jacs.9b06845

Lai, T.Y.; Tao, L.; Britt, R.D.; Power, P.P. *J. Am. Chem. Soc.* **2019**, *141*, 12527-12530.

3.1 Introduction

Heavier group 14 element analogues of alkynes, the dimetallynes REER (E= Si, Ge, Sn, Pb; R= terphenyl or hindered aryl group), have attracted wide interest due to their unusual bonding and high reactivity.[1] Their X-ray crystal structures show that they have a trans-bent geometry in contrast to the familiar linear structures found for their lighter carbon homologues.[2] The trans-bent structures can be rationalized in several ways: the simplest relies on the lower hybridization tendency of the heavier main group p-block elements as a result of the increased spatial disparity of the s- and p- orbital radii with increasing atomic number.[3] Another view is that the EE triple bond consists of two weak donor- acceptor bonds and a π-bond as shown in Scheme 1(a). The trans-bending can also be viewed in terms of a second order Jahn-Teller (SOJT) interaction[4] of an empty σ* and a filled, in-plane π-orbital which have the same symmetry designation (b_u) in bent C_{2h} local symmetry Scheme 1(b). This results in an E-E bond orbital with variable bonding character affording group 14 atoms by a connected σ-, a π- and an in -plane non-bonding or 'slipped'[1d] π- molecular orbital.

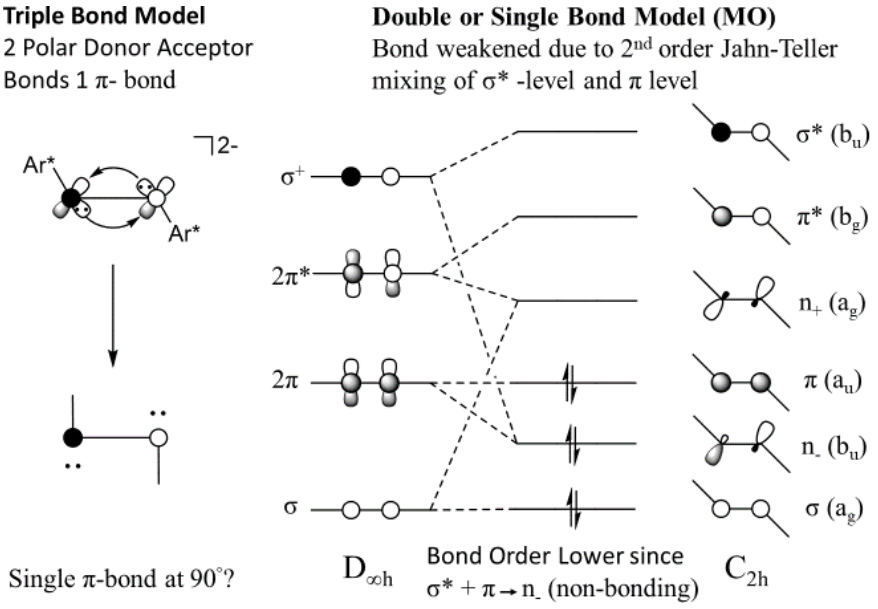

Scheme 1. Two major bonding models for distannyne.

The SOJT effect occurs in the heavier element species due to weaker bonding which affords lower energy differences and, hence a stronger interaction, between filled and empty molecular energy levels of like symmetry. This results in non-bonded electron density at the group 14 atoms which results in bending and also a change in the relative energies and symmetries of the frontier orbitals from π (HOMO) and π* (LUMO) in the linear form to a π (HOMO) and n_+ (LUMO) in the trans-bent configuration.[4] This allows matching of the symmetry of the frontier orbitals of the dimetallynes with those of several important small molecules such as H_2[5-7] and ethylene[8] and also facilitates reactions with other molecules such as cyclopentadiene[9] and metal carbonyls[10] under mild conditions to yield products in which the E-E bonds are broken. Thus, the bonding models in Scheme 1 and the observed reaction patterns suggest that the E-E triple bonds are relatively weak despite the fact that the Sn-Sn bond distance in $Ar^{iPr4}SnSnAr^{iPr4}$, 2.6675(4)Å,[2d] is shorter than the sum (2.8Å)[11] of the single-bond covalent radii of tin (*cf.* 2.780(4) Å Sn-Sn distance in single bonded $Ph_3SnSnPh_3$)[12]. The relative weakness of the E-E triple bonds has been corroborated by

calculations[13] which gave E-E triple bond strengths of 33.8, 25.9 and 17.6 kcal mol^{-1} in the terphenyl germanium, tin and lead $Ar^{iPr6}EEAr^{iPr6}$ dimetallynes.[13a] These numbers are only about 50% of the values (67.0, 61.6 and 54.6 $kcalmol^{-1}$) for 'normal' single bonds between the tetravalent elements in Me_3EEMe_3 molecules.[14]

Parallel investigations of the related sterically hindered stannylene, $:Sn(Ar^{iPr4})_2$ (which also features two-coordinate tin) showed that it unexpectedly reacted with toluene to give the benzyl derivative $Ar^{iPr4}SnCH_2Ph$ in quantitative yield with elimination of $Ar^{iPr4}H$.[15] EPR spectroscopy of the reaction solution revealed that a Sn(I) radical : $\dot{S}nAr^{iPr4}$ was formed. In addition, a trace amount of its dimer, the distannyne $Ar^{iPr4}SnSnAr^{iPr4}$,[2d] was detected by ^1H NMR spectroscopy. These results indicate that cleavage of the Sn-C bond in $:Sn(Ar^{iPr4})_2$ has readily occurred to generate a : $\dot{S}nAr^{iPr4}$ and $\dot{A}r^{iPr4}$ radical pair which then reacts with toluene solvent to afford the benzyl product. This conclusion is also supported by the facile insertion of ethylene into an Sn-C bond in $:Sn(Ar^{iPr4})_2$ or $:Sn(Ar^{iPr6})_2$ at 60°C in benzene.[16] Related two-coordinate germanium(I) radicals was also observed and trapped by Jones and Roesky.[17]

The relatively weak tin-tin bonds calculated for the terphenyl substituted distannynes[13] and the ready detection of the : $\dot{S}nAr^{iPr4}$ radical in solutions of $:Sn(Ar^{iPr4})_2$ suggested that dissociation of $Ar^{iPr4}SnSnAr^{iPr4}$ into the corresponding Sn(I) radicals in accordance with the equilibrium $Ar^{iPr4}SnSnAr^{iPr4} \rightleftharpoons 2 : \dot{S}nAr^{iPr4}$ might also be a possibility. Accordingly, we investigated the dissociation of $Ar^{iPr4}SnSnAr^{iPr4}$ in solution and now present the experimental evidence from ^1H NMR and EPR spectroscopy which demonstrates that $Ar^{iPr4}SnSnAr^{iPr4}$ dissociates reversibly to : $\dot{S}nAr^{iPr4}$ radicals in solution.

3.2 Experimental Details

General Procedures. All operations were carried out under anaerobic and anhydrous conditions using modified Schlenk techniques. All solvents were dried over alumina columns, stored over an Na mirror and degassed prior to use. Ar$^{i\text{Pr4}}$SnSnAr$^{i\text{Pr4}}$ was synthesized via reported literature. The ^{1}H NMR spectroscopic data were collected on a Bruker 500MHz spectrometer. van't Hoff analysis was calculated with reported procedure.

Variable temperature ^{1}H NMR spectroscopy and Van't Hoff analysis of Ar$^{i\text{Pr4}}$SnSnAr$^{i\text{Pr4}}$

Derivation of VT-NMR/van't Hoff Analysis:

Consider the following equilibrium in solution

$$A_2 \rightleftharpoons 2A \quad (1)$$

Where the equilibrium constant is

$$K_c(T) = \frac{[A]^2}{[A_2]} \quad (2)$$

Scaling the concentration by a total concentration resulting in

(C_0= total conc., x_1= conc. ratio of A, x_2= conc. ratio of A_2 and I= Intensity)

$$[A] = 2C_0x_1(T)\,; \qquad [A_2] = C_0x_2(T)\,; \qquad x_2(T) = \frac{I_2}{I_0}$$

Therefore,

$$\frac{K_c(T)}{4C_0} = \frac{(1-x_2)^2}{x_2} \quad (3) \qquad \frac{I_0 K_c}{4C_0} = \frac{(I_0 - I_2)^2}{I_2} \quad (4)$$

Since

$$K_c = K_0 e^{-\frac{a}{T}} \quad a = \frac{\Delta H_d^{298K}}{R} \quad K_0 = e^{\frac{\Delta S}{R}}$$

Equation (4) can be written as

$$f(T) = \ln\left[\frac{(I_0 - I_2)^2}{I_2}\right] = -\frac{\Delta H_d^{298K}}{R}\left(\frac{1}{T}\right) + \ln\left(\frac{I_0 K_0}{4C_0}\right) \quad (5)$$

By Plotting $f(T) vs. (\frac{1}{T})$ with a guessed I_0 and iteratively adjustment of I_0 to

make a best customary linear fit, would result in a slope that equals to $-\frac{\Delta H_d^{298K}}{R}$

Once, I_0 and ΔH_d^{298K} were gained, a posteriori van't Hoff analysis can be used to obtain ΔG_d^{298K}.

VT-NMR/van't Hoff Analysis

The integral for the signal atoms of the, meta-aromatic hydrogen of the central ring were used for the determination of the equilibrium constant for dissociation.

$$f(T) = \ln\left[\frac{(I_0 - I_2)^2}{I_2}\right] = -\frac{\Delta H_d^{298K}}{R}\left(\frac{1}{T}\right) + \ln\left(\frac{I_0 K_0}{4C_0}\right)$$

3.3 Result and Discussion

The work herein consists of a collaborative effect between Dr. Lizhi Tao and myself. I am responsible for the synthesis of the compounds and reaction used throughout the experiment and Dr. Lizhi Tao carried out the EPR experiments and the DFT calculations.

An examination of the ^{1}H NMR and ^{1}H-^{1}H correlation spectra of the distannyne, $Ar^{iPr4}SnSnAr^{iPr4}$ in d_8-toluene showed that the meta- and para- hydrogens of the central aryl ring C_6H_3 moiety of the terphenyl ligand Ar^{iPr4} have chemical shifts of 7.51 and 6.22 ppm respectively in C_7D_8 at 298K. Heating the solution to 367K (Figure 1) afforded relatively large changes in these chemical shifts to 8.3 and 4.55 ppm. Cooling the solution to the starting point at 298K restores the chemical shifts of the signals to their original values at 7.51 and 6.22 ppm.

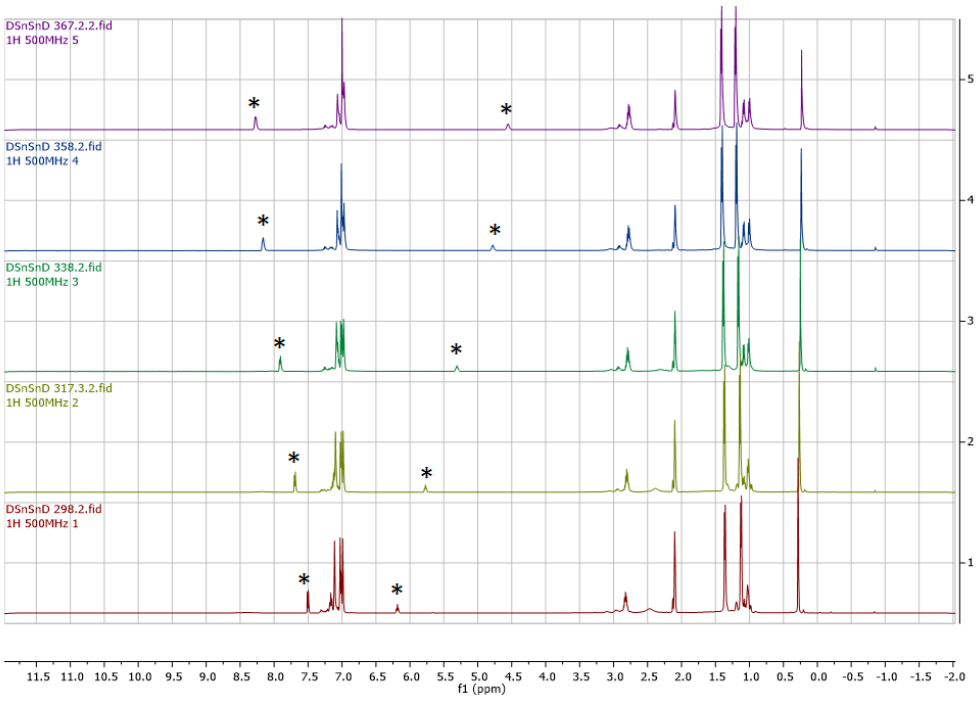

Figure 1. VT ^{1}H NMR Spectra of $Ar^{iPr4}SnSnAr^{iPr4}$ in C_7D_8.

These relatively large chemical shift movements with temperature can be rationalized by postulating the generation of paramagnetic character as a result of the incipient dissociation of the distannyne to $:\dot{S}nAr^{iPr4}$ radicals at higher temperature. The opposite temperature coefficients of the two signals are consistent with a contact shift resulting from the spin polarization through the molecular orbitals of the molecule.[18] Further analysis of the VT ^{1}H NMR data by van 't Hoff analysis (SI)[19] led to the ΔH_{diss} value of 17.2 kcal mol^{-1} for the Sn-Sn bond enthalpy. The $\Delta G_{diss}(298)$= 7.84 kcal mol^{-1} which leads to a K_{diss} value of 1.778x10^{-6}.

The experimental value 17.2±1.7 kcal mol^{-1} for the Sn-Sn bond enthalpy is somewhat lower than the calculated value[13a] and may be regarded as very low in view of the short Sn-Sn distance 2.6675(4) Å and the 51.4 kcal mol^{-1} measured for the longer (2.789(4)Å) single bond in $Ph_3SnSnPh_3$[20] and the 51.5 kcal mol^{-1} in the sterically more crowded $Mes_3SnSnMes_3$ (Mes= C_6H_2-2,4,6-Me_3).[21] Recall that Nagase, Ziegler and their coworkers have calculated[11] the triple bonds in distannynes with the aryl substituents Ar^{iPr6} and Ar^{iPr4} to be 25.9[11a] and 28.7 kcal mol^{-1},[11b] are about half the experimental values for tetra-valent tin-tin single bonds. The computational data were deemed to imply that the REER species did not dissociate to the two ER fragments in solution.[13b] However, the dissociation of the $Ar^{iPr4}SnSnAr^{iPr4}$ to two $:\dot{S}nAr^{iPr4}$ radicals is supported by EPR spectroscopy. The low-temperature (15 K) X-band (9.38 GHz) EPR spectrum of a solid-state solution sample prepared by UV photolysis or thermolysis at 80 °C of $Ar^{iPr4}SnSnAr^{iPr4}$ in toluene for ca. 30 mins displays a radical signal (burgundy trace, Figure 2A) with the *g*-values = [2.030, 1.977, 1.934]. The signal for this radical is very similar to that of the tin(I) radical $:\dot{S}nAr^{iPr4}$ obtained by dissociation of the Sn-C bond in $Sn(Ar^{iPr4})_2$[13] (green trace, Figure 2A) which is also generated by UV photolysis or thermolysis of $Sn(Ar^{iPr4})_2$ at 80 °C in benzene for ca. 30 mins. The temperature

dependence of the EPR spectrum (Figure 2B) suggests that this radical species is monomeric, as the signal intensity behaves according to the Curie law. A large hyperfine splitting of approximately 1687 MHz (61.0 mT) at a magnetic field of 339.1 mT (corresponding to *g* value 1.977) shows that it is a Sn-centered radical (^{119}Sn: I = 1/2, 8.59% abundance; ^{117}Sn: I = 1/2, 7.68% abundance), due to the strong Fermi contact and spin-dipolar interactions of electron spin with $^{117/119}$Sn nuclear spin.[22] This hyperfine coupling value falls within the range (32.9 – 342.6 mT)[23] of mononuclear Sn-centered radicals, and far exceeds the coupling (ca, 0.8 mT) in the ditin radical anion, [Ar$^{i\text{Pr4}}$SnSnAr$^{i\text{Pr4}}$]$^{\bullet-}$,[24,25] where the unpaired electron resides in an out-of-plane π-orbital delocalized over two tin atoms.

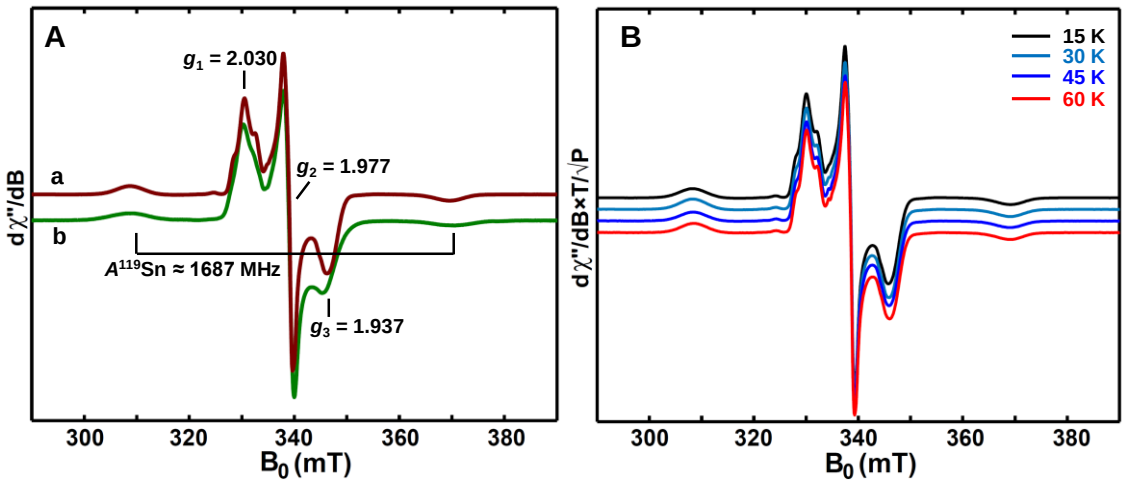

Figure 2. (**A**) The X-band (9.38 GHz) CW EPR spectrum of the radical obtained by UV photolysis/thermolysis at 80 °C of Ar$^{i\text{Pr4}}$SnSnAr$^{i\text{Pr4}}$ (burgundy trace, a) in PhMe for ca. 30 mins. The green trace (b) is the Sn(I) radical intermediate from by UV photolysis/thermolysis at 80 °C of Sn(Ar$^{i\text{Pr4}}$)$_2$ in benzene for ca. 30 mins.[10] Spectrometer settings: 15 K, 0.1 mW power (no saturation), microwave frequency, 9.38 GHz, conversion time, 40 ms, modulation amplitude, 0.8 mT, modulation frequency, 100 kHz. (**B**) Temperature dependence (15 - 60 K) of the EPR spectrum of the radical obtained by UV photolysis/thermolysis of Ar$^{i\text{Pr4}}$SnSnAr$^{i\text{Pr4}}$ at 80°C.

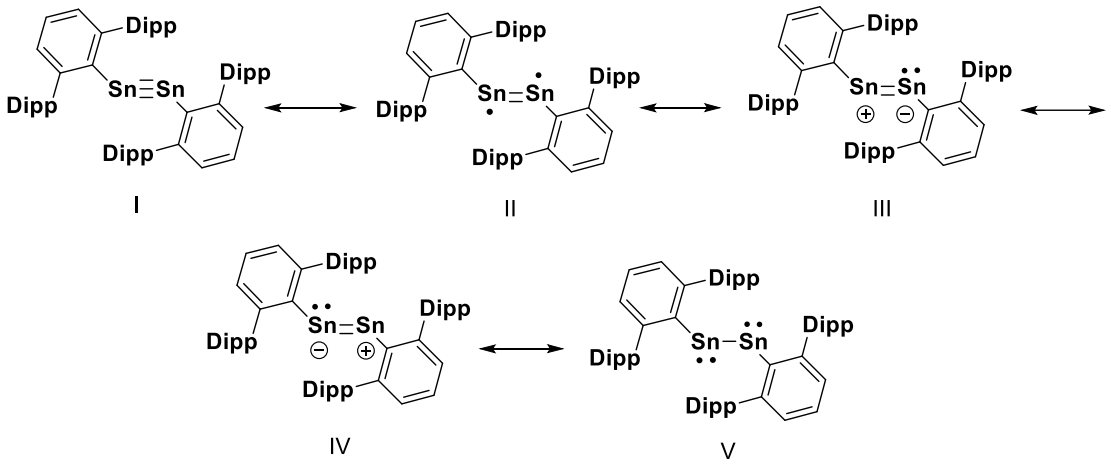

Figure 3. Some resonance structures of $Ar^{iPr4}SnSnAr^{iPr4}$

The EPR and ^1H NMR data clearly indicate that the Sn-Sn bond in $Ar^{iPr4}SnSnAr^{ipr4}$ is weak. However the weakness is not consistent with the short Sn-Sn distance or the simple bonding picture in Scheme 1 or with the resonance structures I-V drawn schematically in Figure 3 which collectively suggest a bond order greater than one (the biradical structure II was not detected by EPR spectroscopy.)

The unique character of the Sn-Sn bonds in $Ar^{iPr4}SnSnAr^{iPr4}$ is consistent charge-shift Sn-Sn bonding[26] and the AIM Calculations of Meng and coworkers which supports this view[27] for the $Ar^{iPr4}EEAr^{iPr4}$ (E=Si-Pb) series. These indicate that the electronic properties are manifested as low electron density between the E atoms, ELF basin centroids not in the region between the E atoms are split into two separate ones and Laplacians of the electron density at the center of the bond that are near zero or slightly positive. All such characteristics are consistent with EE charge shift bonding.[27,28]

3.4 Conclusions

In conclusion, $Ar^{iPr4}SnSnAr^{iPr4}$ was shown to dissociate into two corresponding Sn(I) radicals : $\dot{S}nAr^{iPr4}$ by EPR spectroscopy. The $Ar^{iPr4}SnSnAr^{iPr4} \rightleftharpoons 2 : \dot{S}nAr^{iPr4}$ equilibrium

was also quantified to be 17.2±1.7 kcal mol^{-1} via van't hoff analysis of ^{1}H VT NMR spectroscopy. The EPR and ^{1}H NMR data clearly indicate that the Sn-Sn bond in $Ar^{iPr4}SnSnAr^{ipr4}$ is weak and is consistent with the Sn-Sn bond being a charge-shift bond.

3.5 References

1. a) Rivard E. and Power, P.P. Multiple Bonding in Heavier Element Compounds Stabilized by Bulky Terphenyl Ligands *Inorg. Chem.* **2007**, *46*, 10047-10064. b) Guo, J.-D.; Sasamori, T. Activation of Small Molecules by Compounds that Contain Triple Bonds Between Heavier Group-14 Elements. *Chem. Asian. J.* **2018**, *13*, 3800-3817. c) Wang, Y.; Robinson, G.H. Unique homonuclear multiple bonding in main group compounds *Chem. Commun.,* **2009**, 5201-5213 d) Klinkhammer, K.W. How Can One Recognize a Triple Bond between Main Group Elements? *Angew. Chem. Int. Ed*., **1997**, *36*, 2320-2322. e) Landis, C.R.; Weinhold, F. Origin of Trans-Bent Geometries in Maximally Bonded Transition Metal and Main Group Molecules *J. Am. Chem. Soc*. **2006**, *128*, 7335-7345. f) Ploshnik, E.; Danovich, D.; Hiberty, P.C.; Shaik, S.; The Nature of the Idealized Triple Bonds Between Principal Elements and the σ Origins of Trans-Bent Geometries—A Valence Bond Study *J. Chem. Theory, Comput.* **2011**, *7*, 955-968.
2. a) Pu, L.; Twamley, B.; Power, P.P. Synthesis and Characterization of 2,6-$Trip_2H_3C_6PbPbC_6H_3$-2,6-$Trip_2$ (Trip = C_6H_2-2,4,6-i-Pr): A Stable Heavier Group 14 Element Analogue of an Alkyne *J. Am. Chem. Soc.,* **2000**, *122*, 3524-3525 b) A. Sekiguchi; R. Kinjo; M. Ichinohe, A Stable Compound Containing a Silicon-Silicon Triple Bond. *Science*, **2004**, *305*, 1755–1757. c) Stender, M.; Philips, A.D.; Wright, R.J.; Philip P.P. Synthesis and Characterization of a Digermanium Analogue of an Alkyne. *Angew. Chem. Int. Ed.* **2002**, *41*, 1785-1787. d) Philips, A.D.; Wright, R.J.; Olmstead,

M.M.; Power, P.P. Synthesis and Characterization of 2,6-$Dipp_2$-$H_3C_6SnSnC_6H_3$-2,6-$Dipp_2$ (Dipp = C_6H_3-2,6-*i*-Pr_2): A Tin Analogue of an Alkyne. *J. Am. Chem. Soc.* **2002**, *124*, 5930-5931. e) Sugiyama, Y.; Sasamori, T.; Hosoi, Y.; Furukawa, Y.; Takagi, N. Nagase, S.; Tokitoh, N. Synthesis and Properties of a New Kinetically Stabilized Digermyne: New Insights for a Germanium Analogue of an Alkyne. *J. Am. Chem. Soc.* **2006**, *128*, 1023-1031. f) Sasamori, T.; Hironaka, K.; Sugiyama, Y.; Takagi, N.; Nagase, S.; Hosoi, Y.; Furukawa, Y.; Tokitoh, N. Synthesis and Reactions of a Stable 1,2-Diaryl-1,2-dibromodisilene: A Precursor for Substituted Disilenes and a 1,2-Diaryldisilyne. *J. Am. Chem. Soc.* **2008**, *130*, 13856-13857. g) Hadlington, T.J.; Hermann, M.; Li, J.; Frenking, G.; Jones, C. Activation of H_2 by a Multiply Bonded Amido–Digermyne: Evidence for the Formation of a Hydrido–Germylene *Angew. Chem. Int. Ed.,* **2013**, *52*, 10199–10203.

3. Kutzelnigg, W. Chemical Bonding in the Higher Main Group Elements *Angew. Chem. Int. Ed.* **1984,** *23*, 272-295.
4. Wedler, H.B.; Wendelboe, P.; Power, P.P. Second-Order Jahn-Teller (SOJT) Structural Distortions in Multiply Bonded Higher Main Group Compounds. *Organometallics*, **2018**, *37*, 2929-2936
5. a) Peng, Y.; Brynda, M.; Ellis, B.D.; Fettinger, J.C.; Rivard, E.; Power, P.P. Addition of H_2 to distannynes under ambient conditions. *Chem. Commun.,* **2008**, 6042-6044. b) Mandal, S.K.; Roesky, H.W. Group 14 Hydrides with Low Valent Elements for Activation of Small Molecules *Acc. Chem. Res.* **2012**, *45*, 298-307
6. Hadlington, T.J.; Jones, C. A singly bonded amido-distannyne: H_2 activation and isocyanide coordination. *Chem. Commun.* **2014**, *50*, 2321-2323.
7. Wang, S.; Sherbow, T.J.; Berben, L.A.; Power, P.P. Reversible Coordination of H_2 by a Distannyne. *J. Am. Chem. Soc.*, **2018**, *140*, 590-593

8. Peng, Y.; Ellis, B.D.; Wang, X.; Fettinger, J.C.; Power, P.P. Reversible Reactions of Ethylene with Distannynes Under Ambient Conditions. *Science*, **2009**, *325*, 1668-1670.
9. a) Summerscales, O.T.; Caputo, C.A.; Knapp, C.E.; Fettinger, J.C.; Power, P.P. The Role of Group 14 Element Hydrides in the Activation of C–H Bonds in Cyclic Olefins. *J. Am. Chem. Soc.* **2012**, *134*, 14595-14603. b) Summerscles, O.T.; Fettinger, J.C.; Power, P.P. C–H Activation of Cycloalkenes by Dimetallynes (M = Ge, Sn) under Ambient Conditions. *J. Am. Chem. Soc.*, **2011**, *133*, 11960-11963.
10. McCrea-Hendrick. M.L.; Caputo, C.A.; Linnera, J.; Vasko, P.; Weinstein, C.M.; Fettinger, J.C.; Tuononen, H.M.; Power, P.P. Cleavage of Ge–Ge and Sn–Sn Triple Bonds in Heavy Group 14 Element Alkyne Analogues $(EAr^{iPr4})_2$ (E = Ge, Sn; Ar^{iPr4} = C_6H_3-2,6(C_6H_3-2,6-$iPr_2)_2$) by Reaction with Group 6 Carbonyls. *Organometallics*, **2016**, *35*, 2759-2767.
11. Pyykkö P.; Atsumi, M. Molecular single-bond covalent radii for elements 1-118. *Chem. Eur. J*, **2009**, *15*, 186-197.
12. Preut, V.H.; Haupt, J.-J., Huber, F. Die Kristall-und Molekularstruktur des Hexaphenyl-distannans. *Z. Anorg. Allg. Chem.*, **1973**, *396*, 81-89.
13. (a)Takagi, N; Nagase, S. Substituent Effects on Germanium- Germanium and Tin-Tin Triple Bonds. *Organometallics* **2001**, *20*, 5498-5500. (b) Seidu, I.; Seth, M.; Ziegler, T. Role Played by Isopropyl Substituents in Stabilizing the Putative Triple Bond in Ar'EEAr' [E = Si, Ge, Sn; Ar' = C_6H_3-2,6-(C_6H_3-2,6-$iPr_2)_2$] and Ar*PbPbAr* [Ar* = C_6H_3-2,6-(C_6H_2-2,4,6-$iPr_3)_2$]. *Inorg. Chem.*, **2013**, *52*, 8378-8388.
14. Luo, Y-R. Comprehensive Handbook of Chemical Bond Energies, CRC Press, Boca Raton, Fl, 2007.
15. Lai, T-Y.; Fettinger, J.C.; Power, P.P. Facile C–H Bond Metathesis Mediated by a Stannylene. *J. Am. Chem. Soc.* **2018**, *140*, 5674-5677.

16. Lai, T-Y.: Guo, J.D.; Fettinger, J.C.; Nagase, S.; Power, P.P Facile insertion of ethylene into a group14 element-carbon bond: effects of the HOMO-LUMO energy gap on reactivity *Chem. Commun*. **2019**, *55*, 405-407.

17. (a) Woodul, W.D.; Carter, E. Müller, R.; Richards, A.F.; Stasch, A.; Kaupp, M.; Murphy, D.M.; Driess, M.; and Jones, C. A Neutral, Monomeric Germanium(I) Radical *J. Am. Chem. Soc*. **2011**, *133*, 10074-10077. (b) Siddiqui, M.M.; Sarkar, S.K.; Sinhababu, S.; Ruth, P.N.; Herbst-Irmer, R.; Stalke, D.; Ghosh, M.; Fu, M.; Zhao, L.; Casanova, D.; Frenking, G.; Schwederski, B.; Kaim, W.; and Roesky, H.W. Isolation of Transient Acyclic Germanium(I) Radicals Stabilized by Cyclic Alkyl(amino) Carbenes *J. Am. Chem. Soc*. **2019**, *141*, 1908-1912.

18. Köhler F.H. in eMagRes, Wiley, Chichester, 2011, Paramagnetic Complexes in Solution: The NMR Approach https://doi.org/10.1002/9780470034590.emrstm1229.

19. Rösel, S.; Becker, J.; Allen, W.D.; Schreiner, P.R. Probing the Delicate Balance between Pauli Repulsion and London Dispersion with Triphenylmethyl Derivatives *J. Am. Chem. Soc*. **2018**, *140*, 14421-14432

20. Carson, A.S.; Laye, P.G.; Spencer, J.A.; Steele, W.V. The enthalpy of combustion of organo-metallic compounds measured with a vacuum-jacketed aneroid calorimeter. The enthalpy of formation of di-tin hexaphenyl and some associated bond energies. *J. Chem. Thermodynamics*, **1970**, *2*, 659-664.

21. El-Faragy, A.F.; Lehnig, M.; Neumann, W.P. Über sterisch gehinderte freie Radikale, IX. Zur Gewinnung und Struktur von Stannylradikalen $R_3Sn.$ mit raumfüllenden Gruppen. *Chem. Ber*. **1982**, *115*, 2783-2794.

22. Morton, J.; Preston, K., Atomic parameters for paramagnetic resonance data. *J. Magn. Reson.* **1978,** *30*, 577-582.

23. a) Becker, M.; Förster, C.; Franze, C.; Hartrath, J.; Kirsten, E.; Knuth, J.; Klinkhammer, K.W.; Sharma, A.; Hinderberger, D.; *Inorg. Chem.*, **2008**, *47*, 9965–9978. b) Sekiguchi, A.; Fukawa, T.; Lee, V.Y.; Nakamoto, M. Tin-Centered Radical and Cation: Stable and Free. *J. Am. Chem. Soc.*, **2003**, *125*, 9250–9251

24. Olmstead, M.M.; Simons, R.S.; Power, P.P. Synthesis and Characterization of $[Sn_2\{C_6H_3\text{-}2,6(2,4,6\text{-}iPr_3C_6H_2)_2\}_2]\text{-}\bullet$: A Singly Reduced Valence Isomer of a "Distannyne". *J. Am. Chem. Soc.*, **1997**, *119*,11705–11706.

25. Jung, Y.; Brynda, M.; Power, P.P.; Head-Gordon, M. Ab Initio Quantum Chemistry Calculations on the Electronic Structure of Heavier Alkyne Congeners: Diradical Character and Reactivity. *J. Am. Chem. Soc.* **2006**, *128*, 7185-7192.

26. a) Shaik, S.; Danovich, D.; Wu, Wei, Hiberty, P.C. Charge-shift bonding and its manifestations in chemistry. *Nature Chemistry*, **2009**, *1*, 443-449 b) Sini, G.; Maitre, P.; Hiberty, P.C.; Shaik, S.S. Covalent, ionic and resonating single bonds *J. Mol. Sruct.* **1991**, *229*, 163-169 c) Shaik, S.; Danovich, D.; Silvi, B.; Lauvergnat, D.L.; Hiberty, P.C. Charge-Shift Bonding—A Class of Electron-Pair Bonds That Emerges from Valence Bond Theory and Is Supported by the Electron Localization Function Approach. *Chem. Eur. J.* **2005**, *11*, 6358-6371.

27. Huo, S.; Li, X.; Zeng, Y.; Sun, Z.; Zheng, S.; Meng, L. Nature of E–E bonds in heavier ditetrel alkyne analogues ArEEAr (Ar = $C_6H_3\text{-}2,6(C_6H_3\text{-}2,6\text{-}iPr_2)_2$; E = Si, Ge, Sn, and Pb) *New J. Chem.* **2013**, *37*, 3145-3151.

28. Charge-Shift bonding represents a fourth type of element-element bonding in addition to covalent, ionic, and metallic bonds.

29. A higher energy (37.3 kcal mol^{-1}) was calculated for the distannyne TbtSnSnTbt[13] (Tbt= $C_6H_2\text{-}2,4\text{-}6\text{-}\{CH(SiMe_3)_2\}_3$). The difference corresponds to the shorter distance (2.659Å) calculated for TbtSnSnTbt vs the 2.900 Å calculated for $Ar^{iPr6}SnSnAr^{iPr6}$.[13a] The

difference in values was attributed to the higher degree of twisting calculated for the core array C(ipso)Sn-SnC(ipso) in $Ar^{iPr6}SnSnAr^{iPr4}$

Chapter 4

EPR Spectroscopic Identification of Sn(I) and Ge(III)-hydride Radicals: a Related Radical Mechanism in Heavier Group 14 Element Tetrylene Chemistry

This work is published in Inorganic Chemistry, DOI: 10.1021/acs.inorgchem.9b02504

Tao, L.; **Lai, T.Y.**; Britt, R.D.; Power, P.P. *Inorg. Chem.* **2019**, *58*, 15034-15038.

4.1 Introduction

The heavier group 14 element tetrylenes (:ER_2, E = Si, Ge, Sn, or Pb; R = bulky organic group), as carbene analogues, have garnered much interest given their extensive chemistry and reactivity towards small molecules, such as H_2, CO, NH_3, CO_2, C_2H_4 etc. However, mechanistic understanding the chemistry of these tetrylenes is still limited, although a radical mechanism was first proposed by Lappert and coworkers back to early 1970s.[1] As shown in Scheme 1, during the photolysis of :$Sn^{II}R_2$ (R = $CH(SiMe_3)_2$) that has a singlet (S = 0) configuration with a nonbonding electron pair occupying one of the two valence orbitals, an S = 1/2 paramagnetic species of $\cdot Sn^{III}R_3$ was generated and identified by using electron paramagnetic resonance (EPR) spectroscopy.[1] This $\cdot Sn^{III}R_3$ is the first reported persistent radical of heavier group 14 element.[1] The overall reaction can be viewed as a photochemical disproportionation, and a Sn(I) radical intermediate : $\dot{S}nR$ was hypothesized to be generated via Sn−C bond cleavage during the photolysis reaction.

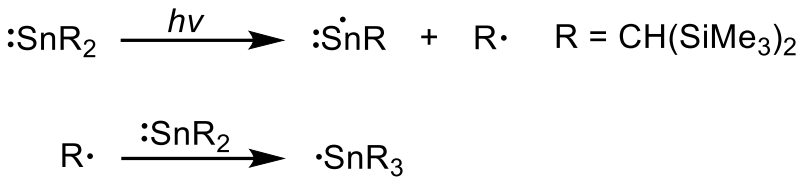

Scheme 1. Photochemical disproportionation of :SnR_2 (R = $CH(SiMe_3)_2$).

However, this one-coordinated radical intermediate, i.e. a tetrelyne : ĖR, has never been isolated. The most probable reason is that such species dimerize rapidly to form a range of heavier alkyne analogues ditetrelynes REER (R = bulky substituent) or higher oligomer $(ER)_n$ (n = 4, 6, 8 etc). Besides Lappert and coworkers' early work (*vide supra*),[1] an : ĖR radical intermediate was later suggested by a number of reports[2] where a tetrylene (:ER_2) is heated, or during the reaction of Si_2Cl_6 or GeI_2 with an organolithium reagent[3], or during the reduction of an aryl tetrel halide with KC_8 to afford ditetrylynes (Scheme 2),[3,4] which describe instances of reactions in which radicals were proposed as intermediates.

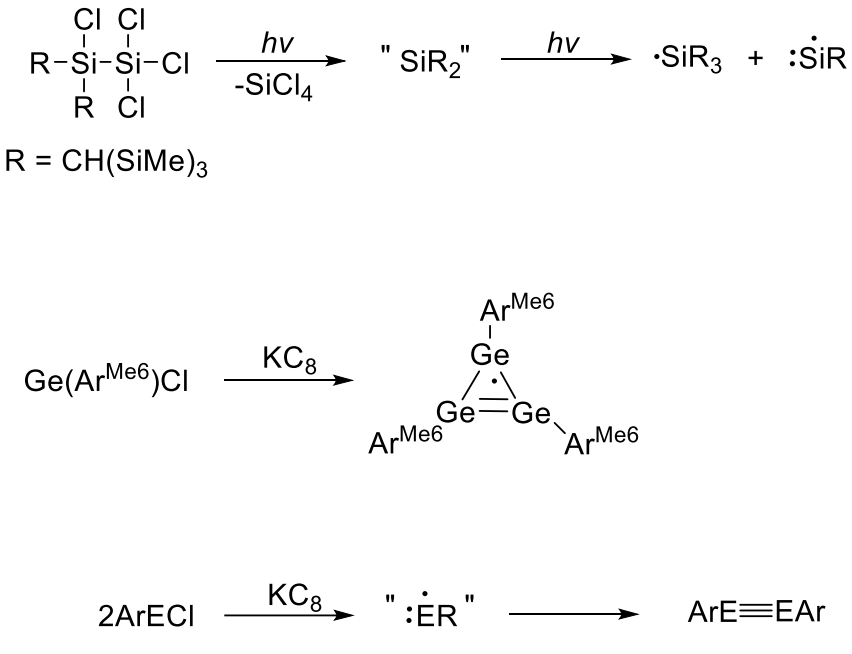

Scheme 2. Reactions in which tertelyne molecules (: ĖR radical, E = Ge, Sn, Pb) have been proposed as intermediates.

On the other hand, several groups have used the extremely bulky ligand R which can both chelate and provide considerable steric shielding to the E center to isolate an electronically and kinetically stabilized mononuclear two-coordinated radicals. In 2011, Jones and coworkers reported the first monomeric Ge(I) radical that is stabilized by nitrogen coordination from the bidentate β-diketiminato ligand, as illustrated in Scheme 3.[6] This radical was synthesized by the reduction of a β-diketiminato Ge(II) chloride with sodium napthalenide or with a magnesium(I) dimer LMgMgL (L= $[(MesNCMe)_2CH]^-$; Mes= mesityl), thus, affording crystals of the neutral Ge(I) compound, as shown in Scheme 3. This Ge(I) species was characterized by using X-ray crystallography, EPR spectroscopy as well as theoretical calculations, which supported a neutral, monomeric Ge(I) π radical.[7-9]

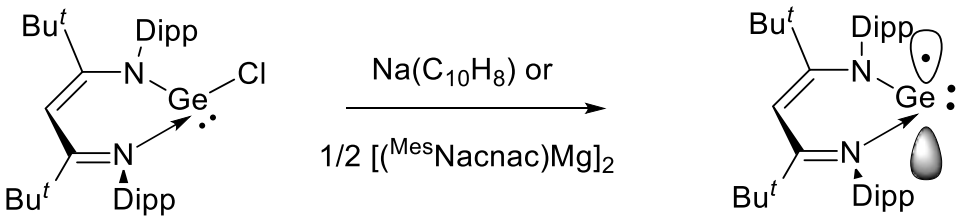

Scheme 3. Synthesis of a mononuclear Ge(I) germyne radical.

Recently, we reported the detection of a one-coordinated Sn(I) radical (:$\dot{S}$nR) during the photolysis or thermolysis at 80 °C of the stannylene $Sn(Ar^{iPr4})_2$, Ar^{iPr4} = C_6H_3-2,6-(C_6H_3-2,6-$^i Pr_2$)$_2$ by using EPR spectroscopy.[10] This Sn(I) radical is an intermediate in facile C-H bond metathesis that involves the stannylene $Sn(Ar^{iPr4})_2$ and alkyl arenes.[10] Herein we extend the study and report a series of germanium and tin radicals that are generated during the photolysis/thermolysis of the tetrylenes, including $Sn(Ar^{iPr4})_2$, $Sn(Ar^{iPr6})_2$, $Ge(Ar^{iPr4})_2$, and $Ge(Ar^{iPr6})_2$. Both tin and germanium radical species were trapped and identified by using EPR spectroscopy complemented with theoretical calculations. The tin radical intermediate we trapped during the photolysis/thermolysis of diarylstannylene of $Sn(Ar^{iPr4})_2$ or $Sn(Ar^{iPr6})_2$ is a

one-coordinated S = 1/2 Sn(I) radical, i.e., $:\dot{S}nR$ (R = Ar^{iPr4} or Ar^{iPr6}). In contrast, the germanium radical that we trapped during the photolysis/thermolysis of diarylgermylene of $Ge(Ar^{iPr4})_2$ or $Ge(Ar^{iPr6})_2$ is an S = 1/2 Ge(III)-hydride species, i.e., ·GeHRR' (R = Ar^{iPr4} or Ar^{iPr6}, R' is a quaternary carbon). This could be due to the greater reactivity Ge(I) radical intermediate $(:\dot{G}eR)$id and the greater strength of a Ge-H bond. The Ge(III)-hydride species we trapped arises from the insertion of the active Ge(I) radical intermediate in a C-H bond. This work provides insights into the radical mechanistic understanding of the heavier group 14 element tetrylenes chemistry.

4.2 Experimental Details

Sample preparations. All operations were carried out under anaerobic and anhydrous conditions using modified Schlenk techniques. All solvents were dried over alumina columns, stored over an Na mirror and degassed prior to use. Synthesis of $Ge(Ar^{iPr4})_2$ and $Ge(Ar^{iPr6})_2$ followed the procedures that have been described in the literature. A Rayonet-200 photochemical reactor with a wavelength range of 253–570 nm at approximately 35 W was used for photolysis reaction. The EPR samples were prepared by UV light exposure at room temperature for ~30 min in benzene before being flash frozen in liquid nitrogen. The thermolysis treated samples are prepared by heating at 80 °C for ~30 min in benzene before being flash frozen in liquid nitrogen.

X-band CW EPR spectroscopy. The X-band (9.38 GHz) continuous-wave (CW) EPR spectra were recorded on a Bruker (Billerica, MA) EleXsys E500 spectrometer which is equipped with a super-high Q resonator (ER4122SHQE). Cryogenic temperatures were achieved and controlled using an ESR900 liquid helium cryostat in conjunction with a temperature controller (Oxford Instruments ITC503) and gas flow controller. CW EPR data were collected under

slow-passage, non-saturating conditions at 15 K. The spectrometer settings were as follows: conversion time = 40ms, modulation amplitude = 0.3mT, and modulation frequency = 100 kHz; other settings are given in corresponding figure captions. Spectral simulations were performed using the Easyspin 5.1.10 toolbox within the MatLab software suite (The Mathworks Inc., Natick, MA).

Q-band EPR spectroscopy. Q-band two pulse electron spin-echo (ESE)-detected field swept EPR spectrum ($\pi/2$-τ-π-τ-echo) was collected at 34.220 GHz using a Bruker (Billerica, MA) EleXsys E580 spectrometer equipped with a 10 W amplifier and a R.A. Isaacson cylindrical TE011 resonator in an Oxford CF935 cryostat. Pulse sequences were programmed with the PulseSPEL programmer via the XEPR interface. Experiment parameters: 10 K, microwave frequency = 34.220 GHz, $\pi/2$ = 12ns and τ = 300 ns.

Q-band pulse ENDOR spectroscopy. Q-band (~34.0 GHz) pulse Davies-ENDOR experiments were performed on a Bruker Biospin EleXsys 580 spectrometer equipped with a 10 W amplifier and a R.A. Isaacson cylindrical TE_{011} resonator in an Oxford CF935 cryostat. ENDOR measurements were performed at 10 K by employing the Davies pulse sequence (π-RF-$\pi/2$-τ-π-τ-echo) for larger hyperfine couplings. ENDOR spectra were collected stochastically by randomly 4 hopping the RF excitation frequency. Pulse sequences were programmed with the PulseSPEL programmer via the XEPR interface.

For a single molecular orientation with respect to the applied magnetic field, a nucleus (N) with nuclear spin of I = 1/2 (e.g., ^{1}H) that is hyperfine coupled to an S = 1/2 electron spin will give rise to two ENDOR transitions appearing at positions that are a function of ν_N, the

nuclear Larmor frequency, and *A*, the orientation-dependent hyperfine coupling value. If $\nu_N > A/2$, the observed ENDOR transitions are centered at the νN of the nucleus and split by the hyperfine coupling *A*.

A variable mixing-time (VMT) ENDOR experiment was conducted to determine the absolute sign of the hyperfine coupling A at a given field position. As shown in Figure S2 in the Appendix III, the pulse sequence of VMT Davies-ENDOR is π-RF-t_{mix}-$\pi/2$-τ-π-τ-echo. Various mixing-times t_{mix} ranging from 1 μs to 200 μs were used and the default delay time for the microwave pulse after RF was 1 μs for the regular ENDOR experiment. For an S = 1/2, I = 1/2 spin system, as the mixing time t_{mix} is increased to a length on the order of the electron-spin relaxation time, the ENDOR response corresponding to $M_s = +1/2$ (α) electron spin manifold decreases more rapidly than the response corresponding to $M_s = -1/2$ (β) manifold. By comparing the relative intensity of the ν_+ (the high RF frequency peak) and ν_- (the low RF frequency peak) ENDOR transitions for the ENDOR spectra acquired at different t_{mix}, we can match each transition to their corresponding electron spin manifold and determine the sign of *A*.

Density functional theory (DFT) computations. All calculations were carried out using the ORCA 4.0.1 quantum chemistry program. Unrestricted Kohn-Sham geometry optimizations were carried out using BP86 density functional along with the zero-order regular approximation (ZORA) to include the scalar relativistic effects. The ZORA-def2-TZVP basis sets were used for the heavier atom, Ge, while the basis set of SVP was used for light atoms (hydrogen and carbon). The calculations were sped up by employing the resolution of identity (RI) approximation along with the segmented all-electron relativistically contracted (SARC/J) coulomb-fitting auxiliary basis set which is implemented in ORCA 4.0.1. Increased integration

grids (Grid5) and tight SCF convergence were used throughout the calculations. Solvent effects have been considered with conductor-like screening model (COSMO) with a dielectric constant ε of 2.3 for benzene.

EPR parameters for Ge^{III} -hydride model was calculated by using Unrestricted Kohn-Sham (UKS) formalism and employing the hybrid meta-GGA TPSSh wave functional. The ZORAdef2-TZVP basis set was used for Ge, while the basis set of EPR-II was used for C and H. The calculations were sped up by employing the resolution of identity (RI) approximation along with the segmented all-electron relativistically contracted (SARC/J) coulomb-fitting auxiliary basis set. Increased integration grids (Grid5) and tight SCF convergence were used throughout the calculations.

4.3 Results and Discussion

The work herein consists of a collaborative effort between Dr. Lizhi Tao and myself. I am responsible for the synthesis of the compounds and reaction used throughout the experiment and Dr. Lizhi Tao did the EPR experiments and the DFT calculations.

Sn(I) radical intermediate. Previously we reported the EPR spectrum of a Sn(I) radical : $\dot{S}nR$ that is generated by UV photolysis of $Sn(Ar^{iPr4})_2$ or thermolysis at 80 °C in benzene for ca. 30 mins. Herein, photolysis or thermolysis of $Sn(Ar^{iPr6})_2$ in benzene resulted in a similar radical intermediate, with the corresponding low-temperature (15 K) X-band (9.40 GHz) and Q-band (34.34 GHz) EPR spectra given in Figure 1. One paramagnetic species is evident in the spectra and is well simulated by using a rhombic **g** tensor of $[g_1, g_2, g_3] = [2.031, 1.980, 1.940]$ with $g_{iso} = 1.984$ ($g_{iso}^2 = (g_1^2 + g_2^2 + g_3^2)/3$), which is slightly below the usual range ($g_{iso} = 1.988 \sim 2.027$) of typical Sn^{III}-centered radicals (*see* Table 1). Especially, a significant large hyperfine splitting of approximate 1680 MHz (corresponding to 60.6 mT) centered at the magnetic field

of 339.1 mT (corresponding to g_2 value 1.980) is observed in the X-band spectrum. This large hyperfine splitting is characteristic of a heavier element Sn-centered radical due to the strong Fermi-contact (FC) and spin-dipolar interactions of electron spin with $^{117/119}$Sn nuclear spin (^{119}Sn: I = 1/2, 8.59% abundant; ^{117}Sn: I = 1/2, 7.68% abundant). The Fermi-contact and spin-dipolar interactions of electron spin with ^{119}Sn nuclear spin that refer to the isotropic hyperfine interaction of unit spin in 5s orbital and the anisotropic hyperfine interaction of unit spin in 5p orbital are as strong as $a^{FC}(^{119}Sn)$ = -43920 MHz and $P(^{119}Sn)$ = -1831 MHz, respectively.

By spectral simulations of both X-band and Q-band EPR spectra (*see* Figures 1 and S1), the hyperfine tensor **A** of ^{119}Sn in this radical intermediate is determined as $[A_1, A_2, A_3]$ = [±400, ±1680, ±300] MHz. This total ^{119}Sn hyperfine tensor includes three contributions: (i) the isotropic Fermi-contact term a_{iso}; (ii) the anisotropic electron-nuclear spin dipolar term **T**; (iii) the anisotropic orbital term which describes the electron orbital angular momentum dipolar coupling with the nuclear spin and is proportional to the *g*-value deviations from *g*-free electron (g_e = 2.0023). The third-term contribution can be computed by using the $P(^{119}Sn)[\Delta g_1, \Delta g_2, \Delta g_3]$, i.e., [52, 41, 114] MHz, which is relative small. If we solely consider the first and the second term, the hyperfine tensor can be decomposed as $\mathbf{A} = a_{iso} + \mathbf{T}$, where $\mathbf{T} = \rho_{5p}P(^{119}Sn)$ [-2/5, +4/5, -2/5] and $a_{iso} = \rho_{5s}a^{FC}(^{119}Sn)$ with ρ_{5s} and ρ_{5p} describing the corresponding spin density residing in 5s and 5p orbital, respectively. Although we do not know the signs of the principle *A*-values, we noted that the maximum principle *T*-value T_{max} ($\mathbf{T} = [T_1, T_2, T_3]$, $2T \equiv T_{max} = -T_1 - T_3 = +4/5\rho_{5p}P(^{119}Sn)$ with the slight rhombicity of the tensor neglected) has to be negative, due to g_n ^{119}Sn < 0 and the corresponding $P(^{119}Sn)$ < 0 (*vide supra*). Based on the negative T_{max}, the sign of the principle *A*-value is reasonable as [±400, -1680, ±300] MHz (four possibilities, *see* SI for details), resulting in a_{iso} and *T in the range of -316 ~ -793 MHz and -443 ~ -677 MHz, respectively. Now* the spin density on ^{119}Sn can be calculated to be ρ_{5s} = 1.2 ~ 1.8% and ρ_{5p} = 60.4 ~ 92.4%, respectively. The spin-density analysis revealing most of

the electron spin residing in Sn 5p orbital suggests that this tin radical is a π-type radical.

Although tin has two magnetic isotopes, i.e., ^{119}Sn and ^{117}Sn both with nuclear spin I = 1/2, we did not observe two distinct sets of hyperfine splitting which are expected from the couplings of one unpaired electron with these two isotopes. The reason could be a result of their close gyromagnetic ratios (γ) of these two isotopes, with $\gamma(^{119}\text{Sn})/\gamma(^{117}\text{Sn})$ ~1.046, which affords a small difference between $A(^{119}\text{Sn})$ and $A(^{117}\text{Sn})$. Therefore, the hyperfine peaks are broad, as shown in Figure 1, which have the overlap of hyperfine features from two different isotope nuclei.

The ^{119}Sn a_{iso} (*-316* ~ -793 MHz) of this trapped radical intermediate is much smaller than that of those typical $\cdot Sn^{III}R_3$ radicals (*see* Table 1), with the a_{iso} in the range of 926 MHz to 9547 MHz (corresponding to 32.9 mT to 342.6 mT). We rule out the possibility that this trapped tin radical intermediate is a Sn(III) radical, i.e., $\cdot Sn^{III}R_3$, based on the following considerations. First, due to the steric pressure, it is impossible to form a $\cdot SnR_3$ species where R = Ar^{iPr4} or Ar^{iPr6}. Second, we obtained a same EPR spectrum by employing either benzene or ether as the solvent, suggesting that the solvent does not affect the radical species. Therefore, the tin radical should not be $\cdot SnAr^{iPr4}R_2$ or $\cdot SnAr^{iPr6}R_2$, where R = solvent-based ligand. Because if this were the case, the **g** tensor and Sn-hyperfine tensor would be altered, resulting in a different EPR spectrum. In addition, we did not detect other magnetic nuclei (e.g., ^{1}H with I = 1/2) that are superhyperfine strongly-coupled to the tin radical (i.e, as ligands to the tin-center) either from CW EPR or pulse Electron Nuclear Double Resonance (ENDOR) spectra. This is in contrast to the Ge(III)-hydride radical species we will describe in next section.

Taken together, we conclude that a π-type Sn(I) radical intermediate is generated by UV photolysis or thermolysis at 80 °C of $Sn(Ar^{iPr4})_2$ or $Sn(Ar^{iPr6})_2$ in benzene or ether for ca.

30 min. The corresponding EPR analysis supports that it is a Sn(I) radical, formed via Sn−C bond cleavage during the UV photolysis/thermolysis reaction.

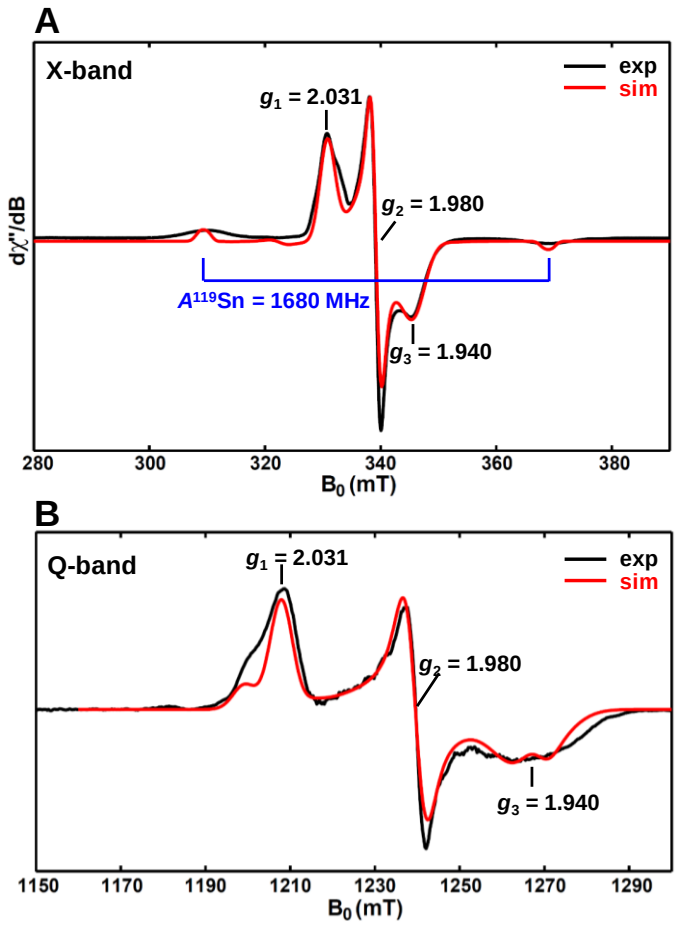

Figure 1. X-band CW EPR spectrum (A) and Q-band (34.0 GHz) pseudo-modulated electron spin-echo detected field-swept EPR spectra (B) of the radical intermediate trapped by UV photolysis of $Sn(Ar^{iPr6})_2$ in benzene for ~30 min. The spectrometer settings are as follows: 15 K, 0.1 mW power (no saturation), microwave frequency, 9.38 GHz, conversion time, 40 ms, modulation amplitude, 0.8 mT, modulation frequency, 100 kHz. The Q-band EPR spectra were recorded at 10 K by using a two-pulse sequence of π/2-τ-π-τ-echo, with π/2 = 12 ns and τ = 300 ns. The modulation amplitude of 3.0 mT was used to convert the absorption spectra to the pseudo-modulated spectra in (B).

The simulation (red trace) parameters are as follows: g = [2.031, 1.980, 1.940], $A^{119}{}_{Sn}$ = [-400, -1680, -300] MHz.

Ge(III)-hydride radical species. Solutions of the compound $Ge(Ar^{iPr4})_2$ or $Ge(Ar^{iPr6})_2$ were subjected to ca. 30 mins of UV photolysis or thermolysis at 80 °C in benzene, and then frozen in order to trap any potential radical intermediates. Analysis by using EPR spectroscopy revealed that photolysis/thermolysis of these two Ge-compounds resulted in the formation of a similar Ge radical, with the low-temperature (15 K) X-band as well as Q-band EPR spectra shown in Figure 2. One paramagnetic component is observed and is well-simulated by using a slightly rhombic **g** tensor of $[g_1, g_2, g_3] = [2.029, 2.003, 1.989]$ with $g_{iso} = 2.007$, which falls in the range ($g_{iso} = 1.999 \sim 2.010$) of typical Ge^{III}-centered radicals (*see* Table 2) but is larger than the $g_{iso} = 1.988$ of the reported neutral Ge(I) radical with a **g** tensor of $[g_1, g_2, g_3] = [2.001, 1.997, 1.968]$.

In addition to the central signal at g ~ 2.0 region, satellite signals split by 90 MHz (corresponding to 3.2 mT) are observed, which is a very characteristic feature arising from the hyperfine coupling interaction with ^{73}Ge nuclear spin ($I = 9/2$, 7.8% abundance). As shown in the zoom-in insets of Figure 2A, the observable six hyperfine peaks are part of the ^{73}Ge-hyperfine pattern displaying total $2I + 1 = 10$ hyperfine splittings, with the remaining four hyperfine peaks buried in the central signal. By spectral simulations of both X-band and Q-band EPR spectra, the ^{73}Ge hyperfine tensor **A** of this radical is determined as an axial tensor $[A_1, A_2, A_3] = [-10, -90, -10]$ MHz, with the signs of the principle *A*-values adopted from DFT predictions described below. As the anisotropic orbital term $P(^{73}Ge)[\Delta g_1, \Delta g_2, \Delta g_3]$ (here, $P(^{73}Ge) = -120$ MHz) is computed to be very small as [3.2, 0.1, 1.6] MHz, its contribution to the hyperfine tensor **A** can be neglected. Then the hyperfine tensor can be decomposed as $\mathbf{A} = a_{iso} + \mathbf{T}$, where $\mathbf{T} = [-T, 2T, -T]$, giving $a_{iso} = -36$ MHz and $T = -26$ MHz. The negative signs are reasonable as $g_n\,^{73}Ge < 0$ (also see above ^{119}Sn hyperfine analysis). Now the spin density on ^{73}Ge can be determined by using $a_{iso} = \rho_{4s} a^{FC}(^{73}Ge)$ and $T = 2/5\rho_{4p} P(^{73}Ge)$, where the $a^{FC}(^{73}Ge)$ and $P(^{73}Ge)$ referring to the Fermi-contact and spin-dipolar interactions of electron

spin with ^{73}Ge nuclear spin are -2363 MHz and -120 MHz, respectively. The spin density localized in 4s orbital (ρ_{4s}) and 4p orbital (ρ_{4p}) are computed as ca. 1.5% and 55%, respectively, with most of the spin density residing in Ge 4p orbital. This suggests that the trapped Ge radical is a π-type radical, similar as the tin π radical we described above.

Of considerable interest, in the X-band EPR spectrum (Figure 2A) we observed significant doublet with a superhyperfine splitting ca. 1.0 mT (corresponding to ~28 MHz) superimposed in the Ge-EPR signal. The splitting is too small to be resolved at higher microwave frequency Q-band EPR spectrum, as seen in Figure 2B. This significant doublet splitting indicates that there is one $I = 1/2$ nuclear spin coupled to the Ge-centered electron spin, with the hyperfine interaction strong enough to be resolved by X-band CW EPR spectrum.

To identify the type of this $I = 1/2$ nuclei spin, we pursued pulse EPR studies ENDOR for this trapped Ge radical. Figure 3 presents the orientation-selected ^{1}H ($I = 1/2$) Davies-ENDOR spectra, which means the ENDOR spectra were recorded at the field positions across the whole EPR envelope. The reason for the orientation-selected pulse EPR study is that the sample is a frozen solution of paramagnets with a **g** tensor of [2.029, 2.003, 1.989] that are anisotropic as revealed by Q-band spectrum (Figure 2B). Orientation-selected ENDOR spectra can capture the full span of the hyperfine interaction tensor **A** and orient the tensor elements to the **g** tensor via a set of experimentally determined Euler angles [α, β, γ]° (zyz convention). In the ^{1}H-ENDOR spectra (Figure 3), besides the central weakly-coupled ^{1}H with the hyperfine couplings < 6 MHz, a distinguishable doublet with the splitting of ~25 MHz is observable in the outer region, which is consistent with the superhyperfine doublet displayed in the X-band CW EPR spectrum (*vide supra*). Taken together, we conclude that there is one ^{1}H strongly-coupled to the Ge-centered π radical, with the weakly-coupled ^{1}H signals (< 6 MHz) arising from those distant protons (e.g., phenyl ring or solvent).

Simulations of the orientation-selected ^{1}H-ENDOR spectra enable us to determine a near-isotropic hyperfine tensor **A** of this strongly-coupled ^{1}H, i.e. [A_1, A_2, A_3] = [-23.0, -20.5, -31.5] MHz, with an Euler angle of [27, 53, -10]° relative to the *g* frame. The relative signs of principal *A*-values are identified from ENDOR spectral simulation; the absolute sign is determined via variable mixing-time (VMT) ENDOR experiment by recording ENDOR spectra at the magnetic field (1223.7 mT) corresponding to g_2 2.007, as shown in Figure 4. As the mixing time t_{mix} is increased from 1 μs (black trace) to 200 μs (red trace), the high RF frequency peak ($\nu_+ = |\nu_N - M_sA|$) of ^{1}H decreases, suggesting that the ν_+ ENDOR transition is corresponding to the α electron spin manifold (M_s = +1/2), giving a negative hyperfine coupling *A*.

Decomposition of the **A** tensor of this strongly-coupled ^{1}H gives a major contribution of a_{iso} = -25 MHz and a small anisotropic dipolar component **T** = [2.0, 4.5, -6.5] MHz. The spin density on the 1s orbital of ^{1}H can be calculated via $a_{iso} = \rho_{1s}a^{FC}(^1H)$, where the Fermi-contact interaction of unit electron spin with ^{1}H nuclear spin $a^{FC}(^1H)$ is +1420 MHz, giving ρ_{1s} = -1.8%. The negative spin population on ^{1}H 1s orbital suggests that the electron spin residing on the strongly-coupled ^{1}H arises from spin polarization that gives excess beta spin (spin down). Taken considerations of both the magnitude and the sign of a_{iso}, this strongly-coupled ^{1}H is a hydride directly coordinated to germanium center. This assignment is corroborated by the following discussion on the unique dipolar component **T** of ^{1}H = [2.0, 4.5, -6.5] MHz, in which $T_{max} < 0$.

The dipolar component **T** of ^{1}H hyperfine tensor arises solely from the through-space dipolar interaction between the electron spin on Ge and the ^{1}H nuclear spin, as there are no local contributions arising from the spin density residing in p-, d- or f-type orbital for ^{1}H. Therefore, by using point-dipole approximation that applies to the case where the distance (*r*) between the electron spin and nuclear spin is longer than 2.5 Å, the **T** = [-*T*, -*T*, 2*T*] can be

computed as $T = \rho_{Ge} g_e g_n \beta_e \beta_n (\mu_0/4\pi h)/r^3$ (ρ_{Ge} is the spin density on Ge). Here, as both g_n ^{1}H and ρ_{Ge} are positive, the $T_{max} \equiv 2T$ should be positive, which contrasts with the negative -6.5 MHz obtained from ENDOR experiment. This suggests that the point-dipole approximation (r > 2.5 Å) does not hold in the case of Ge-hydride. Instead, we employed an empirical approximation model by assuming that the $4p_\pi$ spin density concentrated at two effective spin centers (A and B) of two p-orbital lobes, as illustrated in Figure 5. The spin density residing on either A (0, 0, d) or B (0, 0, -d) is $\rho_A = \rho_B = 0.5\rho_{Ge}$, where d is the distance between the Ge nucleus and each effective lobe center. If the ^{1}H is in the plane of p-orbital node (out-of-plane angle $\theta = 0°$) with a planar geometry, the dipolar hyperfine tensor $\mathbf{T}_{cal} = \rho_A \mathbf{T}_A + \rho_B \mathbf{T}_B$ is computed to be

$$\mathbf{T}_{cal} = \rho_{Ge} g_e g_n \beta_e \beta_n (\mu_0/4\pi h)/(r^2 + d^2)^{5/2}[-r^2 + 2d^2, 2r^2 - d^2, -r^2 - d^2]$$

Here, r is the Ge-H bond length (1. 57 Å based on DFT model described below) and ρGe ≈ 0.80 (taken from DFT calculation). By varying the d value, it was found that the best-match $\mathbf{T}_{cal}$ = [2.47, 4.01, -6.48] MHz with $T_{max} < 0$ is obtained when d = 1.45 Å, very close to the experimental tensor **T** = [2.0, 4.5, -6.5] MHz. The slight rhomibicity can be adjusted by using $\theta = 3.8°$ (*see* two-point point-dipole approximation model in SI, and it is noted that the **T** tensor is very sensitive to the out-of-plane angle θ), which yields $\mathbf{T}_{cal}$ = [2.02, 4.50, -6.53] MHz matching the experimental tensor **T** exactly. Analysis of the unique dipolar component **T** of ^{1}H not only suggests that the Ge-hydride radical is pseudo-planar ($\theta < 3.8°$), but also provides us insights into various radial distributions of the effective spin center of different p orbitals, e.g., d = 1.45 Å for germanium $4p_\pi$ orbital, while d = 0.68 Å for carbon $2p_\pi$ orbital in previous studies, as shown in Figure 5.

Identification of a hydride coordinated to the Ge center with a pseudo-planar geometry suggests that the trapped Ge radical should reasonably be a Ge(III)-hydride radical rather than

a one-coordinated Ge(I) radical. We reasoned that the one-coordinated Ge(I), as an analogue of the Sn(I) radical, generated during photolysis/thermolysis via Ge−C bond cleavage could be too active to be trapped. Instead, the Ge(III)-hydride radical species we detected via EPR spectroscopy arises from the insertion of the active Ge(I) radical intermediate in a C-H bond., i.e., ·GeHRR' (R = Ar^{iPr4} or Ar^{iPr6}, R' is unknown). At this point, we do not know the origin of this C-H insertion. However, based on the ^{1}H-ENDOR experiment we did not detect any signal from beta-proton, as the hyperfine coupling of beta-proton arising from spin hyperconjunction is as strong as the value of hydride but with positive signs that are distinct from the hydride ENDOR described above. This is corroborated by the following DFT calculation. Therefore, the C-H insertion reaction is most likely the tertiary carbon of the isopropyl in phenyl ring (*see* DFT calculation section for details.) We rule out the possibility from the solvent benzene, as the hydride EPR/ENDOR signal was not affected by using the solvent of C_6D_6.

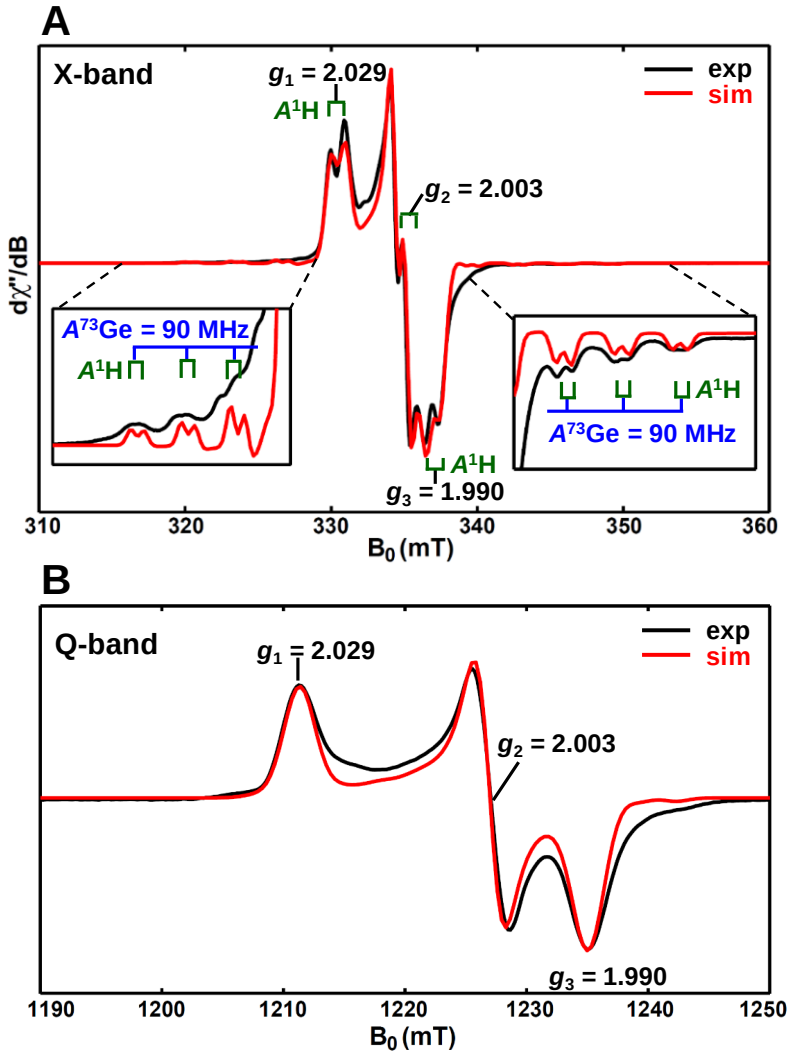

Figure 2. X-band CW EPR spectrum (A) and Q-band (34.0 GHz) pseudo-modulated electron spin-echo detected field-swept EPR spectra (B) of the radical trapped by UV photolysis of $Ge(Ar^{iPr4})_2$ in benzene for ~30 min. The spectrometer settings are as follows: 15 K, 0.1 mW power (no saturation), microwave frequency, 9.38 GHz, conversion time, 40 ms, modulation amplitude, 0.8 mT, modulation frequency, 100 kHz. The Q-band EPR spectra were recorded at 10 K by using a two-pulse sequence of π/2-τ-π-τ-echo, with π/2 = 12 ns and τ = 300 ns. The modulation amplitude of 3.0 mT was used to convert the absorption spectra to the pseudo-modulated spectra in (B).

The simulation (red trace) parameters are as follows: g = [2.029, 2.003, 1.990], A^{73}_{Ge} = [-10, -90, -10] MHz, A^1H = [-23.0, -20.5, -31.5] MHz.

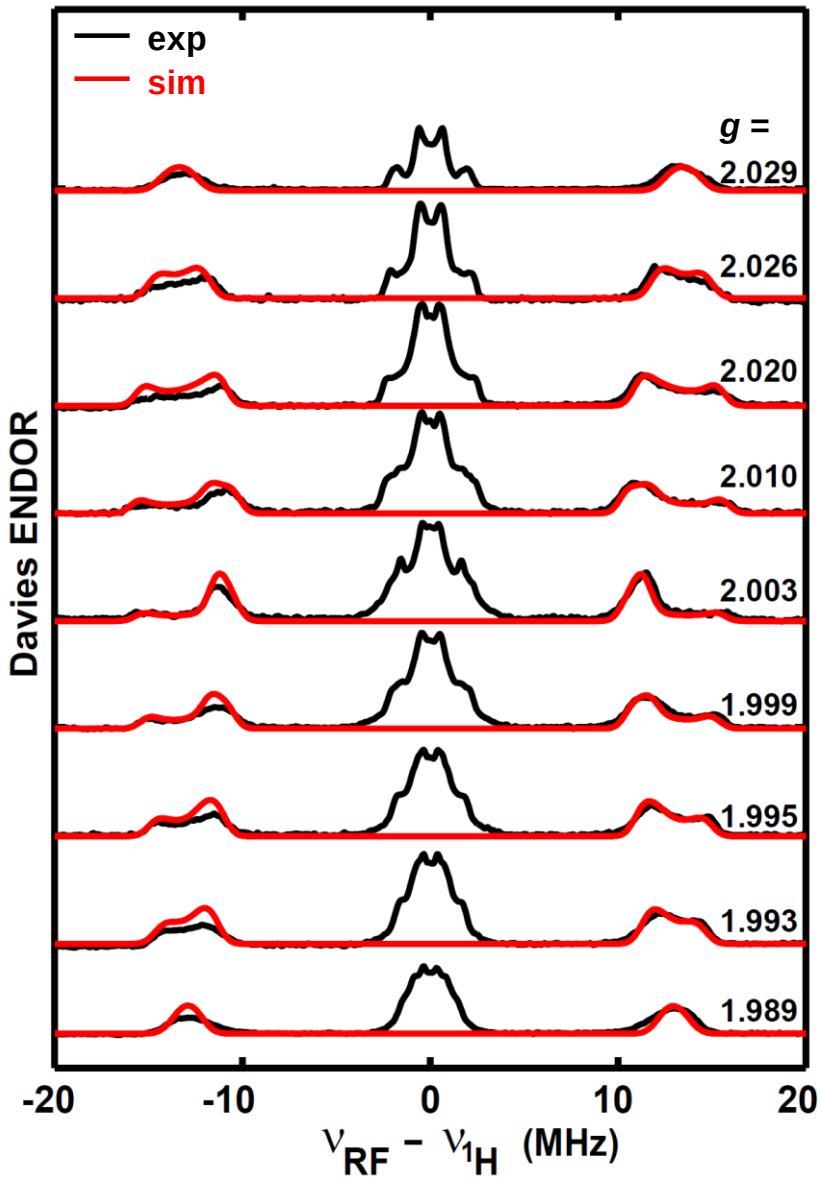

Figure 3. Orientation-selected Q-band (34.30 GHz) ^{1}H-ENDOR spectra of the radical trapped by UV photolysis of Ge(Ar^{iPr4})$_2$ in benzene for ~30 min. All the experimental spectra are in black, while the simulated spectra are in red. Simulation parameters for the hydride is $A(^{1}H)$ = [-23.0, -20.5, -31.5] MHz, Euler angle = [27, 53, -10]°. Spectrometer settings for ^{1}H-ENDOR are 10 K, microwave frequency = 34.30 GHz, microwave inversion pulse π = 80 ns, $\pi/2$ = 12 ns, τ = 300 ns and RF pulse = 20 µs.

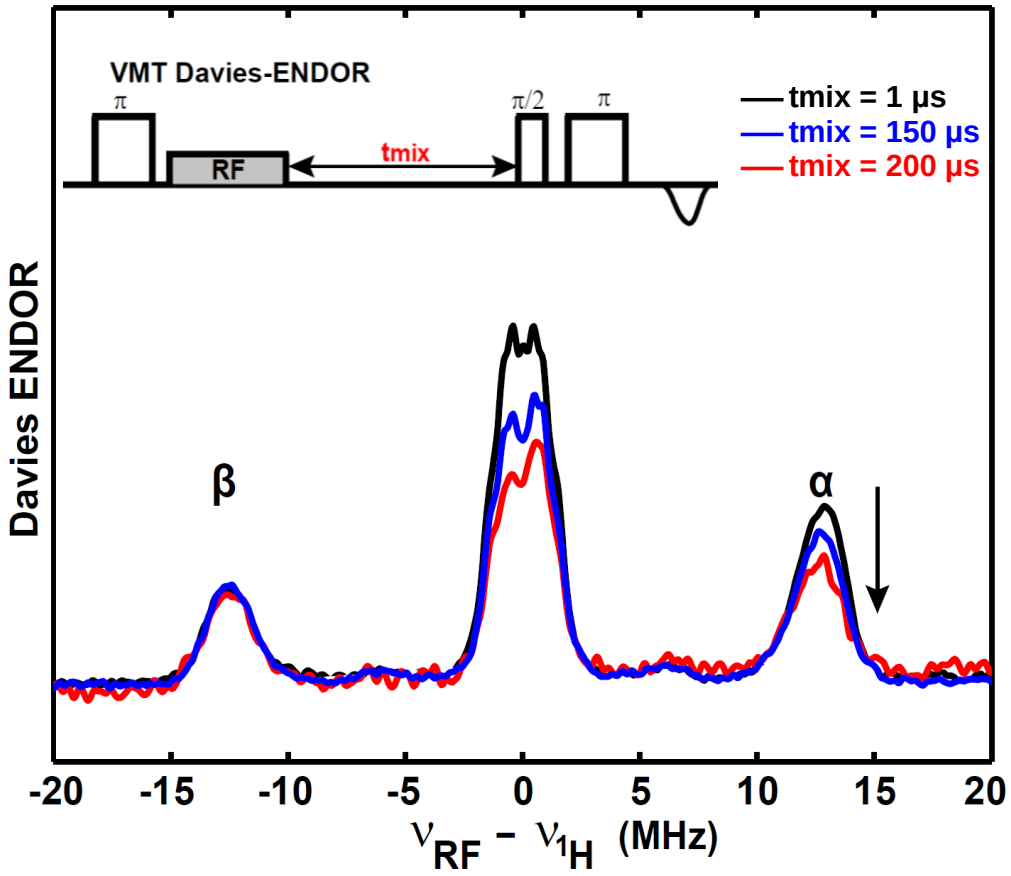

Figure 4. ^{1}H VMT Davies-ENDOR spectra of the radical trapped by UV photolysis of $Ge(Ar^{iPr4})_2$ in benzene for ~30 min recorded at magnetic field of 1223.7 mT (g = 2.003) and T = 10 K. The ENDOR transitions corresponding to β electron spin manifold in the spectra acquired by using various t_{mix} are normalized, with the decreases in the ENDOR transitions corresponding to α spin manifold. Other spectrometer settings are microwave frequency = 34.30 GHz, microwave inversion pulse π = 80 ns, π/2 = 12 ns, τ = 300 ns and RF pulse = 20 µs.

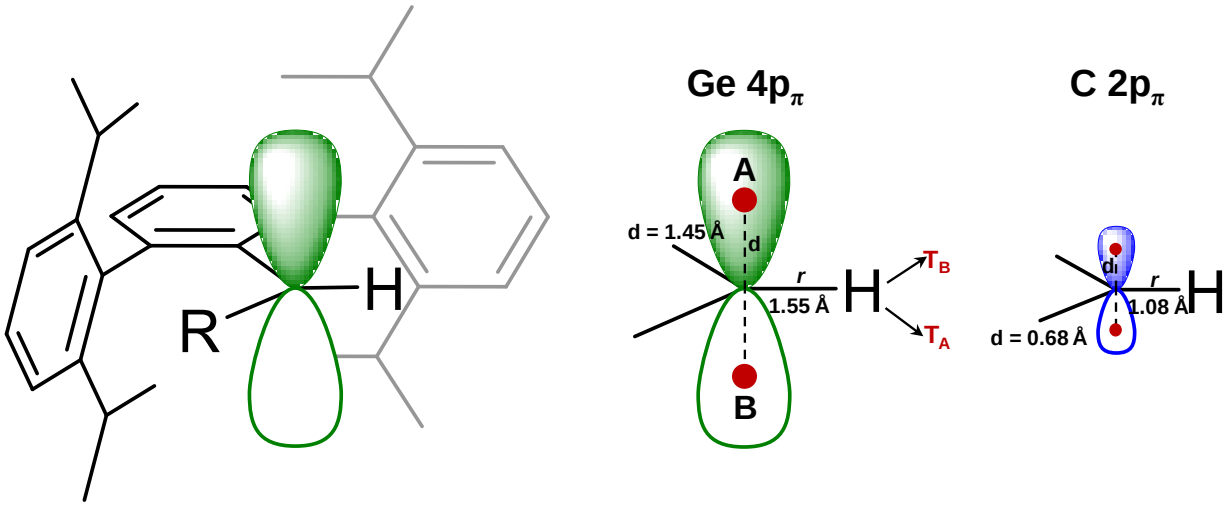

Figure 5. Illustration of the two-point dipole approximation model by assuming that the Ge $4p_\pi$ spin density concentrated at two effective spin centers (A and B) of two p-orbital lobes of Ge radical we trapped. d is the distance between the Ge nucleus and each effective lobe center and *r* is the Ge-H bond length. Here, the out-of-plane angle $\theta = 0°$ (see Figure 7). Previous studies on carbon $2p_\pi$ orbital are also presented for comparison to provide insights into various radial distributions of the effective spin center of different p orbitals.

DFT Calculations. *Sn(I) radical intermediate model*. Based on the crystal structure of $Sn(Ar^{iPr4})_2$, we generated a $:\dot{S}nR$ ($R = Ar^{iPr4}$) intermediate model and performed geometry optimization by using all-electron relativistic calculations, as shown in Figure 6. The calculated Löwdin spin populations shows that the spin density of this Sn(I) radical model is primarily metal tin-based, with most of the spin density (ρ = 82%) residing on Sn and minor spin density (ρ = 9.5%) delocalized to the phenyl ring. The singly occupied molecular orbital (SOMO) for this one-coordinated Sn(I) radical model is a non-bonding molecular orbital dominated by Sn $5p_z$ (spin density ρ = 56%) character, suggesting that this is a π-type radical involving a Sn $5p_z$ orbital and is consistent with the experiment data of the trapped Sn(I) radical intermediate (*vide supra*).

Ge(III)-hydride radical model. As described above, the Ge(III)-hydride radical is most likely formed via a C-H insertion reaction of the $:\dot{G}eR$ ($R = Ar^{iPr4}$) radical that is the Sn(I) analogue but more active. Therefore, we were only able to trap the Ge(III) species rather than Ge(I) intermediate. Based on EPR analysis of the Ge(III)-hydride radical, the C-H insertion reaction is most likely on the tertiary carbon of the isopropyl group in phenyl ring. We therefore built up a corresponding Ge(III)-hydride model, with the optimized geometry shown in Figure 7A. We noted that geometry optimization results in a pyramidal geometry, with the out-plane-angle θ = 22° and the Ge-H bond length r = 1.55 Å. However, the predicted hydride hyperfine coupling tensor **A** = [+101, +108, +112] MHz (Figure 7B) does not match the experimental *A*-values (i.e. [-23.0, -20.5, -31.5] MHz) either in the magnitude or the sign of *A*-values. The predicted positive ^1H hyperfine value suggests that it mainly arises from spin delocalization due to the dominant s-p hybridization in this pyramidal Ge(III)-hydride model, which is obvious not the case of our trapped Ge(III)-hydride radical.

Yonezawa and coworkers' early work employed theoretical calculations to study the relationship between the geometry of $\cdot CH_3$, $\cdot SiH_3$ and $\cdot GeH_3$ radicals and the corresponding hyperfine coupling values. It is suggested that the hyperfine value for hydride is very sensitive to the out-plane-angle θ: with the θ decreasing, the spin-polarizaiton contribution which yields negative hyperfine coupling becomes larger and is dominant in a planar geometry when $\theta = 0°$. Based on their work and our two-point diploe approximation model which suggests $\theta < 3.8°$ (*vide supra*), we built up a corresponding Ge(III)-hydride model with a trigonal planar geometry by constraining the dihedral angle between H-Ge-$C_{isopropyl}$ and H-Ge-C_{phenyl} as 180° on the above optimized pyramidal geometry, as shown in Figure 7C. The predicted ^1H hyperfine coupling tensor **A** is [-40, -43, -58] MHz, with the negative sign arising from spin polarization matching the experimental value. The magnitude of the predicted hyperfine is slightly higher than the experimental value, which could be due to the spin population of the hydride in this model is slightly higher than the trapped radical. The calculated Löwdin spin populations shows that this planar Ge(III)-hydride model are primarily metal germanium-based, with most of the spin density (ρ = 80%) residing on Ge. The SOMO for this planar Ge(III)-hydride model is a non-bonding molecular orbital dominated by Ge $4p_z$ character, suggesting a π-type radical.

Altogether, DFT calculations support that the Ge radical we trapped is a pseudo-planar Ge(III)-hydride radical, which could arise from the C-H insertion reaction of the Ge(I) radical intermediate. Although we do not exactly know the origin of the C-H insertion reaction, it is on a tertiary carbon as no strongly-coupled beta-protons were detected. As shown in a planar Ge(III)-hydride model with a methyl ligand to Ge(III) (Figure Sxx), the predicted hyperfine coupling values of two beta-^1H ([+42, +49, +43] MHz and [+37, +39, +33] MHz) are comparable to that of the hydride ([-41, -43, -58] MHz) in the magnitude but

with positive signs that origin from the spin-hyperconjunction mechanism. We did not detect any beta-proton signal from ENDOR experiment.

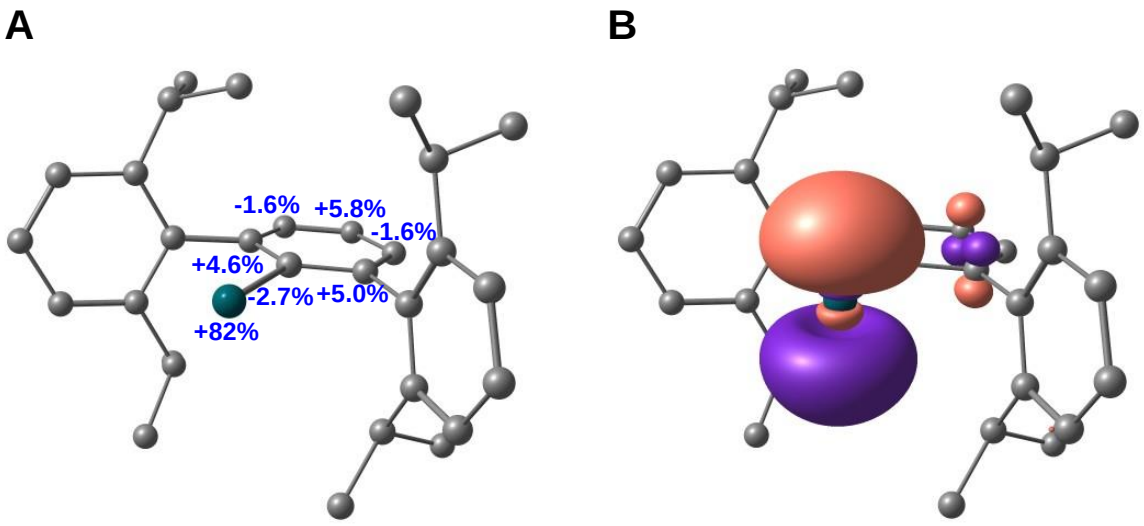

Figure 6. (A) The optimized geometry of : $\dot{S}$nR (R = Ar^{iPr4}) radical intermediate model and the calculated Löwdin spin populations on tin center and the phenyl ring. (B) DFT calculated SOMO of the left Sn(I) radical intermediate model (isosurface value = 0.05 a.u.)

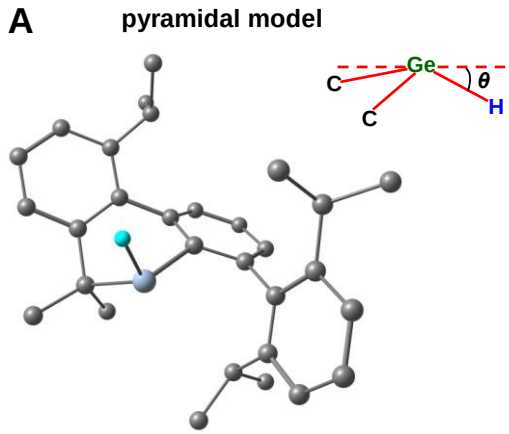

B

	out-of-plane angle (θ)	A ^{73}Ge, MHz	A $^{1}H_{hydride}$, MHz
pyramidal model	22°	[-214, -216, -306]	[+101, +108, +112]
planar model	0°	[-46, -162, -49]	[-40, -43, -58]
exp.	< 3.8°	[-10, -90, -10]	[-23.0, -20.5, -31.5]

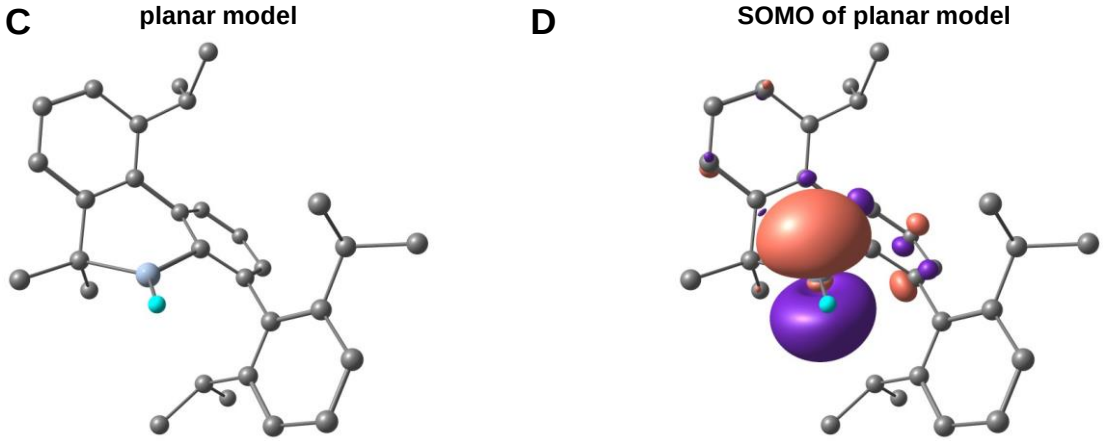

Figure 7. (A) The optimized geometry of Ge(III)-hydride model by presenting a pyramidal geometry for Ge center, with the out-plane-angle θ = 22° and the Ge-H bond length r = 1.55 Å. (B) The DFT-predicted hyperfine coupling values for Ge and the hydride ^{1}H. (C) A trigonal planar geometry of Ge(III)-hydride model by constraining the dihedral angle between H-Ge-$C_{isopropyl}$ and H-Ge-C_{phenyl} as 180° on the above optimized pyramidal geometry shown in Figure A. (D) DFT calculated SOMO of the planar Ge(III)-hydride model shown in Figure C (isosurface value = 0.05 a.u.).

4.4 Conclusions

In summary, photolysis/thermolysis of the tetrylenes, $Sn(Ar^{iPr4})_2$, $Sn(Ar^{iPr6})_2$, $Ge(Ar^{iPr4})_2$, and $Ge(Ar^{iPr6})_2$, led to a Sn(I) intermediate and Ge(III)-hydride radicals which were trapped and characterized by EPR spectroscopy complemented with theoretical calculations. The reason that the Ge(III) radical is trapped instead of a Ge(I) radical intermediate could be due to that the Ge(I) radical (: $\dot{G}eR$) is more reactive than the Sn(I) radical and affords a C-H insertion product, i.e. the Ge(III)-hydride. The new class of tin and germanium radicals characterized in this work provides insights into the radical mechanism pathway of heavier group 14 element tetrylenes chemistry.

4.5 References

1. Davidson, P. J.; Hudson, A.; Lappert, M. F.; Lednor, P. W., Tris[bis(trimethylsilyl)methyl]tin(III), $R_3Sn\cdot$: an unusually stable stannyl radical, from photolysis of R_2Sn. *Journal of the Chemical Society, Chemical Communications* **1973**, 829-830.
2. Asay, M.; Jones, C.; Driess, M., N-Heterocyclic Carbene Analogues with Low-Valent Group 13 and Group 14 Elements: Syntheses, Structures, and Reactivities of a New Generation of Multitalented Ligands. *Chemical Reviews* **2011**, *111*, 354-396.
3. Sekiguchi, A., Disilyne with a silicon-silicon triple bond: A new entry to multiple bond chemistry. *Pure Appl. Chem.* **2008**, *80*, 447-457.
4. Power, P. P., Persistent and Stable Radicals of the Heavier Main Group Elements and Related Species. *Chemical Reviews* **2003**, *103*, 789-810.

5. Hudson, A.; Lappert, M. F.; Lednor, P. W., Subvalent Group 4B metal alkyls and amides. Part 4. An electron spin resonance study of some long-lived photochemically synthesised trisubstituted silyl, germyl, and stannyl radicals. *Journal of the Chemical Society, Dalton Transactions* **1976**, 2369-2375.
6. M. Olmstead, M.; Pu, L.; S. Simons, R.; P. Power, P., Reduction of Ge(Cl)$C_6H_3Mes_2$-2,6 to give the cyclotrigermenyl radical $(GeC_6H_3Mes_2\text{-}2,6)_3\cdot$ and the trigermenyl anion salt $K(GeC_6H_3Mes_2\text{-}2,6)_3$. *Chemical Communications* **1997**, 1595-1596.
7. Pu, L.; Twamley, B.; Power, P. P., Synthesis and Characterization of 2,6-$Trip_2H_3C_6PbPbC_6H_3$-2,6-$Trip_2$ (Trip = C_6H_2-2,4,6-*i*-Pr_3): A Stable Heavier Group 14 Element Analogue of an Alkyne. *Journal of the American Chemical Society* **2000**, *122*, 3524-3525.
8. Phillips, A. D.; Wright, R. J.; Olmstead, M. M.; Power, P. P., Synthesis and Characterization of 2,6-$Dipp_2$-$H_3C_6SnSnC_6H_3$-2,6-$Dipp_2$ (Dipp = C_6H_3-2,6-*i*Pr_2): A Tin Analogue of an Alkyne. *Journal of the American Chemical Society* **2002**, *124*, 5930-5931.
9. Stender, M.; Phillips, A. D.; Wright, R. J.; Power, P. P., Synthesis and Characterization of a Digermanium Analogue of an Alkyne. *Angewandte Chemie International Edition* **2002**, *41*, 1785-1787.
10. Woodul, W. D.; Carter, E.; Müller, R.; Richards, A. F.; Stasch, A.; Kaupp, M.; Murphy, D. M.; Driess, M.; Jones, C., A Neutral, Monomeric Germanium(I) Radical. *Journal of the American Chemical Society* **2011**, *133*, 10074-10077.
11. Egorov, M. P.; Nefedov, O. M.; Lin, T.-S.; Gaspar, P. P., Germylene and Stannylene Anion-Radicals: Generation and Electronic Structure. *Organometallics* **1995**, *14*, 1539-1541.

12. Sekiguchi, A.; Fukawa, T.; Nakamoto, M.; Lee, V. Y.; Ichinohe, M., Isolable Silyl and Germyl Radicals Lacking Conjugation with π-Bonds: Synthesis, Characterization, and Reactivity. *Journal of the American Chemical Society* **2002**, *124*, 9865-9869.
13. Cotton, J. D.; Cundy, C. S.; Harris, D. H.; Hudson, A.; Lappert, M. F.; Lednor, P. W., Photochemical synthesis and electron spin resonance characterisation of stable trivalent metal alkyls (Si, Ge, Sn) and amides (Ge and Sn) of Group IV elements. *Journal of the Chemical Society, Chemical Communications* **1974**, 651-652.
14. Lai, T. Y.; Fettinger, J. C.; Power, P. P., Facile C–H Bond Metathesis Mediated by a Stannylene. *Journal of the American Chemical Society* **2018**, *140*, 5674-5677.
15. Morton, J. R.; Preston, K. F., Atomic parameters for paramagnetic resonance data. *J. Magn. Reson.* **1978**, *30*, 577-582.
16. Solomon, E. I.; Szilagyi, R. K.; DeBeer George, S.; Basumallick, L., Electronic Structures of Metal Sites in Proteins and Models: Contributions to Function in Blue Copper Proteins. *Chemical Reviews* **2004**, *104*, 419-458.
17. Morehouse, R. L.; Christiansen, J. J.; Gordy, W., ESR of Free Radicals Trapped in Inert Matrices at Low Temperature: CH_3, SiH_3, GeH_3, and SnH_3. *The Journal of Chemical Physics* **1966**, *45*, 1751-1758.
18. Jackel, G. S.; Gordy, W., Electron Spin Resonance of Free Radicals Formed from Group-IV and Group-V Hydrides in Inert Matrices at Low Temperature. *Physical Review* **1968**, *176*, 443-452.
19. Fieldhouse, S. A.; Lyons, A. R.; Starkie, H. C.; Symons, M. C. R., Unstable intermediates. Part CXLVII. Electron spin resonance spectra of radicals in irradiated organotin compounds: the radicals R_3Sn, R_4Sn^-, R_5Sn, R_3SnCl^-, Ph_6Sn^{2-}, $H_2\dot{C}Sn(Me)_2SnMe_3$, and $H_2\dot{C}Sn(Me)_2Cl$. *Journal of the Chemical Society, Dalton Transactions* **1974**, 1966-1972.

20. Bennett, J. E.; Howard, J. A., ESR spectra of the trimethyl—tin and trimethyl—lead radicals. *Chemical Physics Letters* **1972**, *15*, 322-324.
21. Berclaz, T.; Geoffroy, M., Paramagnetic damage in X-irradiated tetraphenyltin: Probable trapping of Ph_5Sn. *Radiation Physics and Chemistry* **1978**, *12*, 91-94.
22. Lehnig, M.; Buschhaus, H.-U.; Neumann, W. P.; Apoussidis, T., Electron spin resonance and kinetic studies on tin centered radicals r3sn. with bulky substituents. *Bulletin des Sociétés Chimiques Belges* **1980**, *89*, 907-914.
23. Lehnig, M.; Apoussidid, T.; Neumann, W. P., The configuration of the tin-centered radical R_3Sn (R = 2,4,6-tri-*i*-propyphenyl) as studied by ESR. *Chemical Physics Letters* **1983**, *100*, 189-192.
24. Becker, M.; Förster, C.; Franzen, C.; Hartrath, J.; Kirsten, E.; Knuth, J.; Klinkhammer, K. W.; Sharma, A.; Hinderberger, D., Persistent Radicals of Trivalent Tin and Lead. *Inorganic Chemistry* **2008**, *47*), 9965-9978.
25. Hoffman, B. M., Electron nuclear double resonance (ENDOR) of metalloenzymes. *Accounts of Chemical Research* **1991**, *24*, 164-170.
26. Davies, E. R., A new pulse endor technique. *Physics Letters A* **1974**, 47, 1-2.
27. Epel, B.; Manikandan, P.; Kroneck, P. M. H.; Goldfarb, D., High-field ENDOR and the sign of the hyperfine coupling. *Applied Magnetic Resonance* **2001**, *21*, 287-297.
28. Cano, J.; Ruiz, E.; Alvarez, S.; Verdaguer, M., Spin Density Distribution in Transition Metal Complexes: Some Thoughts and Hints. *Comments on Inorganic Chemistry* **1998**, *20*, 27-56.
29. Schweiger, A.; Jeschke, G., Principles of Pulse Electron Paramagnetic Resonance. Oxford University Press: 2001.
30. Gordy, W., Theory and applications of electron spin resonance. Wiley: New York, 1980.

31. Stoll, S.; NejatyJahromy, Y.; Woodward, J. J.; Ozarowski, A.; Marletta, M. A.; Britt, R. D., Nitric Oxide Synthase Stabilizes the Tetrahydrobiopterin Cofactor Radical by Controlling Its Protonation State. *Journal of the American Chemical Society* **2010**, *132*, 11812-11823.

32. Rao, G.; Altman, A. B.; Brown, A. C.; Tao, L.; Stich, T. A.; Arnold, J.; Britt, R. D., Metal Bonding with 3d and 6d Orbitals: An EPR and ENDOR Spectroscopic Investigation of Ti^{3+}–Al and Th^{3+}–Al Heterobimetallic Complexes. *Inorganic Chemistry* **2019**, *58*, 7978-7988.

33. Gagnon, D. M.; Stich, T. A.; Mehta, A. P.; Abdelwahed, S. H.; Begley, T. P.; Britt, R. D., An Aminoimidazole Radical Intermediate in the Anaerobic Biosynthesis of the 5,6-Dimethylbenzimidazole Ligand to Vitamin B12. *Journal of the American Chemical Society* **2018**, *140*, 12798-12807.

34. Gerson, F.; Huber, W., Electron Spin Resonance Spectroscopy of Organic Radicals. WILEY-VCH Verlag GmbH & Co. KGaA: Weinheim, 2003.

35. Bennett, S. W.; Eaborn, C.; Hudson, A.; Hussain, H. A.; Jackson, R. A., Electron spin resonance spectra of trimethylsilyl, trimethylgermyl and related free radicals in solution. *Journal of Organometallic Chemistry* **1969**, *16*, P36-P38.

36. Geoffroy, M.; Ginet, L.; Lucken, E. A. C., ESR study of the triphenylgermyl radical in a single crystal of triphenylgermane. *Chemical Physics Letters* **1976**, *38*, 321-324.

37. Siddiqui, M. M.; Sarkar, S. K.; Sinhababu, S.; Ruth, P. N.; Herbst-Irmer, R.; Stalke, D.; Ghosh, M.; Fu, M.; Zhao, L.; Casanova, D.; Frenking, G.; Schwederski, B.; Kaim, W.; Roesky, H. W., Isolation of Transient Acyclic Germanium(I) Radicals Stabilized by Cyclic Alkyl(amino) Carbenes. *Journal of the American Chemical Society* **2019**, *141*, 1908-1912.

38. Pantazis, D. A.; Chen, X.-Y.; Landis, C. R.; Neese, F., All-Electron Scalar Relativistic Basis Sets for Third-Row Transition Metal Atoms. *Journal of Chemical Theory and Computation* **2008**, *4*, 908-919.

39. Pantazis, D. A.; Neese, F., All-electron scalar relativistic basis sets for the 6p elements. *Theoretical Chemistry Accounts* **2012**, *131*, 1292.

40. Ohta, K.; Nakatsuji, H.; Maeda, I.; Yonezawa, T., Ab initio calculation of geometries and hfs constants of CH_3, SiH_3 and GeH_3 radicals. *Chemical Physics* **1982**, *67*, 49-58.

41. Stoll, S.; Britt, R. D., General and Efficient Simulation of Pulse EPR Spectra. *Phy. Chem. Chem. Phy.* **2009**, *11*, 6614-6625.

42. Stoll, S.; Schweiger, A., EasySpin, a Comprehensive Software Package for Spectral Simulation and Analysis in EPR. *J. Magn. Reson.* **2006**, *178*0, 42-55.

43. Bruggemann, W.; Niklas, J. R., Stochastic ENDOR. *J. Magn. Reson* **1994**, *108*, 25-29.

44. Neese, F., ORCA-an ab initio, Density Functional and Semiempirical Program Package. University of Bonn: Bonn, Germany, 2007; Vol. v. 2.6-35.

45. Perdew, J. P., Density-functional approximation for the correlation energy of the inhomogeneous electron gas. *Phys. Rev. B* **1986**, *33*, 8822-8824. 1.

46. Becke, A. D., Density-functional exchange-energy approximation with correct asymptotic behavior. *Phys. Rev. AZ* **1988**, *38*, 3098-3100.

47. van Lenthe, E.; Ehlers, A.; Baerends, E.-J., Geometry optimizations in the zero order regular approximation for relativistic effects. *J. Chem. Phys.* **1999**, *110*, 8943-8953.

48. Lenthe, E. v.; Baerends, E. J.; Snijders, J. G., Relativistic regular two-component Hamiltonians. *J. Chem. Phys.* **1993**, *99*, 4597-4610.

49. Wüllen, C. v., Molecular density functional calculations in the regular relativistic approximation: Method, application to coinage metal diatomics, hydrides, fluorides and

chlorides, and comparison with first-order relativistic calculations. *J. Chem. Phys.* **1998**, *109*, 392-399.

50. Klamt, A.; Schuurmann, G., COSMO: a new approach to dielectric screening in solvents with explicit expressions for the screening energy and its gradient. *J. Chem. Soc., Perkin Trans.* **1993**, *2*, 799-805.
51. Blachly, P. G.; Sandala, G. M.; Giammona, D. A.; Bashford, D.; McCammon, J. A.; Noodleman, L., Broken-Symmetry DFT computations for the reaction pathway of IspH, an iron–sulfur enzyme in pathogenic bacteria. *Inorg. Chem.* **2015**, *54*, 6439-6461.
52. Blachly, P. G.; Sandala, G. M.; Giammona, D. A.; Liu, T.; Bashford, D.; McCammon, J. A.; Noodleman, L., Use of Broken-Symmetry Density Functional Theory to characterize the IspH oxidized state: implications for IspH mechanism and inhibition. *J. Chem. Theory Comput.* **2014**, *10*, 3871-3884.
53. Staroverov, V. N.; Scuseria, G. E.; Tao, J.; Perdew, J. P., Comparative assessment of a new nonempirical density functional: Molecules and hydrogen-bonded complexes. *J. Chem. Phys.* **2003**, *119*, 12129-12137.

Chapter 5

Facile Insertion of Ethylene into a Sn-C Bond: Effects of the HOMO-LUMO Energy Gap on Reactivity

This work is published in Chemical Communications, DOI: 10.1039/C8CC08488B

Lai, T.Y.; Guo, J.D.; Fettinger, J.C; Nagase, S.; Power, P.P. *Chem Commun.* **2019**, *55*, 405-407.

5.1 Introduction

The reactions of heavier divalent group 14 element species (tetrylenes) with unsaturated C-C bonds have attracted increasing interest because of their potential relevance for catalysis involving the group 14 molecules.[1] Their relatively low HOMO-LUMO gaps, generate sufficiently high reactivity such that they can often interact with alkenes or alkynes under mild conditions.[2] Several researchers have shown that tetrylenes (ER_2; E= Si, Ge, Sn or Pb), tetrlynes (REER) and tetrylenoids (species in which tetrylenes are stabilized by coordination with a carbene) react with alkynes affording either insertion or cycloaddition products.[2] However, examples of direct reactions between olefins and heavier tetrylenes remain relatively rare in part because of increased HOMO-LUMO energy separations with increasing atomic number, and none has led to insertion into an E-C bond.[3]

In 1994, Ando and coworkers showed that the germylene, (GeR_2, R= $-CH(SiMe_3)_2$) reacted with ethylene to give a 1,2-digermacyclobutane probably via a germirane intermediate (Scheme 1, top).[4] More recently, it was shown that a silylene-phosphine complex[5] and a bis(arylthiolato) silylene[6] reacted in a reversible fashion with ethylene (Scheme 1, middle). The silyl silylene, $:Si\{N(C_6H_3\text{-}2,6\text{-}iPr_2)SiMe_3\}\{Si(SiMe_3)_3\}$, was shown to undergo migratory insertion of ethylene into a Si-Si bond by Rieger and coworkers in 2015 (Scheme 1).[7] However,

no examples of a simple insertion of ethylene or other olefins into group 14 element-carbon bonds has been reported.

For stannylenes, calculations on the reaction of SnH_2 with ethylene suggest that it involves a two-step mechanism to give upon binding a metallocyclopropane with subsequent insertion into the Sn-H bond having a barrier of 12.66 kcal mol^{-1}.[8] In 2008 Banasak-Holl and coworkers[9] reported that a stannylene and a iodobenzene reacted with olefins under mild conditions. The olefin addition products display regioselectivity consistent with a radical induced migratory insertion into a C-H bond.[10]

Nonetheless, the direct reaction of a organostannylene with ethylene or other olefins under ambient or near ambient conditions remained unknown. Herein we report the direct reaction of the diarlystannylenes $Sn(Ar^{iPr4})_2$ and $Sn(Ar^{iPr6})_2$, (Ar^{iPr4} = C_6H_3-2,6-(C_6H_3-2,6-^{i}Pr $_2$)$_2$, Ar^{iPr6} = C_6H_3-2,6-(C_6H_2-2,4,6-^{i}Pr$_3$)$_2$) with ethylene at 60°C which afford products in which one equivalent of ethylene is inserted into one of the Sn-C bonds.

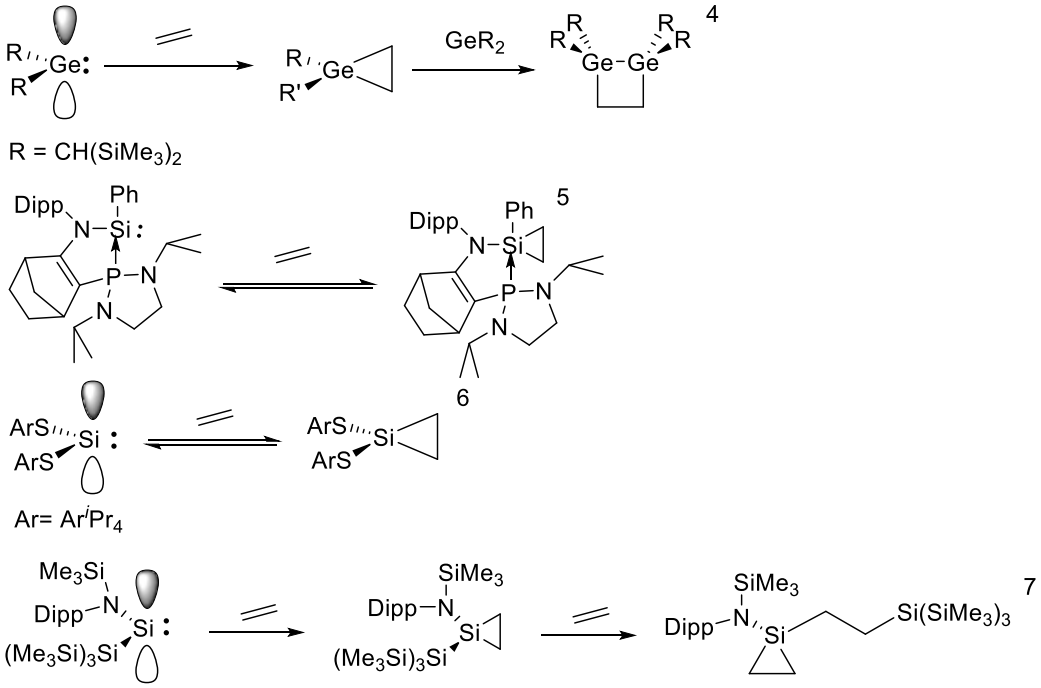

Scheme 1. Reactions of tetrylenes with olefins[4-7]

5.2 Experimental Details

General Procedures. All operations were carried out under anaerobic and anhydrous conditions using modified Schlenk techniques. All solvents were dried over alumina columns and degassed prior to use. The ^{1}H, ^{13}C and ^{119}Sn NMR spectroscopic data were collected on a Bruker 400MHz spectrometer. ^{119}Sn NMR data were referenced to $Sn^{n}Bu_4$ (−11.7 ppm). Infrared spectroscopy was collected as a Nujol mull using a Bruker Tensor 27 IR spectrometer. UV−visible spectroscopy was carried out as dilute hexane solutions in 3.5 mL quartz cuvettes using an Olis 17 Modernized Cary 14 UV/vis/NIR spectrophotometer. $Sn(Ar^{iPr_4})_2$ and $Sn(Ar^{iPr_6})_2$ were synthesized according to literature methods. Ethylene gas was dried via a P_2O_5/Sieves drying column prior to use.

$Ar^{iPr_4}Sn(C_2H_4Ar^{iPr_4})$ (1a) A rapidly stirred solution of $Sn(Ar^{iPr_4})_2$ (1.00 g, 1.09 mmol) in benzene *ca*. 30 mL was treated with an excess of ethylene gas over one hour at 25 °C. The temperature was elevated to 60 °C and stirred for 12h. Upon cooling the solution was filtered using a filter-tipped cannula and concentrated under reduced pressure. Storage of the solution at room temperature afforded **1**. Yield (0.53 g, 51.23%) Mp: 171-176°C, ^{1}H NMR (400 MHz, C_6D_6, 298 K): δ = 0.68 (t, 2H, $^{3}J_{H,H}$=9.6Hz CH_2CH_2Ar), 1.04 (d, 12H $^{3}J_{H,H}$=1.6Hz $CH(CH_3)_2$), 1.05 (d, 12H $^{3}J_{H,H}$=1.6Hz $CH(CH_3)_2$), 1.08 (d, 12H $^{3}J_{H,H}$=4Hz $CH(CH_3)_2$), 1.14(d, 12H $^{3}J_{H,H}$=3.6Hz $CH(CH_3)_2$), 2.17 (t, 2H, $^{3}J_{H,H}$=6.8Hz, CH_2CH_2Ar), 2.71 (m, 4H $^{3}J_{H,H}$=7Hz $CH(CH_3)_2$), 3.07 (m, 4H $^{3}J_{H,H}$=7Hz $CH(CH_3)_2$), 7.03-7.28 (m, 18H *m*-C_6H_3, *p*-C_6H_3, *m*-Dipp and *p*-Dipp; Dipp = 2,6-*i*Pr_2-C_6H_3); $^{13}C\{^{1}H\}$ NMR (126 Hz, C_6D_6, 298 K): 22.85, 23.26, 25.49, 25.90, 30.50, 30.58, 122.97, 123.41, 126.08, 128.61, 129.23, 129.50, 135.87, 139.24, 139.50, 143.58, 143.81, 146.39, 146.49 ; $^{119}Sn\{^{1}H\}$ NMR (186.36 Hz, C_6D_6,

298 K): δ=1806 ppm UV-vis: λ_{max} (nm), ϵ (M^{-1} cm^{-1}) = 482nm, 2130. IR (CsI, nujol, mineral oil; selected, cm^{-1}) : 2950, 1480, 1280, 1100, 1040, 820

$Ar^{iPr6}Sn(C_2H_4Ar^{iPr6})$ (1b) A rapidly stirred solution of $Sn(Ar^{iPr6})_2$ (1.00g,0.924mmol) in benzene *ca*. 30 mL was treated with an excess of ethylene gas over one hour at 25 °C. The temperature was elevated to 60 °C and stirred for 12h. The solution was filtered using a filter-tipped cannula and concentrated under reduced pressure. Storage of the solution at room temperature afforded **1b**. Yield (0.42 g, 40.9%) Mp: 167-175 °C, ^{1}H NMR (400 MHz, C_6D_6, 298 K): δ = 0.95 (t, 2H, $^3J_{H,H}$=5.8 Hz CH_2CH_2Ar), 1.09 (d, 24H $^3J_{H,H}$= 4.8Hz $CH(CH_3)$), 1.21, (d, 24H $^3J_{H,H}$= 4.8Hz $CH(CH_3)$), 1.29 (d, 12H $^3J_{H,H}$=3.6Hz $CH(CH_3)$), 1.31 (d, 12H $^3J_{H,H}$=4Hz $CH(CH_3)$), 2.60 (t, 2H, $^3J_{H,H}$= 4.7Hz, CH_2CH_2Ar), 2.78 (m, 4H $^3J_{H,H}$= 4.7Hz $CH(CH_3)_2$), 2.86 (m, 4H $^3J_{H,H}$= 4.8Hz $CH(CH_3)_2$), 2.97 (m, 2H $^3J_{H,H}$= 4.8Hz $CH(CH_3)_2$), 3.18 (m, 4H $^3J_{H,H}$= 4.8Hz $CH(CH_3)_2$), 7.05-2.25 (m, 14H *m*-C_6H_3, *p*-C_6H_3, and *m*-Trip; Trip = 2,4,6-*i*Pr_2-C_6H_2) $^{13}C\{^1H\}$ NMR (126 Hz, C_6D_6, 298 K): 23.21, 23.71, 24.10, 25.50, 25.92, 30.51, 30.59, 34.14, 34.41, 50.10, 120.34, 120.88, 121.03, 124.45, 25.86, 129.85, 130.10, 133.32, 136.95, 139.57, 143.66, 144.32, 146.05, 147.69, 148.42. $^{119}Sn\{^1H\}$ NMR (186.36 Hz, C_6D_6, 298 K): δ=1946 ppm. UV-vis: λ_{max} (nm), ϵ (M^{-1} cm^{-1}) = 489nm, 2200 IR (CsI, nujol, mineral oil; selected, cm^{-1}) : 2970, 1470, 1260, 1080, 1040

5.3 Results and Discussion

The work herein consists of a collaborative effort of Dr. Jing-Dong Guo and myself. Dr. Guo peformed the DFT calculation. The synthesis, characterization, reaction, and the construction of the paper was carried out by me.

The blue diarylstannylenes, :$Sn(Ar^{iPr4})_2$ (1.00 g, 1.09 mmol),[11] or $Sn(Ar^{iPr6})_2$ (1.00g, 0.924 mmol)[12] in benzene or heptane *ca*. 30 mL were treated with an excess of ethylene gas

over one hour at 25 °C. The temperature was raised to 60 °C and the mixture was stirred for 12h to give a red solution (Scheme 2). Benzene was removed under reduced pressure and replaced by toluene (*ca.* 20mL). Concentration to ca. 10mL followed by storage at ca. -18 °C afforded red crystals of the stannylenes **1a** and **1b** in moderate yield (0.53g, 51.23%) and (0.42 g, 40.9%). The X-ray crystal structures of compounds **1a** and **1b** are shown in Figure 1.

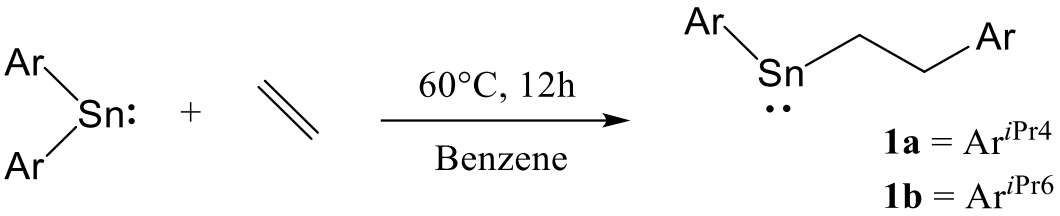

Scheme 2. The reaction of $SnAr_2$ species with ethylene.

The crystal structures illustrate that one ethylene molecule has inserted into one of the Sn-C bonds of each stannylene. The tin atoms have a bent two-coordinate configuration with C-Sn-C angles of 94.7(5)°(**1a**) and 99.06°(**1b**). These are considerably narrower to than those in previously reported, related stannylenes which span the range 107.61(9)° to 123.55(14)°.[11-17] In particular, the C-Sn-C angles may be compared to those of the precursor $Sn(Ar^{iPr4})_2$ (112.77(9)°) and $Sn(Ar^{iPr6})_2$ (112.55(6)) which are significantly wider because of the greater steric repulsion between the two large terphenyl substituents. The Sn-C bond lengths in **1a** and **1b** span the range 2.145(4)-2.210(12)Å which is similar to what is found in other stannylenes and distannenes[11-17] (*cf.* sum, 2.17Å of the single bond radii of carbon, 0.77 Å, and tin ,1.40 Å).[18]

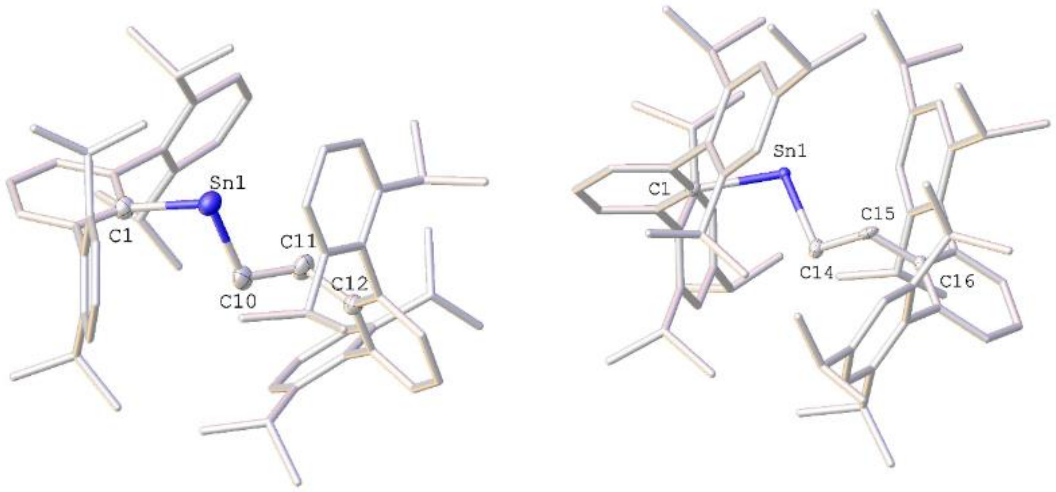

1a **1b**

Figure 1. X-ray crystal structure of $Ar^{iPr4}SnCH_2CH_2Ar^{iPr4}$ (**1a**, left) and $Ar^{iPr6}SnCH_2CH_2Ar^{iPr6}$ (**1b**, right). Hydrogen atoms and co-crystallized solvent molecules are not shown. Selected bond lengths [Å] and angles [°]: **1a:** C1-Sn1: 2.145(4), Sn1-C10: 2.210(12), C10-C11: 1.542(13), C11-C12: 1.50(17), C1-Sn1-C10: 94.7(5), Sn1-C10-C11: 112.6(12), C10-C11-C12: 119.9(14). **1b**: C1-Sn1: 2.1992(12), Sn1-C14: 2.205(2), C14-C15: 1.549(3), C15-C16: 1.492, C1-Sn1-C14: 99.22(1), Sn1-C14-C15: 109.90(18), C14-C15-C16: 116.224

The solution $^{119}Sn\{^1H\}$ NMR spectra of **1a** and **1b** display a single downfield resonance at 1809 and 1946 ppm respectively. These chemical shifts lie within the range (1200-2600ppm) observed for other two-coordinate diorganostannylenes and related species,[19] and may be compared with the ^{119}Sn NMR chemical shifts of $Sn(Ar^{Me6})_2$ (1971ppm),[16] $Sn(Ar^{iPr4})_2$ (2245ppm)[17] and $Sn(Ar^{iPr6})_2$ (2129ppm).[12] The UV-vis spectra show one absorption at 482 nm (**1a**) or 489 nm (**1b**), consistent with an n→p transition for alkyl/aryl stannylene species having a monomeric formulation in solution.[11,12,16,20-22] These values may be compared to those of $Ar^{iPr4}SnCH_2C_6H_5$ (486nm),[20] $Ar^{iPr4}SnCH_2C_6H_4$-3-Me (490nm),[20]

$Ar^{iPr4}SnCH_2CH_2Bu^t$ (486nm),[21] $Ar^{iPr6}SnCH_2CH_2Bu^t$ (484nm),[21] and $Ar^{iPr4}SnR$ (R= norbornyl, 494nm; norbornenyl, 502nm)[22] and $Ar^{iPr4}Sn(norbornyl)SnAr^{iPr4}$ (496nm)[22] which were prepared by the reactions of the respective olefins with the corresponding aryl tin (II) hydrides.

The reaction of $Sn(Ar^{iPr4})_2$ or $Sn(Ar^{iPr6})_2$ to yield **1a** and **1b** was found to be limited to one equivalent of ethylene even in the presence of a large excess of the olefin and extended reaction periods up to 3 days. Cooling the solution to −80°C also afforded no evidence of further ethylene complexation or reaction with **1a** or **1b** on the basis of ^1H NMR spectroscopy. We also tested the reactivity of the related tetrylene, $Sn(Ar^{Me6})_2$, where the tin environment is less hindered. However, no reaction with ethylene was observed under identical conditions to those used for **1a** and **1b**. The counter intuitive reactivity pattern toward ethylene may be compared to the reactions of $Sn(Ar^{Me6})_2$ and $Sn(Ar^{iPr4})_2$ toward H_2, where the less bulky $Sn(Ar^{Me6})_2$ was also found to be unreactive toward H_2 even at elevated temperature. Inspection of the UV-vis spectra of $Sn(Ar^{Me6})_2$, $Sn(Ar^{iPr4})_2$ and $Sn(Ar^{iPr6})_2$ reveals absorptions at 553, 600 and 612 nm respectively which shows that the absorption maximum is shifted to longer wavelengths, hence lower energies, for the more crowded stannylenes and is consistent with a decreasing HOMO-LUMO energy separation as the size of the ligands increase. Attempted reactions of $Sn(Ar^{iPr4})_2$ and $Sn(Ar^{iPr6})_2$ with propene, 2-butene or styrene under similar conditions to those described for ethylene yielded no evidence of reaction apparently for steric reasons.

In contrast to the UV-vis absorptions mentioned above for $Sn(Ar^{iPr4})_2$ (600nm) and $Sn(Ar^{iPr6})2$ (612nm), **1a** (482nm) and **1b** (489nm), have the significantly shorter wavelength values indicating a larger HOMO-LUMO separation. They display no further reactivity with ethylene (cf, $Sn(Ar^{Me6})_2$ has an absorption at 553nm and also does not react with ethylene).

The initial step of the reaction of $Sn(Ar^{iPr4})_2$ with ethylene is calculated to involve the approach of the ethylene molecule at an angle to the $Sn\{C(ipso\}_2$ plane to interact approximately face-on with the Sn 4p-orbital. This is similar to interaction with other small molecules such as H_2, CO and isocyanide.[23,24] This produces a weak ethylene complex (INT-1) (enthalpy of stabilization = -4.7 $kcal^{-1}$) and a slight lengthening of the ethylene C-C double bond. The ethylene is not symmetrically coordinated (the Sn-C distance to the two ethylene differs by over 0.2 Å). The INT-1 complex can further react by two routes involving the transition state TS 1 (ΔH= -2.6 kcal mol^{-1}, ΔG= +10.0kcal mol^{-1}) in which the Sn-C distances to the ethylene become at most equal (2.213 and 2.328 Å) en route to a cyclostannapropane intermediate INT-2 (with equal Sn-C bond lengths to C_2H_4 and a single C-C bond of 1.528 Å). This complex has a positive ΔG value and is thus unstable (ΔH= -3.6 kcal mol^{-1}, ΔG= +9.0kcal mol^{-1}) and does not lead to an inserted product. A somewhat higher energy transition state TS2 (ΔH= +4.8 kcal mol^{-1}, ΔG= +15.3kcal mol^{-1}) in which the ethylene is displaced toward one of the Sn-C(ipso) bonds which is lengthened to Sn-C1 = 2.601 Å (cf. Sn-C2 = 2.28 Å) and simultaneous initial formation of an Sn-C bond to one of the ethylene carbons (ie Sn--C4 = 2.376Å) and a C-C bond to the other ethylene carbon (C1--C3 = 2.72Å) is also calculated. This leads eventually to the formation of the inserted product (PRO) corresponding to the structurally characterized **1a**. This is enthalpically favoured by 47.4 kcal mol^{-1} (cf ΔG= -34.8 kcal mol^{-1}). Attempts to observe the interaction of ethylene and tin in solution (INT-1) at *ca.* −80°C were unsuccessful consistent with the calculated instability of INT-2.

The possibility that the reaction might proceed by a different mechanism, involving homolytic cleavage of an Sn-C bond followed by the reaction of the $\bullet SnAr^{iPr4}/\bullet Ar^{iPr4}$ or $\bullet SnAr^{iPr6}/\bullet Ar^{iPr6}$ radical pairs with ethylene to yield the products as shown (Scheme 3b) was

also investigated. The •SnAr^{iPr4} radical has recently been detected in the metathesis reactions of :Sn(Ar^{iPr4})$_2$ with alkyl benzenes in refluxing toluene. However, the calculations at the B3PW91-D3BJ level indicate a quite high activation barrier (*ca.* 40.6 kcal mol^{-1}) for such a process shown in Scheme 3b

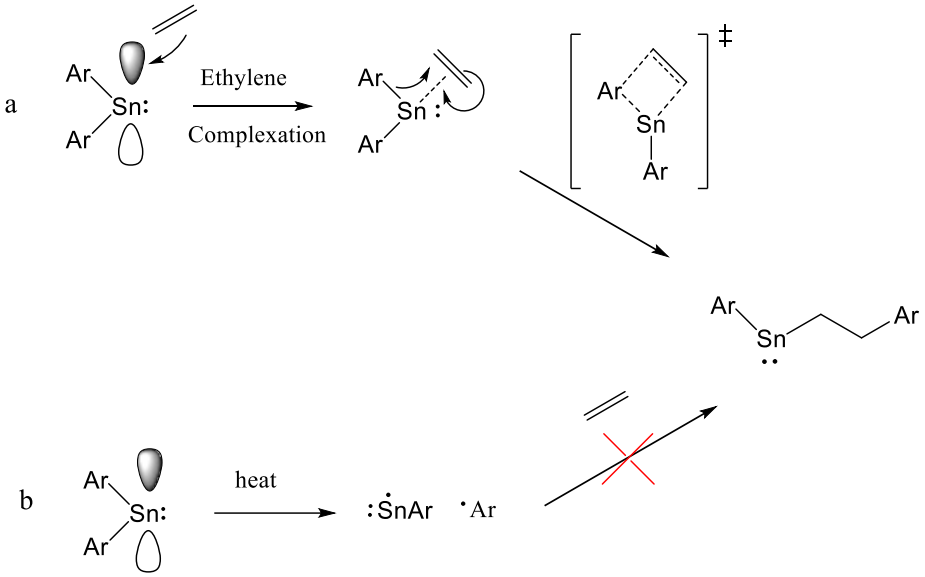

Scheme 3. Two possible ethylene insertion mechanisms for the reactions of the diaryl tin with ethylene.

5.4 Conclusions

In summary, the reaction of Sn(Ar^{iPr4})$_2$ or Sn(Ar^{iPr6})$_2$ with ethylene at 60°C proceeds via a facile migratory insertion route to afford products **1a** and **1b** The downfield ^{119}Sn NMR chemical shifts at 1809 and 1946 ppm. X-ray crystallography confirm these monomeric stannylene structure in the solid state and in solution. Further investigation of the reactivity of this open-shell species in underway.

5.5 References

1. R. Jambor and A. Lyčka *Eur. J. Inorg. Chem.***2017**, 4887–4898
2. a) R. Kinjo; M. Ichinohe; A. Sekiguchi; N. Takagi; M. Sumimoto and S. Nagase, *J. Am. Chem. Soc.*, **2007**, *129*, 7766–7767. b) S.J. Han; T. Sasamori; Y. Mizuhata and N. Tokitoh, *Dalton Trans.*, **2010**, *39*, 9238–9240. c) C. Cui; M.M. Olmstead and P.P. Power, *J. Am. Chem. Soc.*, **2004**, *126*, 5062–5063. d) C. Cui; M.M. Olmstead; J.C. Fettinger; G.H. Spikes and P.P. Power, *J. Am. Chem. Soc*., **2005**, *127*, 17530–17541. e) T.J. Hadlington; J. Li; M. Hermann; A. Davey; G. Frenking and C. Jones, *Organometallics*, **2015**, *34*, 3175–3185. f) L. Zhao; C. Jones and G. Frenking, *Chem. Eur. J.*, **2015**, *21*, 12405–12413. g) T. Sasamori; T. Sugahara; T. Agou; J.-D. Guo; S. Nagase; R. Streubel and N. Tokitoh, *Organometallics*, **2015**, *34*, 2106–2109 h) V. Protchenko; M.P. Blake; A.D. Schwarz; C. Jones; P. Mountford and S. Aldridge, *Organometallics*, **2015**, *34*, 2126–2129 i) F. Lips; A. Mansikkamaki; J.C. Fettinger; H.M. Tuononen; P.P Power, *Organometallics* **2014**, *33*, 6253−6258 j) O.T. Summerscales; J.C. Fettinger; P.P. Power, *J. Am. Chem. Soc*. **2011**, *133*, 11960−11963 k) O.T. Summerscales; C.A. Caputo; C.E. Knapp; J.C. Fettinger; P.P. Power, *J. Am. Chem. Soc.* **2012**, *134*, 14595−14603
3. H. Jacobsen; T. Ziegler, *Comments Inorg. Chem.* **1995**, *17*, 301-317
4. H. Ohgaki; Y. Kabe and W. Ando *Organometallics* **1995**, *14*, 2139-2141
5. R. Rodriguez; D. Gau; T. Kato; N. Saffon-Merceron; A. De Cozar; F.P. Cossio; A. Baceiredo, *Angew. Chem., Int. Ed.* **2011**, *50*, 10414-10416
6. F. Lips; J.C. Fettinger; A. Mansikkamaki; H.M. Tuononen; P.P. Power, *J. Am. Chem. Soc.* **2014**, *136*, 634−637
7. D. Wendel; W. Eisenreich; C. Jandl; A. Pöthig; B. Rieger, *Organometallics* **2016**, *35*, 1-4
8. X.H. Lu; L.M. Zhai; Y.X. Wang, *Chin. J. Chem.* **2001**, *19*, 1053-1057

9. A. Kavara; K.D. Cousineau; A.D. Rohr; J.W. Kampf; M.M. Banaszak-Holl, *Organometallics* **2008**, *27*, 1041-1043
10. J. March, *Advanced Organic Chemistry,* 4th ed.; Wiley: New York, **1992**; pp 743–745
11. G.H. Spikes; Y. Peng; J.C. Fettinger; P.P. Power, *Z. Anorg. Allg. Chem.* **2006**, *632*, 1005−1010
12. M. McCrea-Hendrick; M. Bursch; K.L. Gullett; L.R. Maurer; J.C. Fettinger; S. Grimme; and P.P. Power, *Organometallics*, **2018**, *37*, 2075-2085
13. V.Y. Lee; A. Sekiguchi, *Organometallic Compounds of Low-Coordinate Si, Ge, Sn and Pb: From Phantom Species to Stable Compounds*, John Wiley & Sons, Ltd, Chichester, UK, 2010.
14. M. Asay; C. Jones; and M. Driess, *Chem. Rev.* **2011**, *111*, 354-396
15. Y. Mizuhata; T. Sasamori; and N. Tokitoh, *Chem Rev.* **2009**, *109*, 3479-3511
16. P. Wilfling; K. Schittelkopf; M. Flock; R.H. Herber; P.P. Power; R.C. Fischer, *Organometallics* **2015**, *34*, 2222−2232.
17. R.S. Simons; L. Pu; M.M. Olmstead; P.P. Power, *Organometallics* **1997**, *16*, 1920−1925
18. P. Pyykko; M. Atsumi, *Chem. - Eur. J.* **2009**, *15*, 186-197.
19. a) B. Wrackmeyer, *In Annual Reports on NMR Spectroscopy*; Academic Press: San Diego, CA, 1999; Vol. 38 b) N. Tokitoh; K. Manmaru; R. Okazaki, *Organometallics* **1994**, 13, 167-171 c) M. Weidenbruch; J. Schlaefke; A. Schafer; K. Peters; H.G. von Schnering; H. Marsmann, *Angew. Chem., Int. Ed. Engl.* **1994**, *33*, 1846-1848.
20. T.Y. Lai; J.C. Fettinger and P.P. Power, *J. Am. Chem. Soc.,* **2018**, *17*, 5674-5677
21. S. Wang; M. McCrea-Hendrick; C.M. Weinstein; C.A. Caputo; E. Hoppe; J.C. Fettinger; M.M. Olmstead; P.P. Power, *J. Am. Chem. Soc*. **2017**, *139*, 6596-6604.
22. S. Wang; M. McCrea-Hendrick; C.M. Weinstein; C.A. Caputo; E. Hoppe; J.C. Fettinger; M.M. Olmstead; P.P. Power, *J. Am. Chem. Soc*. **2017**, *139*, 6586-6595.

23. Y. Peng; J.-D. Guo; B.D. Ellis; Z. Zhu; J.C. Fettinger; S. Nagase; P.P. Power, *J. Am. Chem. Soc*. **2009**, *131*, 16272–16282.

24. Z.D. Brown; P.P. Power, *Inorg. Chem.* **2013**, *52*, 6248-6259

Chapter 6

Reversible Binding of Ethylene and Propylene by Germylenes

This work is published in Organometallics, DOI: 10.1021/acs.organomet.9b00109

Lai, T.Y.; Chen, C.Y.; Fettinger, J.C.; Power, P.P. *Organometallics* **2019**, *38*, 1425-1428.

6.1 Introduction

Apart from insertion reactions with their hydride derivatives, the direct reactions of simple olefins with main group compounds, either under ambient or near-ambient conditions, remain relatively rare.[1] For group 14 species, early reports described the cyclo-addition of tetra-tert-butyldisilene with ortho-methylstyrene to yield the [2+2] cycloaddition species 1,1,2,2-tetra-tert-butyl-3-(2-methylphenyl)-1,2-disilacyclobutane,[2] and of tetramesityldisilene and digermene with styrene to yield the corresponding [2+2] cycloaddition products.[3] Later, the silyl substituted disilene $\{(t\text{-}BuMe_2)Si\}_2SiSi\{Si(t\text{-}BuMe_2)_2\}_2$ was shown to react with styrene to give a 1,2-disilacyclobutane species.[4] Similarly, the disilynes $\{(Me_3Si)_2CH\}_2\}_2(i\text{-}Pr)SiSiSiSi(i\text{-}Pr)\{CH(SiMe_3)_2\}_2]$[5] and $\{(t\text{-}Bu_3Si)_2MeSi\}SiSi\{SiMe\{Si(t\text{-}Bu_3)_2\}$[6] were shown to react with 2-butene or ethylene respectively to afford cyclic [2+2] disilene addition products.

In contrast to these simple cyclizations, the reaction of the disilyne BbtSiSiBbt (Bbt= C_6H_2-2,6-$\{CH(SiMe_3)_2\}_2$-4-$\{C(SiMe_3)_3\}$) with ethylene was more complex and the major product featured an ethylene molecule inserted into the SiSi triple bond while two other ethylenes formed a silacylopropane unit at each silicon, ie, a bis(siliranyl)ethane.[7] The reaction of the corresponding digermyne BbtGeGeBbt (Bbt = C_6H_2-2,4,6-$(CH(SiMe_3)_2)_3$)

with ethylene yielded a 1,2-digermacyclobutene and, upon reaction with a further equivalent of ethylene, a 1,4-digermabicyclo[2.2.0]hexane or a bis(germiranyl)ethane.[8]

Reversibility in reactions with small molecules is of importance for further possible applications in catalytic process.[9] The common feature of the reactions discussed above is that under ambient conditions they are all irreversible. However, in 2009 it was shown[10] that the distannynes $Ar^{iPr4}SnSnAr^{iPr4}$ and $Ar^{iPr8}SnSnAr^{iPr8}$ (Ar^{iPr4}=C_6H_3-2,6-(C_6H_3-2,6-iPr_2)$_2$ and Ar^{iPr8}= C_6H-2,6-(2,4,6-C_6H_2-iPr_3)$_2$-3,5-iPr_2) (Scheme 1a) reversibly bind two ethylene molecules at room temperature although the ethylene reactions with the corresponding digermynes proved irreversible. In addition, a very recent report has demonstrated reversibility for the addition of some terminal alkenes to the digermyne BbtGeGeBbt in which one alkene molecule forms a 1,2-digermacyclobutane product (Scheme 1b).[11] Reversible reactions of ethylene with certain phosphine complexed silylenes (Scheme 1c)[12] and dithiolatosilylenes were also described and the silacyclopropane intermediates were isolated and structurally characterized (Scheme 1d).[13] Nonetheless, no reversible olefin complexation by simple tetrylene derivatives of the heavier elements, germanium, tin or lead has been reported.

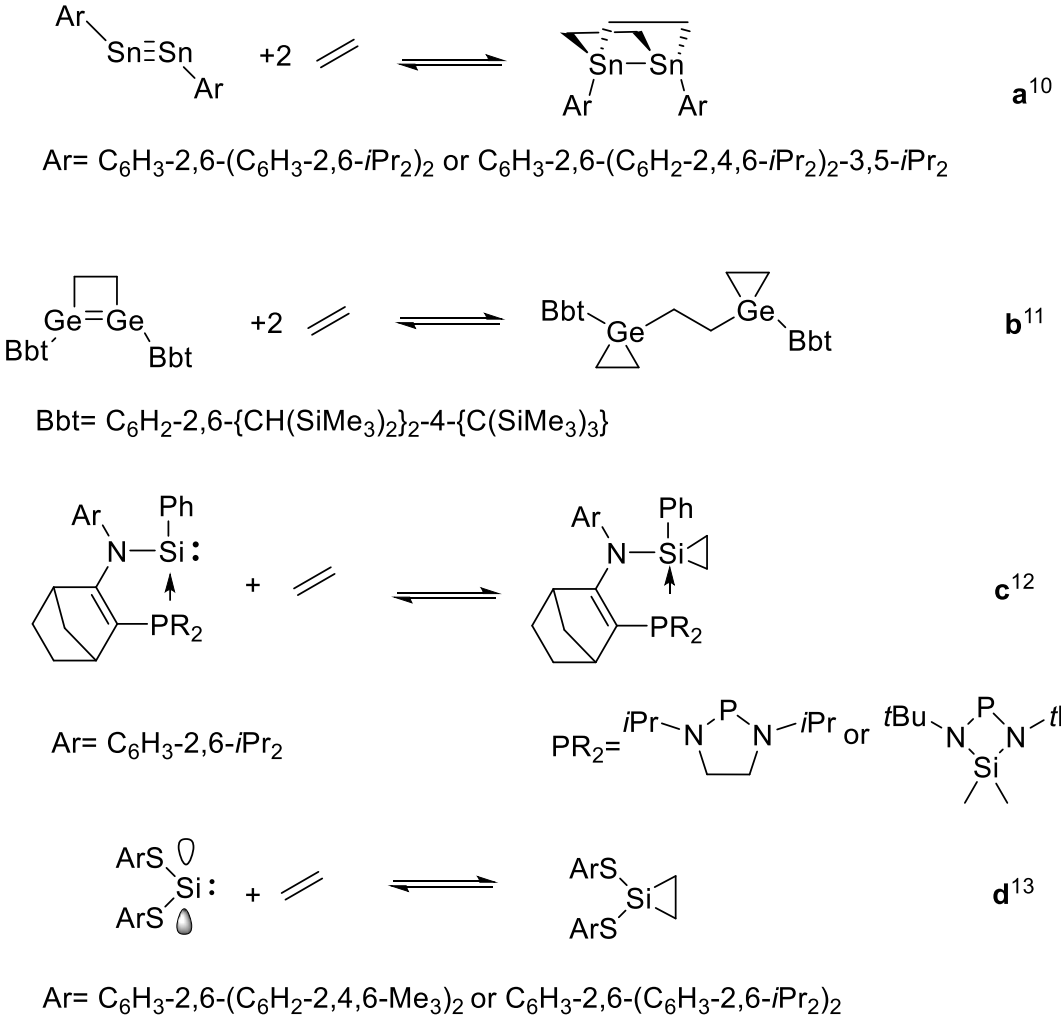

Scheme 1. Illustration of the known reversible reactions of main group compounds with ethylene at or near room temperature.[10-13]

Herein, we report the first examples of reversible olefin binding by stable, two-coordinate germylenes, presumably via an intermediate π-complex.[14] We demonstrate that $Ge(Ar^{Me6})_2$[15] and $Ge(Ar^{iPr4})_2$[16] react reversibly with ethylene, and that $Ge(Ar^{iPr4})_2$ also reversibly binds propylene at room temperature in toluene (**Scheme 2**, top). We show also that at elevated temperature $Ge(Ar^{iPr4})_2$ reacts with ethylene to yield the ethyl substituted digermene $\{Ge(Et)(Ar^{iPr4})\}_2$ with elimination of one equivalent of $Ar^{iPr4}H$ (**Scheme 2**, bottom). The products were analyzed via X-ray crystallography and ^1H NMR Spectroscopy.

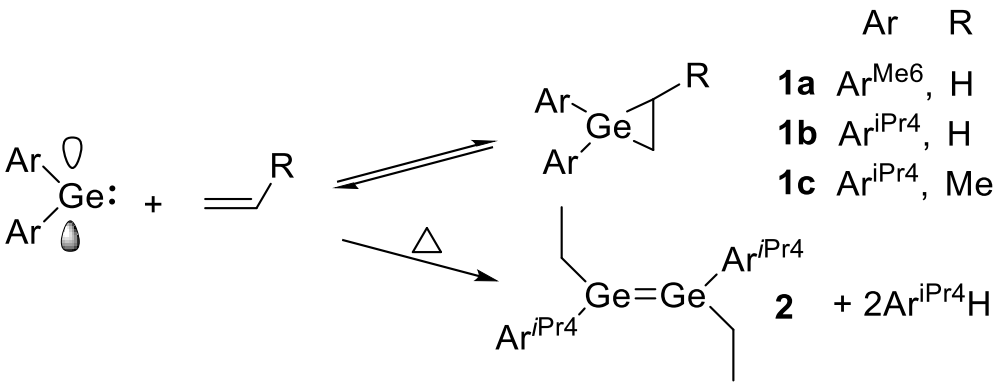

Scheme 2. Reactions of diarylgermylenes with olefins

6.2 Experimental Details

General Procedures. All operations were carried out under anaerobic and anhydrous conditions using modified Schlenk techniques. All solvents were dried over alumina columns and degassed prior to use. The ^{1}H and ^{13}C NMR spectroscopic data were collected on a Bruker 400/500MHz or a Varian 600MHz spectrometer. VT ^{1}H NMR data were recorded on a Bruker 500 instrument. $Ge(Ar^{Me_6})_2$ and $Ge(Ar^{iPr_4})_2$ were synthesized according to literature methods. Ethylene and propylene gas were dried via a P_2O_5/Sieves drying column prior to use.

$(Ar^{Me_6})_2Ge(C_2H_4)$ (1a) In a J. Young NMR tube, $Ge(Ar^{Me6})_2$ (0.033g 0.047mmol) was added and dissolved in d8-toluene *ca.* 0.5ml . The solution was degassed twice and backfilled with ethylene. To ensure complete reaction of the NMR sample, the NMR was left at RT for a day prior to NMR spectroscopy. ^{1}H NMR (500MHz, C_7D_8, 248K): 0.53(s, 4H, C**H**Ge), 1.76(s, 24H, o-Me), 2.24(s, 12H, p-Me), 6.5-7.5(14H aromatic Hs)

$(Ar^{iPr_4})_2Ge(C_2H_4)$ (1b) A rapidly stirred solution of $Ge(Ar^{iPr4})_2$ (1.00 g, 1.15 mmol) in toluene *ca*. 30 mL was degassed 3 times then treated with ethylene gas. Storage of the solution at -30°C afforded **1b**. Yield (0.3g, 29%) Mp: 112°C (turned blue), ^{1}H NMR (500MHz, C_7D_8, 248K): -0.04/0.51(t, 4H, GeC**H**), 0.66(d, 6H, C**H**$_3$CH), 0.97/0.98/1.64/1.25 (d, 48H, C**H**$_3$CH), 1.66(m, 4H, CH_3C**H**), 3.32(m, 4H, CH_3C**H**). ^{13}C NMR (126MHz, C_6D_6, 298K): 5.94, 11.46, 27.23, 28.39, 28.48, 29.75, 30.82, 30.97, 31.23, 31.64, 34.17, 34.89, 34.96, 36.74, 127.19, 127.6, 128.46, 130.51, 132.96, 134.29, 138.65, 139.04, 140.03, 146.53, 147.74, 149.96, 151.22, 152.13, 152.91, 153.09, 153.34.

$(Ar^{iPr_4})_2Ge(C_3H_6)$ (1c) In a J. Young NMR tube, $Ge(Ar^{iPr4})_2$ (0.03g mmol) added was dissolved in d8-toluene and the solution is degassed twice and backfilled with propylene. To ensure complete reaction the NMR sample, the NMR was left at RT for a day prior the NMR recording. However, the resulting broadening makes it difficult for NMR recording. The germirane signals are hidden in the isopropyl signals. ^{1}H NMR (500MHz, C_7D_8, 248K): 0.38/0.54/0.73/0.99/1.21(d, 48Hs C**H**$_3$CH) 3.28(m, 4H, CH_3C**H**), 4.02(m, 4H, CH_3C**H**)

$[(Ar^{iPr_4})Ge(C_2H_5)]_2$ (2) A rapidly stirred solution of $Ge(Ar^{iPr4})_2$ (0.68 g, 0.78 mmol) in toluene *ca*. 30 mL was degassed 3 times then treated with ethylene gas. The solution was heated to 80°C for 12 h. The solution is concentrated to *ca.* 20mL and storage at -30°C afforded **2**. Yield: (0.125g, 32%).

Variable temperature ^{1}H NMR spectroscopy and Van't Hoff analysis of 1a

The integral atoms of the, o-Me group of $Ge(Ar^{Me6})_2$, free ethylene and Me of the germirane in compound **1a** were used for the determination of the equilibrium constant for the conversion of the germylene with ethylene to give the germirane.

The equilibrium constant was calculated according to equation 1.

$$K_{eq} = \frac{[Germirane]}{[Germylene][ethylene]} \text{ (eq1)}$$

The Van't Hoff equation, equation 2, was used in order to determine ΔH and ΔS from the slope and the intercept of the plot of ln K_{eq} against 1/T.

$$lnK_{eq} = -\frac{\Delta H}{R}\left(\frac{1}{T}\right) + \frac{\Delta S}{R} \text{ (eq. 2)}$$

6.3 Results and Discussion

The work herein consists of a collaborative effort of Ms. Kelly L. Gullett, Ms. Chia-Yuan Chen and myself. Ms. Gullett initiated the study and carried out the variable temperature UV-visible spectroscopy. I am responsible for the synthesis, reaction, X-ray crystallography, ^{1}H NMR spectroscopy, variable temperature ^{1}H NMR spectroscopy and the construction of the paper. Ms. Chen assisted me with the characterization of the products.

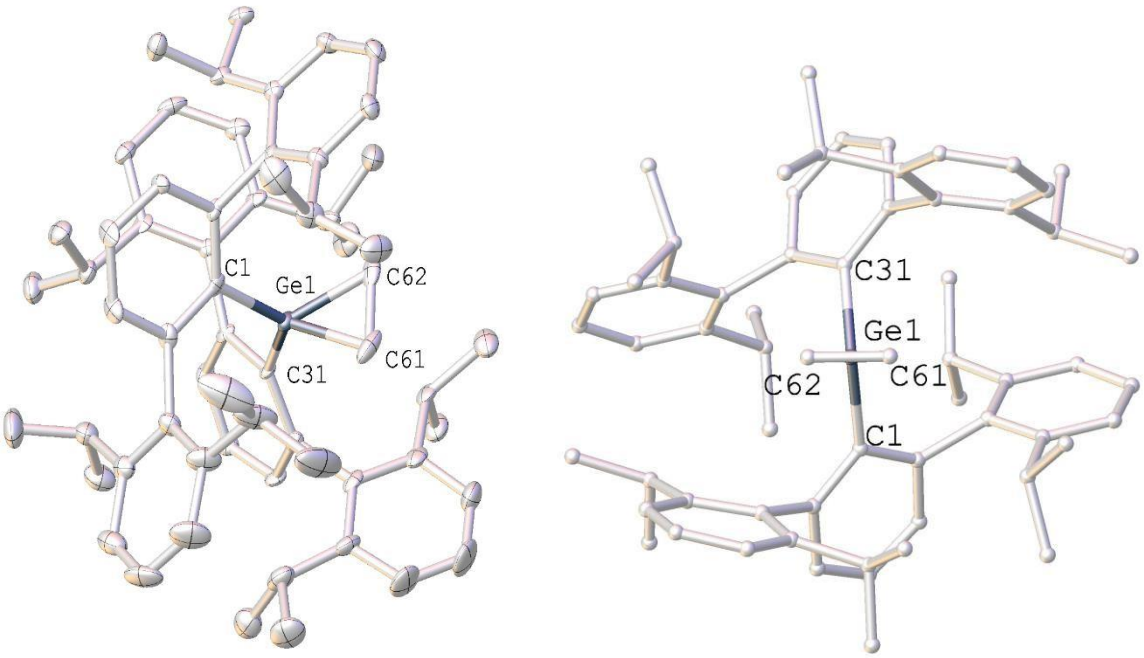

Figure 1. Two views of the thermal ellipsoid (30%) of $(Ar^{iPr4})_2GeCH_2CH_2$ (**1b**). Hydrogen atoms and cocrystallized toluene molecules are not shown. Selected bond distances (Å) and angles (deg): Ge1-C62: 1.944(7), Ge1- C61: 1.946(6), Ge1-C1:1.970(6), Ge1-C41: 1.972(7), C62-C61: 1.514(9), C61-Ge1-C62: 45.8(3), C1-Ge1-C31: 121.6(2).

The reaction with the olefins were carried out by dissolving the germylene in toluene to give a purple ($Ge(Ar^{Me6})_2$) or blue ($Ge(Ar^{iPr4})_2$) solution. Exposure of these solutions under an olefin atmosphere at room temperature results in very pale solution in 30 minutes. Colorless crystals of the germirane, $(Ar^{iPr4})_2GeCH_2CH_2$, **1b** were obtained by cooling a toluene solution to *ca.* -30°C (crystals of **1a** were also obtained but they were unsuitable for X-ray crystallographic studies.) and storage for 12 h at that temperature. The germanium atom is four coordinate and has an irregular tetrahedral coordination geometry (Figure 1, left). The C1-Ge1-C31 angle and the C61-Ge1-C62 angle between the two aryl ligands are 121.6(2)° and 45.8(3)° respectively. The torsion angles between the two planes defined by

the Ge1-C1-C31 and Ge1-C61-C63 arrays are 86.2(4)° (Figure 1, right). Within the girmirane ring the C-Ge-C and Ge-C parameters are similar to those in other girmiranes which spans the range 1.931-2.069Å.[8,15] The C-C bond length within the germirane ring (1.514(9) Å) is similar to those in compound, BbtGe(C_2H_4)C_2H_4Ge(C_2H_4)BbT (1.546(4) Å).[8] On the other hand it is shorter than the C-C distance in {($Me_3Si)_2$HC}Ge(N-phenylmaleimide) (1.63(4))[17] as a result of steric hindrance and is longer than that in {($Me_3Si)_2$HC}Ge(tetramethylbutatriene) (1.470(15))[17] where there is conjugation with the two doubly bonded substituents.

The ^{1}H NMR spectrum of $(Ar^{Me6})_2GeCH_2CH_2$ in toluene-d8 solution displays a signal due to uncomplexed ethylene at 5.30 ppm and a signal at 0.55 ppm corresponding to the complexed molecule. A variable temperature ^{1}H NMR study was performed and a Van't Hoff analysis of the reaction of ethylene with Ge(Ar^{Me6})$_2$ afforded ΔH_{assn}= -44.69kJ mol^{-1}, ΔS_{assn}= -159.82 JK^{-1} and ΔG_{assn} = -6.3 kJ mol^{-1} at 298K. Similarly, a Van't Hoff analysis of the reaction of Ge(Ar^{iPr4})$_2$ with ethylene yields the parameters ΔH_{assn}= -1.36 kJ mol^{-1}, ΔS= 19.78 J K^{-1} and ΔG_{assn} = -7.25 kJ mol^{-1} at 298K. The corresponding data for the reaction of Ge(Ar^{iPr4})$_2$ and propylene are ΔH_{assn}= -1.362 kJ mol^{-1}, ΔS_{assn}= 2.579 J K^{-1} and ΔG_{assn}= -2.1 kJ mol^{-1} at 298K. For the reaction of Ge(Ar^{Me6})$_2$ and propylene, the ^{1}H NMR spectrum of the reaction solution displays little change up to 203K.

For the previously known reversible reaction of the silylene Si(SAr^{iPr4})$_2$ with ethylene,[13] the experimentally determined thermodynamic parameters via ^{1}H variable temperature NMR spectroscopy are ΔH_{assn}= -83.61±8.4 kJ mol^{-1} and ΔG_{assn}= -24.9±2.5 kJ mol^{-1} at 300 K. In the case of the phosphine complexed silylenes (Scheme 1c) with ethylene,[12] experimentally determined thermodynamic parameters by VT ^{31}P NMR

spectroscopy are ΔH_{assn} = -37.7 kJ mol^{-1}, ΔS_{assn} = -118.6 J mol^{-1}K^{-1} and ΔG_{ass}= 2.3 kJ mol^{-1} at 337 K.

In comparison, our compounds have generally low values: *cf* **1a**, ΔG_{ass}= -6.3 kJ mol^{-1} (298K), **1b** ΔG_{ass}= -7.25 kJ mol^{-1}(298K), and **1c** ΔG = -2.1 kJ mol^{-1}. Thus the interaction of the germylene with olefins (- 6.3. kJ mol^{-1}) is only slighter stronger than the corresponding interaction with bulkier alkynes: 3-hexyne (-5.11kJ mol^{-1}).[18] The calculated ΔG values for the reaction of Si(SAr^{iPr4})$_2$ with ethylene and acetylene are -24 kJ mol^{-1}(experimental) and -75 kJ mol^{-1}(DFT) respectively.[19]

The lack of reactivity of Ge(Ar^{Me6})$_2$ with propylene can be explained on the basis of the increased steric repulsion of that olefin in comparison to ethylene. However the more sterically hindered germylene, Ge(Ar^{iPr4})$_2$, reacted with both ethylene and propylene. This counter-intuitive reactivity pattern toward propylene brings to mind the reaction of Sn(Ar^{Me6})$_2$ and Sn(Ar^{iPr4})$_2$ with ethylene, where the less bulky species Sn(Ar^{Me6})$_2$ also did not react with ethylene even at elevated temperature whereas Sn(Ar^{iPr4})$_2$ reacted readily.[20] Inspection of the UV-vis spectra of Sn(Ar^{Me6})$_2$ and Sn(Ar^{iPr4})$_2$ reveals absorptions at 553 and 600 nm respectively showing that the more crowded stannylene has a decreased HOMO-LUMO energy separation. In the case of Ge(Ar^{Me6})$_2$ and Ge(Ar^{iPr4})$_2$ the UV absorptions are 578 and 608,[15,16] again showing a smaller HOMO-LUMO gap for the more sterically crowded Ge(Ar^{iPr4})$_2$. Upon reaction with ethylene the more reactive Ge(Ar^{iPr4})$_2$, also yielded a slightly more negative ΔG in comparison to that of Ge(Ar^{Me6})$_2$ (**1b** (ΔG_{assn} = -6.85 kJ mol^{-1} at 298K) vs **1a** (ΔG_{assn} = -6.3 kJ mol^{-1} at 298K)).

Previously, our group reported that Sn(Ar^{iPr4})$_2$ undergoes a facile migratory insertion reaction with ethylene at 60 °C to afford the alkyl aryl stannylene, Ar^{iPr4}SnCH$_2$CH$_2$Ar^{iPr4}.[20]

In an attempt to observe a similar reaction for the germanium species, $Ge(Ar^{iPr4})_2$ was heated under ethylene to 60 °C in hexane. The resulting product (Scheme 2, bottom) proceeded via an insertion of the ethylene into a Ge-H bond that was generated via Ge-C cleavage of a Ge-Ar^{iPr4} bond, followed by a H abstraction from the $:\dot{G}eAr^{iPr4}$ radical.[21] Compound **2** and its crystal structure had been previously reported.[22] However, in that case it was synthesized by the reaction of EtMgBr with $Ge(Ar^{iPr4})Cl$.

6.4 Conclusions

In conclusion, the diarylgermylenes, $Ge(Ar^{Me6})_2$ and $Ge(Ar^{iPr4})_2$, have been shown to reversibly coordinate ethylene.[23] The more sterically crowded, but more reactive $Ge(Ar^{iPr4})_2$, was shown to bind propylene as well. The thermodynamic parameters were experimentally determined by VT ^1H NMR spectroscopy which provide values that are consistent with the observed reversibility in these reactions. The reaction of $Ge(Ar^{iPr4})_2$ with ethylene at 60°C in hexane resulted in the hydrogermylation product **2** by Ge-C bond cleavage and H abstraction.

6.5 References

1. Possibly, the earliest, well documented examples are the reactions with group 13 hydrides. See: (a) Hurd, D.T. The Reactions of Diborane with Hydrocarbons *J. Am. Chem. Soc.* **1948**, *70*, 2053-2055. Ziegler, K.; Gellert, H.G.; Kuehlhorn,H.; Martin, H.; Meyer, K.; Nagel, K.; Sauer,H.; Zosel, K. Aluminium-organische Synthese im Bereich olefinischen Kohlenwasserstoffe *Angew. Chem.* **1952**, *64*, 323-350. Reversible olefin complexation with aluminium. see: (b) Radzewich, C.E.; Coles, M.P. and Jordan, R.F. Reversible Ethylene Cycloaddition Reactions of Cationic Aluminum ß-Diketiminate Complexes. *J. Am. Chem.*

Soc. **1998**, *120*, 9384-9385. (c) Bakewell, C.; White A.J.P.; Crimmin, M.R. Reversible alkene binding and allylic C-H activation with an aluminium(I) complex. *Chem. Sci.* **2019**, *10*, 2452-2458

2. Weidenbruch, M.; Kroke, E.; Marsmann, H.; Pohl,S.; Saak,W. Disilene and Silylene Additions to the Double Bonds of Alkenes and 1,3-Dienes;: Molecular Structure of a [2+2] Cycloaddition Product *J. Chem. Soc. Chem. Commun*. **1994**,1223-12224.
3. Dixon, C.E.; Cooke, J.A.; Baines, K. M. The Reaction of Group 14 Dimetallenes with Alkenes: Electron-Poor Alkenes *Organometallics* **1997**, *16*, 5437-5440.
4. Iwamoto, T.; Sakurai, H.; Kira, M. Bimolecular Reactions of Tetrakis(trialkylsilyl)disilenes with Various Reagents *Bull. Chem. Soc. Jpn*. **1998**, *71*, 2741-2747.
5. Sekiguchi, A.; Kinjo, R.; Ichinohe, M. A Stable Compound with a Silicon Silicon Triple Bond *Science* **2004**, *305*, 1755-1757.
6. Wiberg, N.; Vashist, S.K.; Fischer, G.; Mayer, P. Disilynes (III) A Relatively Stable Disilyne RSi=SiR (R= $SiMe(SiBu^t_3)_2$ *Z. Anorg. Allg. Chem*. **2004**, *630*, 1823-1828.
7. Han, J. S.; Sasamori,T.; Mizuhata, Y.; Tokitoh,N. Reactivity of an Aryl Substuted Silicon-Silicon Triple Bond: Reactions of a 1,2-Diaryldisilyne with Alkenes, *J. Am. Chem. Soc.* **2010**, *132*, 2546-2547.
8. Sasamori,T.; Sugahara, T; Agou, T; Sugamata, K.; Guo, J.-D.; Nagase, S.; Tokitoh, N. Reaction of a Diaryldigermyne with Ethylene, *Chemical Science* **2015**, *6*, 5526-5530.
9. Chu, T.; Nikonov, G.I.; Oxidative Addition and Reductive Elimination at Main-Group Element Centers, *Chem. Rev.* **2018**, *118*, 3608-3680
10. Peng,Y. ;Ellis, B.D. Wang, X.; Fettinger, J.C.; Power, P.P. Reversible Reactions of Ethylene with Distannynes Under Ambient Conditions *Science* **2009**, *325*, 1168-1670.
11. Sugahara, T.; Guo, J.-D.; Sasamori, T.; Nagase, S.; Tokitoh, N. Reversible addition of terminal Alkenes to digermynes. *Chem. Commun*. **2018,** 54**,** 519-522.

12. Rodriguez, R. C.; Gau, D,; Kato, T.; Saffon-Merceron, N.; de Cozar, A.; Cossio, F.P.; Baceiredo, A. Reversible Binding of Ethylene to Silylene–Phosphine Complexes at Room Temperature *Angew. Chem. Int. Ed.* **2011**, *50*, 10414-10416.
13. Lips F. Fettinger, J. C.; Mansikkamaki, A.; Tuononen, H.; Power, P.P. Reversible Complexation of Ethylene by a Silylene under Ambient Conditions *J. Am. Chem. Soc.* **2014**, *136*, 634-637.
14. Billone, P.S.; Beleznay, K.; Harrington, C.R.; Huck, L.A. and Leigh, W.J. A Glimpse at the Chemistry of GeH_2 in Solution. Direct Detection of an Intramolecular Germylene-Alkene π-Complex *J. Am. Chem. Soc.* **2011**, *133*, 10523-10534
15. Simons, R.S.; Pu, L.; Olmstead, M.M. and Power, P.P. Synthesis and Characterization of the Monomeric Diaryls M{C_6H_3-2,6-Mes_2}$_2$ (M= Ge, Sn, or Pb; Mes= 2,4,6-$Me_3C_6H_2$-) and Dimeric Aryl-Metal Chlorides[M(Cl){C_6H_3-2,6-Mes_2}]$_2$(M= Ge or Sn) *Organometallics*, **1997**, *16*, 1920-1925.
16. Spikes, G.H.; Peng, Y.; Fettinger, J.C.; and Power, P.P. Synthesis and Characterization of the Monomeric Sterically Encumbered Diaryls E{C_6H_3-2,6-(C_6H_3-2,6-*i*Pr_2)$_2$}$_2$ (E=Ge, Sn, or Pb, *Z. Anorg. Allg. Chem.* **2006**, *632*, 1005-1010
17. Ando, W.; Ohgaki, H.; Kabe, Y. Stable germirane derivatives, *Angew. Chem., Int. Ed. Engl.* **1994**, *33*, 659-661
18. Lai, T.Y.; Gullet, K.L.; Chen C.-Y.; Fettinger J.C.; and Power, P.P. Reversible Complexation of Alkynes by a Germylenes *Organometallics* **2019**, *38*, 1421−1424
19. This finding is consistent with the greater strain energy calculated for a silacyclopropane and silacyclopropene. (a) Gordon, M. S. Ring strain in cyclopropane, cyclopropene, silacyclopropane, and silacyclopropene, *J. Am. Chem. Soc.* **1980**, *102*, 7419-7422. (b) Lips, F.; Masikkamäki, A.; Fettinger, J. C.; Tuononen, H. M.; Power, P. P. Reactions of Alkenes and Alkynes with an Acyclic Silylene and Heavier Tetrylenes under Ambient

Conditions, *Organometallics* **2014**, *33*, 6253−6258 (c) Su, M.-S. and Chu, S.-Y. Theoretical Studies of the Additions of Germylenes to Ethylene, *J. Am. Chem. Soc.* **1999**, *121*, 11478-11485.

20. Lai. T.Y.; Guo, J.-D.; Fettinger, J.C.; Nagase, S. and Power P.P. Facile Insertion of Ethylene into a Group 14 Element-Carbon Bond: Effects of the HOMO–LUMO Energy Gap on Reactivity, *Chem Commun*. **2019**, *55*, 405-407
21. Lai, T.Y.; Britt, R.D.; Power, P.P. Germanium Hydride Radical Trapped during the Photolysis/Thermolysis of Diarylgermylene *Inorg. Chem.* **2019**, *58*, 15034-15038..
22. Stender, M.; Pu. L. and Power, P.P. Stabilized Terphenyl-Substituted Digermene Derivatives of Simple Organic Groups and Their Halide Precursors: Preference for Symmetrically Bonded Structures, *Organometallics*, **2001**, *20*, 1820-1824.
23. A video recording of the reversible reaction between $Ge(Ar^{iPr4})_2$ with ethylene is also given in the supporting information

Chapter 7

Reversible Complexation of Alkynes by a Germylene

This work is published in Organometallics, DOI: 10.1021/acs.organomet.9b00077

Lai, T.Y.; Gullett, K.L.; Chen, C.Y.; Fettinger, J.C.; Power, P.P. *Organometallics*, **2019**, *38*, 1421-1424.

7.1 Introduction

The reactions of heavier group 14 tetrylenes (ER_2; E= Si, Ge, Sn) with alkynes have attracted increasing interest due to their potential relevance for catalysis involving group 14 species.[1] The relatively modest energy gap between the occupied lone pair and empty valence frontier p-orbitals of the tetrylenes facilitate high reactivity so that reactions with alkynes may occur under ambient conditions (Scheme 1).[2] Several groups have shown that the heavier tetrylenes react with alkynes to afford either insertion or cycloadditon products.[3] However, examples of reversible reactions of alkynes with heavier tetrylenes remain extremely rare, in part because the product metallocyclopropenes are relatively stable, thereby hindering the reverse reaction. Calculations for the reaction of $Si(SAr^{iPr4})_2$[4] with alkenes and alkynes show that the product of its reaction with acetylene $(Ar^{iPr4}S)_2SiC(H)=C(H)$ is 51 kJ mol^{-1}; more favored than the product, $(Ar^{iPr4}S)_2SiCH_2\text{-}CH_2$, $Ar^{iPr4} = C_6H_3\text{-}2,6(C_6H_3\text{-}2,6\text{-}iPr_2)_2$, from its reaction with ethylene.[5] The activation barriers for both reactions were calculated to be 54 kJ mol^{-1} (Gibbs free energy of reactants set at zero) and the relative energy of the product is −75 kJ mol^{-1}. In addition, Ohshita and coworkers[6] reported high stability for the silacyclopropene, $Mes_2SiC(Ph)=C(Ph)$, which releases diphenylacetylene only upon heating at 250° C for 24h. Sekiguchi and coworkers[7] showed that the germacyclopropene $(^iPr_3Si)_2GeC(SiMe_3)=C(SiMe_3)$, releases

bis(trimethylsilyl)acetylene only upon reduction with lithium metal with formation of a 1,1-dilithiogermane $(^{i}Pr_3Si)_2GeLi_2$.

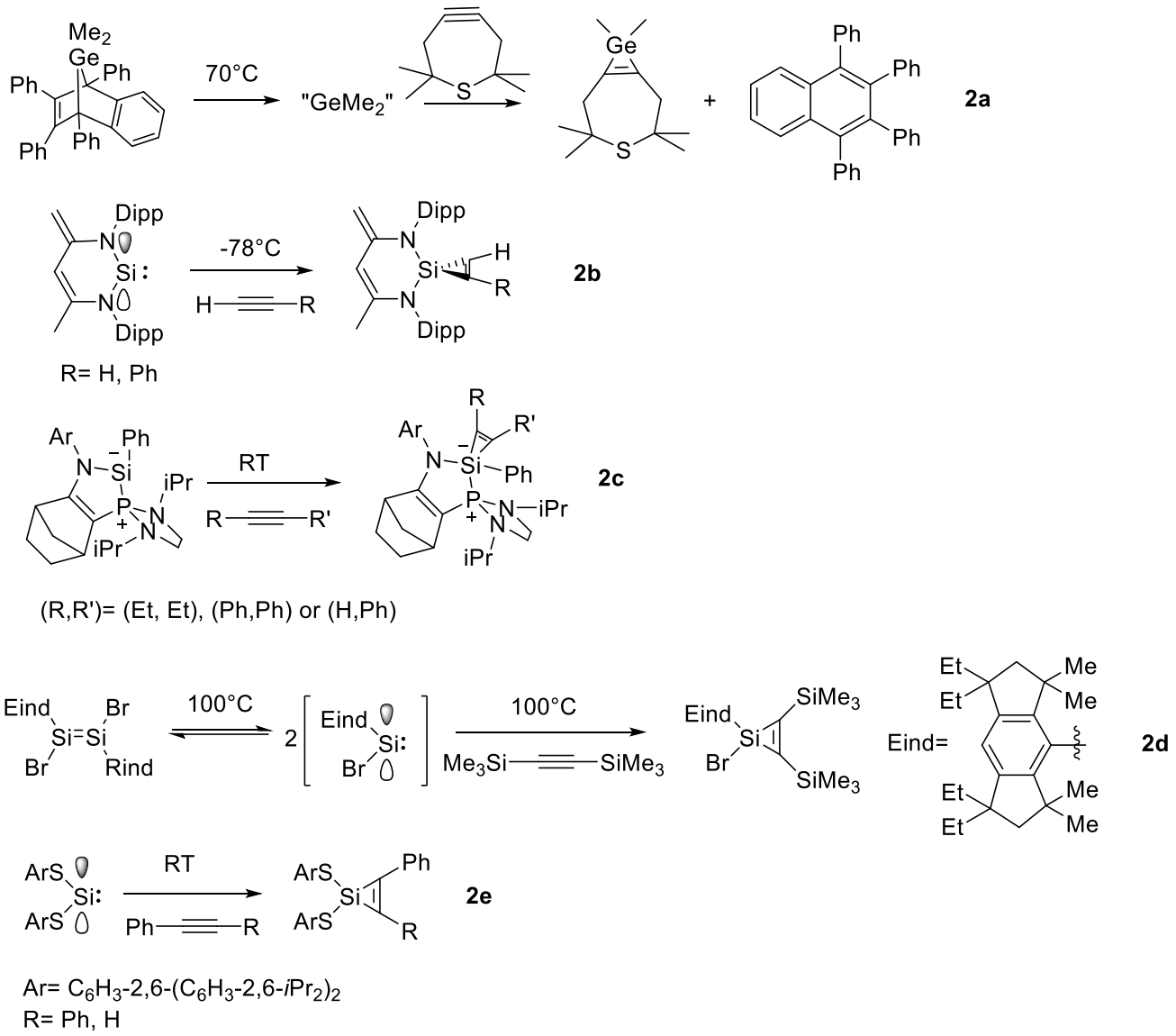

Scheme 1. Some reactions of tetrylenes with alkynes[2]

The only known reversible complexation of an alkyne by a tetrelyene was described by Sita and cowokers in 1988. In this case it involved a reaction with a strained alkyne 3,3,6,6-tetramethyl-1-thiacyclohept-4-yne which afforded the stannacyclopropene product as indicated in Scheme 2.[8]

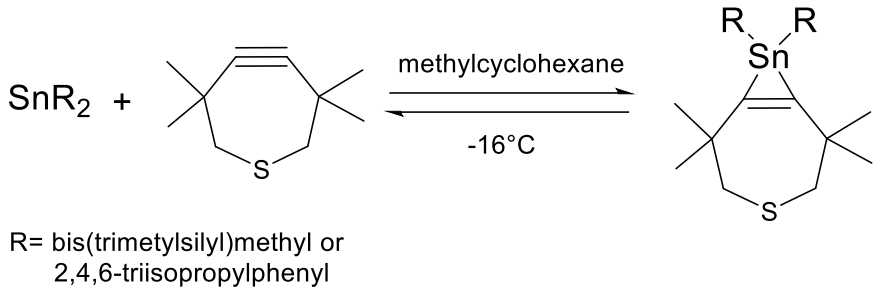

R= bis(trimetylsilyl)methyl or
2,4,6-triisopropylphenyl

Scheme 2. Reversible complexation of a strained cyclic alkyne with a diorganostannylene.[8]

The reaction is believed to occur as a result of the increased reactivity of the thiocycloheptyne arising from its strained structure. Calculations for the reaction of SnH_2 with HC≡CH to form the parent stannacyclopropene $H_2SnC(H)=C(H)$, show that it has a relatively low activation energy barriers (37.6 kJ mol^{-1}) for the forward and reverse reactions. It should be kept in mind that stannylenes are inherently more stable than their lighter congeners which also tends to favor olefin or alkyne dissociation.[9]

In contrast, reversible complexation of a strain free alkyne with heavier tetrylenes under ambient or near ambient conditions is currently unknown. In this chapter we report the reversible complexation of a diarylgermylene, $Ge(Ar^{Me6})_2$, (Ar^{Me6}= C_6H_3-2,6(C_6H_2-2,4,6-$Me_3)_2$) to four unstrained alkynes 3-hexyne, diphenylacetylene, trimethylsilylacetylene and phenylacetylene (**Scheme 3**). The germacyclopropene (germirene) products (**Scheme 3**) were isolated and the thermodynamic parameters for the reactions were analyzed by ^{1}H NMR spectroscopy. In addition, the structures of **1a** and **1d** were determined by X-ray crystallography.

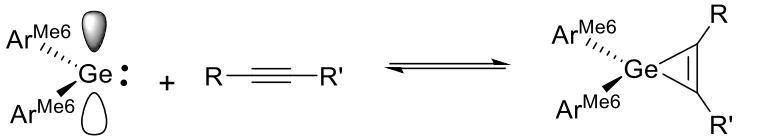

R = CH_2CH_3 , Ph, H, or $SiMe_3$

1a, R,R'= CH_2CH_3
1b, R,R'= Ph
1c, R,R'= H, $SiMe_3$
1d, R,R'= H, Ph

Scheme 3. Reversible complexation of alkynes by diarylgermylene.

7.2 Experimental Details

General Procedures. All operations were carried out under anaerobic and anhydrous conditions using modified Schlenk techniques. All solvents were dried over alumina columns, stored over an Na mirror and degassed prior to use. 3-hexyne, diphenylacetylene, trimethylsilylacetylene and phenylacetylene are stirred over sieves and distilled prior to use. $Ge(Ar^{Me6})_2$, (Ar^{Me6}= C_6H_3-2,6(C_6H_2-2,4,6-Me_3)$_2$) was prepared according to literature procedures.[S1] VT ^{1}H NMR data were recorded on a Bruker 500 instrument. The ^{1}H and ^{13}C NMR spectra were referenced to residual d8-toluene.

(Ar^{Me6})$_2$GeC(CH_2CH_3)C(CH_2CH_3) (1a): $Ge(Ar^{Me6})_2$ (0.5g 0.71mmol) was dissolved in hexane (*ca.* 15mL) and excess 3-hexyne (0.8mL, 7.1mmol) was added. The resulting colorless solution was stored at RT for 2 days affording **1a** as colorless crystals. Yield (0.31g, 55.9 %) Mp: 124°C (turned purple), ^{1}H NMR (400MHz, C_6D_6, 298K): 1.06 (t, 6H, $CH_2C\mathbf{H_3}$), 1.53 (s, 4H, CH_3) , 1.89 (s, 4H, CH_3), 2.02 (s, 4H, CH_3), 2.12 (m, 4H, $C\mathbf{H}_2CH_3$), 2.17 (s, 4H, CH_3), 2.28 (s, 4H, CH_3), 2.36 (s, 4H, CH_3), 6-8(m, 14H, aromatic Hs). ^{13}C NMR (126MHz, C_6D_6, 298K): 14.50, 20.82, 22.53, 23.02, 23.52, 128.60, 129.89, 130.81, 136.26, 137.81, 139.15, 142.55, 150.51.

$(Ar^{Me6})_2GeC(Ph)=CPh)$(1b): In a J. Young NMR tube, $Ge(Ar^{Me6})_2$ (0.033g 0.047mmol) added was dissolved in d8-toluene and 1 equivalent of diphenylacetylene (0.047mmol) was added. To ensure complete reaction the NMR sample, the NMR was left at RT for a day prior the NMR recording. ^{1}H NMR (500MHz, C_7D_8, 248K): 1.62 (s, 4H, CH_3), 1.66 (s, 4H, CH_3), 1.74 (s, 4H, CH_3), 1.92 (s, 4H, CH_3), 2.12 (s, 4H, CH_3), 2.34 (s, 4H, CH_3), 6-8, (m, 24H, aromatic Hs)

$(Ar^{Me6})_2GeC(H)=C(SiMe_3)$(1c): In a J. Young NMR tube, $Ge(Ar^{Me6})_2$ (0.033g 0.047mmol) added was dissolved in d8-toluene and 1 equivalent of trimethylsilylacetylene (0.047mmol) was added. To ensure complete reaction the NMR sample, the NMR was left at RT for a day prior the NMR recording. ^{1}H NMR (500MHz, C_7D_8, 218K): 0.06(s, 9H, Si**Me**$_3$), 1.79 (s, 24H, o-Me), 2.35 (s, 12H, p-Me), 6-8, (m, 14H, aromatic Hs), 8.62 (s, 1H, **H**C-Ge-CMe_3)

$(Ar^{Me6})_2GeC(H)=C(Ph)$(1d): $Ge(Ar^{Me6})_2$ (0.5g 0.71mmol) was dissolved in hexane (*ca.* 15mL) and excess phenylacetylene (0.8mL, 7.1mmol) was added. The resulting colorless solution was stored at RT for 2 days affording **1d** as colorless crystals. Yield (0.41g, 72%) Mp: 160°C (turned orange), ^{1}H NMR (400MHz, 298K): 1.77 (s, 24H, o-Me), 2.21 (s, 12H, p-Me), 6-7.3, (m, 19H, aromatic Hs), 7.51 (s, 1H, **H**C-Ge-CPh) ^{13}C NMR (126MHz, C_6D_6, 298K): 21.22, 22.38, 127.30, 127.51, 128.40, 128.81, 129.04, 130.44, 132.96, 136.56, 136.96, 137.61, 138.67, 141.22, 149.11, 153.89

Variable temperature ^{1}H NMR spectroscopy and Van't Hoff analysis of 1a

The integration for the signal atoms of the, o-Me group of $Ge(Ar^{Me6})_2$, terminal methyl groups for 3-hexyne and compound **1a** were used for the determination of the equilibrium constant for the conversion of the germylene with 3-hexyne to give the germirene.

The equilibrium constant was calculated according to equation 1.

$$K_{eq} = \frac{[Germirene]}{[Germylene][3-hexyne]} \text{ (eq1)}$$

The Van't Hoff equation, equation 2, was used in order to determine ΔH and ΔS from the slope and the intercept of the plot of ln Keq against 1/T.

$$lnK_{eq} = -\frac{\Delta H}{R}\left(\frac{1}{T}\right) + \frac{\Delta S}{R} \text{ (eq. 2)}$$

7.3 Results and Discussion

The work herein consists of a collaborative effort of Ms. Kelly L. Gullett, Ms. Chia-Yuan Chen and myself. Ms. Gullett initiated the study. The synthesis, reaction characterization, and variable temperature ^{1}H NMR was carried out by me with the assistance of Ms. Chen. I am responsible for the construction of the paper.

The diarylgermylene, $Ge(Ar^{Me6})_2$ (Ar^{Me6} = C_6H_3-2,6-(C_6H_2-2,4,6-Me_3)$_2$),[10] was reacted with an excess of the alkyne in hexanes. The color of the solution immediately changed from purple to colorless. Concentration of the solutions under reduced pressure, and storage at room temperature overnight resulted in colorless crystals in moderate yields. Crystals of **1a** and **1d** proved amenable for X-ray crystallographic studies. The structures (Figure 1) of **1a** and **1d** illustrate that the alkyne forms a [1+2] cycloaddition product with the

germylene. The resulting germirenes have C=C distances of 1.33(3)Å(**1a**) and 1.3351(2)Å (**1d**) which are in the typical range for a carbon-carbon double bond (cf. 1.339 Å in ethylene).[11] The Ge-C bonds in the germirene span the range 1.92-1.97 Å which is slightly shorter than the sum (1.98 Å) of the covalent radii of carbon (0.77Å) and germanium (1.21Å).[12] The C-Ge-C germirene angles are 40.573(9)°(**1a**) and 40.672(9)°(**1d**) and the C-Ge-C angles between the two aryl Ar^{Me6} ligands are 115.079(2)° and 117.483(10)°.

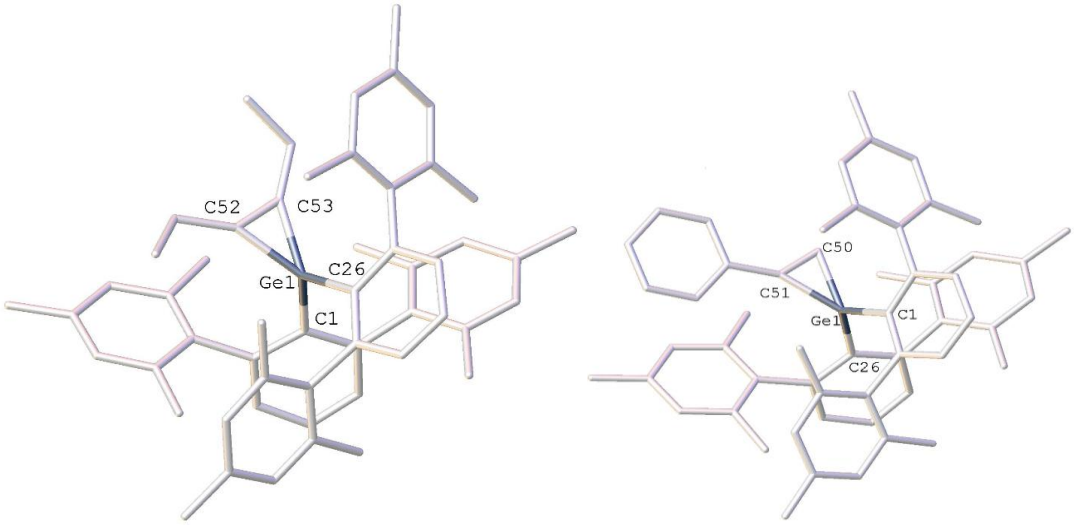

1a **1d**

Figure 1. Stick drawing of the crystal structures of **1a** and **1d**. Hydrogen atoms are not shown. Selected bond distances (Å) and angles (deg): **1a**: Ge1-C1:1.970(2), Ge1-C26: 1.9730(19), Ge1-C52: 1.91928(6) Ge1-C53: 1.92611(5) C52-C53: 1.33(3) C11-Ge1-C17: 40.573(9), C3-Ge1-C7:115.079(2) **1d**: Ge1-C1: 1.9680(16), Ge1-C26:1.9670(13), Ge1-C51: 1.9277(3) Ge1-C50: 1.9139(3) C51-C50: 1.3351(2) C51-Ge1-C50: 40.672(9) C1-Ge1-C26:117.483(10).

The Ge-C and C=C bond distances are similar to those in the small number of known germirenes which span the range 1.88-1.929 Å and 1.324-1.39 Å.[13-16] The C-Ge-C

germacyclopropene ring angle is also in close agreement with those in the reported germirenes $Me_2Ge(C_{10}H_{16}S)$ (40.5(3)°),[2a] $Ar_2GeC(CF_3)=C(CF_3)$ (Ar= 2-tert-butyl-4,5,6-trimethyl-phenyl) (39.94(13)°),[13] $\{(Me_3Si)_2CH\}_2Ge(C_{14}H_{17}N_3O)$ (43.3(6)°),[14] and $[(IDipp)\{(SiMe_3)CH\}GeC(H)=C(Ph))][BAr^F_4]$ (40.79(15)°).[15]

The angles between the two terphenyl ligands in the germirene **1a** (115.079(2)°) and **1d** (117.483(10)°), display only small changes from that in the precursor germylene (114.4(2)°). It seems likely that this small difference facilitates the reversibility of the reaction since the C-Ge-C angle remains almost unchanged during the process.

The ^{1}H NMR spectrum of **1a** (*cf* Figure AVI1.) shows that the signal for terminal methyl group of the uncomplexed 3-hexyne molecule (1.00 ppm) is shifted upfield to 0.94 ppm upon binding the alkyne. A Van't Hoff analysis of the association of 3-hexyne using variable temperature (276- 318 K) ^{1}H NMR spectroscopy affords the values ΔH_{assn}= -16±1.12 kJmol^{-1}, $\Delta S_{assn=}$ -36.62±2.56 J K^{-1} mol^{-1} and ΔG_{assn}= -5.11±0.36 kJ mol^{-1} at 298K. Similarly, a Van't Hoff analysis of the association of diphenylacetylene using variable temperature (258-298 K) ^{1}H NMR spectroscopy affords ΔH_{assn}= -6.47±0.61 kJ mol^{-1}, $\Delta S_{assn=}$ -2.65±0.25 J K^{-1} and ΔG_{assn}= -5.65±0.536 kJ mol^{-1} at 298K. The corresponding data for the reaction (208- 248 K) with trimethylsilylacetylene are ΔH_{assn}= -42.48±2.97 kJ mol^{-1}, $\Delta S_{assn=}$ -159.9±11.2 J K^{-1} mol^{-1} and a positive ΔG_{assn}(calculated)= 5.16±0.36 kJ mol^{-1} at 298K and ΔG_{assn}(observed)= -2.83±0.20 kJ mol^{-1} at 248K. For the reaction with phenylacetylene the ^{1}H NMR spectrum displays little change up to 353K. However, when **1d** was dissolved in toluene at room temperature, the solution displayed a very pale purple color (Figure S10) indicating that there is a small amount of dissociation, but the concentration of pure germylene was not high enough to be observed by ^{1}H NMR spectroscopy.

For the previously known irreversible reaction of $Si(SAr^{iPr4})_2$ with an alkyne, calculations for the reaction with acetylene yielded the aforesaid activation barrier of 54 kJ mol^{-1}, and ΔG_{assn}= -75 kJ mol^{-1} [4a] as well as a reverse reaction barrier of 129 kJ mol^{-1}. Furthermore, calculations for the reaction of GeH_2 with acetylene at the B3LYP level, shows that ΔG_{assn}= -132 kJ mol^{-1}.[17] The bonding arises from the relatively strong interaction of germylene and acetylene orbitals, to form the germirene, and diminution of the repulsion from the lone pair thereby overcomes the steric repulsion between the two nearby reactants.

For our compounds, the experimental Gibbs free energies are relatively low: **1a** has a ΔG_{assn} value of -5.11 kJ mol^{-1}(298K). For **1b** and **1c** the corresponding values are -5.65 kJ mol^{-1}(298K) and -2.82 kJ mol^{-1}(248K). The relatively small differences in energy may be a reflection of the lack of requirement to distort the geometry of the $Ge(Ar^{Me6})_2$ moiety upon reaction with the alkynes. It is also noteworthy that it is the reactions with the larger alkynes diphenylacetylene, trimethylsilylacetylene and 3-hexyne that are the most reversible perhaps for steric reasons although there may be countered by attractive London dispersion forces. These reactions have ΔG_{assn} values that are slightly negative for **1a** and **1b** and slightly positive for **1c** (ΔG_{assn}= -2.83 kJ mol^{-1} at 248K and ΔG_{assn}= 5.165 kJ mol^{-1} at 298K) at room temperature. In contrast the reaction with the smaller alkyne phenylacetylene approaches irreversiblility with sufficiently limited dissociation in solution that the concentration of $Ge(Ar^{Me6})_2$ is not easily observable by ^{1}H NMR spectroscopy.

7.4 Conclusions

In conclusion, diarylgermylene $Ge(Ar^{Me6})_2$ has been shown to react reversibly with diphenylacetylene, trimetylsilylacetylene and 3-hexyne. Tighter binding was observed with

the less bulky alkyne phenylacetylene although a small equilibrium concentration of the free germylene is apparent from the very faint purple color that appears on dissolving **1d** in toluene.

7.5 References

1. (a) Power P.P. "Main-group elements as transition metals", *Nature*, **2010**, *463*, 171-177 (b) Weetman C., and Inoue S. "The Road Travelled: After Main-Group Elements as Transition Metals" *ChemCatChem* **2018**, *10*, 4213-4288. (c) Erickson, J.D.; Lai, T.Y.; Liptrot, D.J.; Olmstead, M.M.; and Power, P.P.; "Catalytic dehydrocoupling of amines and boranes by an incipient tin(II) hydride" *Chem Commun.* **2016**, *52*, 13656-13659

2. (a) Egorov, M.P.; Kolesnikov, S.P.; Struchkov, Y.T.; Antipin, M.Y.; Sereda, S.V.; and Nefedov, O.M.; "The isolation and X-ray crystal structure of $\Delta^{1,7}$ 2,2,6,6-tetramethyl-4-thia-8,8-dimethyl-8-germabicyclo[5.1.0]octene; The first representative of germirenes" *J. Orgnaomet. Chem.* **1985**, *290*, c27-c30. (b) Yao, S.; van Wullen, C.; Sun, S.-Y. and Driess M.; Dichotomic Reactivity of a Stable Silylene toward Terminal Alkynes: Facile C-H Bond Insertion versus Autocatalytic Formation of Silacycloprop-3-ene" *Angew. Chem. Int. Ed.* **2008,** *47*, 3250-3253. (c) Gau, D.; Rodriguez, R.; Kato, T.; Saffron-Merceron, N.; Baceiredo, A.; "Diastereoselective Synthesis of Bulky, Strongly Nucleophilic, and Configurationally Stable P-Stereogenic Tricyclic Phosphines" *J. Am. Chem. Soc.* **2010**, *132*, 12841-12843. (d) Suzuki, K.; Matuso, T.; Hashizume, D.; and Tamao, K.; "Room-Temperature Dissociation of 1,2-Dibromodisilenes to Bromosilylenes" *J. Am. Chem. Soc.* **2011**, *133*, 19710-19713

3. (a) Sita, L. R.; Bickerstaff, R. D. “Investigation of the Factors Influencing the Structure and Stability of Stannacyclopropenes: The Synthesis and Molecular Structure of Two Derivatives” *Phosphorus, Sulfur, Silicon Relat. Elem.* **1989**, *41*, 31−36. (b) Krebs, A.; Berndt, J. “Synthese zweier germirene” *Tetrahedron Lett.* **1983**, *24*, 4083−4086. (c) Ishida, S.; Iwamoto, T.; Kira, M. “Addition of a stable dialkylsilylene to carbon–carbon unsaturated bonds” *Heteroat. Chem.* **2011**, *22*, 432−437.

4. Rekken, B.D.; Brown, T.M.; Fettinger, J.C. and Power, P.P. “Isolation of a Stable, Acyclic, Two-Coordinate Silylene” *J. Am. Chem. Soc.*, **2012**, *134*, 6504–6507

5. (a) Lips, F; Fettinger, J.C.; Masikkamäki, A..; Tuononen, H. M.; Power, P. P. “Reversible Complexation of Ethylene by a Silylene under Ambient conditions” *J. Am. Chem. Soc.* **2014**, *136*, 634-637 (b) Lips, F.; Masikkamäki, A.; Fettinger, J. C.; Tuononen, H. M.; Power, P. P. “Reactions of Alkenes and Alkynes with an Acyclic Silylene and Heavier Tetrylenes under Ambient Conditions” *Organometallics* **2014**, *33*, 6253−6258. (c) Gordon, M.S. “Ring strain in cyclopropane, cyclopropene, silacyclopropane, and silacyclopropene” *J. Am. Chem. Soc.* **1980**, *102*, 7419-7422. (d) Tsumuraya, T.; Batcheller, S.A. and Masamune, S. “Strained-Ring and Double-Bond Systems Consisting of the Group 14 Elements Si, Ge, and Sn” *Angew. Chem. Int. Ed. Engl.* **1991**, *30*, 902-930.

6. Ohshita J., Honda N., Nada K., Lida T., Mihara T., Matsuo Y., Kunai A., Naka A., and Ishikawa M. “Substitution Effects on the Thermal Extrusion of Silylenes from 1,1-Diarylsilacyclopropenes” *Organometallics*, **2003**, *22*, 2436-2441

7. Sekiguchi, A.; Izumi, R.; Ihara, S.; Ichinohe, M. and Lee, V.Y. “The First Isolable 1,1-Dilithiogermane and Its Unusual Dimeric Structure—An Effective Reagent for the

Preparation of Double-Bonded Derivatives of Group 14 Elements" *Angew. Chem Int. Ed.* **2002**, *41*, 1598-1600

8. Sita, L. R.; Bickerstaff, R. D. " Synthesis and crystal structure of the first stannacyclopropene derivative" *J. Am. Chem. Soc.* **1988**, *110*, 5208-5209

9. (a) Sita, L. R.; Kinoshita, I.; Lee, S. P. " Reactions of stannylenes with alkynes: synthesis and chemical reactivity of a stable 1,2-distannacyclobut-3-ene derivative" *Organometallics* **1990**, *9*, 1644-1650 (b) Boatz, J. A.; Gordon, M. S.; Sita, L. R. " Theoretical studies of the metallacyclopropenes *c*-$[MX_2C_2H_2]$ (M = C, Si, Ge, Sn; X = H, F)" *J. Phys. Chem.***1990**, *94*, 5488-5493

10. Simons, R.S.; Pu, L.; Olmstead, M.M.; and Power, P.P." Synthesis and Characterization of the Monomeric Diaryls $M\{C_6H_3\text{-}2,6\text{-}Mes_2\}_2$ (M = Ge, Sn, or Pb; Mes = 2,4,6-$Me_3C_6H_2$−) and Dimeric Aryl−Metal Chlorides $[M(Cl)\{C_6H_3\text{-}2,6\text{-}Mes_2\}]_2$ (M = Ge or Sn)" *Organometallics*, **1997**, *16*, 1920-1925.

11. (a) Smith, M.B.; March,J. Advanced Organic Chemistry 5th Ed., Wiley, New York, 2001, Chapter 1, p20. (b) Lide, D. R. Handbook of Chemistry and Physics; Chemical Rubber: Boca Raton, **1995**.

12. Pyykkö, P.; Atsumi, M. "Molecular Single-Bond Covalent Radii for Elements 1–118" *Chem. - Eur. J.* **2009**, *15*, 186−197.

13. Meiners, F.; Saak, W.; Weidenbruch, M. "A Germacyclopropene with Electronegative Groups at the Ring Carbon Atoms" *Z. Anorg. Allg. Chem.* **2002**, *628*, 2821-2822.

14. Ando, W.; Ohgaki, H.; Kabe, Y. "Stable Germirane Derivatives" *Angew. Chem. Int. Ed. Engl.* **1994**, *33*, 659-661

15. Rit, A.; Tirfoin, R.; Aldridge, S. "Exploiting Electrostatics to Generate Unsaturation: Oxidative Ge=E Bond Formation Using a Non π-Donor Stabilized [R(L)Ge:]$^{+}$ Cation" *Angew. Chem., Int. Ed.* **2016**, *55*, 378−382

16. A video recording of the reversible reaction between Ge(Ar^{Me6})$_2$ with 3-hexyne is also given in the supporting information.

17. Becerra, R.; Boganov, S.E.; Egorov, M.P.; Faustov, P.E.; Kyrlova, I.V.; Nefedov, O.M.; Promyslov, V.M.; and Walsh R. "An investigation of the germylene addition reaction, GeH_2+C_2H_2: Time-resolved gas-phase kinetic studies and quantum chemical calculations of the reaction energy surface" *Phys. Chem. Chem. Phys*., **2004**, *6*, 3370–3382

Chapter 8

Catalytic Dehydrocoupling of Amines and Boranes by an Incipient Tin(II) Hydride

This work is published in Chemical Communication, DOI: 10.1039/C6CC06963K

Erickson, J. D.; **Lai, T. Y.;** Liptrot, D. J.; Olmstead, M. M.; Power, P. P. *Chem. Commun.* **2016**, *52*, 13656-13659.

8.1 Introduction

Aminoboranes, $R_2N\text{-}BR'_2$, have a growing utility in modern synthetic chemistry. Suginome and coworkers have documented their use as efficient but mild sources of iminium cations that may be used in the reductive amination of aldehydes,[1] in Mannich-type couplings of aldehydes, secondary amines, and silyl ketene acetals.[2] Strecker-type aminative cyanation of aldehydes and ketones to α-amino nitriles through the use of bis(dialkylamino)cyanoboranes has also been explored.[3] Sole and coworkers have further shown aminoboranes may be effective sources of amide ions for β-aminations of α,β-unsaturated carbonyl compounds and cyclic vinyl epoxides.[4] Nikonov and co-workers described a chemoselective imine formation via the reaction of bisborylamines with C=O bonds.[5]

Aminoboranes have previously been synthesized through the action of silicon-nitrogen[6-8] and tin-nitrogen[9-11] bonds upon boranes and haloboranes. Salt metathesis of lithium amides ($R_{3-n}H_nNLi$) (n = 1, 2, 3) with BCl_3 has also been used to afford $(R_{3-n}H_nN)_mBCl_{3-m}$ (m = 1, 2, 3) species.[12, 13] Transamination of triaminoboranes, $B(NR_2)_3$ with secondary amines,

R´$_2$NH, affords unsymmetrical triaminoboranes, $(R_2N)_2BNR´_2$.[14] The production of stoichiometric by-products such as potentially toxic group 14 halides and amines in the aforementioned syntheses, however, makes them unfavorable. Aminoborane production using dehydrogenative coupling between 9-borabicyclo[3.3.1]nonane (9-BBN) and protic amines has been reported,[15-18] and reactivity exists between amines and pinacolborane,[19] but these synthetic routes have not been applied to the parent amine- ammonia.

Catalytic hydroboration of imines has been shown to give access to bisborylamines.[5, 20, 21] The catalytic dehydrocoupling of amine-boranes, $R_nNH_{3-n}\cdot BH_3$ (n = 0, 1, 2), has been a subject of broad study due to their potential use in hydrogen storage applications.[22-28] These reactions are traditionally catalyzed by transition-metal complexes[22, 29] to produce a range of oligoborazane products, although some examples of main-group catalyzed dehydrocouplings also exist.[30, 31] The catalytic dehydrocouplings of amines with monohydrido boranes, however, are limited to a handful of examples.

The sole transition-metal catalyzed dehydrocoupling of amines with monohydridoboranes is Westcott and coworkers' rhodium-based dehydrocoupling.[32] Hill and coworkers have reported a dehydrocoupling of pinacolborane (HBPin) or 9-borabicyclo[3.3.1]nonane (9-BBN) with a range of primary and secondary amines to produce both aminoboranes and amino(diboranes) using the magnesium species β-diketiminate species [(HC{(CMe)(N{C_6H_3-2,6-*i*Pr)}$_2$)MgBu].[33] More recently, Roesky and coworkers have used the aluminum dihydride species (HC{CMe(N{C_6H_3-2,6-Et}$_2$)AlH_2 for the dehydrocoupling of HBPin with a range of amines, thiols, and alcohols.[34] Herein we demonstrate catalytic dehydrocoupling for the first time by group 14 compounds, herein the using terphenyl tin(II) methoxides ({$Ar^{Me}{}_6$Sn(μ-OMe)}$_2$, **1**, and {$Ar^{iPr}{}_4$Sn(μ-OMe)}$_2$), **2**, as pre-catalysts.

8.2 Experimental Details

General experimental procedures.

All manipulations were performed under strictly anhydrous and anaerobic conditions by use of modified Schlenk techniques. All solvents were initially dried using a Grubbs-style solvent purification system and further dried over NaK. Pinacolborane was purchased from Synquest and distilled prior to use. All amines were dried over calcium hydride and distilled prior to use. All NMR spectroscopy was carried out on a Bruker 400 MHz spectrometer. ^{119}Sn NMR was referenced to $SnBu_4$ (-11.7 ppm). Infrared spectroscopy was collected as a Nujol mull using a Bruker Tensor 27 IR spectrometer. Melting points were measured using a Mel-Temp II apparatus using capillary tubes sealed under a nitrogen atmosphere and **1** was synthesized as below and compared to literature.

$\{Ar^{Me_6}SnOMe\}_2$ (1). $\{Ar^{Me_6}SnCl\}_2$ (1.545 g, 3.30 mmol) in Et_2O (*ca.* 50 mL) was cooled to 0 °C and NaOMe (0.1785 g, 3.30 mmol) as a slurry in Et_2O (*ca.* 30 mL) was added dropwise over 30 minutes. The mixture was allowed to warm to room temperature overnight. The resultant yellow solution was filtered and the Et_2O removed under reduced pressure. The remaining yellow powder was washed with cold hexanes (*ca.* 5 mL) to afford **1** as a fine yellow powder. Yield: 1.33 g, 87%.

$\{Ar^{iPr_4}SnOMe\}_2$ (2). $\{Ar^{iPr_4}SnCl\}_2$ (0.5155 g, 0.4672 mmol) in Et_2O (*ca.* 60 mL) was cooled to 0 °C and NaOMe (0.0505 g, 0.9343 mmol) as a slurry in Et_2O (*ca.* 25 mL) was added dropwise over 30 minutes. The mixture was allowed to warm to room temperature overnight. The Et_2O was removed under reduced pressure and hexane (*ca.* 50 mL) was added. The mixture was filtered via cannula, its volume reduced to *ca.* 20 mL, and stored at *ca.* -28 °C overnight to afford orange/yellow crystals. Yield: 0.355 g, 70%. M.p.: 159-166 °C. ^{1}H NMR (400 MHz,

C_6D_6, 25 ºC, ppm): 1.13 (m, 24H, CH(C**H**$_3$)$_2$), 2.11 (s, 6H, OMe), 2.91 (sept, 4H, C**H**(CH$_3$)$_2$), 7.05 (m, 2H), 7.12 (m, 4H), 7.19 (d, 8H, *m*-C_6H_3), 7.31 (t, 4H, *p*-C_6H_3). $^{13}C\{^1H\}$ NMR (126MHz, C_6D_6, 25° C, ppm): 24.37, 24.48, 30.79, 122.90, 129.34, 131.47, 139.73, 141.11, 146.90. IR: 2920 (br), 2850 (s), 1590 (w), 1560 (w), 1450 (m), 1370 (m), 1250 (w), 1050 (br), 800 (w), 750 (w), 710 (w).

{Ar^{Me_6}Sn(μ-NEt$_2$)}$_2$ (3). {Ar^{Me_6}SnCl}$_2$ (0.7902 g, 0.8450 mmol) in Et$_2$O (*ca.* 35 mL) was cooled to 0 °C and LiNEt$_2$ (0.1236 g, 0.9343 mmol) in Et$_2$O (*ca.* 30 mL) was added dropwise over 30 minutes. The mixture was allowed to warm to room temperature overnight. The Et$_2$O was removed under reduced pressure and toluene (*ca.* 50 mL) was added. The mixture was filtered via cannula to afford a copper-colored solution which was reduced in volume to *ca.* 10 mL. Storage at -28 °C for three days afforded copper-colored powder of **3**. Yield:0.176 g, 22.2%. M.p.: 139-144 °C, ^{1}H NMR (400 MHz, C_6D_6, 25 ºC, ppm): 0.81 (t, J_{HH} = 7.0 Hz, 12H, NCH$_2$C**H**$_3$), 2.12 (s, 12H, *p*-Me), 2.27 (s, 24H, *o*-Me), 3.47 (m, 8H, NC**H**$_2$CH$_3$), 6.84 (s, 8H, C_6**H**$_2$), 7.12 (d, J_{HH} = 7.5 Hz, 4H, *m*-C_6H_3), 7.31 (t, J_{HH} = 7.5 Hz, 2H, *p*-C_6H_3). $^{13}C\{^1H\}$ NMR (126MHz, C_6D_6, 25° C, ppm): 20.63, 20.72, 20.89, 21.12, 21.56, 21.71, 128.71, 128.87, 135.24, 135.96, 136.23, 136.65, 138.71, 146.82, 148.60, 175.52. IR: 2950(s), 2900(s), 2850(s), 2650 (br), 1450(m), 1375(m), 1260(s), 1100(m), 1000(m), 800(s), 700(s).

Ar^{Me_6}Sn(μ-NEt$_2$)(μ-H)SnAr^{Me_6} (4). {Ar^{Me_6}SnCl}$_2$ (0.255g, 0.253mmol) in Et$_2$O (*ca.* 20 mL) was cooled to -78 °C and HBPin (36.4μl, 0.253mmol) in Et$_2$O (*ca.* 40 mL) was added dropwise over 30 minutes. The mixture was stirred for 30 min and Et$_2$O was removed under reduced presssure and toluene (*ca.* 70 mL) was added. The resulting mixture was filtered via cannula to afford a copper-colored solution. The toluene was removed under reduced pressure and pentane (*ca.* 30 mL) was added. The mixture was sonicated briefly (ca. 5 minutes) and then allowed to sit until all solid settled. The standing liquor was decanted and the remaining solid

dried under reduced pressure to afford **4** as a yellow powder. Yield: 20%. M.p.: 139-144 ºC. ^{1}H NMR (400 MHz, C_6D_6, 25 ºC, ppm): 0.63 (t, J_{HH} = 7.0 Hz, 6H, $NCH_2C\mathbf{H}_3$), 2.04 (s, 12H, *p*-Me), 2.18 (s, 12H, *o*-Me), 2.26 (s, 12H, *o*-Me), 2.34 (dq, J_{HH} = 13.5/6.7 Hz, 1H, $NC\mathbf{H}_2CH_3$), 2.86 (dq, J_{HH} = 13.5/6.7 Hz, 1H, $NC\mathbf{H}_2CH_3$), 4.10 (s, 1H, Sn**H**Sn, ^{119}Sn satellites $J_{H^{119}Sn}$ = 64 Hz), 6.85 (s, 4H, *m*-C_6H_2), 6.87 (s, 4H, *m*-C_6H_2), 6.92 (d, J_{HH} = 7.5 Hz, 4H, *m*-C_6H_3), 7.12 (t, J_{HH} = 7.5 Hz, 2H, *p*-C_6H_3). ^{13}C{^{1}H} NMR (126MHz, C_6D_6, 25° C, ppm): 16.73 ($NCH_2C\mathbf{H}_3$), 21.28 (*p*-Me), 21.95 (*o*-Me), 22.10 (*o*-Me), 45.50 ($NC\mathbf{H}_2CH_3$), 128.58, 129.09, 129.59, 135.62, 136.35, 136.62, 148.99, 169.37 IR: 2920 (br), 2720 (s), 1450 (s), 1370 (s), 1300 (m), 1255 (s), 1090 (br), 1015 (s), 950 (w), 800 (s), 720 (s),

8.3 Results and Discussion

The work herein consists of a collaborative effort between Jeremy D. Erickson, Dr. David J. Liptrot and myself. I was responsible for the synthesis, characterization, and catalytic study of $\{Ar^{iPr4}Sn(\mu\text{-}OMe)\}_2$, whereas Dr. Erickson carried out the experiments with $Ar^{Me6}Sn(\mu\text{-}OMe)\}_2$. The paper was written in collaboration with J.D. Erickson, Dr. D.J. Liptrot and Prof. P.P. Power.

In an initial investigation, addition of the islolated hydrides $\{Ar^{Me_6}SnH\}_4$[35] and $\{Ar^{iPr_4}SnH\}_2$[36] to a solution of diethylamine and pinacolborane yielded no discernable N-B coupled product. However, Jones and coworkers have previously used a tin(II) alkoxide as a pre-catalyst, which is converted to a tin(II) hydride *in situ*, for the hydroboration of carbonyls.[37] Gratifyingly, addition of one equivalent of HBPin to $\{Ar^{Me_6}Sn(\mu\text{-}OMe)\}_2$, **1**,[38] produced resonances in the ^{1}H and ^{11}B NMR spectra which indicated formation of $\{Ar^{Me_6}SnH\}_4$ and PinBOMe.[37] Addition of a catalytic amount of $\{Ar^{Me_6}Sn(\mu\text{-}OMe)\}_2$ to a solution of Et_2NH and

HBPin afforded visible gas evolution and the ^{11}B NMR spectrum indicated the disappearance of the doublet HBPin signal at 28 ppm and the appearance of a singlet at 24 ppm, that matched the reported chemical shift of $PinBNEt_2$ (See SI).[33]

To investigate the scope of the catalytic activity accessible with the pre-catalysts **1** and **2**, the reactions of HBPin with a range of primary and secondary amines were carried out using 2.5 mol % of the pre-catalysts in C_6D_6 at *ca.* 298 K (Table 1).

Table 1. Amines dehydrocoupled with HBPin catalyzed by **1** and **2** (Scheme 1).

$R^1R^2NH + HBPin \xrightarrow[2.5\ \%\ \{ArSnOMe\}_2\ (Ar = Ar^{Me_6}, Ar^{iPr_4})\ C_6D_6]{} R^1R^2N{-}BPin + H_2$

	Catalyst:	**{Ar^{Me_6}Sn(μ-OMe)}$_2$ (1)**			**{Ar^{iPr_4}Sn(μ-OMe)}$_2$ (2)**		
Amine	**Product**	**Reaction**	**t(h)**	**Conv. (%)**	**Reaction**	**t(h)**	**Conv. (%)**
*n*BuNH$_2$	PinBN(H)*n*Bu	1a	10	99	1b	1	99
*s*BuNH$_2$	PinBN(H)*s*Bu	2a	13	99	2b	48	30
Aniline	PinBN(H)Ph	3a	12	99	3b	2	99
4-Fluoroaniline	PinBN(H)(4-F-Ph)	4a	5	99	4b	1	99
4-Chloroaniline	PinBN(H)(4-Cl-Ph)	5a	9	99	5b	2	99
4-Bromoaniline	PinBN(H)(4-Br-Ph)	6a	9	99	6b	2	99
4-Ethylaniline	PinBN(H)(4-C$_2$H$_5$-Ph)	7a	26	95	7b	3	99
2,6-Diisopropylaniline	PinBN(H)Dipp	8a	78	70	8b	-	-
3,5-Dichloroaniline	PinBN(H)(3,5-Cl-Ph)	9a	7	99	9b	2	99
Et$_2$NH	PinBNEt$_2$	10a	9	99	10b	-	-
*i*Pr$_2$NH	PinBN*i*Pr$_2$	11a	10	99	11b	-	-
Cy$_2$NH	PinBNCy$_2$	12a	49	99	12b	-	-
Ph$_2$NH	PinBNPh$_2$	13a	100	15	13b	-	-

$(Me_3Si)_2NH$	No reaction	14a	-	-	14b	-	-
NH_3	$PinBNH_2$	15a	12*	99	15b	12*	99
$PinBNH_2$	$(PinB)_2NH$	16a	12*	99	16b	12*	99

Reaction conditions: $\{Ar^{Me_6}Sn(\mu\text{-}OMe)\}_2$ (1.85 μmol) or $\{Ar^{iPr_4}Sn(\mu\text{-}OMe)\}_2$ (1.85 μmol) with amines (74.1 μmol) and pinacolborane (74.1 μmol) in C_6D_6 (0.60 mL) at room temperature, determined by ^1H NMR and ^{11}B spectroscopy. See SI for ^1H, ^{11}B, and ^{13}C spectra of products. *Reactions with NH_3 were carried out at low temperature and warmed slowly overnight (*ca.* 12h), precluding the accurate assessment of reaction times.

The majority of reactions proceeded with >99% conversion to the aminoborane, most within 24 hours, slowing or failing only with bulky amines (Scheme 1). For example, the dehydrocoupling of dicyclohexylamine and HBPin $\{Ar^{Me_6}Sn(\mu\text{-}OMe)\}_2$ (entry 14a) required 49 hours to reach completion, and the dehydrocoupling of diphenylamine or 2,6-diisopropylaniline with HBPin (entries 10a, 15a) did not reach completion after 3-4 days. The dehydrocoupling of hexamethyldisilazane (entry 16a) with HBPin was not observed. No evidence of dehydrocoupling was observed when $\{Ar^{iPr_4}Sn(\mu\text{-}OMe)\}_2$ was added to HBPin and these amines (entries 14b, 15b, 16b). Furthermore, no reaction was observed for 2,6-diisopropylaniline, iPr$_2$NH, or diethylamine with HBPin (entries 10b, 12b, and 13b) with this catalyst. We attribute this difference in reactivity to the greater steric demands of the Ar^{iPr_4} ligand. The dehydrocoupling rate of HBPin and anilines (entries 4-7) was also dependent on the aryl ring substituents. Para-fluorine, -bromine, and -chlorine substituents all increase the rate of reaction relative to aniline, whereas para-ethylaniline displayed a slower rate of dehydrocoupling with HBPin.

The background reaction for a number of these dehydrocouplings was assessed at the concentrations used for the catalytic study; in each case after 12 hours the conversion was very low (*n*-butylamine 32%; diethylamine, 20%; 4-ethylaniline, 26%) or non-existent (ammonia) indicating the importance of **1** and **2** as precatalysts. Hill and coworkers reported dehydrocoupling of amines and boranes using a 10% loading of [(HC{(CMe)(N{C_6H_3-2,6-*i*Pr_2})}$_2$)MgBu] and observed full conversion to the aminoborane within one hour.[33] While dehydrocoupling reactions using {Ar$^{Me}{}_6$Sn(μ-OMe)}$_2$ and {Ar$^{iPr}{}_4$Sn(μ-OMe)}$_2$ also largely reach full conversion, the reaction times are notably slower. Furthermore, attempts to synthesize aminodi(boranes) from the primary amines of entries 1-9 by the addition of two-fold excess of HBPin were unsuccessful at room temperature. We again attribute these difference to the steric demands of the terphenyl ligands. However, the conversion times by {Ar$^{Me}{}_6$Sn(μ-OMe)}$_2$ and {Ar$^{iPr}{}_4$Sn(μ-OMe)}$_2$ are shorter than the aluminum-catalyzed dehydrocoupling of amines and boranes observed by Roesky and coworkers.[34]

Both {Ar$^{Me}{}_6$Sn(μ-OMe)}$_2$ and {Ar$^{iPr}{}_4$Sn(μ-OMe)}$_2$ were observed to dehydrocouple NH_3 and HBPin. The reactions with ammonia were carried out at low temperature and allowed to warm slowly overnight, precluding accurate assessment of reaction times (see Table 1). The appearance of a methyl-proton signal at 1.10 ppm and an amine-proton signal at 1.75 ppm in the ^{1}H spectrum, accompanied by a singlet ^{11}B NMR chemical shift at 25 ppm, supports the successful synthesis of PinBNH_2 (See SI). The precipitation of black solid was observed using both pre-catalysts along with signals attributed to Ar$^{Me}{}_6$H or Ar$^{iPr}{}_4$H in the ^{1}H NMR spectrum, suggesting decomposition of the catalyst. The addition of a second equivalent of HBPin and 1.85 μmol of {Ar$^{Me}{}_6$Sn(μ-OMe)}$_2$ or {Ar$^{iPr}{}_4$Sn(μ-OMe)}$_2$ led to the disappearance of the aforementioned signals and the appearance of a broad singlet at 25 ppm in the ^{11}B NMR spectrum, and in the ^{1}H NMR spectrum a new pinacol signal at 1.04 ppm and a broad signal at

3.31 ppm corresponding to the N-bound proton. The tri-borylated product $N(BPin)_3$ was not observed, even with a 5-fold excess of HBPin. Heating these reaction mixtures resulted in the appearance of black precipitate and the observation of $Ar^{Me_6}H$ or $Ar^{iPr_4}H$ in ^1H NMR spectra of the resulting mixtures. Nevertheless, this is a striking result bearing in mind the commercial significant of ammonia and the transformations to which bisborylamines can be subjected.

In order to provide insight into the mechanism, a number of stoichiometric studies were undertaken. The isolated tin hydride, $\{Ar^{Me_6}SnH\}_4$ did not prove catalytically competent for B-N dehydrocoupling (*vide supra*) and was not seen to react with an equimolar amount of Et_2NH. Addition of a one or two equivalents of aniline to $\{Ar^{iPr_4}Sn(\mu\text{-}H)\}_2$ showed no evidence of protonolysis by ^1H NMR spectroscopy, however in the presence of a tenfold excess of both aniline and pinacolborane, dehydrocoupling was observed to proceed. To assess the possible effects of hydride formation *in situ*, **1** was reacted with equimolar amounts of Et_2NH and PinBH, whereupon formation of $\{Ar^{Me_6}SnH\}_4$ and no consumption of Et_2NH was the sole observable reaction. These observations indicate that well defined tin hydrides of high molecularity (i.e. >2) are not catalytically relevant intermediates.

In order to assess the viability of tin(II) amide intermediates, $\{Ar^{Me_6}Sn(\mu\text{-}NEt_2)\}_2$ (**3**) was synthesised via salt metathesis from $\{Ar^{Me_6}Sn(\mu\text{-}Cl)\}_2$ and $LiNEt_2$. In the presence of excess iPr_2NH no discernible transamination occurred, however addition of one equivalent of PinBH resulted in ^{11}B NMR resonances indicating the consumption of the borane and formation of $PinBNEt_2$. Reinvestigation of this reaction on a larger scale allowed isolation of crystals of $\{Ar^{Me_6}Sn(\mu\text{-}NEt_2)(\mu\text{-}H)SnAr^{Me_6}\}$ (**4**). Addition of a second equivalent of PinBH yielded the off-cycle $\{Ar^{Me_6}SnH\}_4$.

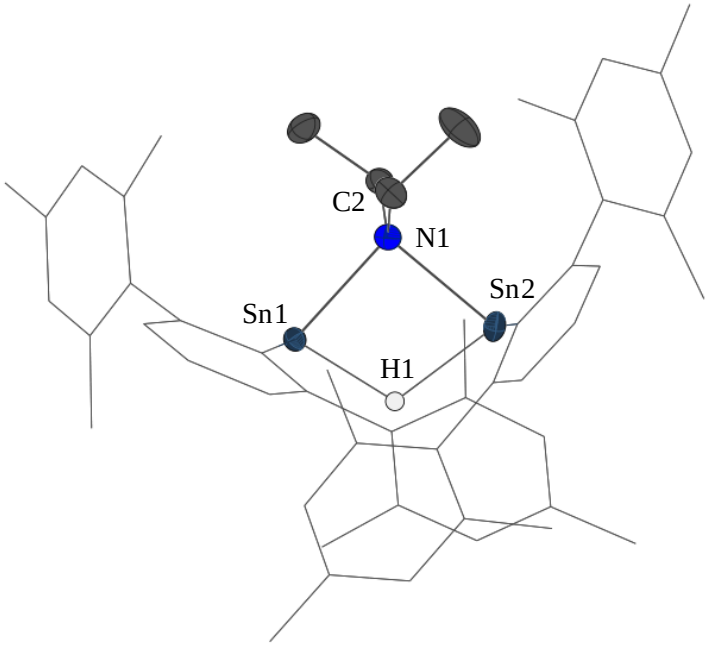

Figure 1 A plot of the crystallographically characterized structure of **4** showing the planar core, ellipsoid probability at 50% for core atoms, hydrogens not bound to tin atoms and two toluene molecules are not shown for clarity. Selected bond lengths (Å) and angles (°): Sn1-N1 2.246(3), Sn2-N1 2.256(3), Sn1-H1 1.73(1), Sn2-H1 1.734(8), Sn1-N1-Sn2 91.4(1), Sn1-H1-Sn2 136(1), N1-Sn1-H1 66.1(7), N1-Sn2-H1 65.9(7).

It is thus reasonable to suggest that whilst well defined, high molecularity tin hydrides are not catalytic intermediates herein, oligomeric mixed amide hydride and amide species are likely to be. Furthermore, it is evident that addition of the Lewis acidic borane is essential for activity and addition of **1** to an equimolar mixture of phenylsilane and Et_2NH gave no indication of dehydrocoupling activity. Thus borates derived from the interaction of Sn-H or Sn-NR_2 moieties with PinBH are essential to catalytic activity.

Finally, the investigation of **1** and **2** as precatalysts allows evaluation of the effect of ancillary ligation on the catalysis. Remarkably, whilst **1** is more tolerant of substrate bulk, **2** consistently provides faster catalysis for amines where it shows any competence. This

strongly indicates that the formation of a lower molecularity or more open oligomer is essential to activity, a situation favoured by the bulkier Ar^{iPr_4}. Thus, the catalysis is likely to be predicated on a series of σ-bond metathesis steps wherein formation of hydrido- and amidoborates facilitates cleavage of tightly-bound tin clusters and yields dehydrocoupling activity, a mechanism not dissimilar to that derived for the magnesium catalysed N-B dehydrocoupling postulated by Hill and co-workers.

8.4 Conclusions

In conclusion, the facile dehydrocoupling of primary or secondary amines with HBPin was accomplished through the use of the pre-catalysts $\{Ar^{Me_6}Sn(\mu\text{-}OMe)\}_2$ and $\{Ar^{iPr_4}Sn(\mu\text{-}OMe)\}_2$. The rate and scope of aminoborane production showed a strong dependence upon the identity of the ancillary ligands at the metal center, and also the electronic nature of the amine, as is especially apparent in reactions with substituted anilines. The potential intermediate $\{Ar^{Me_6}Sn(\mu\text{-}NEt_2)\}_2$ was obtained from the reaction of $\{Ar^{Me_6}Sn(\mu\text{-}Cl)\}_2$ and $LiNEt_2$ which was also competent as a pre-catalyst for amine and borane dehydrocoupling and could be converted into $\{Ar^{Me_6}Sn(\mu\text{-}NEt_2)(\mu\text{-}H)SnAr^{Me_6}\}$ via the addition of pinacol borane. These, combined with stoichiometric studies indicate the importance of the Lewis acid partner in dehydrocoupling. Finally, this work describes the first report of amine-borane dehydrocoupling for ammonia, a significant step in the activation of this utility chemical.

8.5 References

1. M. Suginome, T. Tanaka and T. Hasui, *Synlett*, 2006, 1047-1050.
2. M. Suginome, L. Uehlin and M. Murakami, *J. Am. Chem. Soc.*, 2004, **126**, 13196-13197.
3. M. Suginome, A. Yamamoto and Y. Ito, *Chem. Comm.*, 2002, 1392-1393.

4. C. Sole and E. Fernandez, *Angew. Chem., Int. Ed.*, 2013, **52**, 11351-11355.
5. A. Y. Khalimon, P. Farha, L. G. Kuzmina and G. I. Nikonov, *Chem. Commun.*, 2012, **48**, 455-457.
6. B. Wrackmeyer, H. E. Maisel and M. Herberhold, *J. Organomet. Chem.*, 2001, **637–639**, 727-732.
7. J. F. Janik, C. K. Narula, E. G. Gulliver, E. N. Duesler and R. T. Paine, *Inorg. Chem.*, 1988, **27**, 1222-1227.
8. B. Wrackmeyer, B. Schwarze and W. Milius, *J. Organomet. Chem.*, 1995, **489**, 201-205.
9. T. Seifert, W. Storch and M. Vosteen, *European Journal of Inorg. Chem.*, 1998, 1343-1349.
10. T. Gasparis-Ebeling and H. Nöth, *Chem. Ber.*, 1990, **123**, 261-269.
11. H. Nöth, P. Otto and W. Storch, *Chem. Ber.*, 1986, **119**, 2517-2530.
12. T. Yijun, L. Xiao, CN 101440101, **2009**.
13. G. Zhinong, L. Xiao, CN 102093399, **2011**.
14. R. J. Brotherton and T. Buckman, *Inorg. Chem.*, 1963, **2**, 424-425.
15. B. Singaram, *Heteroatom Chemistry*, 1992, **3**, 245-249.
16. M. Yalpani, R. Boese and R. Köster, *Chem. Ber.*, 1990, **123**, 1275-1283.
17. M. Yalpani, R. Boese and R. Köster, *Chem. Ber.*, 1990, **123**, 1285-1291.
18. M. Yalpani, R. Köster, R. Boese and W. A. Brett, *Angew. Chem. Int. Ed.*, 1990, **29**, 302-304.
19. E. A. Romero, J. L. Peltier, R. Jazzar and G. Bertrand, *Chem. Commun.*, 2016, **52**, 10563-10565.
20. A. Y. Khalimon, P. M. Farha and G. I. Nikonov, *Dalton Trans.*, 2015, **44**, 18945-18956.
21. C. Weetman, M. D. Anker, M. Arrowsmith, M. S. Hill, G. Kociok-Kohn, D. J. Liptrot and M. F. Mahon, *Chem. Sci.*, 2016, **7**, 628-641.

22. A. Staubitz, A. P. M. Robertson and I. Manners, *Chem. Rev.*, 2010, **110**, 4079-4124.

23. N. C. Smythe and J. C. Gordon, *Eur. J. Inorg. Chem.*, 2010, 509-521.

24. C. W. Hamilton, R. T. Baker, A. Staubitz and I. Manners, *Chem. Soc. Rev.*, 2009, **38**, 279-293.

25. B. Peng and J. Chen, *Energy Environ. Sci.*, 2008, **1**, 479-483.

26. V. M. Parvanov, G. K. Schenter, N. J. Hess, L. L. Daemen, M. Hartl, A. C. Stowe, D. M. Camaioni and T. Autrey, *Dalton Trans.*, 2008, 4514-4522.

27. F. H. Stephens, V. Pons and R. T. Baker, *Dalton Trans.*, 2007, 2613-2626.

28. R. J. Keaton, J. M. Blacquiere and R. T. Baker, *J. Am. Chem. Soc.*, 2007, **129**, 1844-1845.

29. R. Waterman, *Chem. Soc. Rev.*, 2013, **42**, 5629-5641.

30. K. A. Erickson, D. S. Wright and R. Waterman, *J. Organomet. Chem.*, 2014, **751**, 541-545.

31. R. J. Less, R. L. Melen and D. S. Wright, *RSC Adv.*, 2012, **2**, 2191-2199.

32. C. M. Vogels, P. E. O'Connor, T. E. Phillips, K. J. Watson, M. P. Shaver, P. G. Hayes and S. A. Westcott, *Can. J. Chem.*, 2001, **79**, 1898-1905.

33. D. J. Liptrot, M. S. Hill, M. F. Mahon and A. S. S. Wilson, *Angew. Chem., Int. Ed.*, 2015, **54**, 13362-13365.

34. Z. Yang, M. Zhong, X. Ma, K. Nijesh, S. De, P. Parameswaran and H. W. Roesky, *J. Am. Chem. Soc.*, 2016, **138**, 2548-2551.

35. P. Vasko, S. Wang, H. M. Tuononen and P. P. Power, *Angew. Chem. Int. Ed.*, 2015, **54**, 3802-3805.

36. E. Rivard, J. Steiner, J. C. Fettinger, J. R. Giuliani, M. P. Augustine and P. P. Power, *Chem. Commun.*, 2007, 4919-4921.

37. T. J. Hadlington, M. Hermann, G. Frenking and C. Jones, *J. Am. Chem. Soc.*, 2014, **136**, 3028-3031.

38. J. D. Erickson, P. Vasko, R. D. Riparetti, J. C. Fettinger, H. M. Tuononen and P. P. Power, *Organometallics*, 2015, **34**, 5785-5791.

Chapter 9

N-N Double Bond Cleavage and Azobenzene Rearrangement with C-C Bond Formation Induced by a Germylene

This work is submitted to *Organometallics*

9.1 Introduction

The reactivity of heavier group 14 element tetrylenes (:ER_2, E = Si, Ge, Sn, or Pb; R = bulky organic group) with unsaturated species has attracted much interest owing to their applications in the synthesis of heterocyclic compounds and related derivatives.[1] In particular, the interaction of main group metal compounds with diazenes RN=NR and their further reactions[2] are of interest since they may provide new species as well as a greater understanding of the mechanism of enzymatic dinitrogen reduction by nitrogenase where it has been shown that hydrazines, hydrazide, and diazenes are important intermediates.[3] In this respect, azobenzene is the most studied organic diazene since it is one of the simpler derivatives of the parent diamine (HN=NH), which is an important intermediate in the reduction sequence.[4]

In 2012, Roesky and coworkers. reported the synthesis of the main group diaziridine via the reaction of a silylene, L^1Si^tBu (L^1 = $PhC(N^tBu_2)$, with azobenzene(**Scheme 1, a**).[5] The same group also showed that the silylene L^1SiNPh_2 reacts with azobenzene via the activation of the ortho C-H moiety of the phenyl substituent of the azobenzene the subsequent migration of the hydrogen atom from the phenyl ring to one of the nitrogen atoms (**Scheme 1, b**).[6] The stannylene SnR_2 [R = 2-$(Me_2NCH_2)C_6H_4$] and silylene (L^1SiCl) were

demonstrated independently by Růžička[7] and Roesky[8] to react with azobenzene to afford in polycyclic products via the activation of two phenyls C-H bonds (**Scheme 1, c and d**).

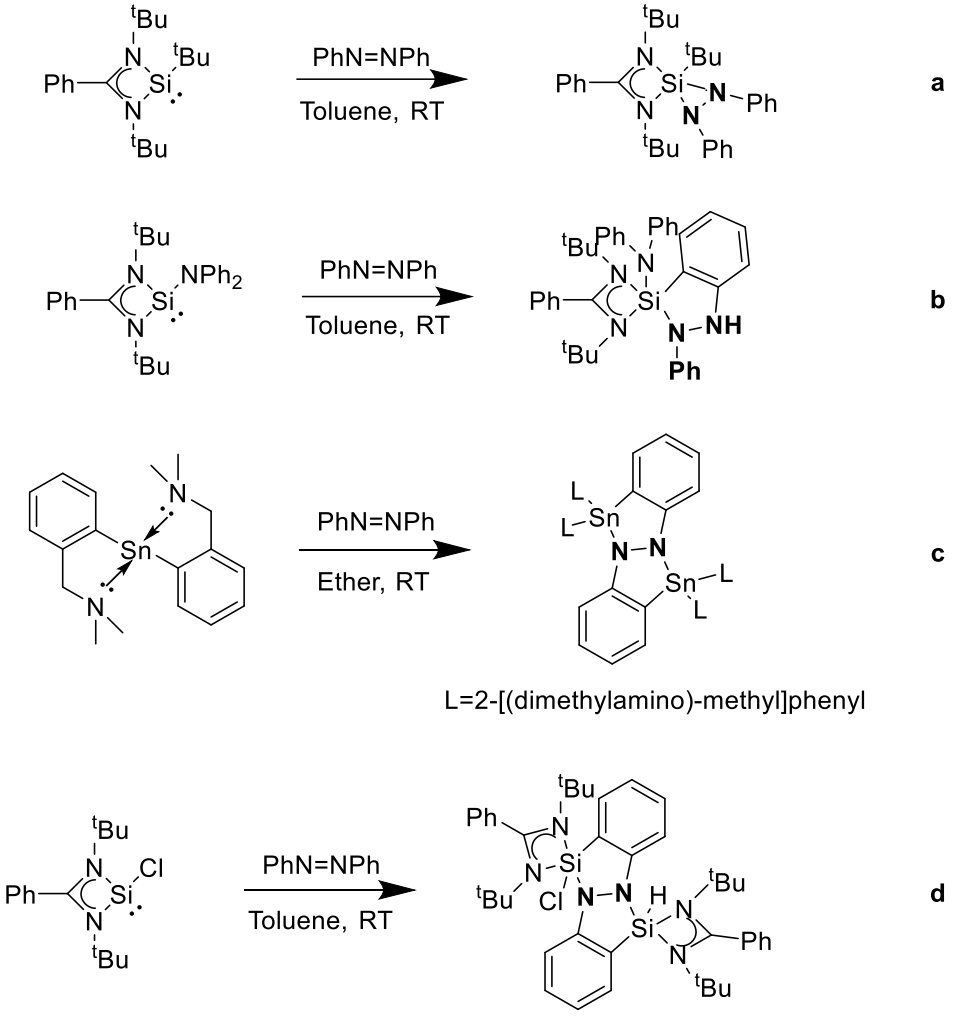

Scheme 1. Some known reactions of tetrylenes with azobenzene (Mes= C_6H_2-2,4,6-Me_3).[5-8]

The N-N bond is preserved in all these reactions. The sole example of N-N bond cleavage in azobenzene by a tetrylene was described by Weidenbruch and coworkers in 1998 (**Scheme 2**).[9] They observed the formation of a 1,2 diaza-sila-indane derivative, which was proposed to proceed via the reaction of a photolytically generated silylene with azobenzene to

generate an intermediate siladiaziridine followed by the insertion of the N-N single bond into the *o*-C-H bond of the phenyl ring.

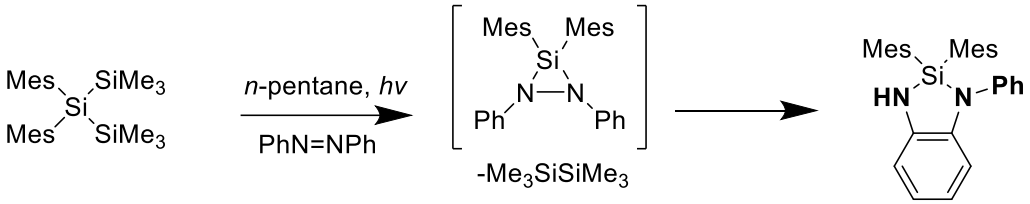

Scheme 2. N-N bond cleavage of azobenzene by a silylene intermediate.[9]

Reactions of germylenes with azobenzene are currently unknown and in general N-N double bond cleavage by main group species is rare.[10] In this chapter we show that germylene, $Ge(Ar^{Me6})_2$ (Ar^{Me6} = C_6H_3-2,6-(C_6H_2-2,4,6-Me_3)$_2$),[11] reacts with azobenzene at room temperature to form the Ge^{IV} diamido products **1a** and **1b** (**Scheme 3**). In contrast, heating the reaction with bulkier diazenes such as 1,2-bis(2,6-diethylphenl)diazene or 1,2-bis(1,3,5-trimetylphenyl)diazene, for 2 days resulted in the decomposition of the starting germylene via activation of a methyl group from a flanking mesityl ring of the Ar^{Me6} ligand (**Scheme 3**) to give the Ge(IV) hydride species **2** illustrated in **Figure AVIII6** and **AVIII8** in the Appendix p322 and p324. The products were characterized by X-ray crystallography and ^{1}H NMR spectroscopy.

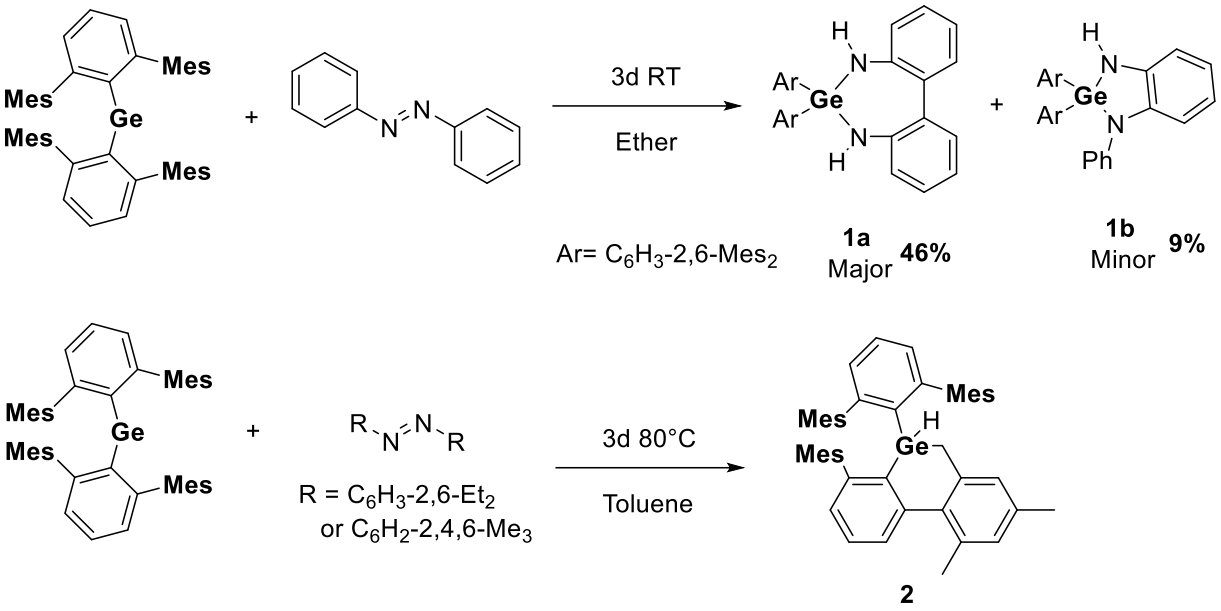

Scheme 3. N=N double bond cleavage of azobenzene via reactions with a diarylgermylene.

9.2 Experimental Details

General Experimental Details.

All operations were carried out under anaerobic and anhydrous conditions using modified Schlenk techniques. All solvents were dried over alumina columns and degassed prior to use. The ^{1}H and ^{13}C NMR spectroscopic data were collected on a Bruker 400MHz spectrometer. Azobenzene, 1,2-bis(2,6-diethylphenl)diazene and 1,2-bis(1,3,5-trimetylpehnyl)diazene were purchased from Sigma-Aldrich and purified via sublimation. $Ge(Ar^{Me_6})_2$ and $Sn(Ar^{Me_6})_2$ were synthesized according to literature methods.

$Ge(Ar^{Me6})_2${N(H)(Ph)-o(Ph)(H)N}(1a): A Et_2O solution (30mL) of $Ge(Ar^{Me6})_2$ (0.80g, 1.14mmol) and azobenzene (0.208g, 1.14mmol) was stirred at room temperature for 3 days. Et_2O was removed under reduced pressure and the resulting solid was washed with 5mL of cold Et_2O twice. The resulting solid was redissolved in toluene. Storage of solution at -30°C

for 3 days results in **1a** as colorless crystals. Yield (0.42g, 46%) Mp: 132-136°C, ^{1}H NMR (400MHz, C_6D_6, 298K): 1.43 (s, 6H, CH_3), 1.54 (s, 6H, CH_3), 1.84 (s, 6H, CH_3), 1.87 (s, 6H, CH_3), 1.90 (s, 6H, CH_3), 2.25 (s, 6H, CH_3), 2.55 (s, 2H, NH) 6-8(m, 21H, aromatic Hs). ^{13}C{^{1}H} NMR (126MHz, C_6D_6, 298K): 20.26, 20.60, 20.80, 21.24, 22.28, 23.62, 119.02, 120.55, 126.57, 126.79, 128.20, 128.71, 128.96, 129.53, 130.84, 130.98, 131.23, 133.26, 134.41, 136.64, 141.13, 146.52, 148.86, 149.76.

Ge(Ar^{Me6})$_2${N(H)-o-C$_6$H$_4$N(Ph)}(1b): A Et_2O solution (30mL) of Ge(Ar^{Me6})$_2$ (0.80g, 1.14mmol) and azobenzene was stirred at room temperature for 3 days. Et_2O was removed under reduced pressure and the resulting solid was washed with 5mL of cold Et_2O twice. The two washed solution was combined, and the solvents was removed in vacuo. The resulting solid was redissolved in THF. Reduced in volume and storage of solution at room temperature for 2 days gave **1b** as pale yellow crystals. Yield (92 mg, 9.2%) Mp: 139-143°C. ^{1}H NMR (400MHz, C_6D_6, 298K): 1.12 (s, 3H, CH_3), 1.34 (s, 3H, CH_3), 1.58 (s, 3H, CH_3), 1.64 (s, 3H, CH_3), 1.70 (s, 3H, CH_3), 1.85 (s, 3H, CH_3), 1.87 (s, 3H, CH_3), 1.89 (s, 3H, CH_3), 1.91 (s, 3H, CH_3), 2.05 (s, 3H, CH_3), 2.24 (s, 3H, CH_3), 2.29 (s, 3H, CH_3), 2.90 (s, 1H, NH). ^{13}C{^{1}H} NMR (126MHz, C_6D_6, 298K): 20.41, 20.54, 20.60, 21.41, 21.53, 21.79, 22.21, 22.28, 22.46, 22.57, 23.01, 110.24, 112.61, 114.77, 118.75, 119.29, 119.81, 128.90, 129.23, 129.40, 130.05, 130.38, 131.09, 131.25, 131.81, 132.00, 133.80, 134.86, 135.10, 135.37, 135.94, 136.20, 136.24, 136.59, 136.70, 137.39, 137.87, 138.52, 138.59, 139.82, 140.66, 141.08, 141.63, 141.81, 143.95, 146.98, 148.07, 150.68, 151.34

9.3 Results and Discussion

The diarylgermylene, $Ge(Ar^{Me6})_2$, reacted with one equivalent of azobenzene upon stirring in diethyl ether at ambient temperature. Over 3 days there was a color change of the solution from the dark purple of the germylene to the bright yellow of the products. After filtration, concentration of the solution under reduced pressure and storage at room temperature for 2 days give pale yellow crystals were obtained. These crystals incorporated the products **1a** and **1b** in good overall yield (72%). X-ray diffraction studies afforded the structure shown in **Figure AVIII7** p323. which results from a co-crystallizing **1a** and **1b** in a 2:1 ratio. Separation of **1a** and **1b** was accomplished by washing the yellow crystals with cold ether which removes **1b** from **1a**. Pure crystals were obtained by recrystallizing **1a** from toluene and **1b** from THF.

The crystal structures (**Figure 1**) of **1a** and **1b** were also determined, and these illustrate the different rearrangements undergone by azobenzene upon reaction with the germylene. The resulting aza-germa-indane has a Ge-N distance of 1.826(10)/1.822(10) Å(**1a**) and 1.822(7)/1,871(7) Å(**1b**) which are in the typical range for a Ge-N single bond[12] and agree with the sum (1.92 Å) of the covalent single bond radii of nitrogen (0.71 Å) and germanium (1.21 Å).[13] The Ge-C bonds to the aryl ligands in **1a** and **1b** span the range 1.97-2.02 Å which is similar to the sum (1.98 Å) of the covalent radii of carbon (0.77Å) and germanium (1.21Å).[13] The N-Ge-N angles are 102.85(5)° for **1a** and 86.87(14)° for **1b** while the C(Ar)-Ge-C(Ar) angles in **1a** (113.11(4)°) and **1b** (111.77(8)°), display only small changes from that in the precursor germylene (114.4(2)°).[11] The torsion angle between the two-phenyl rings in the terphenyl moiety of **1a** is 44.73(4)°, which is in close agreement with the structure of the only other known main group 2,2-biphenyldiamide complex, 6,7-dibenzo-1,3,2-diazaphosphepanes(46.06(12)°).[14] In comparison to an uncomplexed 2,2-

biphenyldiamine, which has a torsion angle of 58.24(15)°,[15] the structures of **1a** and **1b** show a significantly greater degree of steric congestion.

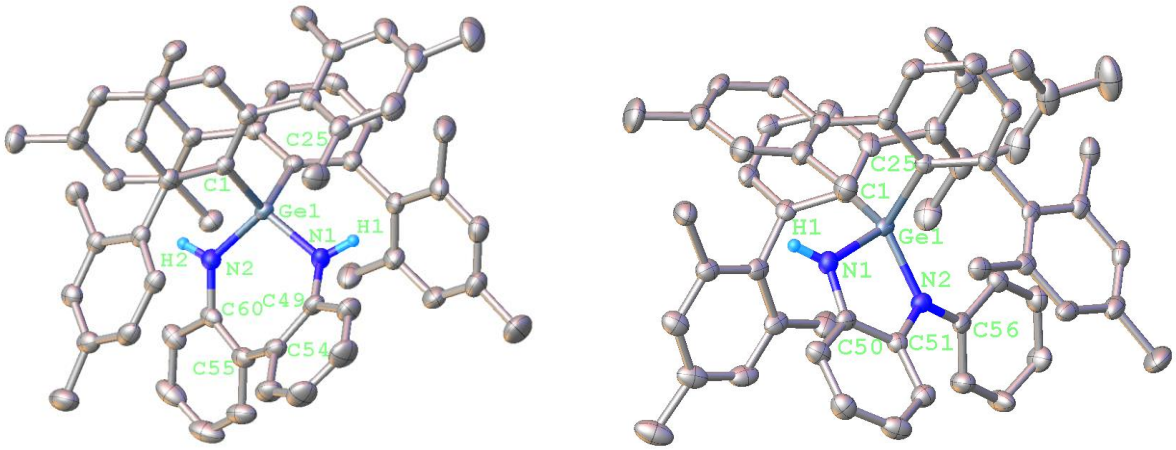

1a **1b**

Figure 1. Molecular structure of **1a** and **1b**. Hydrogen atoms and solvent molecules are not shown. Carbon atoms are shown in pale gray. Selected bond length(Å) and bond angles(°). **1a**: Ge1-N1: 1.826(10), Ge1-N2: 1.822(10), Ge1-C1: 2.00(4), Ge1-C25: 2.00(4), C-25-Ge1-C1: 113.11(4) and N1-Ge1-N2: 102.85(5). **1b:** Ge1-C1: 2.03(2), Ge1-C25: 1.97(19), Ge1-N1:1.822(7), Ge1-N2: 1.871(7), C1-Ge1-C25: 111.77(8) and N1-Ge1-N2: 86.87(14).

The ^{1}H NMR spectrum of **1a** displays six signals corresponding to six methyl protons of the Ar^{Me6} ligands that range from 1.48 to 2.25 ppm. A singlet at 2.55 ppm is due to the two chemically equivalent N-H protons. The ^{1}H NMR spectrum of **1b** features 12 singlets for the methyl protons of equal intensity that range from 1.12 to 2.29. A signal at 2.90 corresponds to the single amine proton.

A proposed mechanism for these reactions is shown in **Scheme 4**. The reaction is initiated by the complexation of diarylgermylene with azobenzene forming a germadiaziridine intermediate species via a [1+2] cycloaddition.[16] The resulting germadiaziridine in path 1 and path 2 in **Scheme 4** may then undergo two different

rearrangements by the cleavage of the N-N bond.[17] It should be noted that no EPR signal was detected and attempts to trap a possible radical intermediate in the reaction sequence with organic spin-traps (TEMPO, AIBN) have so far been unsuccessful. We propose that the reaction proceeds through a five-membered (**Scheme 4, Path I**) or four-membered (**Scheme 4, Path II**) ring intermediate, followed by a [1,3]-H shift reestablishing aromaticity.[6,10,18] The instability of the diaziridine combined with the steric congestion produced by the bulky m-terphenyl substituents at germanium on azobenzene which forces the two-phenyl rings into proximity facilitates the N=N bond cleavage to yield the mixture of products **1a** and **1b**.

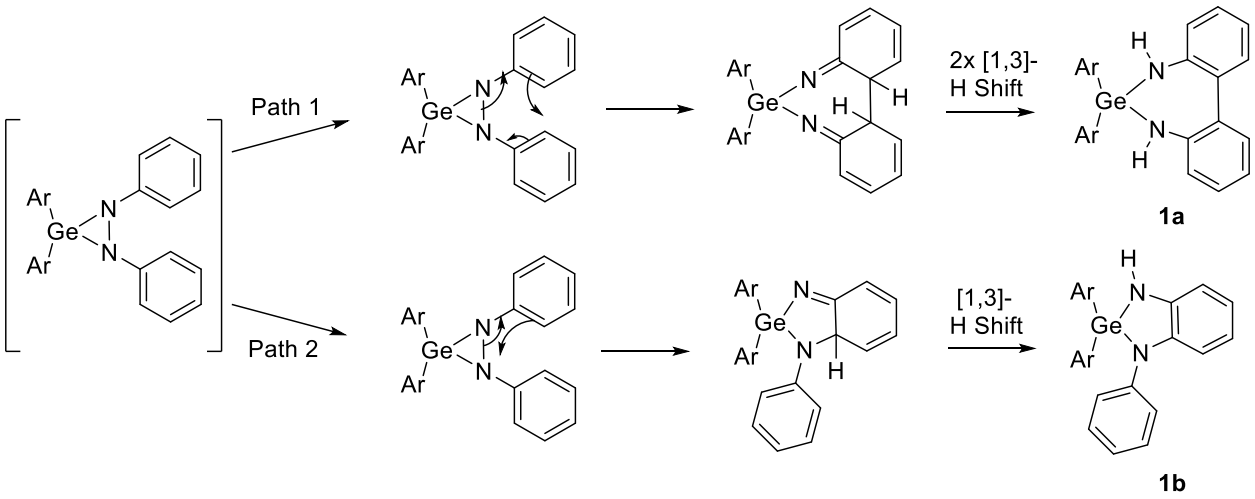

Scheme 4. Proposed mechanisms for the formation of **1a** and **1b** (Ar= C_6H_3-2,6-(C_6H_2-2,4,6-$Me_3)_2$).

In attempts to selectively synthesize the reaction products, a range of reaction conditions was screened. The solvent was demonstrated to not affect the selectivity and changing the reaction temperature does not afford a reaction. Heating the reaction mixture to 60°C in THF or toluene for 3 days resulted in the decomposition of the germylene. Crude ^{1}H NMR displays a Ge-H signal at 4.43ppm which suggests a C-H activation at the mesityl flanking ring. A similar reaction was observed by Aldridge for [Ar^{Me6}Ge(B(NDippCH)$_2$)][20] where the germylene was stirred at room temperature for 12 hours. Reaction with more

sterically demanding organic diazene compounds such as 1,2-bis(2,6-diethylphenl)diazene or 1,2-bis(1,3,5-trimetylphenyl)diazene did not yield a reaction at room temperature.

We also investigated the reaction of the analogous tin species, $Sn(Ar^{Me6})_2$, with azobenzene in a similar manner to $Ge(Ar^{Me6})_2$. However, no reaction was observed under similar reaction conditions. This may be due to the increased HOMO-LUMO energy separation with increasing atomic number (Ge vs Sn) and the weaker bonds to tin in the products.[21] The reactivity difference may be compared to the reaction of $Ge(Ar^{iPr4})_2$ and $Sn(Ar^{iPr4})_2$ with ethylene and alkynes, where $Ge(Ar^{Me6})_2$ forms metallocyclopropane[22] and propenes[23] at room temperature, whereas $Sn(Ar^{iPr4})_2$ resulted in migratory insertion products under elevated temperatures and with no metallacycles being observed.[24]

9.4 Conclusions

In summary, the reaction of $Ge(Ar^{Me6})_2$ with azobenzene at room temperature resulted in two Ge^{IV} diamide products **1a** and **1b**. Compound **1a** represents a new type of rearrangement for azobenzene. Attempts to change the ratio of the two products by heating the solution gave an intramolecular C-H activation of the *ortho*-methyl group in the flanking mesityl ring. ^{1}H NMR spectroscopy and X-ray crystallography confirm these observations. Further investigation of this reaction in potential catalysis is underway.

9.5 References

1. a) Mizuhata, Y.; Sasamori, T. Tokitoh N. "Stable Heavier Carbene Analogues" *Chem. Rev.* **2009**, *109*, 3479–3511 b) Nansuch, F.; Groll, L.; Inoue S. "Recent advances of group 14 dimetallenes and dimetallynes in bond activation and catalysis" *Chem. Sci.*, **2021**, *12*, 2001-2015. c) Asay, M.; Jones C.; Driess M. "N-Heterocyclic Carbene Analogues with Low-Valent Group 13 and Group 14 Elements: Syntheses, Structures, and Reactivities of

a New Generation of Multitalented Ligands" *Chem. Rev.* **2011**, *111*, 354–396. d) Power, P.P. "Main-group elements as transition metals" *Nature*, **2010**, *463*, 171-177. e) Weetman C.; Inoue S. "The Road Travelled: After Main-group Elements as Transition Metals" *ChemCatChem.* **2018**, *10*, 4213-4228.

2. a) Niecke, E.; Link, M.; Nieger, M. "Reversible [4 + 1]-Selbstaddition von Alkyl(arylimino)phosphanen und regioselektive Cycloaddition mit (E)- und (Z)-Azobenzol" *Chem. Ber.* **1992**, *125*, 2635-2640. b) Baker, R.J.; Jones, C.; Mills, D.P.; Murphy, C.M.; Hey-Hawkins, E.; Wolf R. "The reactivity of gallium-(i), -(ii) and -(iii) heterocycles towards Group 15 substrates: attempts to prepare gallium–terminal pnictinidene complexes" *Dalton Trans.*, **2006**, 64-72. c) Azhakar, R.; Sarish, S.P.; Tavčar, G.; Roesky, H.W.; Hey, J.; Stalke D.; Koley, D. "Formation of Silicon Centered Spirocyclic Compounds: Reaction of N-Heterocyclic Stable Silylene with Benzoylpyridine, Diisopropyl Azodicarboxylate, and 1,2-Diphenylhydrazine" *Inorg. Chem.* **2011**, *50*, 3028–3036. d) Leung, W-P.; Kan, K-W.; So C-W.; Mak, T.C.W. "Formation of Germenes from Bis(germavinylidene)" *Organometallics* **2007**, *26*, 3802–3806.

3. a) Lukoyanov, D.; Dikanov, S.A.; Yang, Z.-Y.; Barney, B.M.; Samoilova, R.I.; Narasimhulu, K.V.; Dean, D.R.; Seefeldt, L.C.; Hoffman, B.M. "ENDOR/HYSCORE Studies of the Common Intermediate Trapped during Nitrogenase Reduction of N_2H_2, CH_3N_2H, and N_2H_4 Support an Alternating Reaction Pathway for N_2 Reduction" *J. Am. Chem. Soc.* **2011**, *133*, 11655-11664. b) Nazari, N. "Homogeneous iron complexes for the conversion of dinitrogen into ammonia and hydrazine" *Chem. Soc. Rev.*, **2010**, *39*, 4044-4056. c) Barney, B.M.; McClead, J.; Lukoyanov, D.; Laryukhin, M.; Yang, T. C.; Dean, D.R.; Hoffman, B.M.; Seefeldt, L.C. "Diazene (HN = NH) Is a Substrate for Nitrogenase: Insights into the Pathway of

N_2 Reduction." *Biochemistry* **2007**, *46*, 6784−6794 d) McKenna, C.E.; Simeonov, A.M.; Eran, H.; Bravo-Leerabhandh, M. "Reduction of Cyclic and Acyclic Diazene Derivatives by Azotobacter vinelandii Nitrogenase: Diazirine and trans-Dimethyldiazene" *Biochemistry*, **1996**, *35*, 4502-4514. e) Lukoyanov, D.; Yang, Z.-Y.; Barney, B.M.; Dean, D.R.; Seefeldt, L.C.; Hoffman, B.M. "Unification of reaction pathway and kinetic scheme for N_2 reduction catalyzed by nitrogenase" *Proc. Natl. Acad. Sci. U.S.A.* **2012**, *109*, 5583-5587 f) Buscagan, T.M.; Rees. D.C "Rethinking the Nitrogenase Mechanism: Activating the Active Site" *Joule*, **2019**, *3*, 2662-2678.

4. a) Guillemot, G.; Solari, E.; Scopelliti, R.; Floriani, C. "Molybdenum(IV)-d^2 Reactivity in a Quasiplanar Oxo-Environment Modeled by Calix[4]arene: The Reductive Cleavage of N=N Double Bond and the Formation of 1-Metallacyclopropene from the Corresponding Alkyne Complexes" *Organometallics* **2001**, *12*, 2446–2448. b) Smith, J.M.; Lachicotte, R.J.; Holland, P.L. "N=N Bond Cleavage by a Low-Coordinate Iron(II) Hydride Complex" *J. Am. Chem. Soc.* **2003**, *125*, 15752–15753. c) Bellow, S.M.; Arnet, N.A.; Gurubasavaraj, P.M. Brennessel, W.W.; Bill, E.; Cundari, T.R.; Holland, P.L. "The Mechanism of N–N Double Bond Cleavage by an Iron(II) Hydride Complex" *J. Am. Chem. Soc.* **2016**, *138*, 12112–12123. d) Oguni, N.; Shimazu, S.; Nakamura, A. "Nitrogenase Model Reaction: Electron-Transfer Reduction of Phenylacetylene and Azobenzene by Catalysis of Copolypeptide–Molybdenum Complexes in Protic Solvent" *Polymer Journal*, **1980**, *12*, 891-897. e) Fardiner, M.G. Stringer, D.N. "Dinitrogen and Related Chemistry of the Lanthanides: A Review of the Reductive Capture of Dinitrogen, As Well As Mono- and Di-aza Containing Ligand Chemistry of Relevance to Known and Postulated Metal Mediated Dinitrogen Derivatives" *Materials*, **2010**, *3*, 841-862.
5. Azhakar, R.; Roesky, H.W.; Ghadwal, R.S.; Holstein, J.J.; Dittrich, B. "An access to base-stabilized three-membered silicon heterocycles" *Dalton Trans.*, **2012**, *41*, 9601-

9603.

6. Azhakar, R. Roesky, H.W.; Wolf, H.; Stalke, D. “Reactivity of Stable Heteroleptic Silylene $PhC(NtBu)_2SiNPh_2$ toward Diazobenzene and N-Benzylidineaniline” *Organometallics* **2012**, *31*, 8608–8612.
7. Padeˇlková, C.; Nechaev, M.; Lycˇka, A.; Holubová, J.; Zevaco, T.A.; Růžička, A. “Reactivity of C,N-Chelated Stannylene with Azobenzene” *Eur. J. Inorg. Chem.* **2009**, 2058–2061.
8. Khan, S.; Sen, S.S.; Michel, R.; Kratzert, D.; Roesky, H.W.; Stalke, D. “Formation of a Unsymmetrical Ring System via C–H Bond Activation of Diazobenzene by Stable N-Heterocyclic Chlorosilylene ($PhC(N^tBu)_2SiCl$)” *Organometallics*, **2011**, *30*, 2643–2645.
9. Weidenbruch, M.; Olthoff, S.; Saak, W.; Marsmann, H. “Silylene Reactions with Nitrogen Multiple Bonds: Additions and Rearrangements” *Eur. J. Inorg. Chem.* **1998**, 1755-1758.
10. Zhu, H.; Chai, J.; Fan, H.; Roesky, H.W.; Nehete, U.N.; Schmidt, H-G. Noltemeyer, M. “A Rearrangement of Azobenzene upon Interaction with an Aluminum(I) Monomer LAl {L = $HC[(CMe)(NAr)]_2$, Ar = 2,6-$^iPr_2C_6H_3$}” *Eur. J. Inorg. Chem.* **2005**, 2147-2150.
11. Simons, R.S.; Pu, L.; Olmstead, M.M.; and Power, P.P.” Synthesis and Characterization of the Monomeric Diaryls $M\{C_6H_3\text{-}2,6\text{-}Mes_2\}_2$ (M = Ge, Sn, or Pb; Mes = 2,4,6-$Me_3C_6H_2$−) and Dimeric Aryl−Metal Chlorides $[M(Cl)\{C_6H_3\text{-}2,6\text{-}Mes_2\}]_2$ (M = Ge or Sn)” *Organometallics*, **1997**, *16*, 1920-1925.
12. Lappert, M. F.; Protchenko, A.; Power, P. P.; Seeber, A. *Metal Amide Chemistry*; John Wiley & Sons: 2008; p279
13. Pyykko, P.; Atsumi, M. “Molecular Single-Bond Covalent Radii for Elements 1–118” *Chem. - Eur. J.* **2009**, *15*, 186-197.
14. Nifantiev, E.; Zavalishina, A. I.; Orzhekovskaya, E. I.; Nurkulov, N. N.;Vasyanina, L. K.;

Bekker, A. R.; Belskii, V. K.; Stash, A.I. "Higher 1,3,2-diazaphosphocyclanes. V. 4,5; 6,7- Dibenzo 1,3,2-diazaphosphepanes" *Phosphorus, Sulfur, and Silicon and the Related Elements* **1997**, *123*, 89-110.

15. Ottersen, T. "The Crystal and Molecular structure of 2,2'-Diaminodiphenyl at -165ºC" *Acta Chem. Scand.* **1977**, *31*, 480-484

16. a) Sekiguchi, A.; Izumi, R.; Ihara, S.; Ichinohe, M.; Lee, V.Y. "The First Isolable 1,1-Dilithiogermane and Its Unusual Dimeric Structure–An Effective Reagent for the Preparation of Double-Bonded Derivatives of Group 14 Element" *Angew. Chem. Int. Ed.* **2002**, *4*, 1598-1600. b) Sasamori, T.; Sugahara, T.; Agou, T.; Sugarmata, K.; Guo, J.-D.; Nagase, S.; Tokitoh, N. "Reaction of a diaryldigermyne with ethylene" *Chem, Sci*, **2015**, *6*, 5526-5530 c) Ohgaki, H.; Kabe, Y.; Ando, W. "Reaction of a Germylene with Ethylene: A Stable Digermacyclobutane via a Germirane Intermediate" *Organometallics* **1995**, *14*, 2139-2141. d) Ando, W.; Ohgaki, H.; Kabe, Y. "Stable Germirane Derivatives" *Angew. Chem. Int. Ed. Engl.* **1994**, *33*, 659-661. e) Walewska, M.; Hlina, J.; Baumgartner, J.; Müller, T.; Marschner, C. "Basic Reactivity Pattern of a Cyclic Disilylated Germylene" *Organometallics*, **2016**, *35*, 2728-2737.

17. a) Nielsen, I.M.B. "Ab Initio Study of Aziridines and Diaziridines: Nitrogen Inversion, Ring Opening, and Thermochemistry" *J. Phys. Chem. A* **1998**, *102*, 3193-3201. b) Nevárez, N.; Woerpel, K.A. "Dearomatization Reactions of Aryl-Substituted Silaaziridines" *J. Org. Chem.* **2008**, *73*, 8113–8115

18. a) Ghlogo, G.; Osella, S.; Maranzana, A.; Tonachini, G. "The Mechanism of the Acid-Catalyzed Benzidine Rearrangement of Hydrazobenzene: A Theoretical Study" *Eur. J. Org. Chem.*, **2011**, 2326-2333. b) Zurita, D.A.; Flores-Alamo, M.; García, J.J. "Catalytic transfer hydrogenation of azobenzene by low-valent nickel complexes: a route to 1,2-disubstituted benzimidazoles and 2,4,5-trisubstituted imidazoline" *Dalton Trans.*, **2016**,

45, 10389-10401.

19. Ring strain example: a) Casadei, M.A.; Galli, C.; Mandolini, L. "Ring-Closure Reactions. 22.1 Kinetics of Cyclization of Diethyl (ω-Bromoalkyl)malonates in the Range of 4- to 21- Membered Rings. Role of Ring Stain. *J. Am. Chem. Soc.* **1984**, *106*, 1051-1056. Kinetic/thermodynamic control examples in ring-opening or ring expansion: b) Lam, J.L.; Pham, H.V.; Houk, K.N.; Vanderwal, C.D. "Computation and Experiment Reveal That the Ring-Rearrangement Metathesis of Himbert Cycloadducts Can Be Subject to Kinetic or Thermodynamic Control" *J. Am. Chem. Soc.* **2013**, *135*, 17585-17594.
20. Usher, M.; Protchenko, A.V.; Rit, A.; Campos, J.; Kolychev, E. L.; Tirfoin, R.; Aldridge, S. "A Systematic Study of Structure and E–H Bond Activation Chemistry by Sterically Encumbered Germylene Complexes" *Chem. Eur J.* **2016**, *22*, 11685-11698.
21. Burdett, J.K. *Molecular Shapes* (Wiley-Interscience, New York, 1980).
22. Gullett, K.L.; Lai, T.Y.; Chen, C-Y; Fettinger J.C.; Power, P.P. "Reversible Binding of Ethylene and Propylene by Germylenes" *Organometallics* **2019**, *38*, 1425-1428.
23. Lai, T.Y.; Gullett, K.L.; Chen, C-Y.; Fettinger, J.C.; Power, P.P. "Reversible Complexation of Alkynes by a Germylene" *Organometallics* **2019**, *38*, 1421-1424.
24. Lai, T.Y.; Guo, J-D.; Fettinger, J.C.; Nagase, S.; Power, P.P. "Facile insertion of ethylene into a group 14 element-carbon bond: effects of the HOMO–LUMO energy gap on reactivity" *Chem. Commun.*, **2019**, *55*, 405-407

Appendix I

Supporting Information for Chapter 2: Facile C-H Bond Metathesis Mediated by a Stannylene

Figure AI1. ^{1}H NMR Spectrum of **1a** (400 MHz, C_6D_6, 298K, ppm)

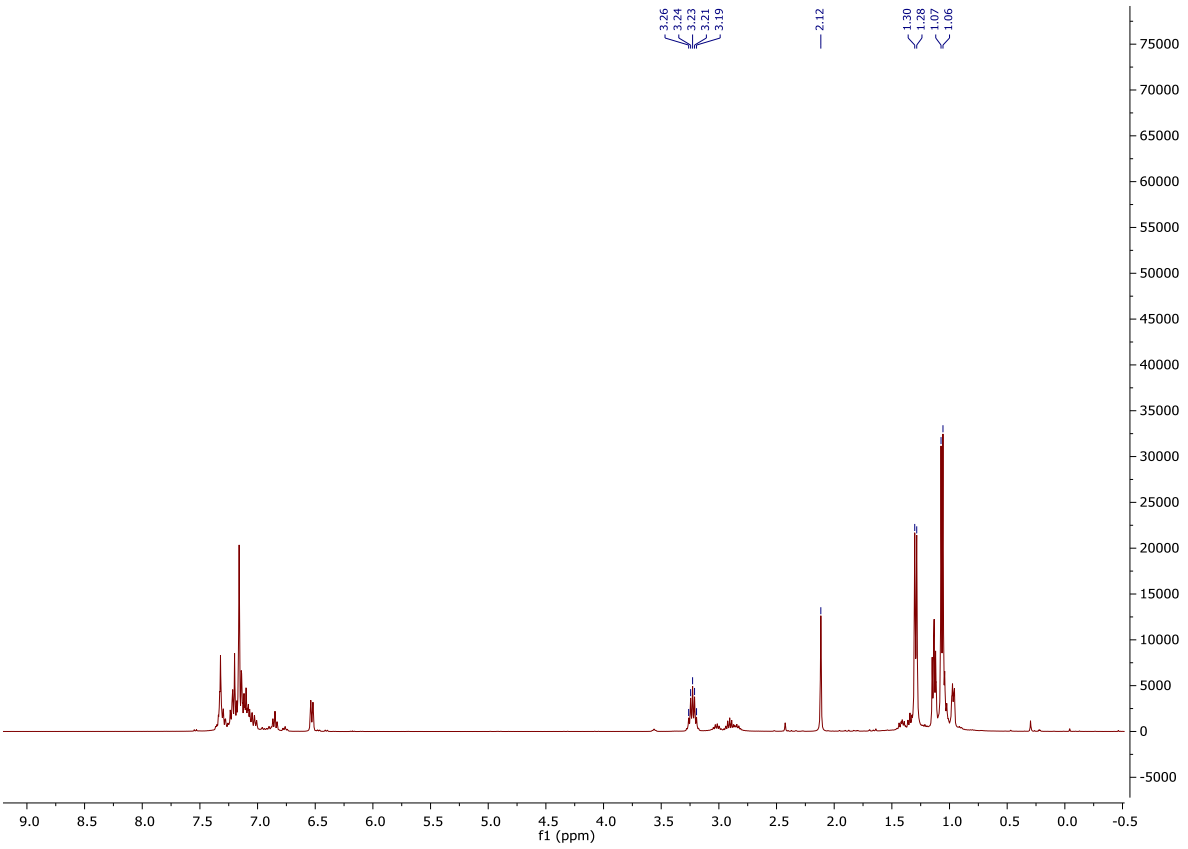

Figure AI2. ^{13}C NMR Spectrum of **1a** (126 MHz, C_6D_6, 298K, ppm)

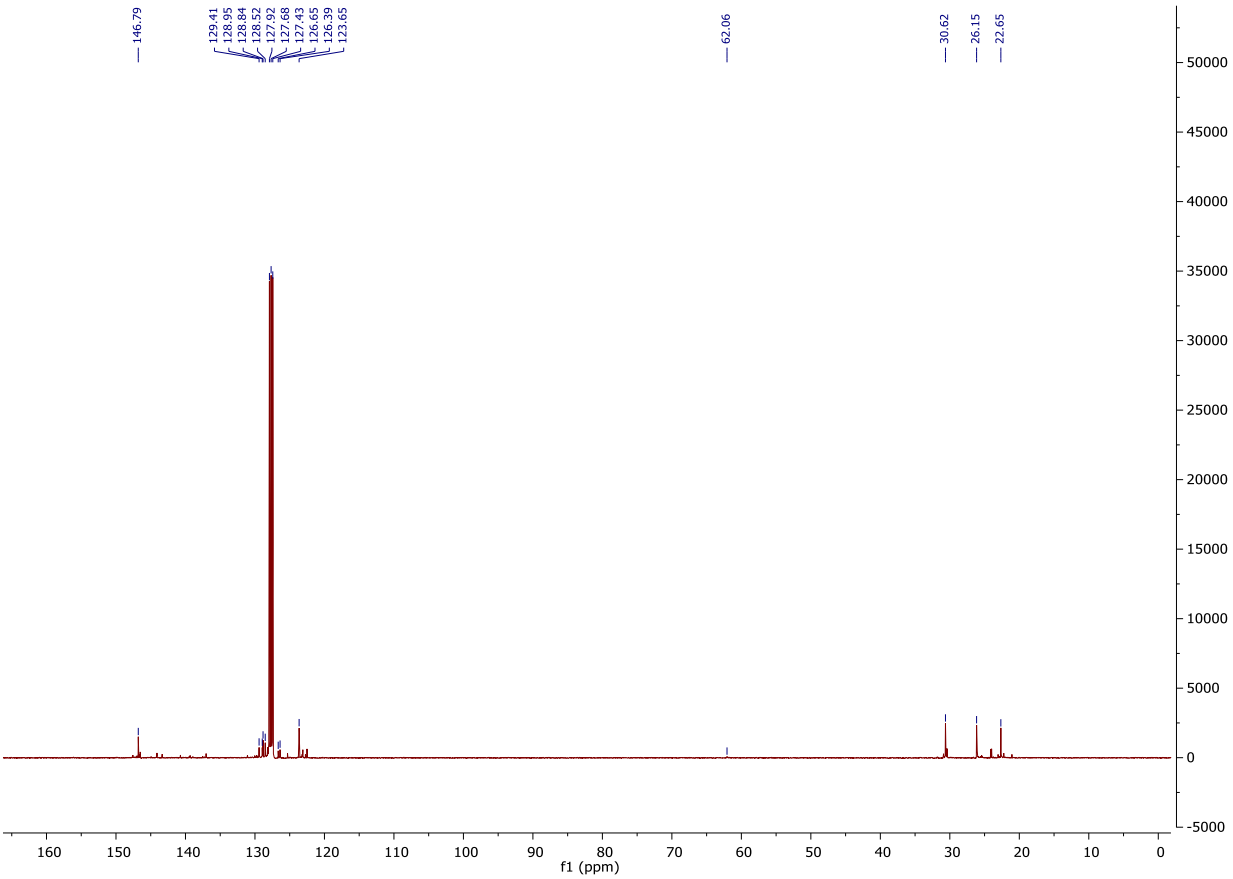

Figure AI3. ^{119}Sn NMR Spectrum of **1a** (186.36 MHz, C_6D_6, 298K, ppm)

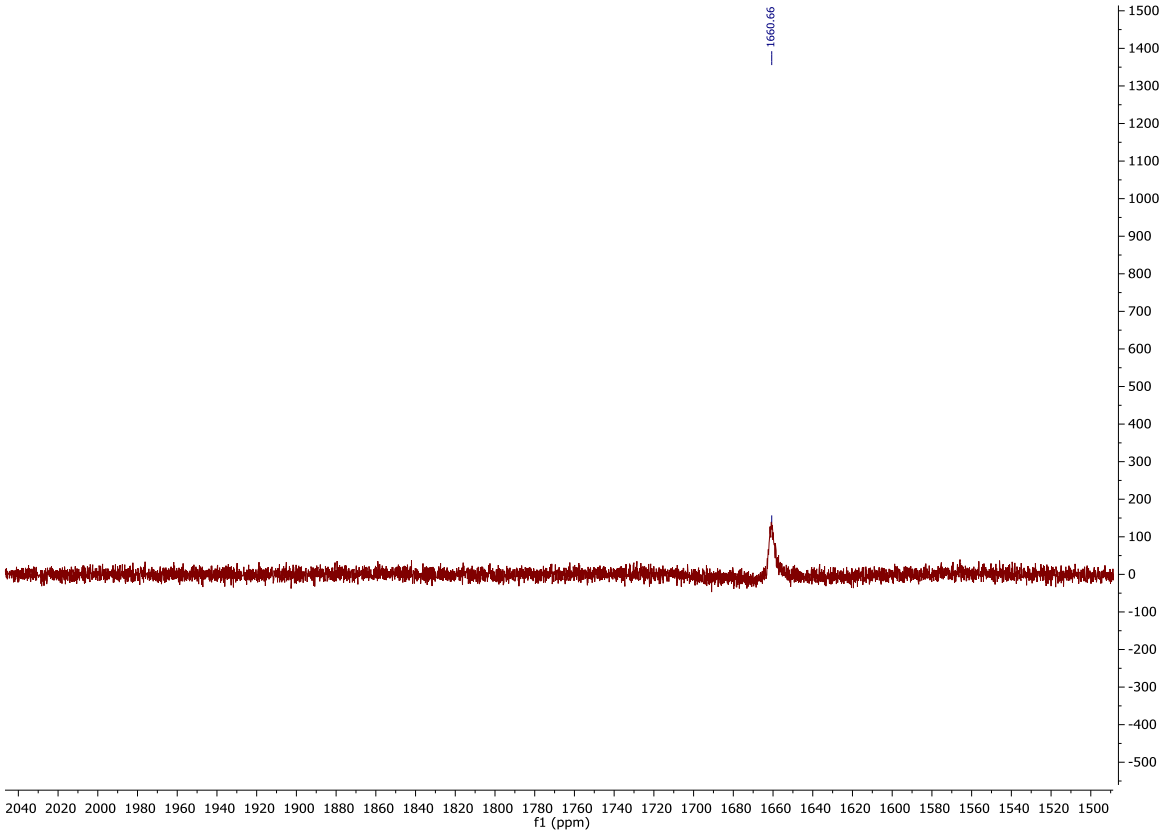

Figure AI4. ^{1}H NMR Spectrum of **1b** (400 MHz, C_6D_6, 298K, ppm)

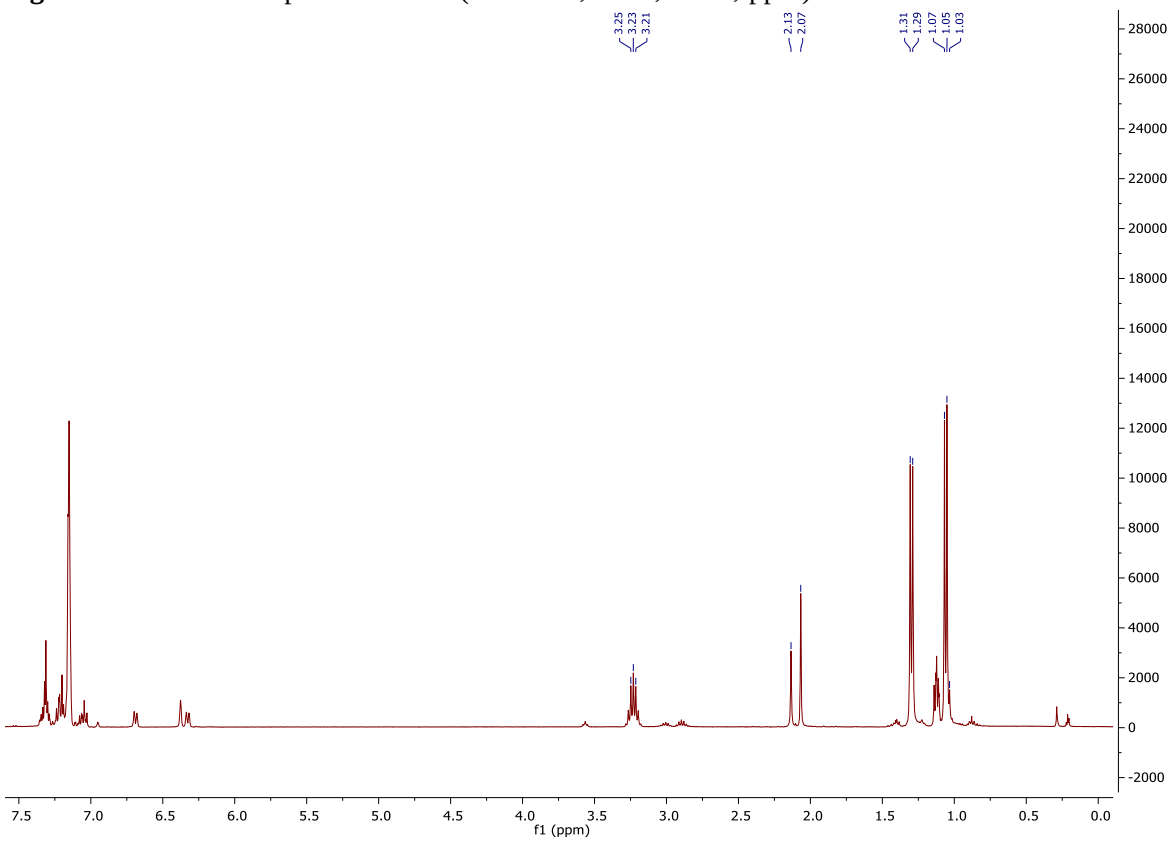

Figure AI5. ^{13}C NMR Spectrum of **1b** (126 MHz, C_6D_6, 298K, ppm)

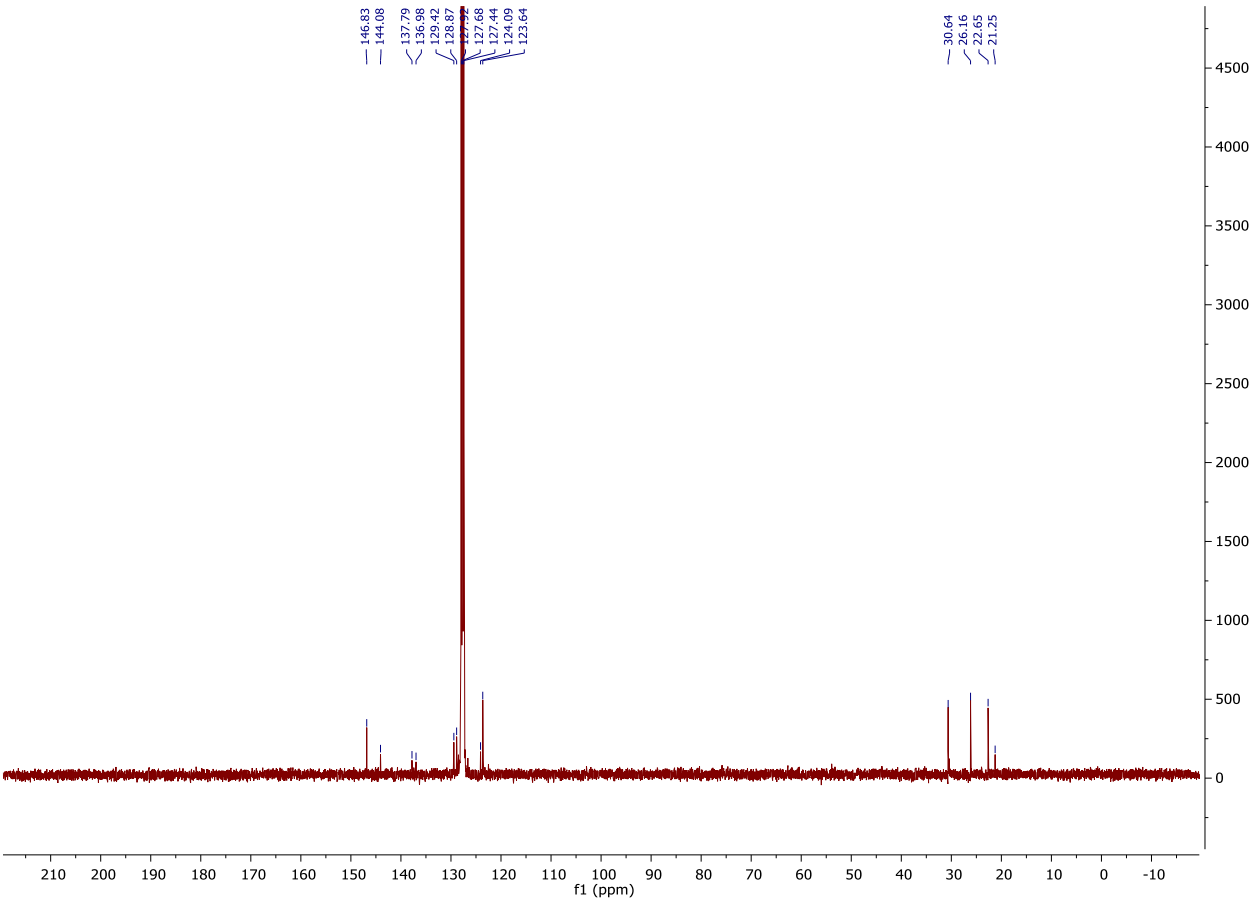

Figure AI6. ^{119}Sn NMR Spectrum of **1b** (186.36 MHz, C_6D_6, 298K, ppm)

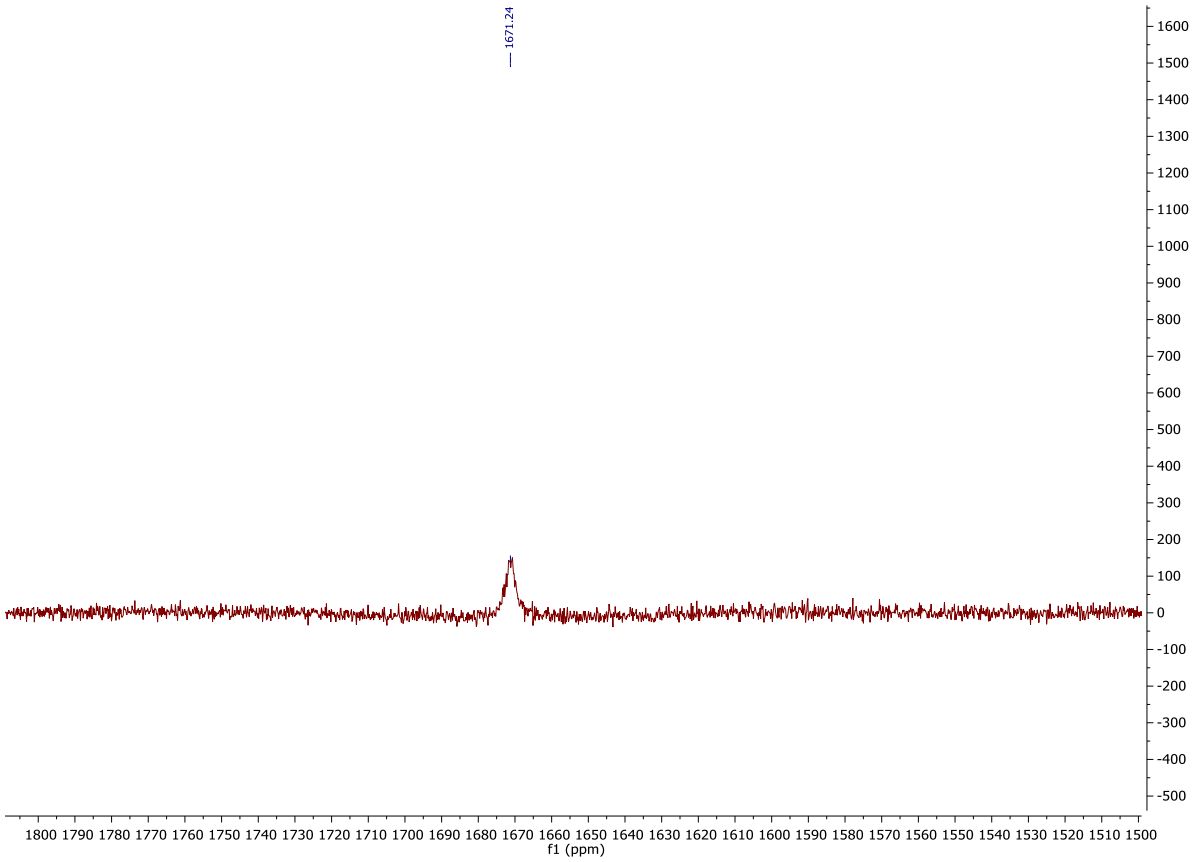

Figure AI7. ^{1}H NMR Spectrum of **1c** (400 MHz, C_6D_6, 298K, ppm)

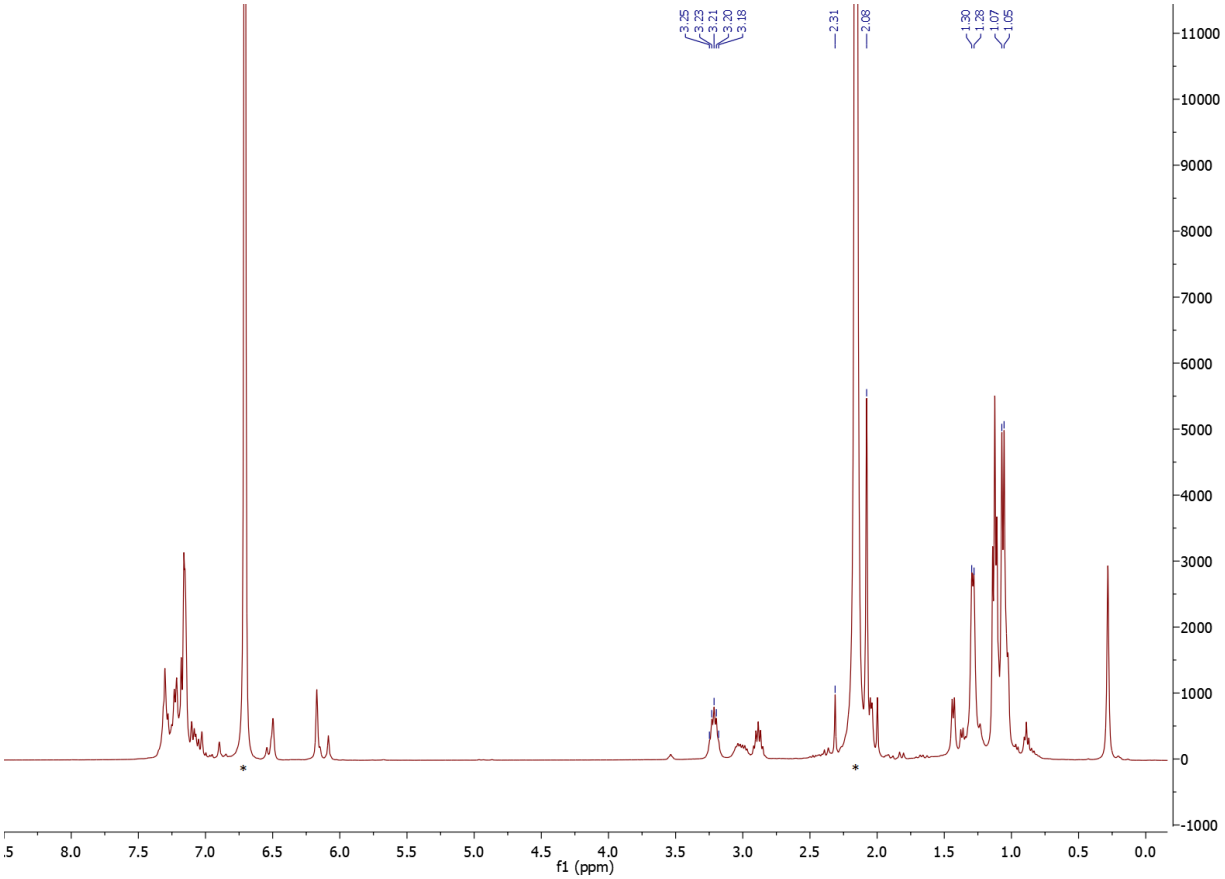

*=Residual Mesitylene

Figure AI8. ^{13}C NMR Spectrum of **1c** (126 MHz, C_6D_6, 298K, ppm)

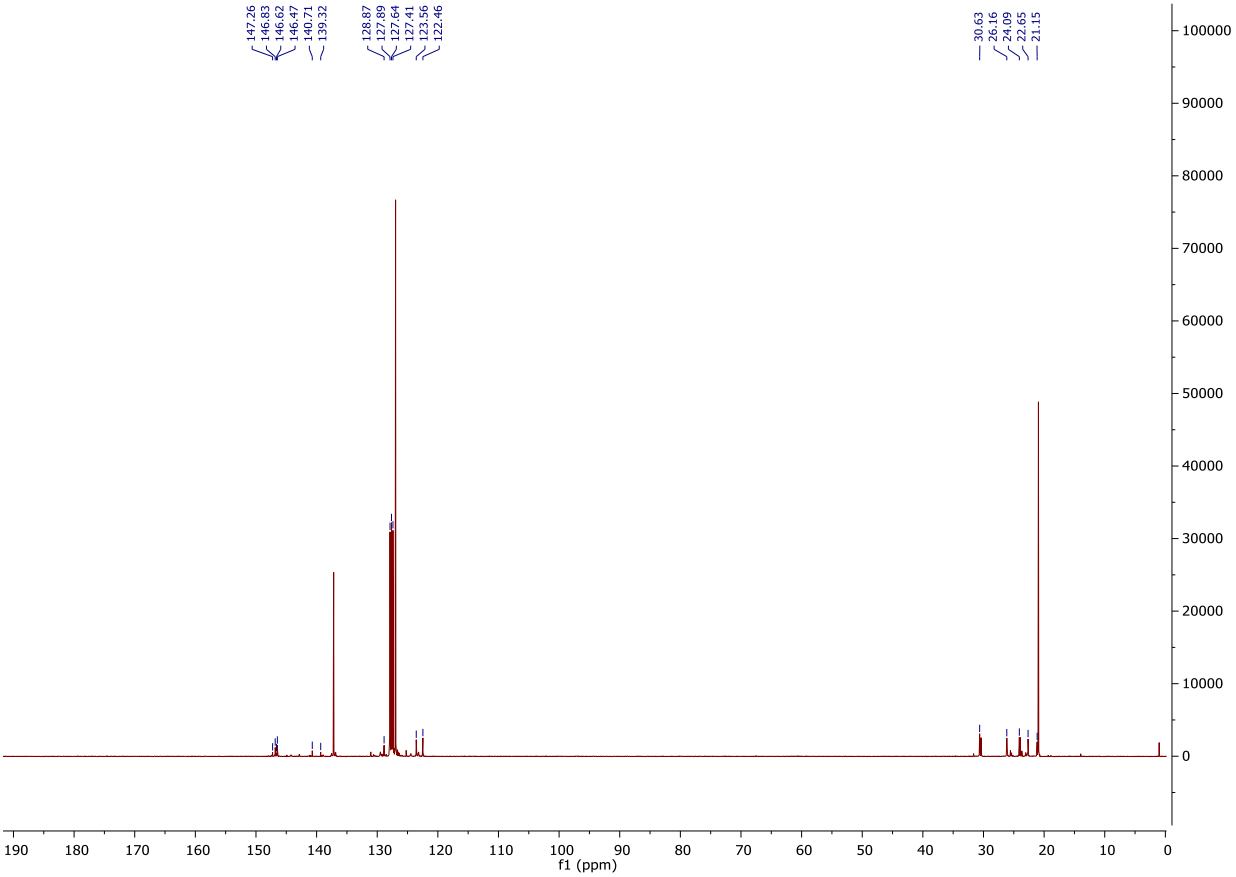

Figure AI9. ^{119}Sn NMR Spectrum of **1b** (186.36 MHz C_6D_6, 298K, ppm)

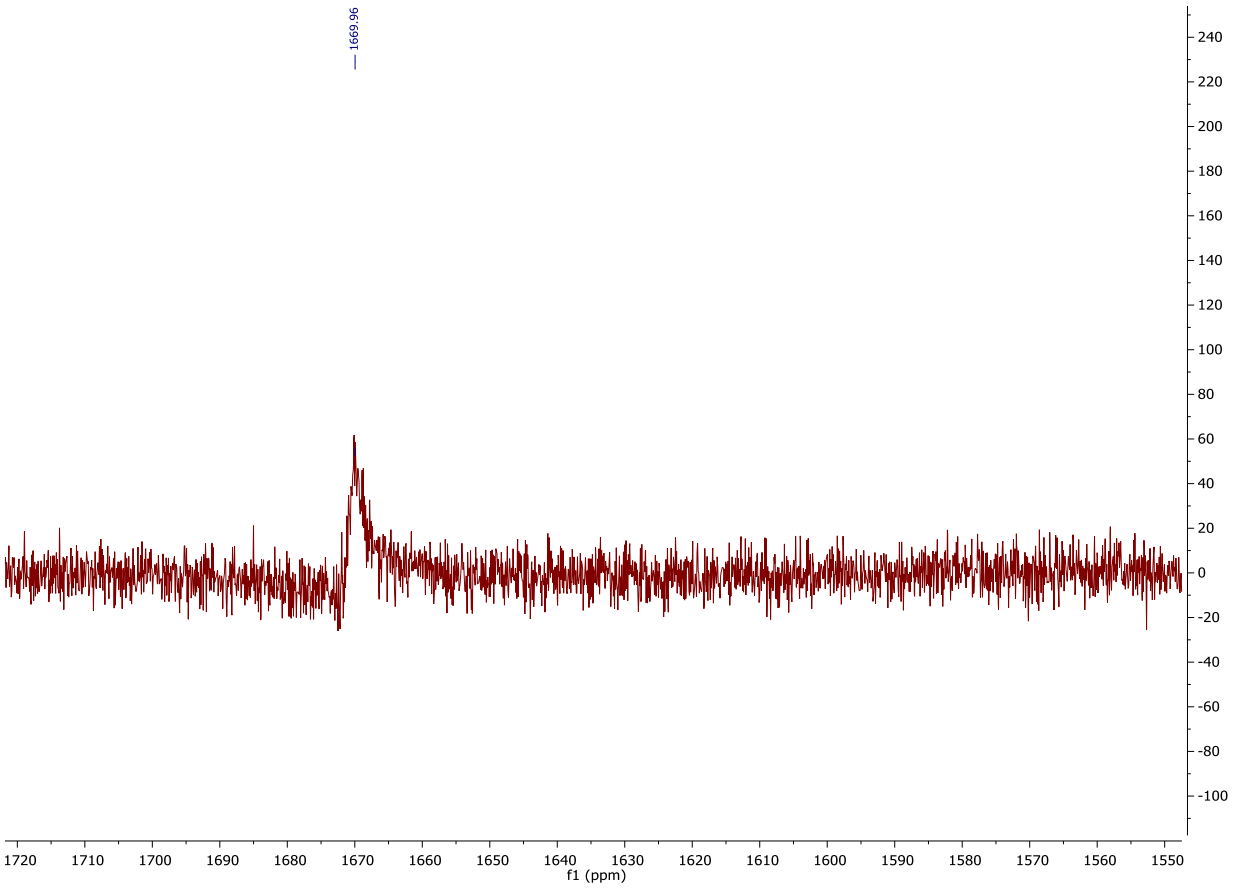

Table AI1. Selected X-ray Crystallographic Data for **1a** and **1b**

Compound	**1a**	**1b**
Formula weight, $gmol^{-1}$	C88 H104 Sn2 · C7H8	C76 H92 Sn2 · C6H14
T (K) / *l* (Å)	90(2) K / 0.71073 Å	100(2) K / 0.71073 Å
Crystal system	Triclinic	Monoclinic
Space group / *Z*	P-1	$P2_1/n$
a, Å	11.7763(7) Å	16.0453(11) Å
b, Å	12.8319(7) Å	11.7131(8) Å
c, Å	13.7749(8) Å	19.0503(13) Å
α, °	110.6153(8)°	90°
β, °	101.7165(8)°	93.4712(17)
γ, °	96.6480(8)°	90°
V, $Å^3$	1867.42(19) $Å^3$	3573.7(4) $Å^3$
ρ, mg m^{-3}	1.244 Mg/m^3	1.155 Mg/m^3
Abs. coeff., mm^{-1}	0.712 mm^{-1}	0.736 mm^{-1}
F(000)	732	1296
Crystal size, mm^3	0.451 x 0.309 x 0.246 mm^3	0.608 x 0.229 x 0.146 mm^3
θ range, °	1.637 to 30.641°	2.371 to 30.569°
Reflns collected	22365	20613
Ind. reflns	11466	10866
R(int)	0.0135	0.0209
Obs. reflns [$I > 2\sigma(I)$]	10639	9366
Completeness to 2θ	100.0	99.8
Goodness-of-fit F^2	1.054	1.105
Final *R* [$I > 2\sigma(I)$]	R1 = 0.0235 wR2 = 0.0597	R1 = 0.0416 wR2 = 0.1021
R (all data)	R1 = 0.0261 wR2 = 0.0608	R1 = 0.0491 wR2 = 0.1053

Appendix II

Supporting Information for Chapter 3: Reversible Sn-Sn Triple Bond Dissociation in a Distannyne: Support for Charge Shift Bonding Character

Figure AII1. VT ^{1}H NMR Spectrum of $Ar^{iPr4}SnSnAr^{iPr4}$ (500 MHz, C_6D_6, 298K to 358K ppm)

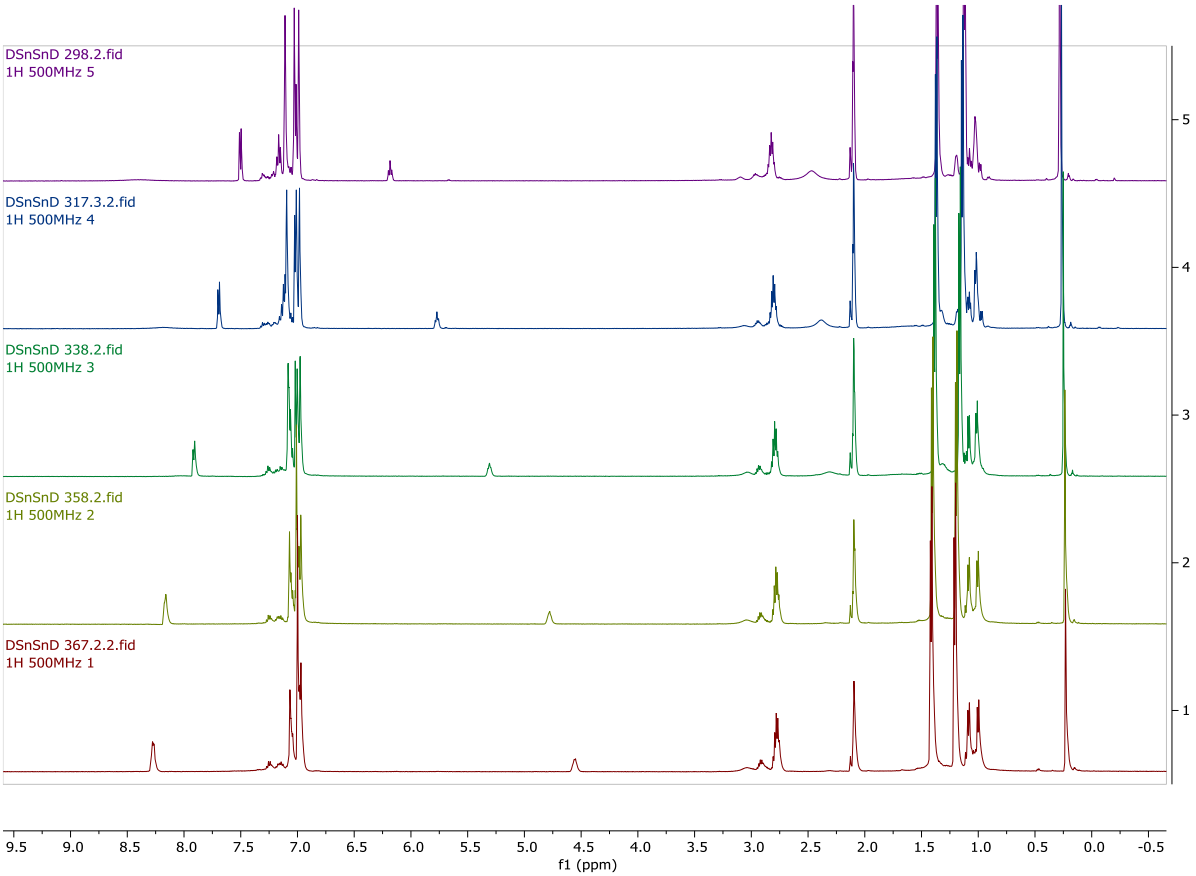
DSnSnD 298.2.fid
1H 500MHz 5
DSnSnD 317.3.2.fid
1H 500MHz 4
DSnSnD 338.2.fid
1H 500MHz 3
DSnSnD 358.2.fid
1H 500MHz 2
DSnSnD 367.2.2.fid
1H 500MHz 1
5
4
3
2
1
9.5 9.0 8.5 8.0 7.5 7.0 6.5 6.0 5.5 5.0 4.5 4.0 3.5 3.0 2.5 2.0 1.5 1.0 0.5 0.0 -0.5
f1 (ppm)

Variable temperature ^{1}H NMR spectroscopy and Van't Hoff analysis of Ar^{iPr4}SnSnAr^{iPr4}

The integral for the signal atoms of the, meta aromatic hydrogen of the central ring were used for the determination of the equilibrium constant for dissociation.

$$f(T) = \ln\left[\frac{(I_0 - I_2)^2}{I_2}\right] = -\frac{\Delta H_d^{298K}}{R}\left(\frac{1}{T}\right) + \ln\left(\frac{I_0 K_0}{4C_0}\right)$$

I0	T	I2	f(T)	1/T	f(T)
2.335	298	2.275	-6.4488	0.003356	-6.4488
2.335	317	2.2197	-5.1178	0.003155	-5.117
2.335	328	2.08425	-3.5010	0.003049	-3.501
2.335	338	1.9272	-2.4500	0.002959	-2.450
2.335	358	1.8261	-1.953	0.002793	-1.953

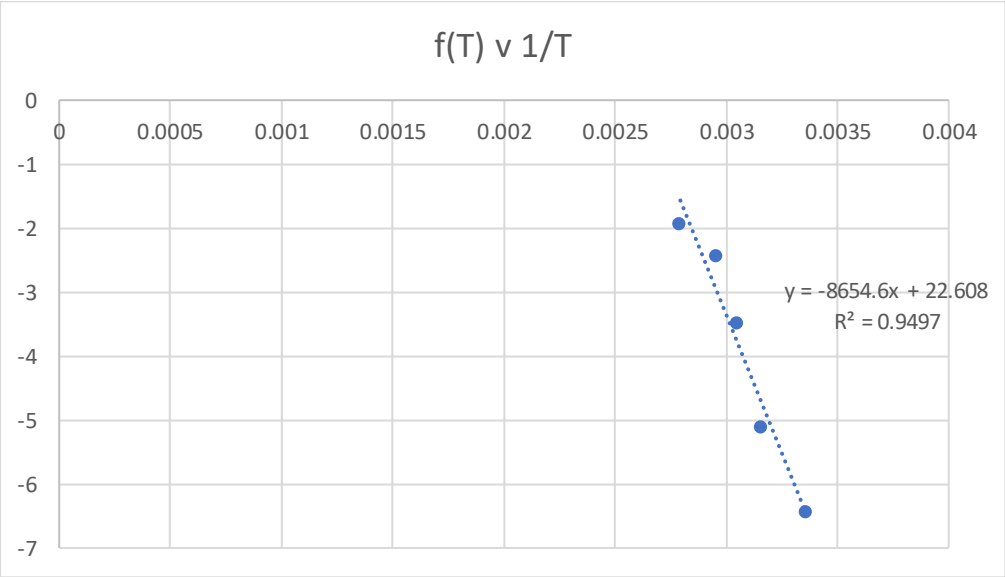

K	lnK	1/T
1.74845E-06	-13.256	0.003356
6.61755E-06	-11.925	0.003155
3.33323E-05	-10.309	0.003049
9.53456E-05	-9.258	0.002959
0.000156702	-8.7611	0.002793

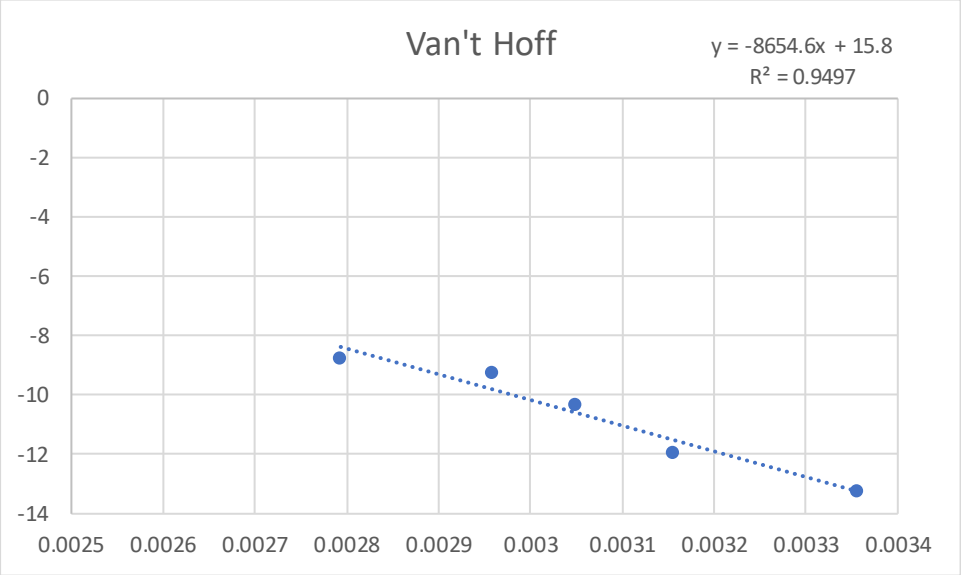

ΔH_d^{298K} = 17.2±1.7 kcal mol^{-1}

ΔS_d = 31.4±3.14 cal mol^{-1} K^{-1}

ΔG_d^{298K} = 7.84±0.78 kcal mol^{-1}

Estimate of Error:

The uncertainty in the integration was estimated to be 10% due to broadening. The VT apparatus indicated an uncertainty in the temperature of 1°C. The concentration is accurate ca. 5%.

Appendix III

Supporting Information for Chapter 4: A Novel Germanium Hydride Radical Trapped During the Photolysis/Thermolysis of Diarylgermylene

Table AIII1. EPR Parameters for Selected Mononuclear Germanium-centered Radicals.

Radical	*g*-values = [g_1, g_2, g_3]	g_{iso}[a]	a_{iso} ^{73}Ge		Ref.
			mT	MHz	
·GeH_3	[2.017, 2.017, 2.003]	2.012	7.5	211	1-2
·$GeMe_3$	-	2.010	8.47	238	3
·$GePh_3$	[2.009, 2.007, 2.001]	2.005	-8.4[e]	-236[e]	4
·$Ge[CH(SiMe_3)_2]_3$	-	2.0078	9.2	258	5
·$Ge[N(SiMe_3)_2]_3$	-	1.999	17.1	478	5
·$Ge(SiMeBu^t_2)_3$		2.0229	2.0	56	6
$\{:Ge[CH(SiMe_3)_2]_2\}^{\cdot-}$	-	2.0125	1.25	35	7
Cy-cAAC:GeN($SiMe_3$)Dip[b]	[2.016, 2.004, 1.9975]	2.003	-		8
Me-cAAC:GeN($SiPh_3$)Mes[b]	[2.018, 2.004, 1.995]	2.005	-		8
neutral Ge(I) radical[c]	[2.001, 1.997, 1.968]	1.988	**A** = [±82.5, ±37.5, ±42.0] MHz, $\lvert a_{iso}\rvert$ = 54 MHz		9
Ge^{III}-hydride[d]	[2.029, 2.003, 1.990]	2.007	**A** = [-10, -90, -10] MHz,[e] a_{iso} = -37 MHz		this chapter

[a] $g_{iso}^2 = (g_1^2 + g_2^2 + g_3^2)/3$.

[b] cAAC = cyclic alkyl(amino) carbenes.

[c] [(^{But}Nacnac)Ge:]·, where ^{But}Nacnac = {[N(Dip)C(Bu^t)]$_2$CH}$^-$, Dip = $C_6H_3Pr^i_2$-2,6.

[d] *g* values from both X-band and Q-band EPR; *A* values from X-band EPR. This radical is retained upon warming up to room temperature and re-cooled down to cryo-temperature.

[e] The sign of the hyperfine is determined, with the others undetermined.

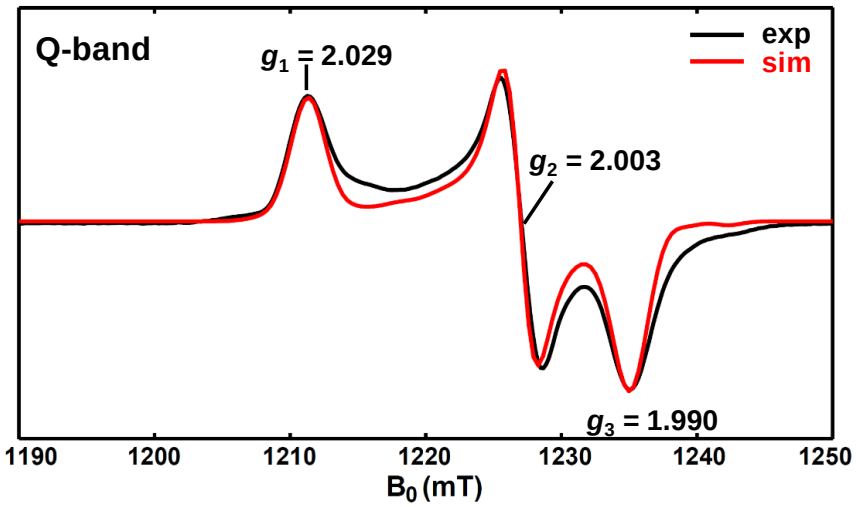

Figure AIII1. Q-band (34.22 GHz) pseudo-modulated electron spin-echo detected field-swept EPR spectrum of the radical trapped by UV photolysis of $Ge(Ar^{iPr4})_2$ in benzene for ~30 min, with the corresponding X-band CW-EPR spectrum shown in Figure 1. The ^{1}H-hyperfine splitting is masked by greater effects of *g*-anisotropy in the higher microwave-frequency/magnetic field Q-band EPR spectrum. The simulation (red trace) parameters are as follows: g = [2.029, 2.003, 1.990], A^{73}Ge = [-10, -90, -10] MHz (7.8% abundance), A^1H = [-23.0, -20.5, -31.5] MHz. The parameters are taken from X-band EPR and ENDOR simulations.

The absolute sign of $^{1}H_{hydride}$

The absolute sign is determined via variable mixing-time (VMT) ENDOR experiment[6] by recording ENDOR spectra at the magnetic field (1223.7 mT) corresponding to g_2 2.003, as shown in Figure S2. As the mixing time t_{mix} is increased from 1 μs (black trace) to 200 μs (red trace), the high RF frequency peak ($\nu_+ = |\nu_N - M_s A|$) of ^{1}H decreases, suggesting that the ν_+ ENDOR transition corresponds to the α electron spin manifold (M_s = +1/2), giving a negative hyperfine coupling A.

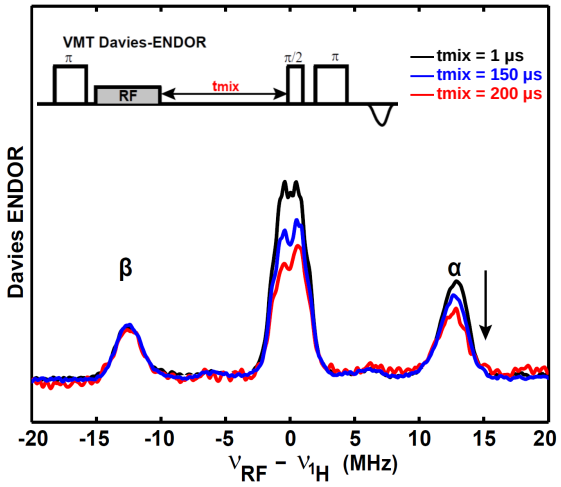

Figure AIII2. ^{1}H VMT Davies-ENDOR spectra of the radical trapped as a result of UV photolysis of $Ge(Ar^{iPr4})_2$ in benzene for ~30 min recorded at magnetic field of 1223.7 mT (g = 2.003) and T = 10 K, acquired by using various t_{mix}. The ENDOR transitions corresponding to β electron spin manifold (M_s = -1/2) are normalized, with the decrease in the ENDOR transitions corresponding to α spin manifold (M_s = +1/2). Other spectrometer settings are microwave frequency = 34.30 GHz, microwave inversion pulse π = 80 ns, π/2 = 12 ns, τ = 300 ns and RF pulse = 20 μs.

Matlab code for two-point dipole approximation model

```
% displaced point dipole for 1H with p orbital treating as two points

clear all;
TH =@(r) gfree*nucgval('1H')*bmagn*nmagn*1e-7/planck/((r/1e9)^3);

 rho = 0.80; % population of Ge 4p orbital
disp = 1.45; % displacement of 4p lobes in angstroms
% coordinates of up and down lobes of pi orbitals
Geu = [0 0 disp].';
Ged = [0 0 -disp].';
Genode = [ 0 0 0].';

PDBZ = [0; 0; 1]; %reference axis for rotation matrix

%population of p orbital
p1 = [0.5, 0.5, 0].'; %divided into three fragments [lobe lobe node];
proj = rho*p1;
j = 1;

rGeH = 1.57; % Ge --- H internuclear distance in angstroms
theta = 0*pi/180; % angle between Ge --- H vector and 4p orbital node plane
NucPos = [0, rGeH*cos(theta), rGeH*sin(theta)].'; %coordinates of hyperfine coupled nucleus in 3-D
space
%vectors between nucleus and lobes of pi orbitals in PDB frame
GeHu = (NucPos-Geu);
GeHd = (NucPos-Ged);
GeHnode = (NucPos-Genode);

ZC = [GeHu GeHd GeHnode];

Anet1 = 0; %initialize Anet
for i = 1:3;
   rA = ZC(:,i);
   zA = rA/norm(rA);
   yA = cross(zA,PDBZ); yA = yA/norm(yA);
   xA = cross(yA,zA); xA = xA/norm(xA);
   R_A = [xA yA zA];
   Adip = [-1 0 0; 0 -1 0; 0 0 2]*TH(norm(rA));
   Aint = R_A*Adip*R_A.'; % transform point-dipole frame into PDB frame
   Anet1 = (proj(i)*Aint) + Anet1; % weight intrinsic A_dip by projection factor and add to total
effective anisotropic hyperfine
end
[R1, A1] = eig(Anet1); % diagonalization of the summed A_dip matrix
sort(diag(A1))
```

The out-of-plane angle θ

By using the two-point dipole approximation model (the above Matlab code), the corresponding dipolar-component tensor $\mathbf{T}_{cal}$ can be obtained by varying the out-of-plane angle θ. As shown in Table S2, the $\mathbf{T}_{cal}$ for the hydrides are very sensitive to the out-plane-angle θ. $\mathbf{T}_{cal}$ is close to the experimental tensor when θ is in the range of 0 ~ 5°, suggesting the Ge^{III}-hydride radical we trapped is in a pseudo-planar geometry.

Table AIII2. The calculated dipolar-component **T** of ^{1}H-hyperfine tensor for the hydride with varying out-of-plane angle θ by using the above two-point dipole approximation model.

Out-of-plane angle (θ)	**T** (MHz)
0°	[2.47, 4.01, -6.48]
1°	[2.43, 4.05, -6.48]
2°	[2.32, 4.17, -6.49]
3°	[2.17, 4.34, -6.51]
4°	[1.99, 4.55, -6.54]
5°	[1.79, 4.78, -6.57]
6°	[1.57, 5.04, -6.61]
7°	[1.36, 5.30, -6.66]
8°	[1.14, 5.58, -6.72]
9°	[5.88, 0.90, -6.78]
10°	[6.18, 0.67, -6.85]
exp.	[2.0, 4.5, -6.5]

A pyramidal model

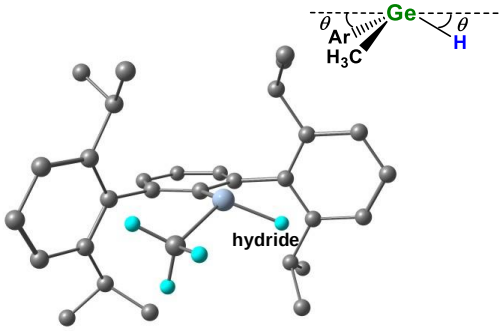

B

	out-of-plane angle (θ)	A ^{73}Ge, MHz	A $^{1}H_{hydride}$, MHz
pyramidal model	17°	[-186, -283, -187]	[+39, +48, +52]
planar model	0°	[-37, -144, -38]	$[-41, -43, -58]_{hydride}$
			$[+42, +43, +49]_{\beta\text{-}^1H_a}$
			$[+37, +33, +39]_{\beta\text{-}^1H_b}$
exp.	≈ 0°	[-10, -90, -10]	[-23.0, -20.5, -31.5]

C planar model

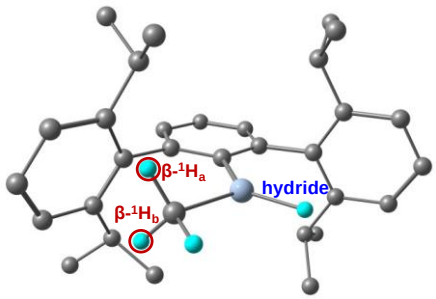

D SOMO of planar model

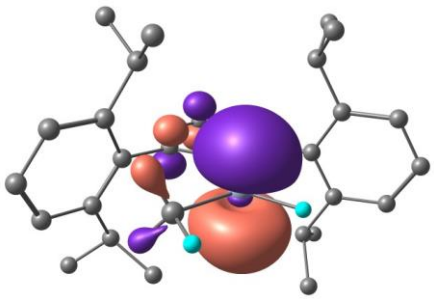

Figure AIII3. (A) The optimized geometry of Ge^{III}-hydride model with a methyl ligand to Ge^{III} by presenting a pyramidal geometry for Ge center, with the out-plane-angle θ = 17° and the Ge-$H_{hydride}$ bond length r = 1.57 Å. (B) The DFT-predicted hyperfine-coupling values for Ge, the hydride and beta-^{1}H. (C) A trigonal-planar geometry of Ge^{III}-hydride model by constraining the dihedral angle between H-Ge-C_{methyl} and H-Ge-C_{phenyl} as 180° on the above optimized pyramidal geometry shown in Figure A. (D) DFT calculated SOMO of the planar Ge^{III}-hydride model shown in Figure C (isosurface value = 0.05 a.u.).

The calculated hyperfine coupling constants of two beta-^{1}H ([+42, +49, +43] MHz and [+37, +39, +33] MHz) of the planar-germanium model are comparable in magnitude to that observed for the hydride ([-41, -43, -58] MHz), but with positive signs that originate from a spin-hyperconjunction mechanism. We did not detect any signals in the ENDOR experiment that would correspond to these calculated hyperfine values from beta-^{1}H.

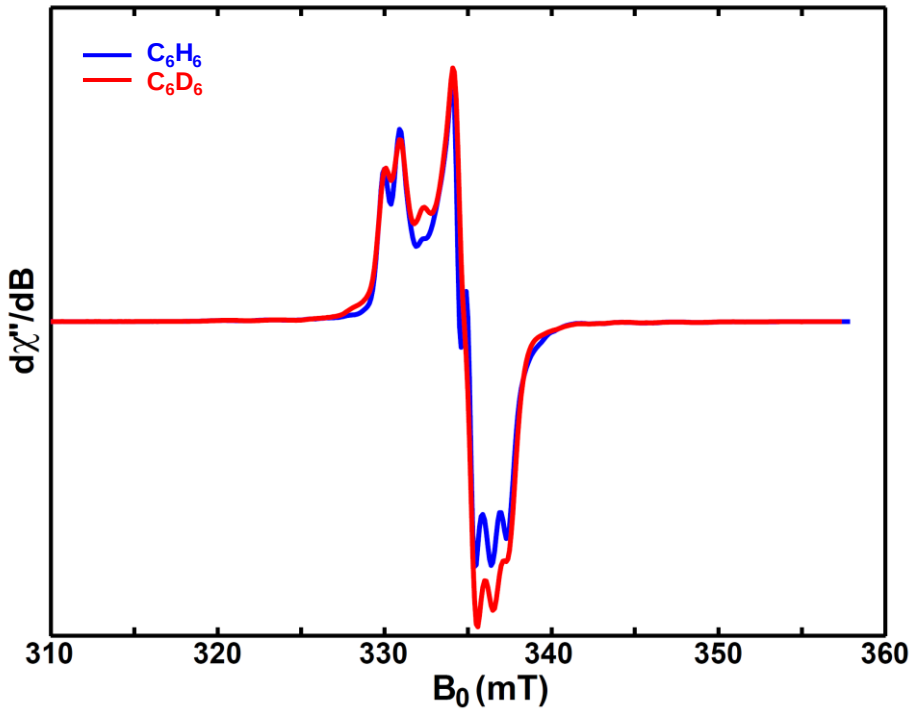

Figure AIII4. X-band (15 K) CW-EPR spectrum of the radical trapped by UV photolysis of $Ge(Ar^{iPr4})_2$ in benzene (blue trace: C_6H_6; red trace: C_6D_6) for ~30 min.

A pyramidal model

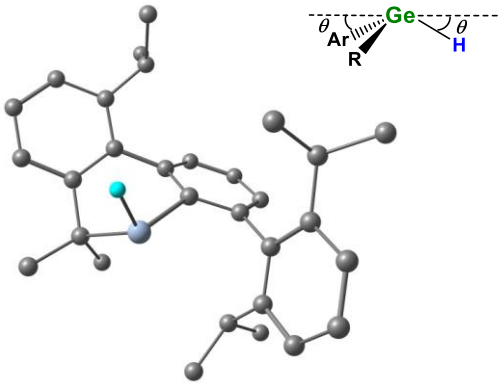

B

	out-of-plane angle (θ)	A ^{73}Ge, MHz	A $^{1}H_{hydride}$, MHz
pyramidal model	22°	[-214, -216, -306]	[+101, +108, +112]
planar model	0°	[-46, -162, -49]	[-40, -43, -58]
exp.	≈ 0°	[-10, -90, -10]	[-23.0, -20.5, -31.5]

C planar model

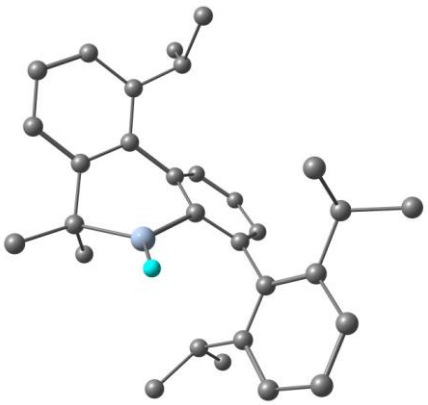

D SOMO of planar model

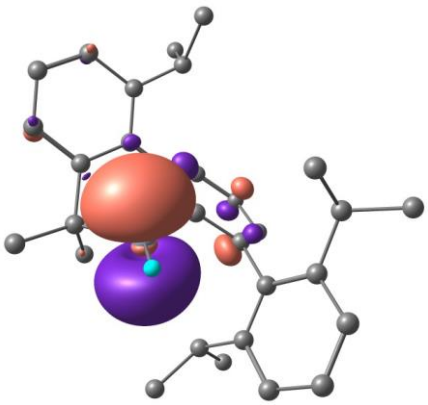

Figure AIII5. (A) The optimized geometry of the Ge^{III}-hydride radical model by presenting a pyramidal coordination for the germanium atom (no beta-proton in this model), with the out-plane-angle θ = 22° and the Ge-H bond length r = 1.57 Å. (B) The DFT-predicted hyperfine coupling values for germanium and the hydride ^{1}H. (C) A trigonal planar geometry of the Ge^{III}-hydride radical model by constraining the dihedral angle between H-Ge-$C_{isopropyl}$ and H-Ge-C_{phenyl} as 180° on the above optimized pyramidal geometry shown in Figure A. (D) DFT calculated SOMO of the planar the Ge^{III}-hydride radical model shown in Figure C (isosurface value = 0.05 a.u.).

Yonezawa and coworkers[10] employed theoretical calculations to study the relationship between the geometry of •CH_3, •SiH_3 and •GeH_3 radicals and the corresponding hyperfine coupling values of the hydrides. They suggested that these hyperfine-coupling values are very sensitive to the out-plane-angle θ: as θ decreases, the spin-polarization contribution, which yields negative hyperfine coupling, becomes larger and is dominant in a planar geometry when θ = 0°, as is approximately the case here for the Ge^{III}-hydride radical.

Table AIII3. Cartesian coordinates of the optimized geometry of the Ge^{III}-hydride radical model by presenting a pyramidal geometry for Ge center (shown in Figure S5A).

Atom	x	y	z
Ge	0.896286	-1.483529	0.306499
H	2.352041	-1.368852	-0.286240
H	-2.203062	-5.481734	-0.526697
H	-3.373405	-4.352445	-2.441315
H	-2.520858	-2.181050	-3.326677
H	2.467544	-6.681698	1.718716
H	1.793196	-5.978515	4.012978
H	-0.066157	-4.347232	4.331740
H	0.568170	-5.679636	-1.368563
H	2.239442	-3.851946	-1.192529
H	2.877045	-5.177363	-2.217200
H	3.455004	-4.990676	-0.525999
H	1.046228	-7.988709	-0.428219
H	2.772940	-7.539255	-0.249902
H	2.032300	-7.581346	-1.872279
H	-1.751404	-2.580738	1.458618
H	-0.436812	-1.557125	3.346143
H	-1.324553	-2.583444	4.520872
H	-2.214022	-1.379222	3.547980
H	-3.127123	-4.626756	1.794849
H	-3.791913	-3.254674	2.743322
H	-2.852102	-4.548456	3.564008
H	0.925486	2.303547	-1.589968
H	1.312247	2.449924	-4.036325
H	0.800140	0.494338	-5.498723
H	0.391417	1.260040	1.728131
H	1.593877	1.525840	0.427676
H	-1.704462	-0.013479	1.368875
H	-2.108716	-0.739348	-0.219973
H	-2.150465	1.037962	-0.014523
H	-0.472335	-2.801746	-4.241527
H	-2.183921	-1.419064	-5.463977
H	-1.335187	-2.556531	-6.564473
H	-0.913106	-0.814941	-6.568096
H	1.972726	-2.532389	-4.681173
H	1.616101	-1.524841	-6.120042
H	1.101593	-3.239059	-6.083351
H	0.017424	2.383379	0.389729
C	-0.253889	-2.663036	-0.790800
C	-0.730772	-3.896533	-0.294329
C	-1.837493	-4.517206	-0.911768
C	-2.484418	-3.888616	-1.987165
C	-2.001754	-2.669545	-2.488501
C	-0.863021	-2.055335	-1.920936

C	-0.059844	-4.505981	0.898833
C	0.991185	-5.444482	0.709830
C	1.646661	-5.960241	1.845291
C	1.269788	-5.564840	3.136933
C	0.226645	-4.645811	3.313969
C	-0.451024	-4.100559	2.205467
C	1.436539	-5.839581	-0.696168
C	2.565737	-4.910862	-1.185850
C	1.841595	-7.317727	-0.811873
C	-1.623211	-3.144295	2.405608
C	-1.382370	-2.112476	3.517660
C	-2.923588	-3.938086	2.639305
C	-0.276519	-0.804229	-2.497216
C	0.079371	0.300072	-1.640333
C	0.658183	1.448847	-2.224039
C	0.881188	1.533725	-3.604053
C	0.578869	0.441807	-4.421646
C	0.024431	-0.742356	-3.888448
C	-0.123723	0.251088	-0.129169
C	0.510545	1.417275	0.637349
C	-1.603595	0.113151	0.272150
C	-0.136078	-1.931967	-4.836548
C	-1.201444	-1.666139	-5.915806
C	1.215402	-2.325293	-5.464113

Table AIII4. Cartesian coordinates of the geometry of the Ge^{III}-hydride radical model by presenting a planar geometry for Ge center (shown in Figure 4 of Chapter 4).

Atom	x	y	z
Ge	0.896000	-1.484000	0.306000
H	2.158000	-1.779000	1.203000
H	-2.203000	-5.482000	-0.527000
H	-3.373000	-4.352000	-2.441000
H	-2.521000	-2.181000	-3.327000
H	2.468000	-6.682000	1.719000
H	1.793000	-5.979000	4.013000
H	-0.066000	-4.347000	4.332000
H	0.568000	-5.680000	-1.369000
H	2.239000	-3.852000	-1.193000
H	2.877000	-5.177000	-2.217000
H	3.455000	-4.991000	-0.526000
H	1.046000	-7.989000	-0.428000
H	2.773000	-7.539000	-0.250000
H	2.032000	-7.581000	-1.872000
H	-1.751000	-2.581000	1.459000
H	-0.437000	-1.557000	3.346000
H	-1.325000	-2.583000	4.521000
H	-2.214000	-1.379000	3.548000
H	-3.127000	-4.627000	1.795000
H	-3.792000	-3.255000	2.743000
H	-2.852000	-4.548000	3.564000
H	0.925000	2.304000	-1.590000
H	1.312000	2.450000	-4.036000
H	0.800000	0.494000	-5.499000
H	0.391000	1.260000	1.728000
H	1.594000	1.526000	0.428000
H	0.017000	2.383000	0.390000
H	-1.704000	-0.013000	1.369000
H	-2.109000	-0.739000	-0.220000
H	-2.150000	1.038000	-0.015000
H	-0.472000	-2.802000	-4.242000
H	-2.184000	-1.419000	-5.464000
H	-1.335000	-2.557000	-6.564000
H	-0.913000	-0.815000	-6.568000
H	1.973000	-2.532000	-4.681000
H	1.616000	-1.525000	-6.120000
H	1.102000	-3.239000	-6.083000
C	-0.254000	-2.663000	-0.791000
C	-0.731000	-3.897000	-0.294000
C	-1.837000	-4.517000	-0.912000
C	-2.484000	-3.889000	-1.987000
C	-2.002000	-2.670000	-2.489000
C	-0.863000	-2.055000	-1.921000

C	-0.060000	-4.506000	0.899000
C	0.991000	-5.444000	0.710000
C	1.647000	-5.960000	1.845000
C	1.270000	-5.565000	3.137000
C	0.227000	-4.646000	3.314000
C	-0.451000	-4.101000	2.205000
C	1.437000	-5.840000	-0.696000
C	2.566000	-4.911000	-1.186000
C	1.842000	-7.318000	-0.812000
C	-1.623000	-3.144000	2.406000
C	-1.382000	-2.112000	3.518000
C	-2.924000	-3.938000	2.639000
C	-0.277000	-0.804000	-2.497000
C	0.079000	0.300000	-1.640000
C	0.658000	1.449000	-2.224000
C	0.881000	1.534000	-3.604000
C	0.579000	0.442000	-4.422000
C	0.024000	-0.742000	-3.888000
C	-0.124000	0.251000	-0.129000
C	0.511000	1.417000	0.637000
C	-1.604000	0.113000	0.272000
C	-0.136000	-1.932000	-4.837000
C	-1.201000	-1.666000	-5.916000
C	1.215000	-2.325000	-5.464000

Table AIII5. Cartesian coordinates of the optimized geometry of the Ge^{III}-hydride radical model by presenting a pyramidal geometry for Ge center (shown in Figure AIII3A).

Atom	x	y	z
Ge	1.580544	0.789507	0.725189
H	2.283364	1.630708	-0.373278
H	-2.222882	-2.676975	0.488049
H	-3.412945	-1.531565	-1.404544
H	-2.444400	0.573350	-2.385057
H	2.167943	-4.596293	2.357839
H	1.958939	-3.662081	4.655514
H	0.524026	-1.664486	5.075946
H	0.021987	-3.512959	-0.474821
H	1.813935	-1.846161	-0.884658
H	2.103470	-3.332023	-1.839670
H	3.062662	-3.024945	-0.354616
H	0.537007	-5.752804	0.611757
H	2.286367	-5.439615	0.369078
H	1.206518	-5.573982	-1.044279
H	-1.171606	0.260710	2.293760
H	0.665093	1.174483	3.734293
H	-0.101721	0.450211	5.188386
H	-0.957567	1.720230	4.265003
H	-2.805110	-1.411215	3.149418
H	-2.993776	0.158762	4.001617
H	-2.169126	-1.214909	4.813696
H	-0.247021	5.248751	-1.007003
H	1.241230	5.232286	-3.009100
H	1.827371	3.076123	-4.121553
H	-1.580931	2.066723	0.572665
H	-1.555462	3.842369	2.290887
H	0.109849	3.517950	1.704040
H	-0.768504	4.990340	1.167404
H	-3.556314	3.594430	0.686082
H	-3.288100	2.991948	-0.984710
H	-2.814059	4.664528	-0.550051
H	0.631844	-0.282025	-2.799657
H	-0.706273	0.500545	-4.756189
H	0.642140	-0.561245	-5.285943
H	0.758740	1.216149	-5.498811
H	3.015425	0.419834	-2.471846
H	3.055833	1.101527	-4.129151
H	2.818690	-0.657908	-3.895334
H	2.525204	-0.755111	2.578931
H	3.255915	-1.138822	0.981723
H	3.794030	0.331858	1.882021
C	2.928008	-0.317726	1.648137
C	-0.022803	-0.076900	-0.020817

C	-0.587894	-1.255876	0.542463
C	-1.800206	-1.765851	0.036515
C	-2.466028	-1.124169	-1.018787
C	-1.926455	0.050048	-1.566582
C	-0.724333	0.586601	-1.068716
C	0.087111	-1.950637	1.681163
C	0.873258	-3.111725	1.436903
C	1.543879	-3.706254	2.523117
C	1.426360	-3.182453	3.819618
C	0.624320	-2.057648	4.052826
C	-0.053498	-1.423010	2.992332
C	0.999662	-3.682105	0.022835
C	2.054614	-2.924850	-0.808828
C	1.270335	-5.193955	-0.004443
C	-0.959064	-0.224870	3.267694
C	-0.298973	0.833314	4.165572
C	-2.308993	-0.699666	3.840095
C	-0.199364	1.872045	-1.626025
C	-0.528474	3.091987	-0.978119
C	-0.000524	4.292448	-1.493718
C	0.836502	4.285491	-2.618757
C	1.162016	3.073103	-3.244000
C	0.658434	1.851469	-2.755897
C	-1.461688	3.114916	0.229695
C	-0.884722	3.913459	1.409927
C	-2.859284	3.619520	-0.177372
C	1.042689	0.535980	-3.426155
C	0.397650	0.415654	-4.819178
C	2.568132	0.341465	-3.483526

Table AIII6. Cartesian coordinates of the geometry of the Ge^{III}-hydride radical model by presenting a planar geometry for Ge center (shown in Figure AIII3C).

Atom	x	y	z
Ge	1.672000	0.649000	0.671000
H	2.509000	1.891000	0.265000
H	1.983000	-0.233000	3.088000
H	2.739000	-1.342000	1.891000
H	3.558000	0.212000	2.314000
H	-2.223000	-2.677000	0.488000
H	-3.413000	-1.532000	-1.405000
H	-2.444000	0.573000	-2.385000
H	2.168000	-4.596000	2.358000
H	1.959000	-3.662000	4.656000
H	0.524000	-1.664000	5.076000
H	0.022000	-3.513000	-0.475000
H	1.814000	-1.846000	-0.885000
H	2.103000	-3.332000	-1.840000
H	3.063000	-3.025000	-0.355000
H	0.537000	-5.753000	0.612000
H	2.286000	-5.440000	0.369000
H	1.207000	-5.574000	-1.044000
H	-1.172000	0.261000	2.294000
H	0.665000	1.174000	3.734000
H	-0.102000	0.450000	5.188000
H	-0.958000	1.720000	4.265000
H	-2.805000	-1.411000	3.149000
H	-2.994000	0.159000	4.002000
H	-2.169000	-1.215000	4.814000
H	-0.247000	5.249000	-1.007000
H	1.241000	5.232000	-3.009000
H	1.827000	3.076000	-4.122000
H	-1.581000	2.067000	0.573000
H	-1.555000	3.842000	2.291000
H	0.110000	3.518000	1.704000
H	-0.769000	4.990000	1.167000
H	-3.556000	3.594000	0.686000
H	-3.288000	2.992000	-0.985000
H	-2.814000	4.665000	-0.550000
H	0.632000	-0.282000	-2.800000
H	-0.706000	0.501000	-4.756000
H	0.642000	-0.561000	-5.286000
H	0.759000	1.216000	-5.499000
H	3.015000	0.420000	-2.472000
H	3.056000	1.102000	-4.129000
H	2.819000	-0.658000	-3.895000
C	2.578000	-0.279000	2.158000
C	-0.023000	-0.077000	-0.021000

C	-0.588000	-1.256000	0.542000
C	-1.800000	-1.766000	0.037000
C	-2.466000	-1.124000	-1.019000
C	-1.926000	0.050000	-1.567000
C	-0.724000	0.587000	-1.069000
C	0.087000	-1.951000	1.681000
C	0.873000	-3.112000	1.437000
C	1.544000	-3.706000	2.523000
C	1.426000	-3.182000	3.820000
C	0.624000	-2.058000	4.053000
C	-0.053000	-1.423000	2.992000
C	1.000000	-3.682000	0.023000
C	2.055000	-2.925000	-0.809000
C	1.270000	-5.194000	-0.004000
C	-0.959000	-0.225000	3.268000
C	-0.299000	0.833000	4.166000
C	-2.309000	-0.700000	3.840000
C	-0.199000	1.872000	-1.626000
C	-0.528000	3.092000	-0.978000
C	-0.001000	4.292000	-1.494000
C	0.837000	4.285000	-2.619000
C	1.162000	3.073000	-3.244000
C	0.658000	1.851000	-2.756000
C	-1.462000	3.115000	0.230000
C	-0.885000	3.913000	1.410000
C	-2.859000	3.620000	-0.177000
C	1.043000	0.536000	-3.426000
C	0.398000	0.416000	-4.819000
C	2.568000	0.341000	-3.484000

Reference for Appendix III

1. Morehouse, R. L.; Christiansen, J. J.; Gordy, W., ESR of free radicals trapped in inert matrices at low temperature: CH_3, SiH_3, GeH_3, and SnH_3. *J. Chem. Phys.* **1966,** *45* (5), 1751-1758.
2. Jackel, G. S.; Gordy, W., Electron spin resonance of free radicals formed from Group-IV and Group-V hydrides in inert matrices at low temperature. *Phys. Rev.* **1968,** *176* (2), 443-452.
3. Bennett, S. W.; Eaborn, C.; Hudson, A.; Hussain, H. A.; Jackson, R. A., Electron spin resonance spectra of trimethylsilyl, trimethylgermyl and related free radicals in solution. *J. Organomet.Chem.* **1969,** *16* (2), P36-P38.
4. Geoffroy, M.; Ginet, L.; Lucken, E. A. C., ESR study of the triphenylgermyl radical in a single crystal of triphenylgermane. *Chem. Phys. Lett.* **1976,** *38* (2), 321-324.
5. Cotton, J. D.; Cundy, C. S.; Harris, D. H.; Hudson, A.; Lappert, M. F.; Lednor, P. W., Photochemical synthesis and electron spin resonance characterisation of stable trivalent metal alkyls (Si, Ge, Sn) and amides (Ge and Sn) of Group IV elements. *J. Chem. Soc., Chem. Commun.* **1974,** (16), 651-652.
6. Sekiguchi, A.; Fukawa, T.; Nakamoto, M.; Lee, V. Y.; Ichinohe, M., Isolable silyl and germyl radicals lacking conjugation with π-bonds: synthesis, characterization, and reactivity. *J. Am. Chem. Soc.* **2002,** *124* (33), 9865-9869.
7. Egorov, M. P.; Nefedov, O. M.; Lin, T.-S.; Gaspar, P. P., Germylene and stannylene anion-radicals: generation and electronic structure. *Organometallics* **1995,** *14* (3), 1539-1541.
8. Siddiqui, M. M.; Sarkar, S. K.; Sinhababu, S.; Ruth, P. N.; Herbst-Irmer, R.; Stalke, D.; Ghosh, M.; Fu, M.; Zhao, L.; Casanova, D.; Frenking, G.; Schwederski, B.; Kaim, W.; Roesky, H. W., Isolation of transient acyclic germanium(I) radicals stabilized by cyclic alkyl(amino) carbenes. *J. Am. Chem. Soc.* **2019,** *141* (5), 1908-1912.
9. Woodul, W. D.; Carter, E.; Müller, R.; Richards, A. F.; Stasch, A.; Kaupp, M.; Murphy, D. M.; Driess, M.; Jones, C., A neutral, monomeric germanium(I) radical. *J. Am. Chem. Soc.* **2011,** *133* (26), 10074-10077.
10. Ohta, K.; Nakatsuji, H.; Maeda, I.; Yonezawa, T., Ab initio calculation of geometries and hfs constants of CH_3, SiH_3 and GeH_3 radicals. *Chem. Phys.* **1982,** *67* (1), 49-58

Appendix IV

Supporting Information for Chapter 5: Facile Insertion of Ethylene into a Group 14 Element-Carbon Bond: Effects of the HOMO-LUMO Energy Gap on Reactivity

Figure AIV1. ^{1}H NMR spectrum for $Ar^{iPr_4}SnC_2H_4Ar^{iPr_4}$ (400 MHz, C_6D_6, 298K, ppm)

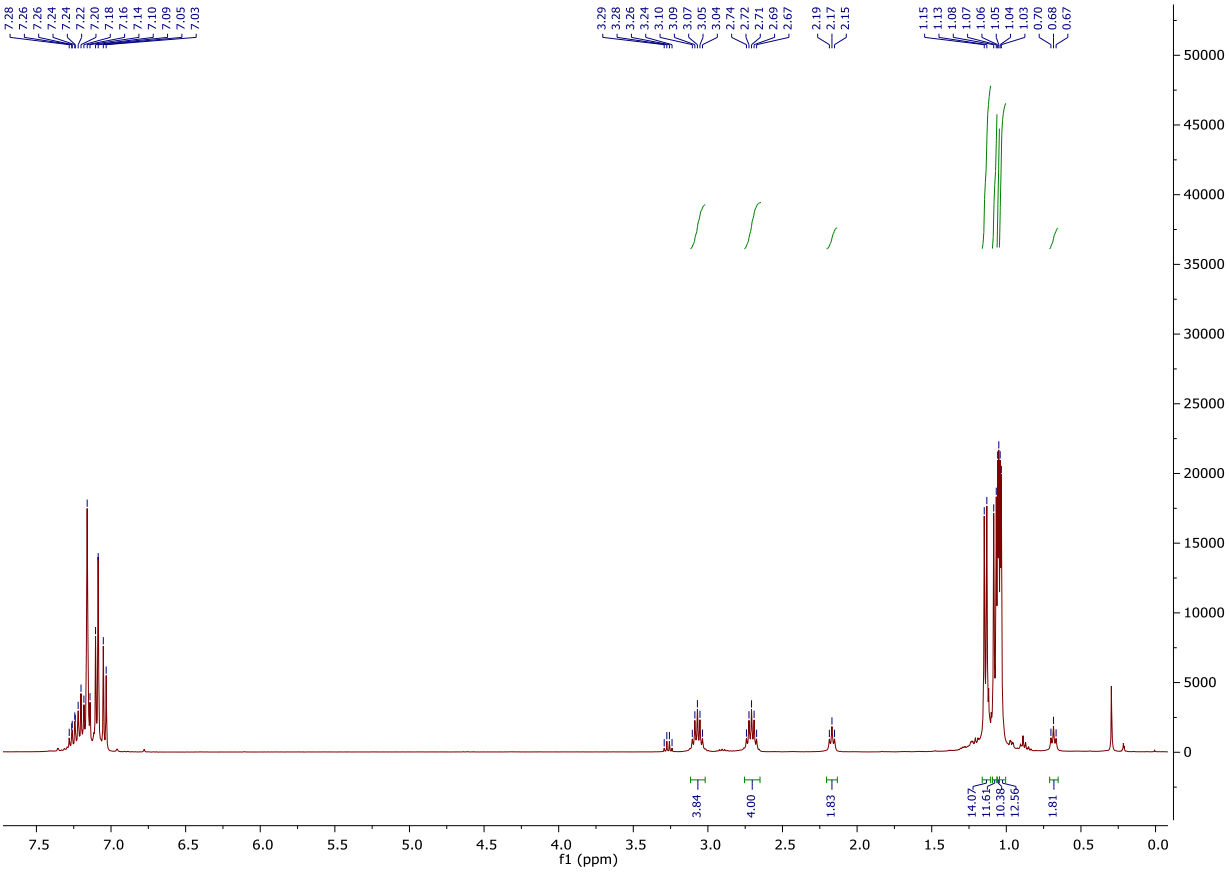

Figure AIV2. $^{13}C\{^{1}H\}$ NMR spectrum for $Ar^{iPr_4}SnC_2H_4Ar^{iPr_4}$ (126 MHz, C_6D_6, 298 K, ppm)

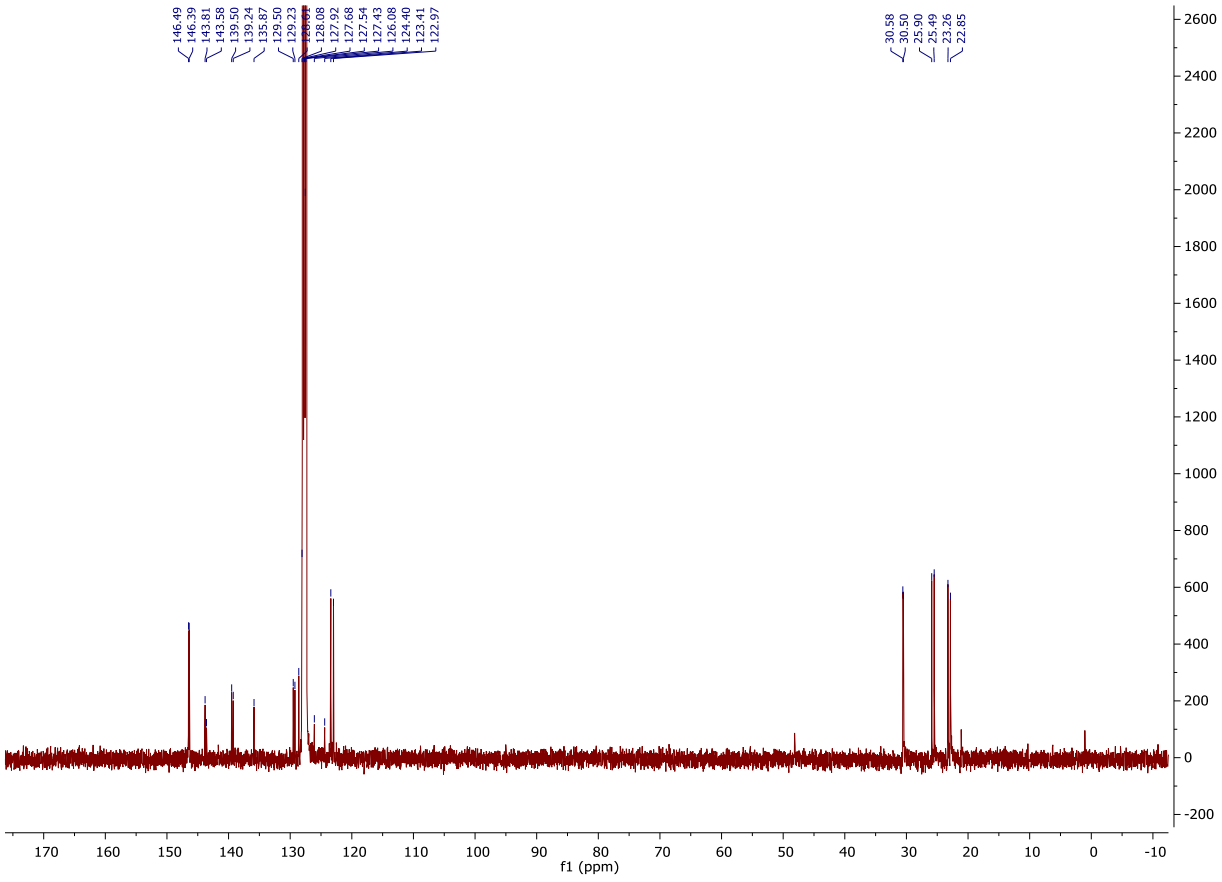

Figure AIV3. $^{119}Sn\{^{1}H\}$ NMR spectrum for $Ar^{iPr_4}SnC_2H_4Ar^{iPr_4}$ (186.36 MHz, C_6D_6, 298K, ppm)

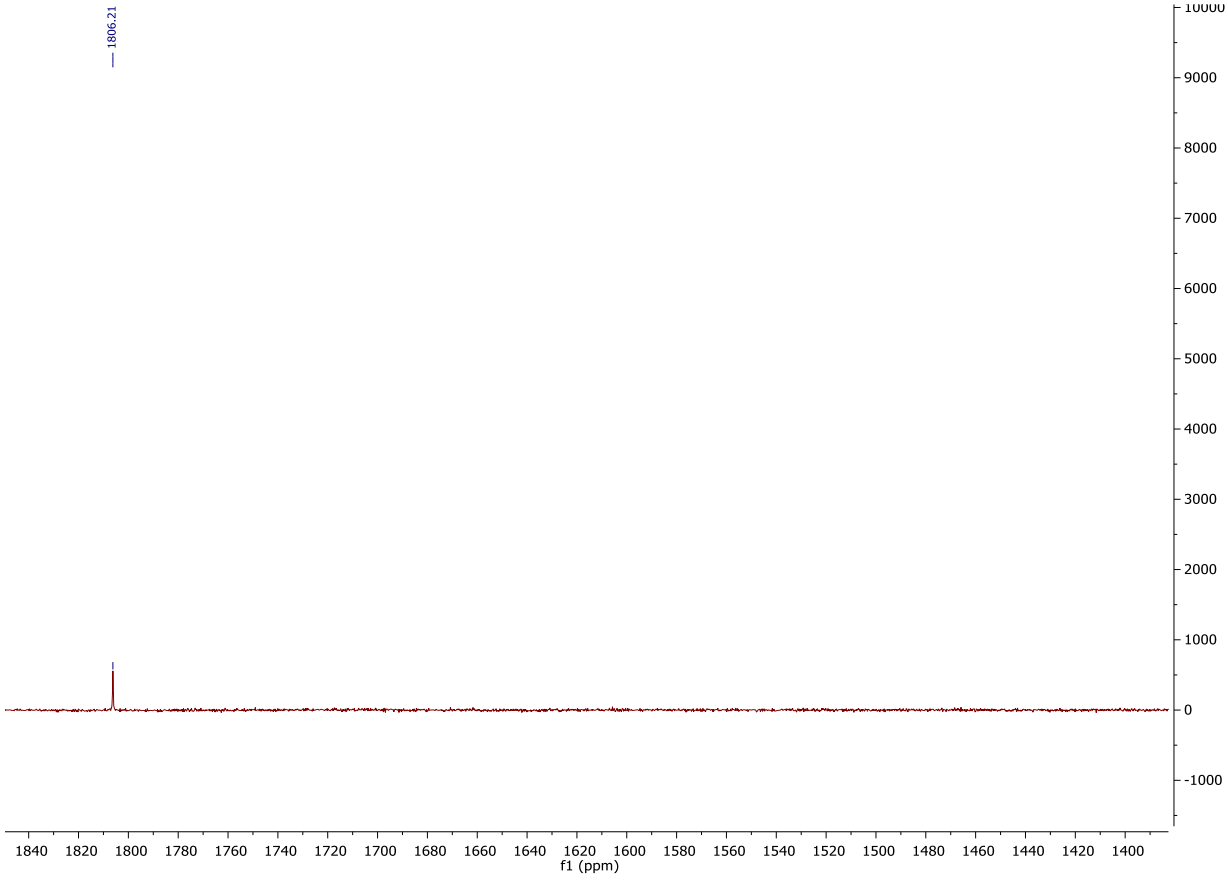

Figure AIV4. ^{1}H NMR spectrum for $Ar^{iPr_6}SnC_2H_4Ar^{iPr_6}$ (400 MHz, C_6D_6, 298K, ppm)

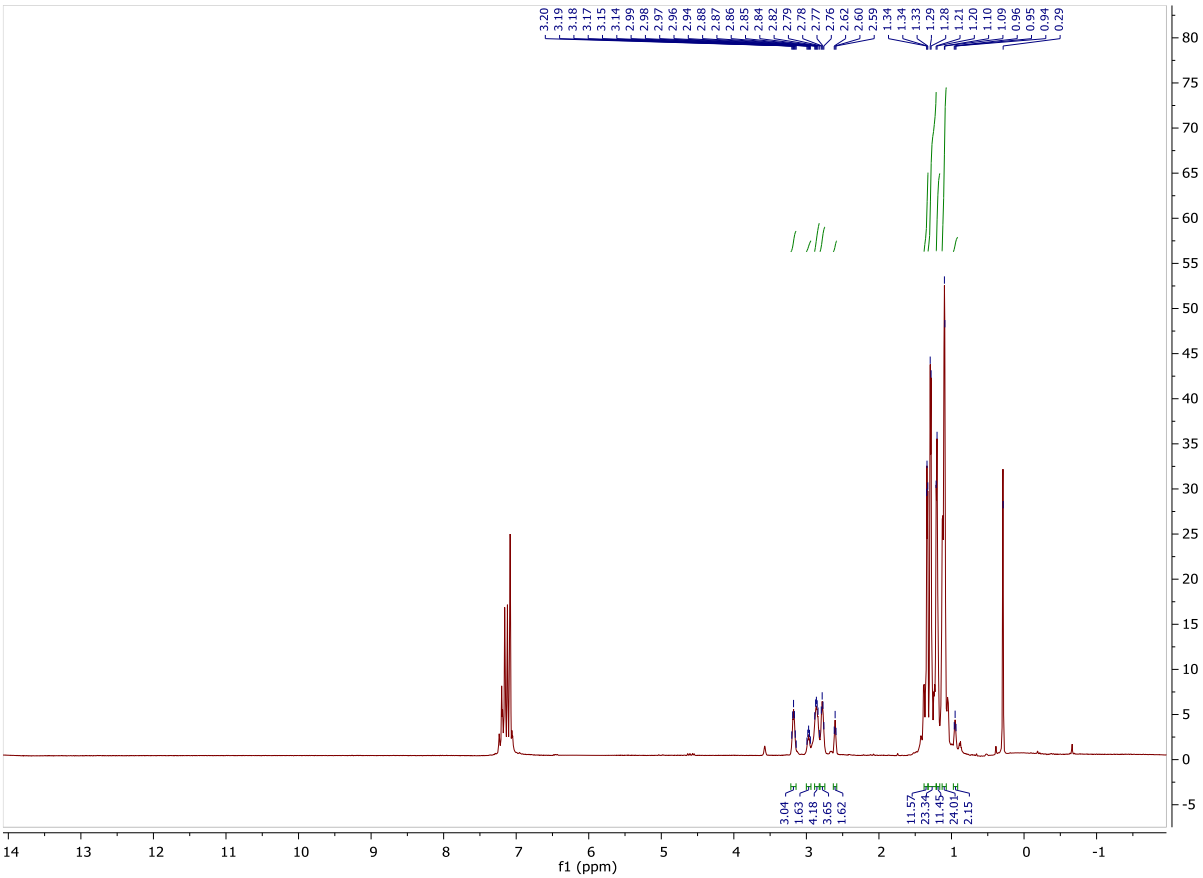

0.29= Silicon grease impurity

Figure AIV5. $^{13}C\{^{1}H\}$ NMR spectrum for $Ar^{iPr_6}SnC_2H_4Ar^{iPr_6}$ (126 MHz, C_6D_6, 298 K, ppm)

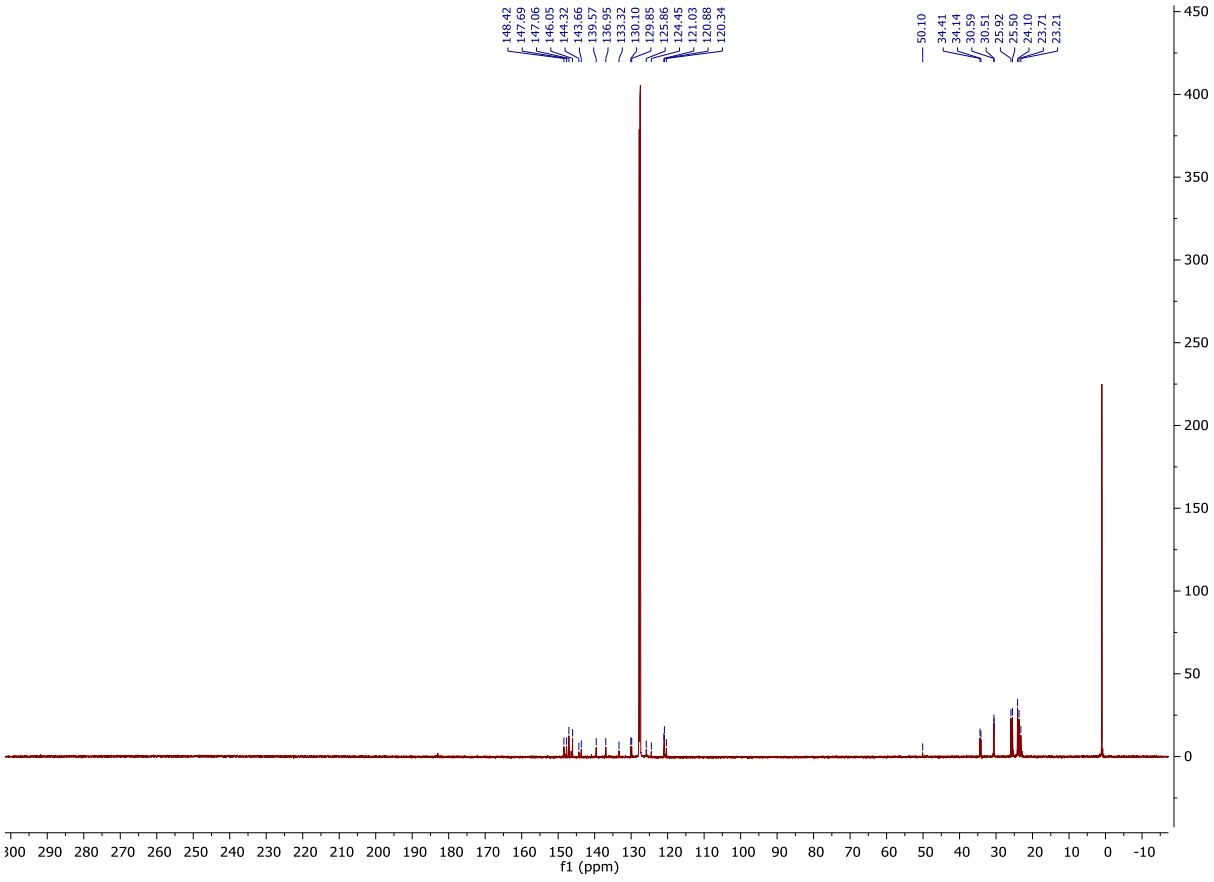

Figure AIV6. $^{119}Sn\{^{1}H\}$ NMR spectrum for $Ar^{iPr_6}SnC_2H_4Ar^{iPr_6}$ (186.36 MHz, C_6D_6, 298K, ppm)

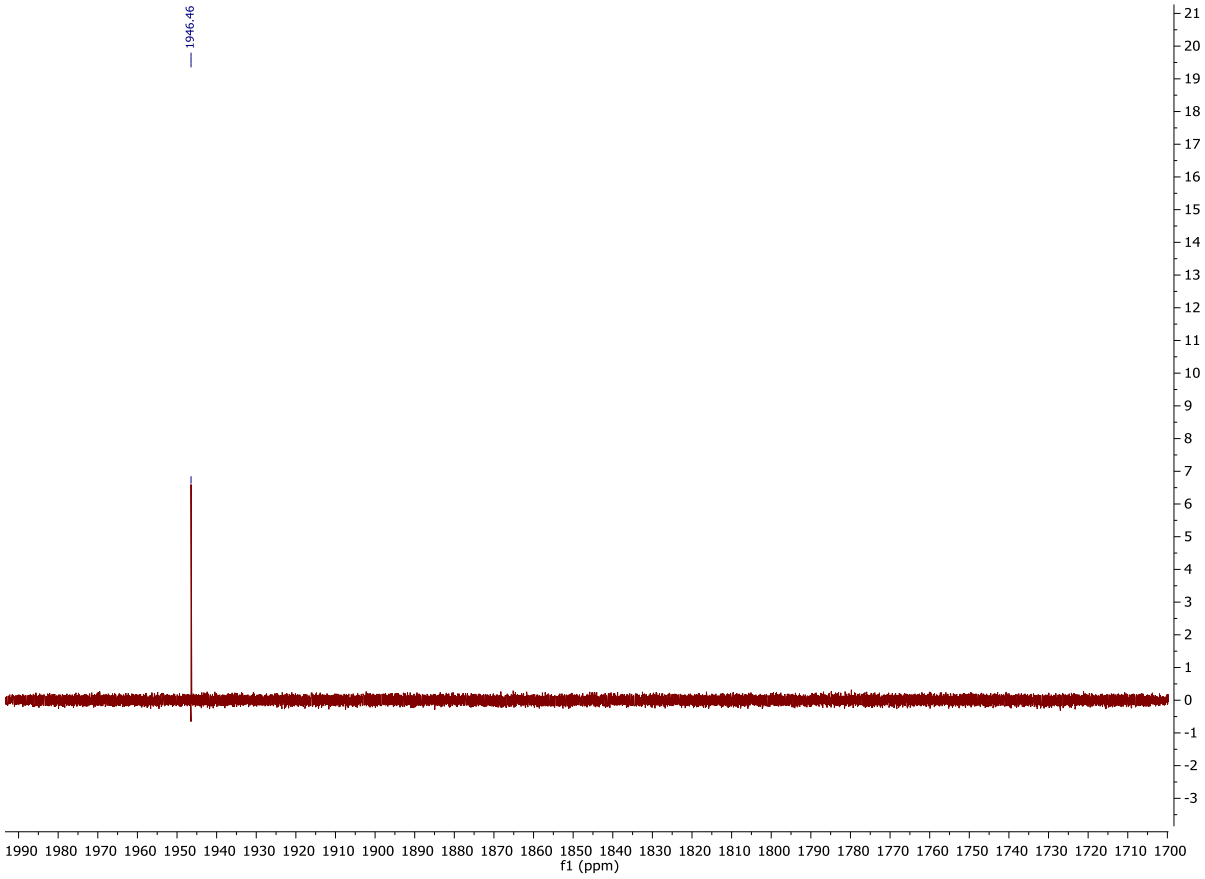

Table AIV1. Selected X-ray Crystallographic Data for **1a** and **1b**

Compound	**1a**	**1b**
Formula weight, $gmol^{-1}$	C62 H78 Sn	C84 H126 Sn
T (K) / *l* (Å)	90(2) K / 0.71073 Å	100(2)K/ 0.71073
Crystal system	Orthorhombic	Monoclinic
Space group / *Z*	$Pna2_1$	P2/n
a, Å	16.2901(9) Å	15.3139(10) Å
b, Å	15.1083(8) Å	12.2886(8) Å
c, Å	21.8016(12) Å	20.4790(14) Å
α, °	90°	90°
β, °	90°	92.374(3)°
γ, °	90°	90°
V, $Å^3$	5365.7(5) $Å^3$	3850.6(4) $Å^3$
ρ, mg m^{-3}	1.166Mg/m^3	1.082 Mg/m^3
Abs. coeff., mm^{-1}	0.512 mm^{-1}	0.372 mm^{-1}
F(000)	2000	1360
Crystal size, mm^3	0.385 x 0.258 x 0.257 mm^3	0.560 x 0.490 x 0.314 mm^3
θ range, °	2.248 to 30.628°	2.324 to 27.524°
Reflns collected	63919	32439
Ind. reflns	16425	8853
R(int)	0.0249	0.0207
Obs. reflns [$I > 2\sigma(I)$]	15193	8015
Completeness to 2θ	99.9%	99.9%
Goodness-of-fit F^2	1.122	1.034
Final *R* [$I > 2\sigma(I)$]	R1 = 0.0419 wR2 = 0.0928	R1 = 0.0326 wR2 = 0.0799
R (all data)	R1 = 0.0458 wR2 = 0.0942	R1 = 0.0370, wR2 = 0.0824

Figure AIV7. Calculation Details of the Reaction of $Sn(Ar^{iPr6})_2$ and Ethylene

Optimization/freq: TPSSTPSS-D3(BJ)/Lanl2dz+d(Sn)/6-31G(d) (others)
Single point calc.: TPSSTPSS-D3(BJ)/[4333111/433111/43]+2d (Sn)/6-311G(d,p) (others)

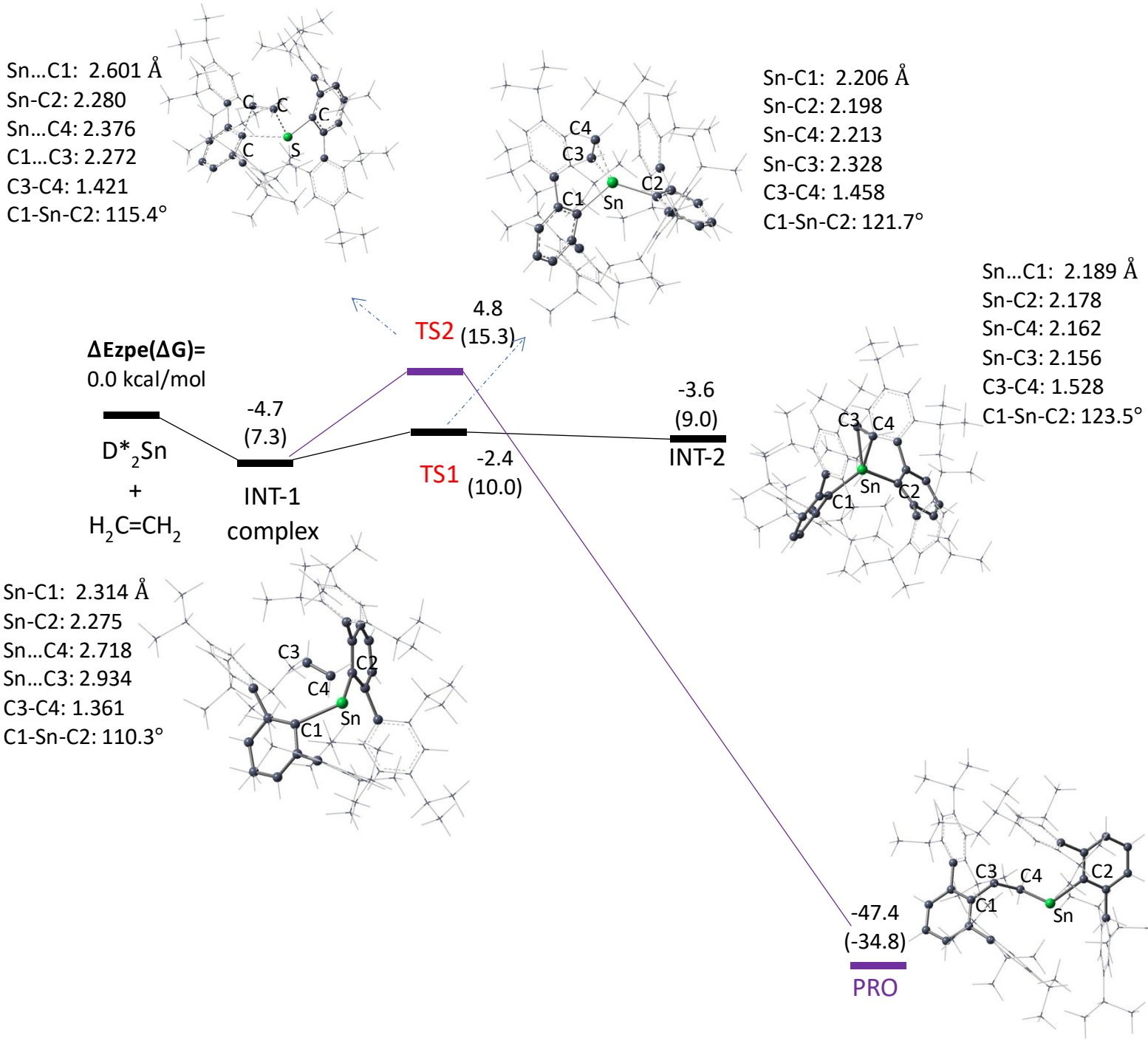

Figure AIV8. Calculation Details of the Reaction of $Sn(Ar^{iPr4})_2$ and Toluene

Reaction of stannylene with toluene

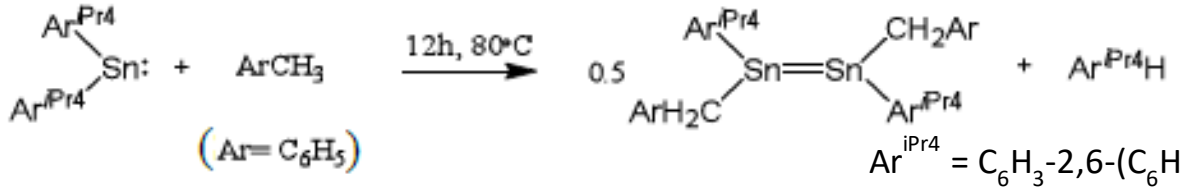

Ar^{iPr4} = C_6H_3-2,6-(C_6H_3-2,6-iPr_2)$_2$

Reaction mechanisms

Optimization/Freq.: B3PW91-D3(BJ)//Lanl2dz+d (Sn)/3-21G(others)
Single point calc. B3PW91-D3(BJ)//[4333111/433111/43]+2d (Sn)/6-311G(d,p) (others)

1. Radical reaction

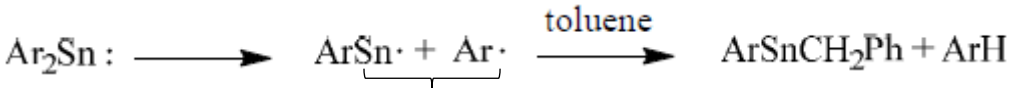

ΔEzpe=0.0 kcal/mol
ΔG=0.0 kcal/mol

67.2(R.T.), for Ar= Ar^{iPr4}
44.8(R.T.)/40.6 (80°C), for Ar= Ar^{iPr4}

2. $SnAr_2^{iPr4}$: [singlet state] ⟷ [triplet state]

ΔEzpe=0.0 kcal/mol
ΔG=0.0 kcal/mol

21.8 (R.T.)
20.6 (R.T.)/21.1 (80°C)

Ar_2Sn: + $PhCH_3$

ΔEzpe=0.0 kcal/mol
ΔG=0.0 kcal/mol

TS_concerted_singlet
37.4 (R.T.)
49.3 (R.T.)/51.4 (80°C)

50.4 (R.T.)
64.8 (R.T.)/67.6 (80°C)

M06-2X level

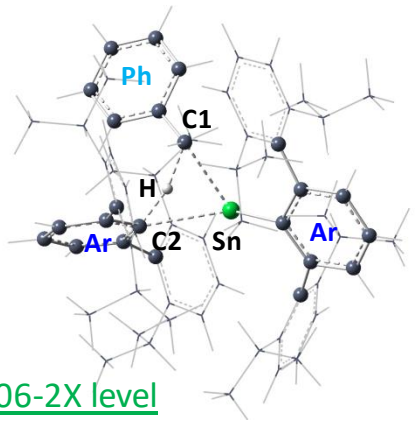

TS_concerted_triplet
> 70 (R.T.)

Sn-C1: 2.591 Å
Sn-C2: 2.765
C1-H: 1.468
C2-H: 1.371

Appendix V

Supporting Information for Chapter 6: Reversible Binding of Ethylene and Propylene by Germylenes

Figure AV1. ^{1}H NMR Spectrum of **1a** (600 MHz, C_7D_8, 273K, ppm)

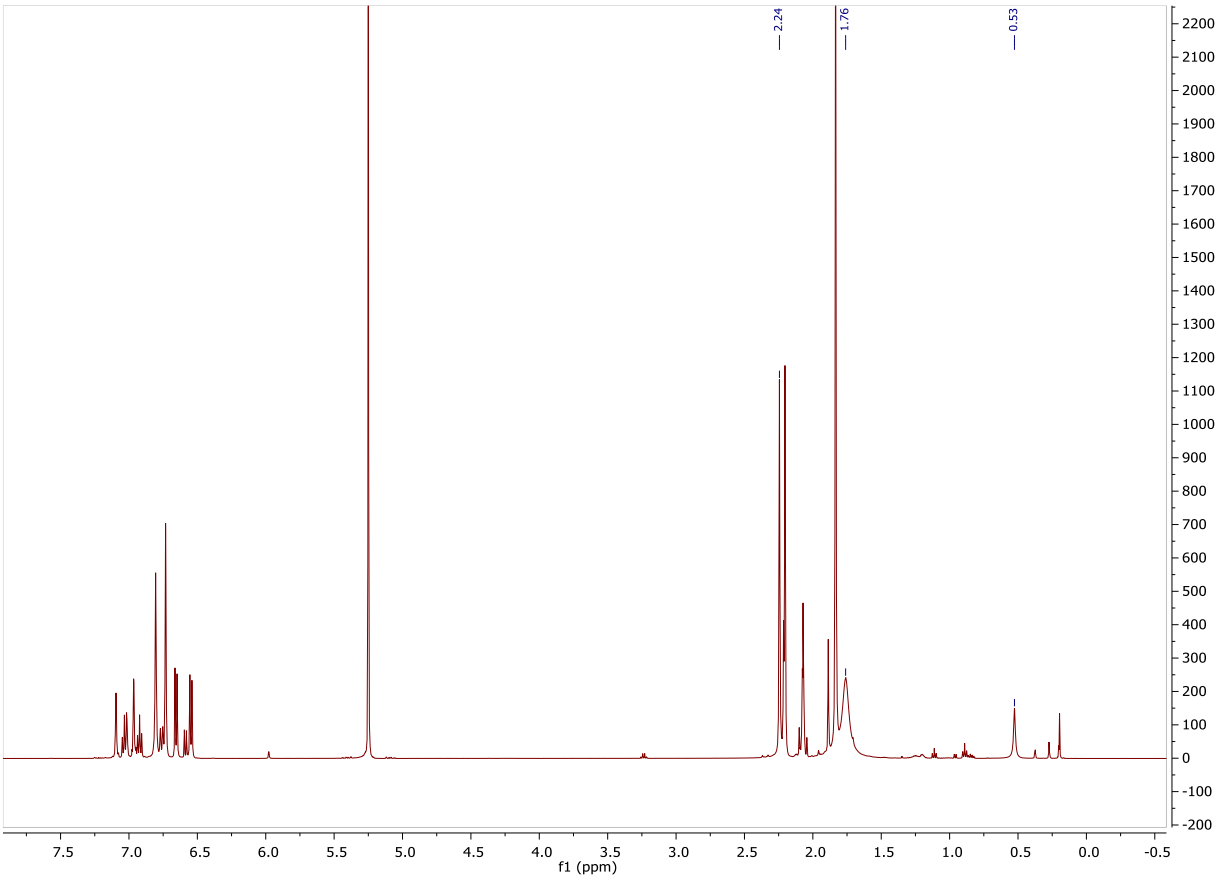

Figure AV2. ^{1}H NMR Spectrum of **1b** (500 MHz, C_7D_8, 298K, ppm)

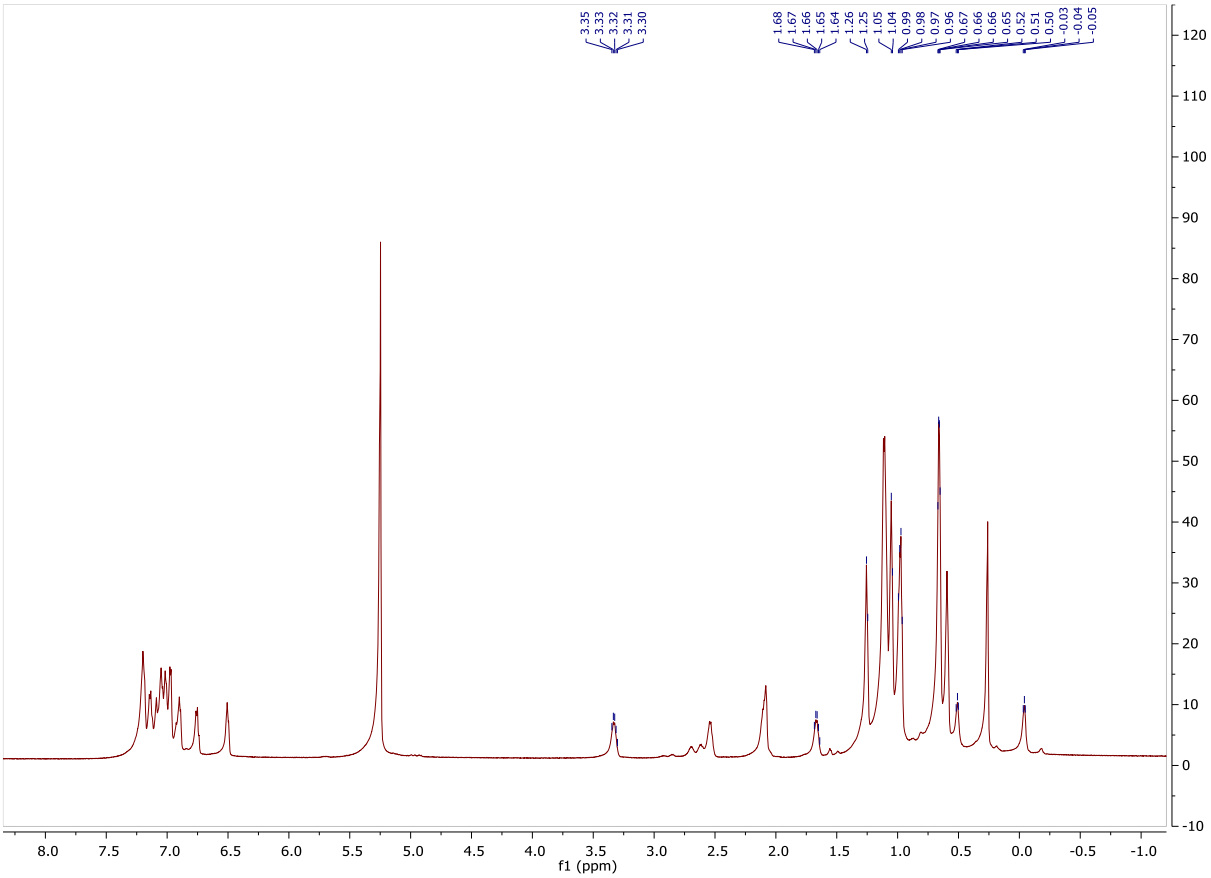

Figure AV3. ^{13}C NMR Spectrum of **1b** (126 MHz, C_6D_6, 298K, ppm)

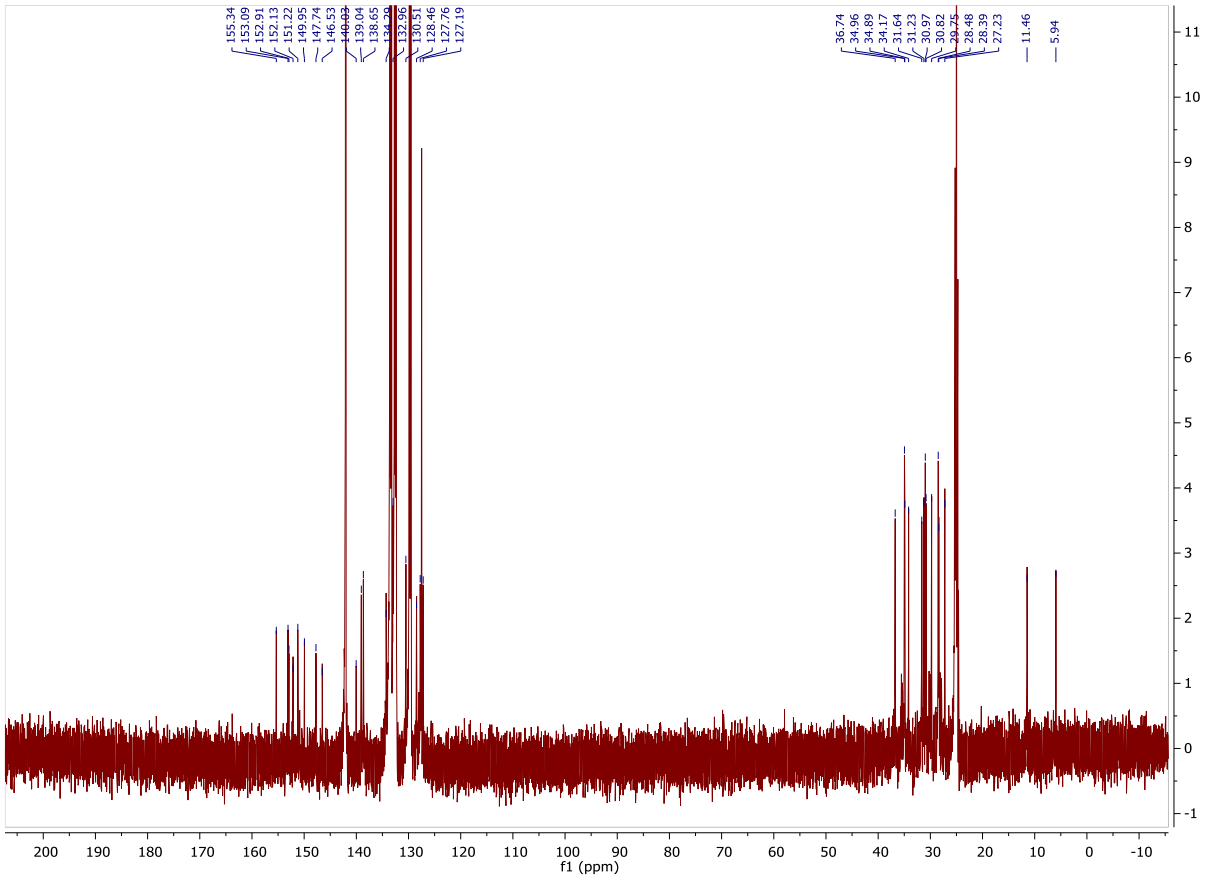

Figure AV4. ^{1}H NMR Spectrum of **1c** (500 MHz, C_7D_8, 248K, ppm)

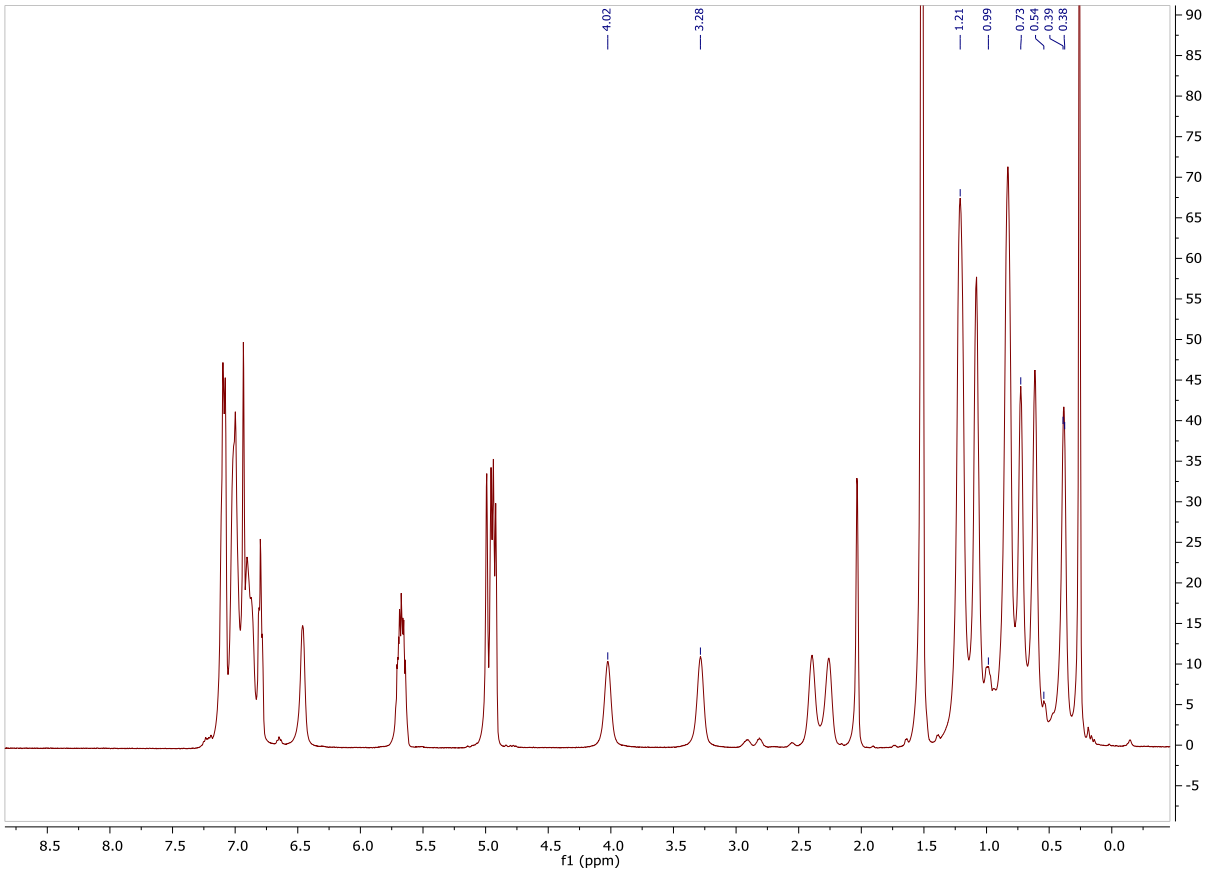

Variable temperature ^{1}H NMR spectroscopy and van't Hoff analysis of **1a**

The integral atoms of the, o-Me group of $Ge(Ar^{Me6})_2$, free ethylene and Me of the germirane in compound **1a** were used for the determination of the equilibrium constant for the conversion of the germylene with ethylene to give the germirane.

The equilibrium constant was calculated according to equation 1.

$$K_{eq} = \frac{[Germirane]}{[Germylene][ethylene]} \text{ (eq1)}$$

The Van't Hoff equation, equation 2, was used in order to determine ΔH and ΔS from the slope and the intercept of the plot of ln Keq against 1/T.

$$lnK_{eq} = -\frac{\Delta H}{R}\left(\frac{1}{T}\right) + \frac{\Delta S}{R} \text{ (eq. 2)}$$

Figure AV5. ^{1}H NMR spectrum for **1a** at various temperatures from 257 to 298 K (500 MHz, C_7D_8)

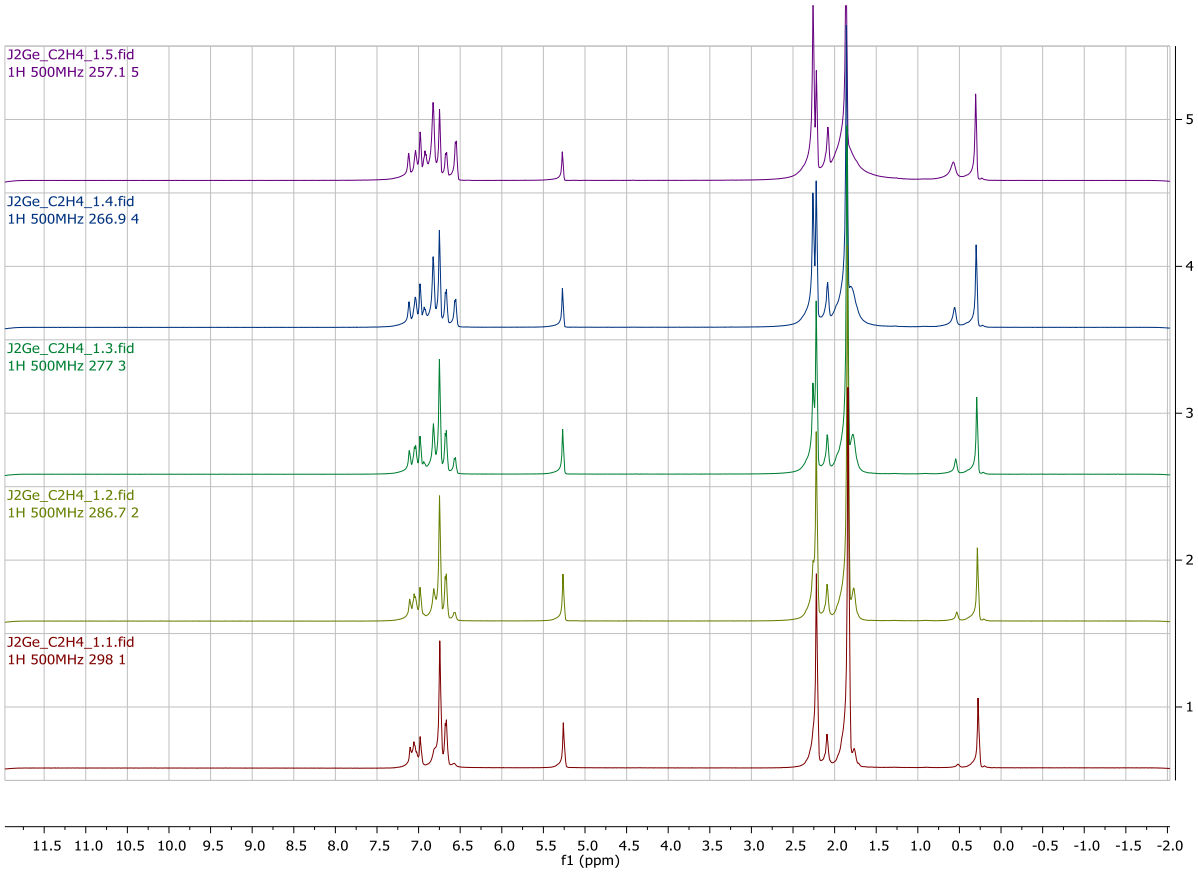

T	$Ge(Ar^{Me6})_2$	Ethylene	complex	
298	249.4	26.76	4	Intensity
286	245.64	27.41	6.02	
278	239.72	25.67	12.68	
268	228.85	24.28	23.63	

T	$Ge(Ar^{Me6})_2$	Ethylene	complex	Scale to number of Hydrogens
298	10.39166667	6.69	1	
288	10.235	6.8525	1.505	
278	9.988333333	6.4175	3.17	
268	9.535416667	6.07	5.9075	

T	$Ge(Ar^{Me6})_2$	Ethylene	complex	
298	0.000228617	0.00014718	0.000022	mol
288	0.00022517	0.000150755	0.00003311	
278	0.000219743	0.000141185	0.00006974	
268	0.000209779	0.00013354	0.000129965	

T	$Ge(Ar^{Me6})_2$	Ethylene	complex	Concentration Volume
298	0.457233333	0.29436	0.044	5.00E-04
288	0.45034	0.30151	0.06622	
278	0.439486667	0.28237	0.13948	
268	0.419558333	0.26708	0.25993	

van't Hoff analysis of Figure AV5.

T	Keq	lnK	1/T
298	0.326	-1.118	0.0033
288	0.488	-0.718	0.0035
278	1.124	0.1168	0.00362
268	2.319	0.841	0.0037

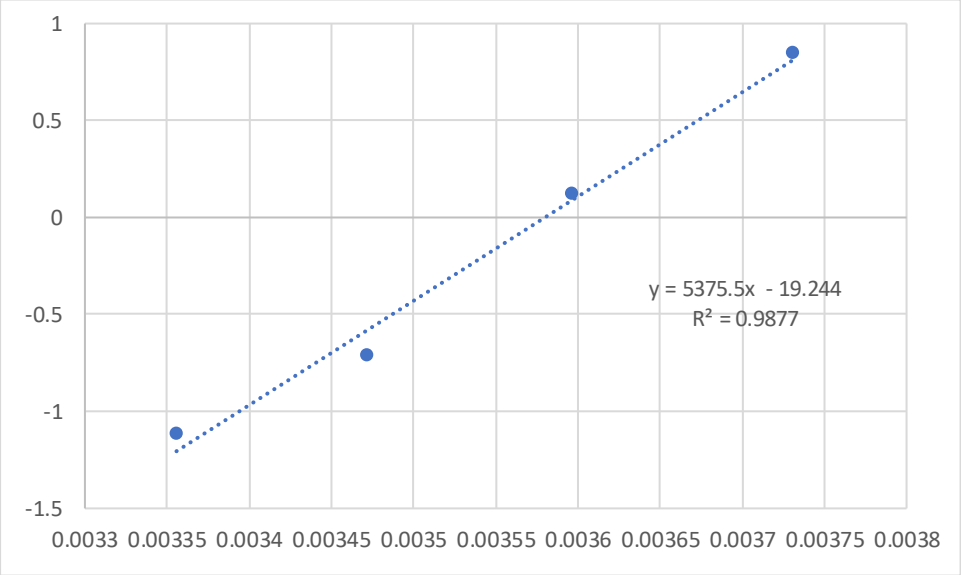

ΔH_{ass}= -44.69 kJ mol^{-1}

ΔS_{ass}= -159.82 J K^{-1} mol^{-1}

ΔG_{ass}(298K)= -6.3 kJ mol^{-1}

Estimate of Error:

The uncertainty in the integration was estimated to be 5%. The VT apparatus indicated an uncertainty in the temperature of 1°C. The concentration is accurate ca. 5% and 2% for the germylene.

Variable temperature ^{1}H NMR spectroscopy and Van't Hoff analysis of **1b**

The integral atoms of the, iPr group of $Ge(Ar^{iPr4})_2$, free ethylene and Me of the germirane in compound **1b** were used for the determination of the equilibrium constant for the conversion of the germylene with ethylene to give the germirane.

Figure AV6. ^{1}H NMR spectrum for **1b** at various temperatures from 258 to 298 K (500 MHz, C_7D_8)

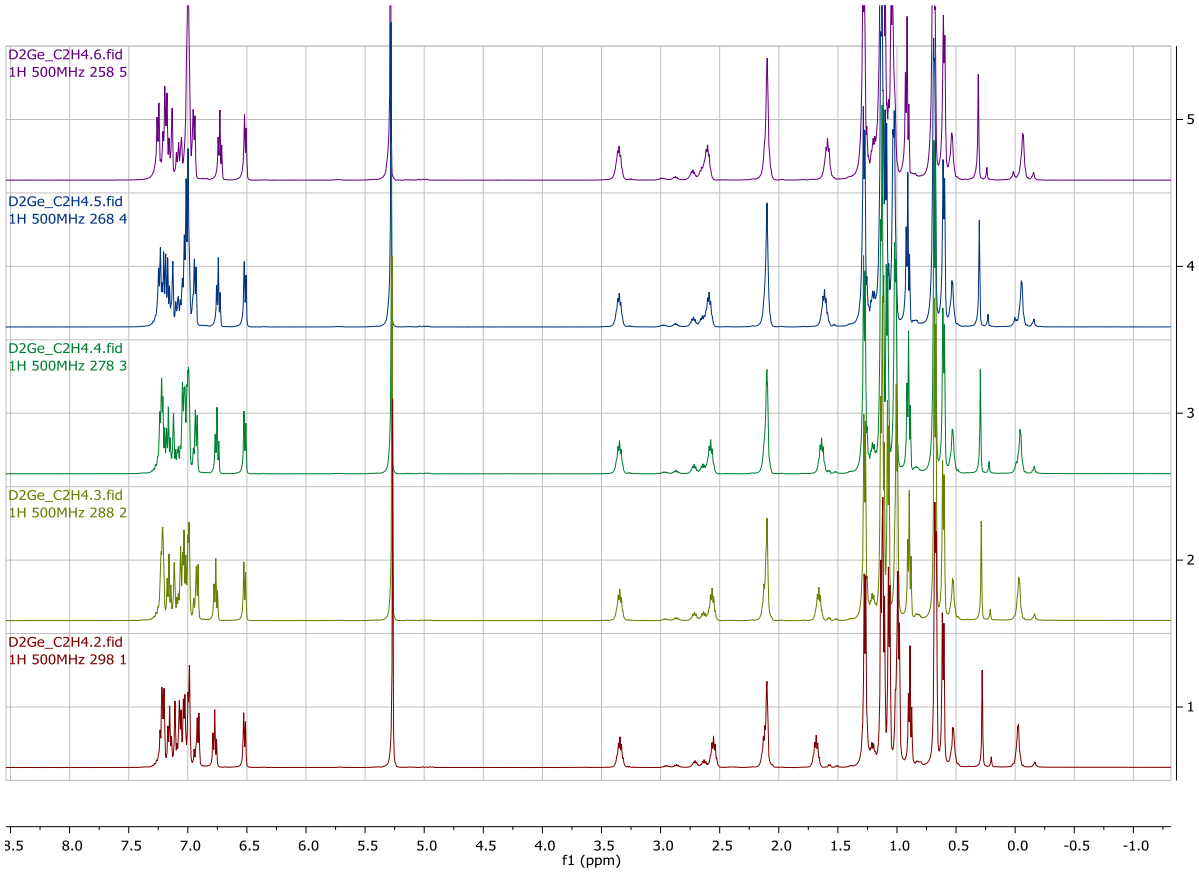

T	$Ge(Ar^{iPr4})_2$	Ethylene	complex	
298	3.97	9.69	4	Intensity
288	3.85	10.19	4.1	
278	3.77	10.53	4.2	
268	3.68	10.81	4.4	
258	3.51	11.69	4.61	

T	$Ge(Ar^{iPr4})_2$	Ethylene	complex	Scale to number of Hydrogens
298	0.49625	2.4225	1	
288	0.48125	2.5475	1.025	
278	0.47125	2.6325	1.05	
268	0.46	2.7025	1.1	
258	0.43875	2.9225	1.1525	

T	$Ge(Ar^{iPr4})_2$	Ethylene	complex	
298	1.09175E-05	0.000053295	0.000022	mol
288	1.05875E-05	0.000056045	0.00002255	
278	1.03675E-05	0.000057915	0.0000231	
268	0.00001012	0.000059455	0.0000242	
258	9.6525E-06	0.000064295	0.000025355	

T	$Ge(Ar^{iPr4})_2$	Ethylene	complex	Concentration Volume
298	0.021835	0.10659	0.044	5.00E-04
288	0.021175	0.11209	0.0451	
278	0.020735	0.11583	0.0462	
268	0.02024	0.11891	0.0484	
258	0.019305	0.12859	0.05071	

van't Hoff analysis of Figure AV6.

T	Keq	lnK	1/T
298	18.9	2.93	0.00335
288	19.0	2.94	0.00347
278	19.23	2.956	0.0036
268	20.11	3.0	0.0037
258	20.42	3.01	0.0039

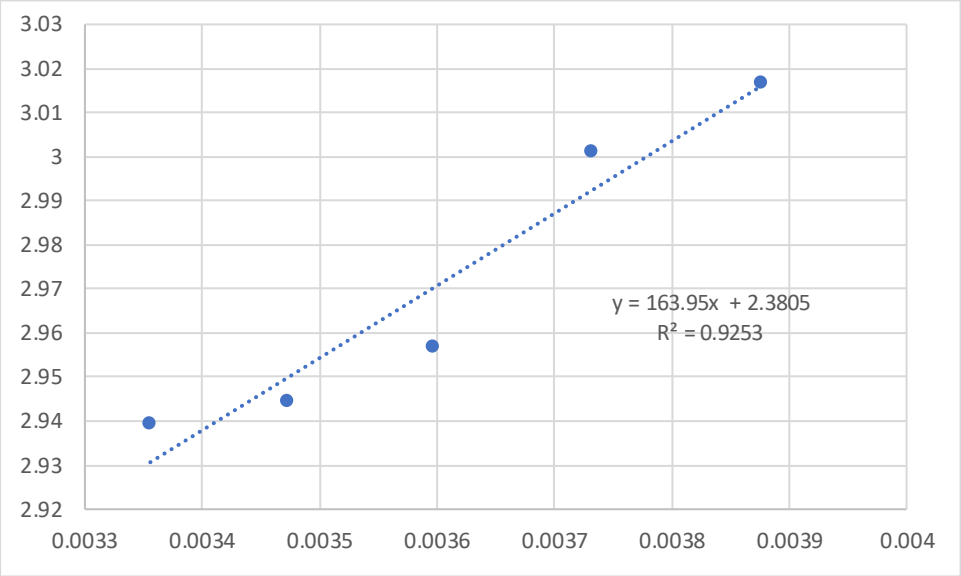

ΔH_{ass}= -1.36 kJ mol^{-1}

ΔS_{ass}= 19.78 J K^{-1} mol^{-1}

ΔG_{ass}(298K)= -7.25 kJ mol^{-1}

Estimate of Error:

The uncertainty in the integration was estimated to be 10% due to broadening. The VT apparatus indicated an uncertainty in the temperature of 1°C. The concentration is accurate ca. 5% and 2% for the germylene.

Variable temperature ^{1}H NMR spectroscopy and Van't Hoff analysis of **1c**

The integral atoms of the, iPr group of $Ge(Ar^{iPr4})_2$, free ethylene and iPr of the germirane in compound **1c** were used for the determination of the equilibrium constant for the conversion of the germylene with ethylene to give the germirane.

Figure AV7.[1]H NMR spectrum for **1c** at various temperatures from 218 to 268 K (500 MHz, C_7D_8)

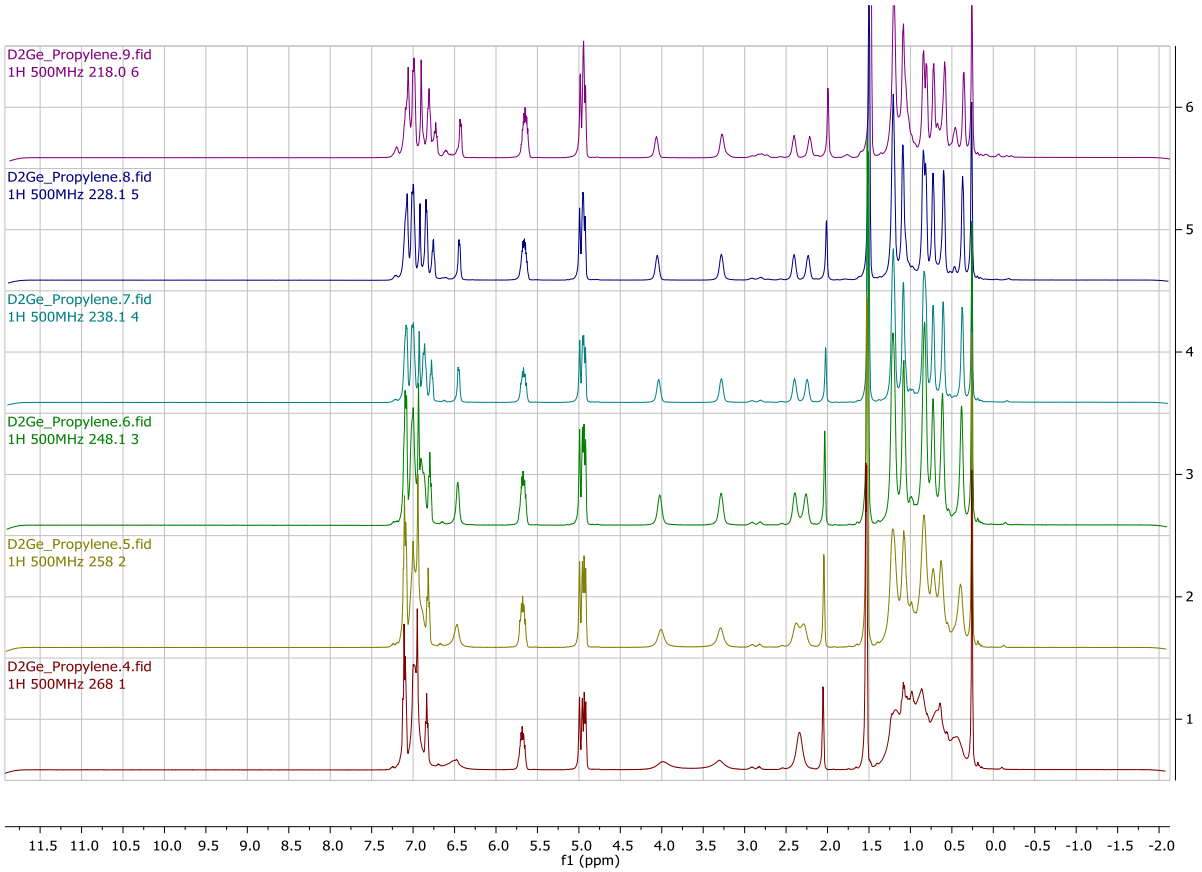

T	$Ge(Ar^{iPr4})_2$	Propylene	complex	
268	10.3	7.04	4	Intensity
258	10.1	7.43	4.3	
248	9.92	8.2	4.68	
238	9.5	8.64	4.87	
228	9.02	8.93	4.99	

T	$Ge(Ar^{iPr4})_2$	Propylene	complex	Scale to number of Hydrogens
268	1.2875	7.04	1	
258	1.2625	7.43	1.075	
248	1.24	8.2	1.17	
238	1.1875	8.64	1.2175	
228	1.1275	8.93	1.2475	

T	$Ge(Ar^{iPr4})_2$	Propylene	complex	
268	0.000028325	0.00015488	0.000022	mol
258	0.000027775	0.00016346	0.00002365	
248	0.00002728	0.0001804	0.00002574	
238	0.000026125	0.00019008	0.000026785	
228	0.000024805	0.00019646	0.000027445	

T	$Ge(Ar^{iPr4})_2$	Propylene	complex	Concentration Volume
268	0.05665	0.30976	0.044	5.00E-04
258	0.05555	0.32692	0.0473	
248	0.05456	0.3608	0.05148	
238	0.05225	0.38016	0.05357	
228	0.04961	0.39292	0.05489	

van't Hoff analysis of Figure AV7

T	Keq	lnK	1/T
268	2.51	0.919	0.0037
258	2.60	0.957	0.00387
248	2.615	0.961	0.00403
238	2.697	0.992	0.00420
228	2.816	1.035	0.004386

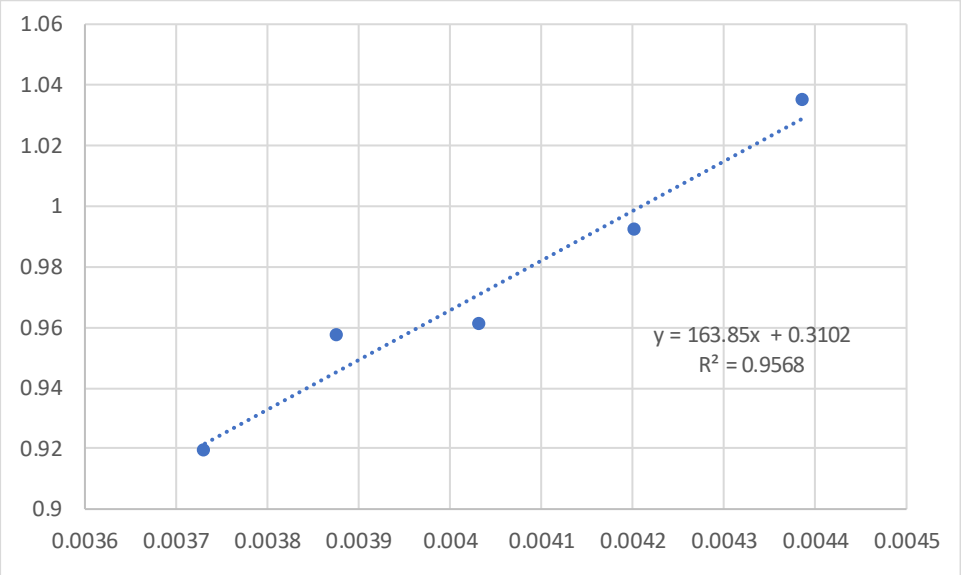

ΔH_{ass}= -1.362 kJ mol^{-1}

ΔS_{ass}= 2.579 J K^{-1} mol^{-1}

ΔG_{ass}(298K)= -2.1 kJ mol^{-1}

Estimate of Error: The uncertainty in the integration was estimated to be 10% due to broadening. The VT apparatus indicated an uncertainty in the temperature of 1°C. The concentration is accurate ca. 5% and 2% for the germylene.

Table AV1. Selected X-ray Crystallographic Data for **1b.**

Compound	**1b**
Formula weight, $gmol^{-1}$	C145 H180 Ge2
T (K) / *l* (Å)	90(2) K / 0.71073 Å
Crystal system	Triclinic
Space group / *Z*	P-1
a, Å	12.408(2) Å
b, Å	19.126(4) Å
c, Å	26.398(5) Å
α, °	93.954(4)°
β, °	91.913(4)°
γ, °	108.740(3)°
V, $Å^3$	5908.3(19) $Å^3$
ρ, mg m^{-3}	1.162 Mg/m^3
Abs. coeff., mm^{-1}	0.560 mm^{-1}
F(000)	2228
Crystal size, mm^3	0.804 x 0.678 x 0.670 mm^3
θ range, °	1.859 to 25.416°.
Reflns collected	19267
Ind. reflns	19267
Obs. reflns [$I > 2\sigma(I)$]	18482
Completeness to 2θ	87.3%
Goodness-of-fit F^2	1.133
Final *R* [$I > 2\sigma(I)$]	R1 = 0.0664 wR2 = 0.1863
R (all data)	R1 = 0.0684 wR2 = 0.1875

Completeness statistics refer to single and composite reflections containing twin component 1 only.

Videos:

https://youtu.be/a1wrfESMbWQ

Appendix VI

Supporting Information for Chapter 7: Reversible Complexation of Alkynes by a Germylene

Figure AVI1. ^{1}H NMR Spectrum of **1a** (400 MHz, C_6D_6, 298K, ppm)

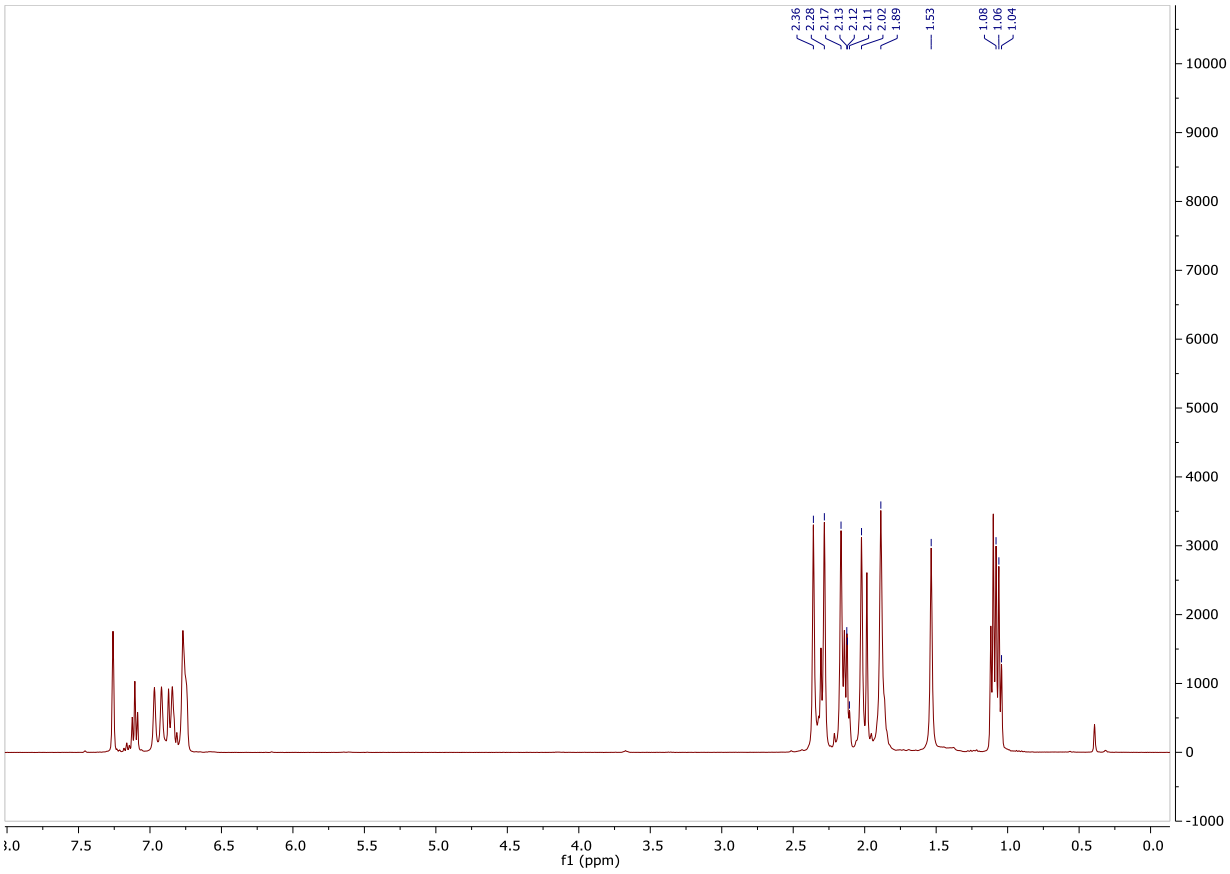

Uncomplexed $Ge(Ar^{Me6})_2$ signals appear at 1.95 and 2.3ppm

Figure AVI2. ^{13}C NMR Spectrum of **1b** (126 MHz, C_6D_6, 298K, ppm)

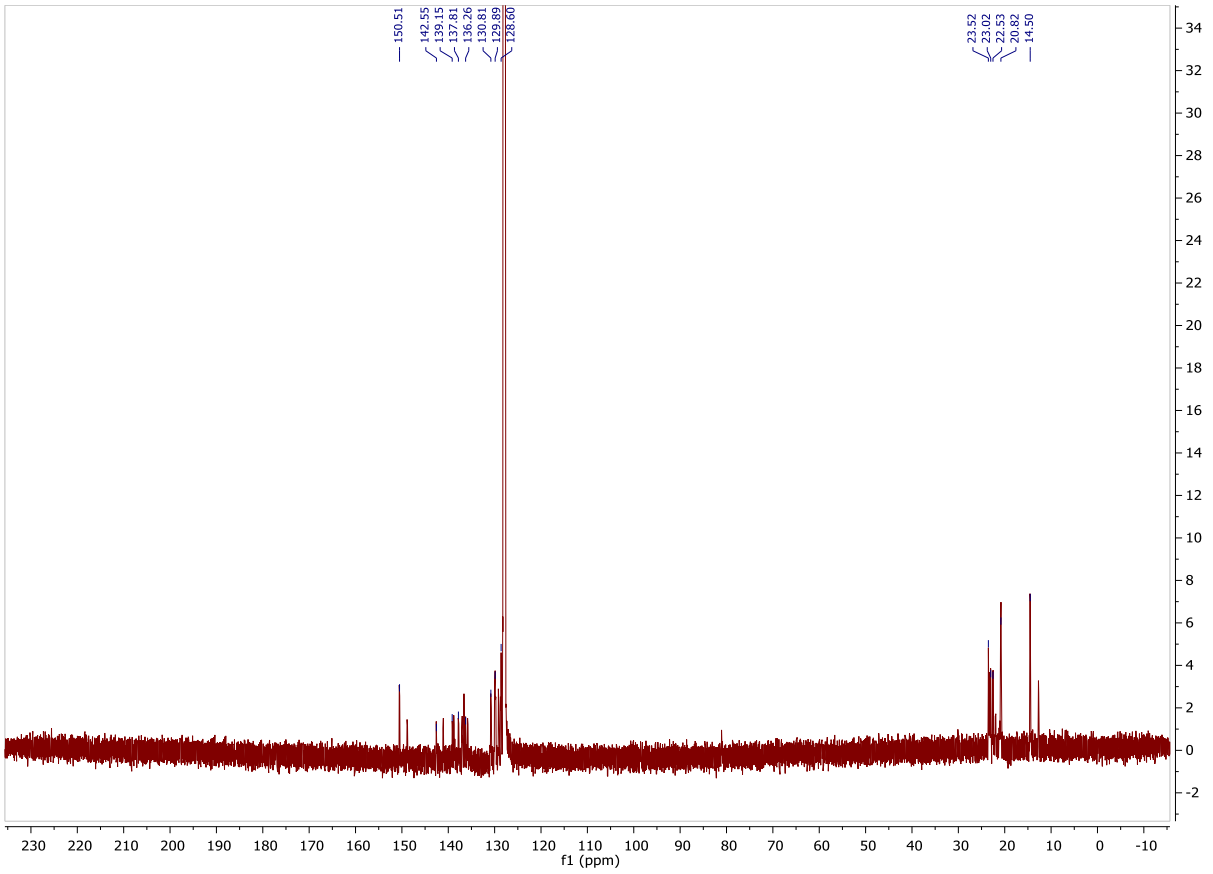

Figure AVI3. ^{1}H NMR Spectrum of **1b** (500 MHz, C_7D_8, 248K, ppm)

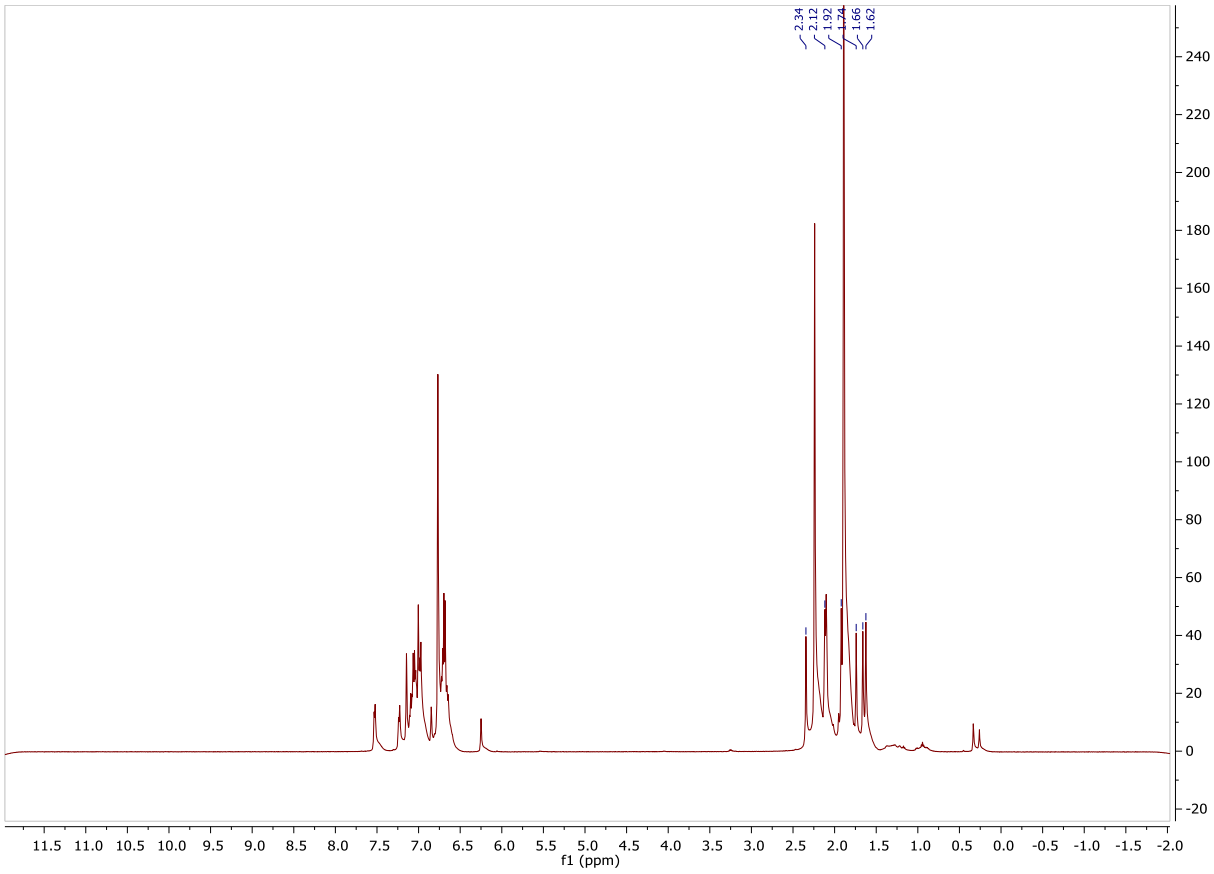

Uncomplexed $Ge(Ar^{Me6})_2$ signals appear at 1.95 and 2.3ppm

Figure AVI4. ^{1}H NMR Spectrum of **1c** (500 MHz, C_7D_8, 218K, ppm)

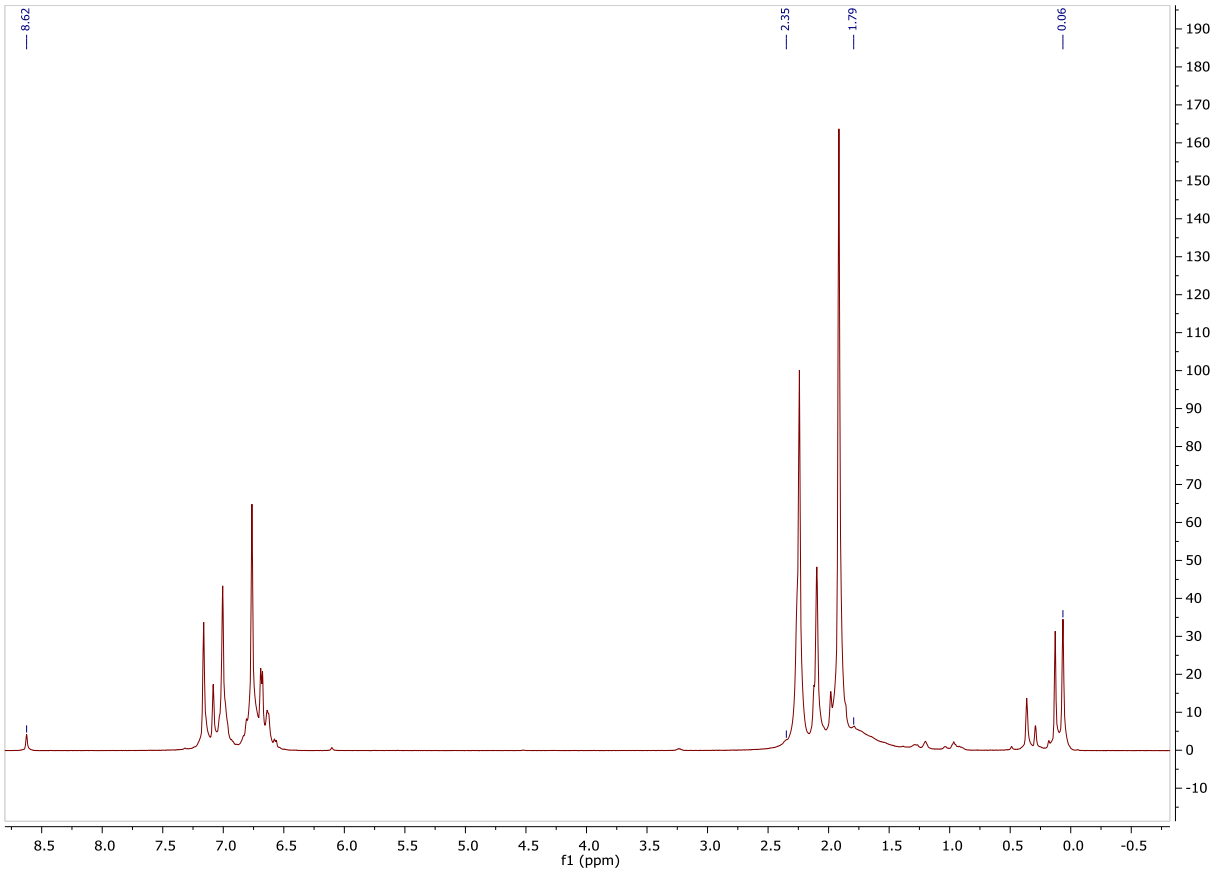

Uncomplexed $Ge(Ar^{Me6})_2$ signals appear at 1.95 and 2.3ppm

Figure AVI5. ^{1}H NMR Spectrum of **1d** (400 MHz, C_6D_6, 298K, ppm)

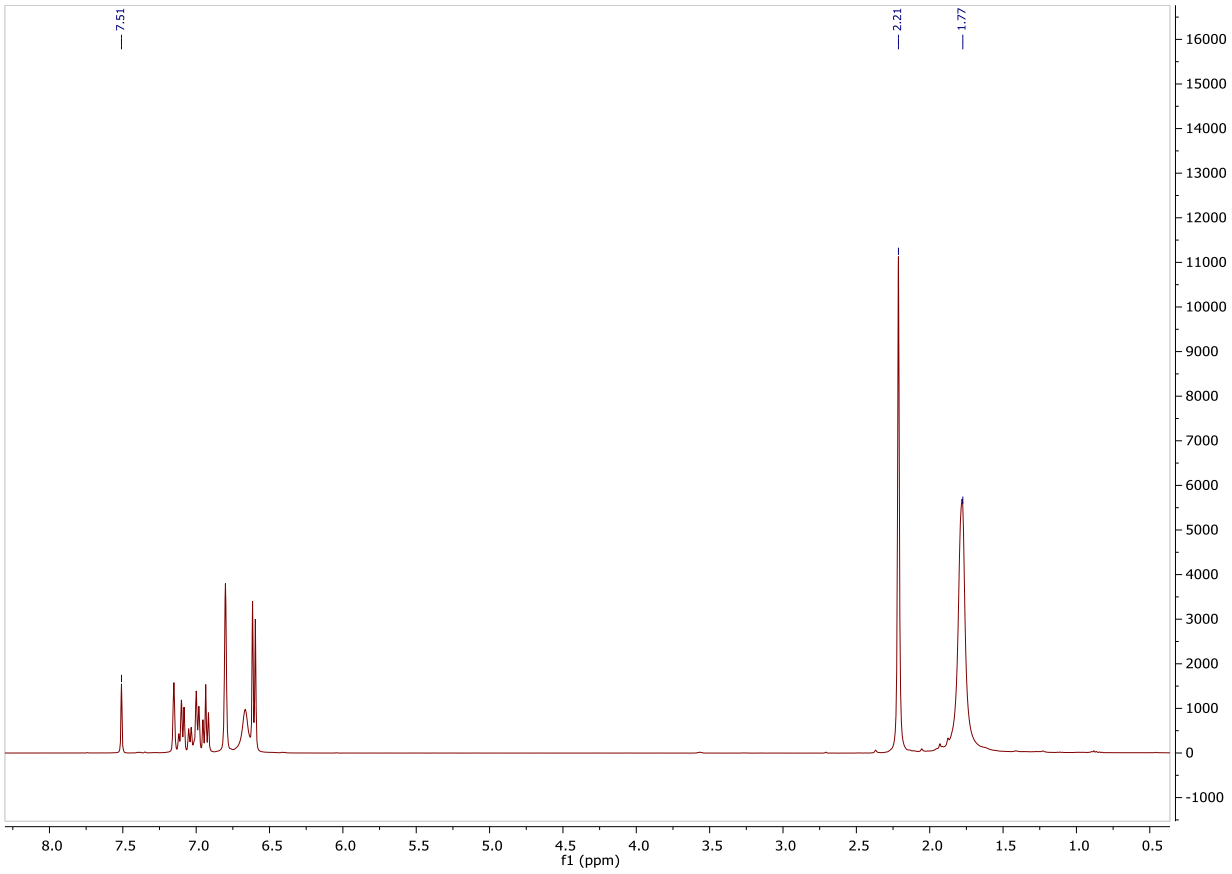

Figure AVI6. ^{13}C NMR Spectrum of **1d** (126MHz, C_6D_6, 298K, ppm)

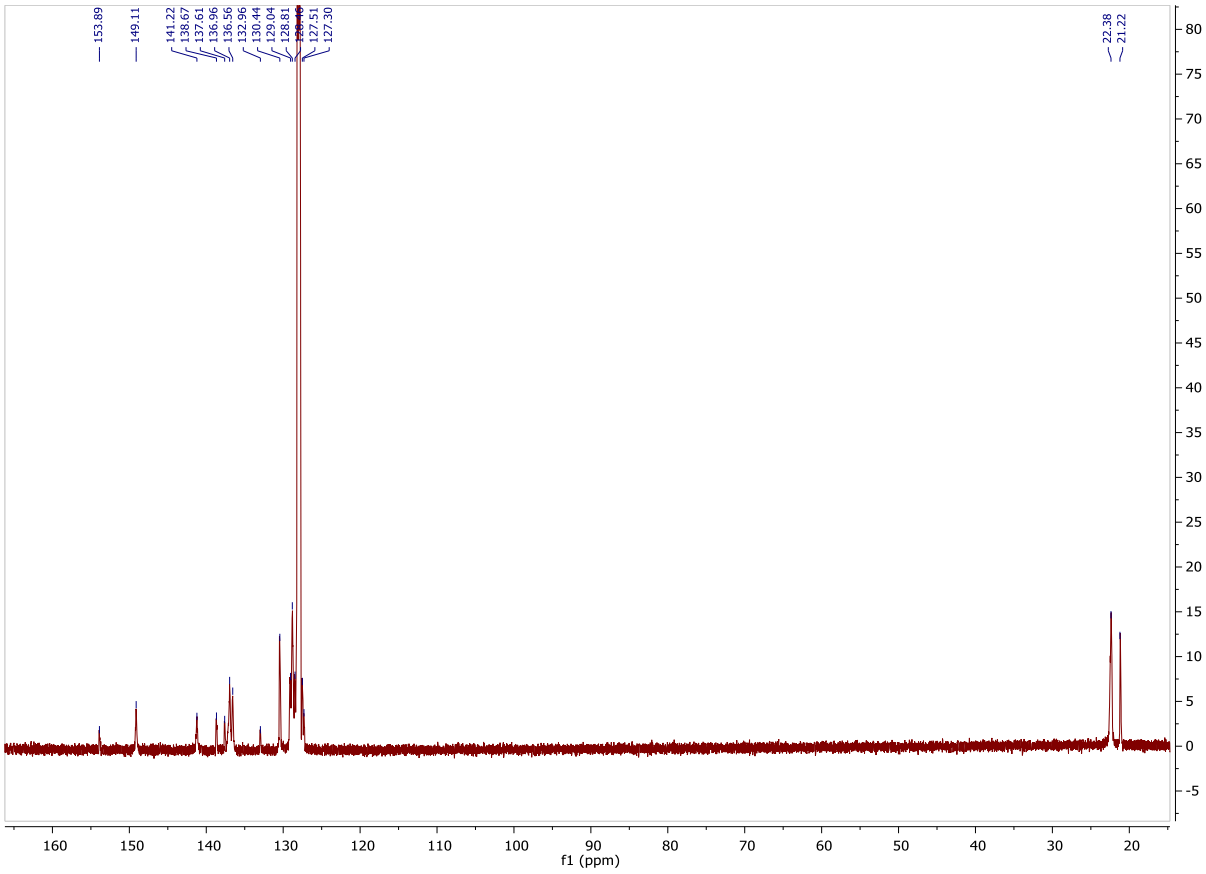

Variable temperature ^{1}H NMR spectroscopy and Van't Hoff analysis of **1a**

The integral for the signal atoms of the, o-Me group of $Ge(Ar^{Me6})_2$, terminal methyl groups for 3-hexyne and compound **1a** were used for the determination of the equilibrium constant for the conversion of the germylene with 3-hexyne to give the germirene.

The equilibrium constant was calculated according to equation 1.

$$K_{eq} = \frac{[Germirene]}{[Germylene][3-hexyne]} \text{ (eq1)}$$

The Van't Hoff equation, equation 2, was used in order to determine ΔH and ΔS from the slope and the intercept of the plot of ln Keq against 1/T.

$$lnK_{eq} = -\frac{\Delta H}{R}\left(\frac{1}{T}\right) + \frac{\Delta S}{R} \text{ (eq. 2)}$$

Figure AVI7. ^{1}H NMR spectrum for **1a** at varrious temperatures from 276 to 318 K (500 MHz, C_7D_8)

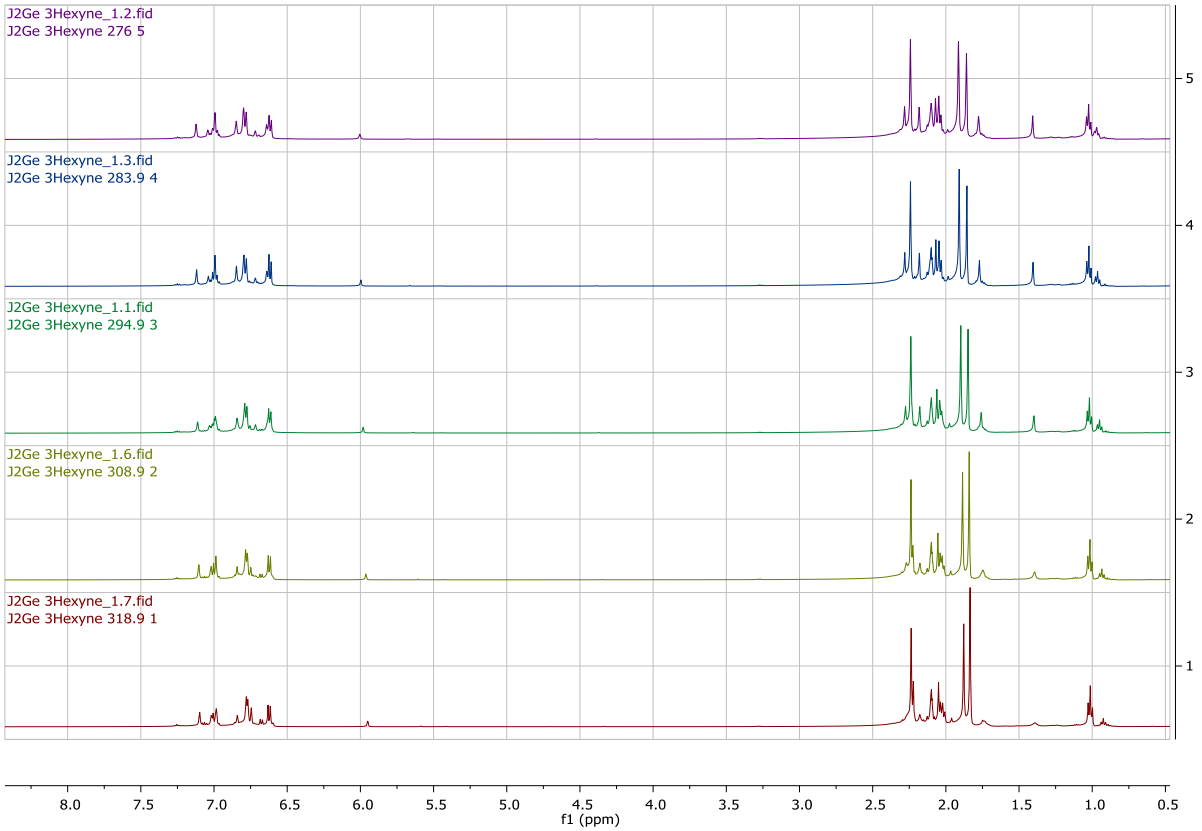

Uncomplexed $Ge(Ar^{Me6})_2$ signals appear at 1.95 and 2.3ppm

T	$Ge(Ar^{Me6})_2$	3-hexyne	complex	
318.9	24	13.55	2.87	Intensity
308	21.57	13.17	3.56	
294.9	19.25	12.59	4.64	
283.9	19.05	12.5	4.93	
276	18.81	12.22	5.23	

T	$Ge(Ar^{Me6})_2$	3-hexyne	complex	Scale to number of Hydrogens
318.9	1	2.258333333	0.478333333	
308	0.89875	2.195	0.593333333	
294.9	0.802083333	2.098333333	0.773333333	
283.9	0.79375	2.083333333	0.821666667	
276	0.78375	2.036666667	0.871666667	

T	$Ge(Ar^{Me6})_2$	3-hexyne	complex	
318.9	0.00002287	5.16481E-05	1.09395E-05	mol
308	2.05544E-05	5.01997E-05	1.35695E-05	
294.9	1.83436E-05	4.79889E-05	1.76861E-05	
283.9	1.81531E-05	4.76458E-05	1.87915E-05	
276	1.79244E-05	4.65786E-05	1.9935E-05	

T	$Ge(Ar^{Me6})_2$	3-hexyne	complex	Concentration Volume
318.9	0.04574	0.103296167	0.021878967	5.00E-04
308	0.041108825	0.1003993	0.027139067	
294.9	0.036687292	0.095977767	0.035372267	
283.9	0.036306125	0.095291667	0.037583033	
276	0.035848725	0.093157133	0.039870033	

van't Hoff analysis of Figure AVI7.

T	Keq	lnK	1/T
318.9	4.63	1.533	0.00313
308	6.5755	1.88	0.00325
294.9	10.0456	2.31	0.0034
283.9	10.863	2.385	0.0035
276	11.939	2.48	0.00362

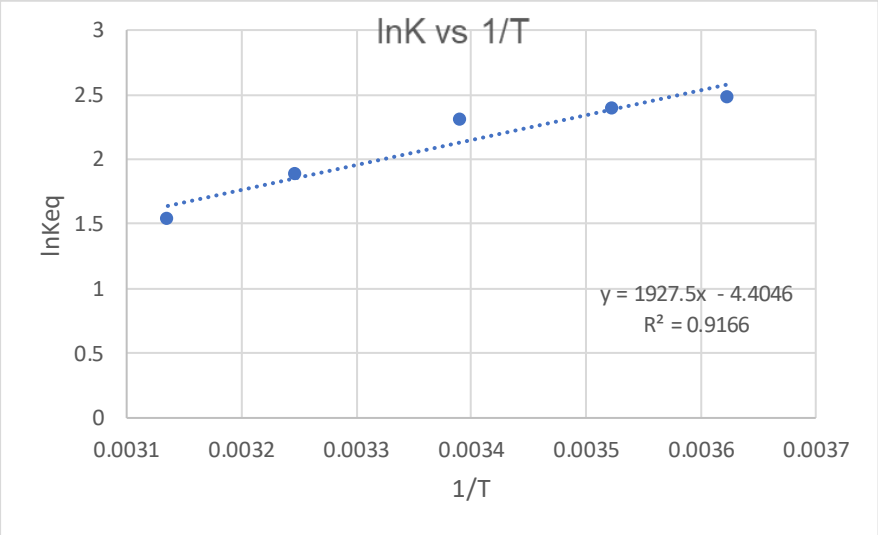

ΔH_{assn}= -16.025 kJ mol^{-1}

ΔS_{assn}= -36.619 J K^{-1} mol^{-1}

ΔG_{assn}(298K)= -5.11 kJ mol^{-1}

Estimate of Error: The uncertainty in the integration was estimated to be 5%. The VT apparatus indicated an uncertainty in the temperature of 1°C. The concentration is accurate ca. 5% and 2% for Tetrylene and 3-hexyne.

Figure AVI8. ^{1}H NMR spectrum for **1b** at various temperatures from 258 to 298 K (500 MHz, C_7D_8)

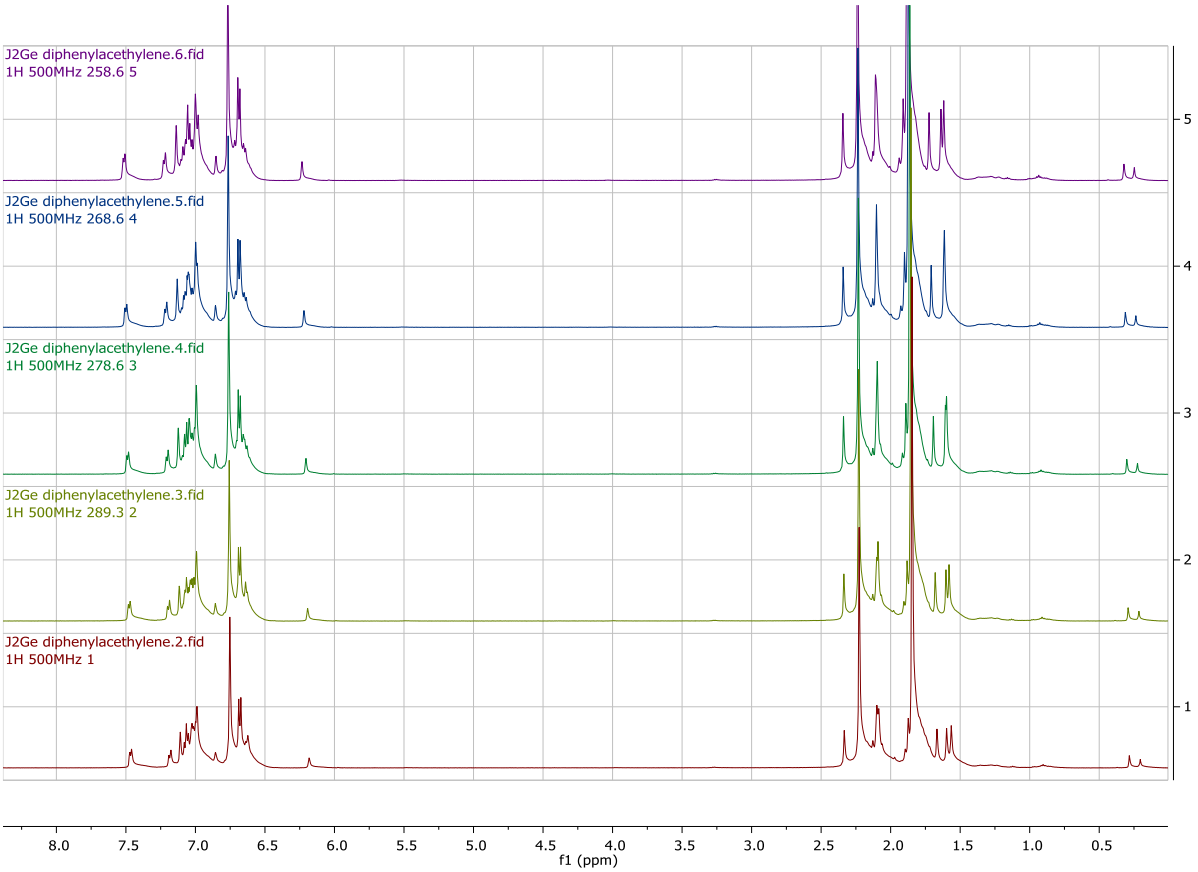

Uncomplexed $Ge(Ar^{Me6})_2$ signals appear at 1.95 and 2.3ppm

Variable temperature ^{1}H NMR spectroscopy and Van't Hoff analysis of **1b**

The integral for the signal atoms of the, o-Me of $Ge(Ar^{Me6})_2$, and p-Me of one of the flanking aryl ring from compound **1b** were used for the determination of the equilibrium constant for the conversion of the germylene with diphenylacetylene to give the germirene.

Note: Unfortunately the uncoordinated diphenylacetylene peak is hidden in the aromatic region, so an assumption was made that the concentration of diphenylacetylene is in equivalent to the concentration of the starting germylene $Ge(Ar^{Me6})_2$. Diphenylacetylene solution was prepared from a serial dilution.

T	$Ge(Ar^{Me6})_2$	complex	
298	12	2.63	Intensity
289.3	11.91	2.99	
278.6	11.85	3.23	
268.6	11.78	3.43	
258.6	11.75	3.86	

T	$Ge(Ar^{Me6})_2$	complex	Scale to number of Hydrogens
298	1	0.438333333	
289.3	0.9925	0.498333333	
278.6	0.9875	0.538333333	
268.6	0.981666667	0.571666667	
258.6	0.979166667	0.643333333	

T	$Ge(Ar^{Me6})_2$	complex	
298	0.00002287	1.00247E-05	mol
289.3	2.26985E-05	1.13969E-05	
278.6	2.25841E-05	1.23117E-05	
268.6	2.24507E-05	1.3074E-05	
258.6	2.23935E-05	1.4713E-05	

T	$Ge(Ar^{Me6})_2$/PhCCPh	complex	Concentration Volume
298	0.04574	0.020049367	5.00E-04
289.3	0.04539695	0.022793767	
278.6	0.04516825	0.024623367	
268.6	0.044901433	0.026148033	
258.6	0.044787083	0.029426067	

van't Hoff analysis of Figure AVI8.

T	Keq	lnK	1/T
298	9.583	2.26	0.00335
289.3	11.06	2.40	0.00345
278.6	12.07	2.491	0.00359
268.6	12.969	2.562	0.00372
258.6	14.67	2.686	0.00387

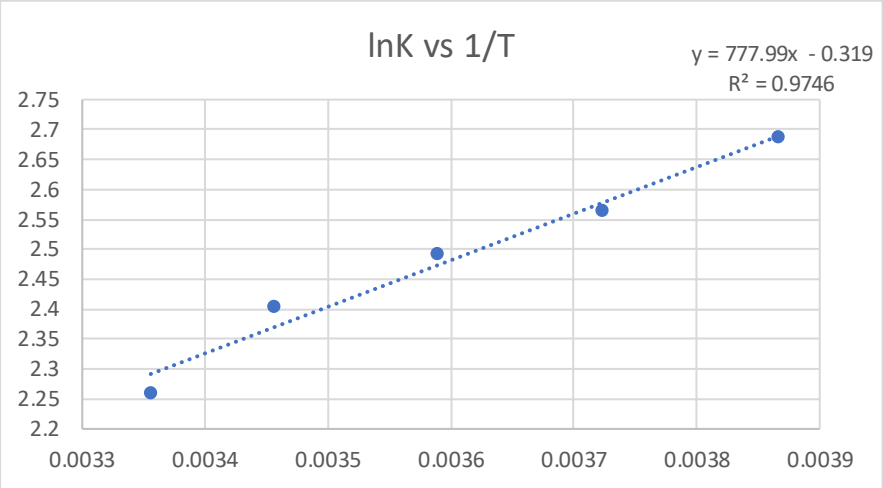

ΔH_{assn}= -6.47 kJ mol^{-1}

ΔS_{assn}= -2.65 J K^{-1} mol^{-1}

ΔG_{assn}(298K)= -5.65 kJ mol^{-1}

Estimate of Error: The uncertainty in the integration was estimated to be 5%. The VT apparatus indicated an uncertainty in the temperature of 1°C. The concentration is accurate ca. 5% and 5% for Tetrylene and diphenylacetylene.

Figure AVI9. ^{1}H NMR spectrum for **1c** at various temperatures from 208 to 248 K (500 MHz, C_7D_8)

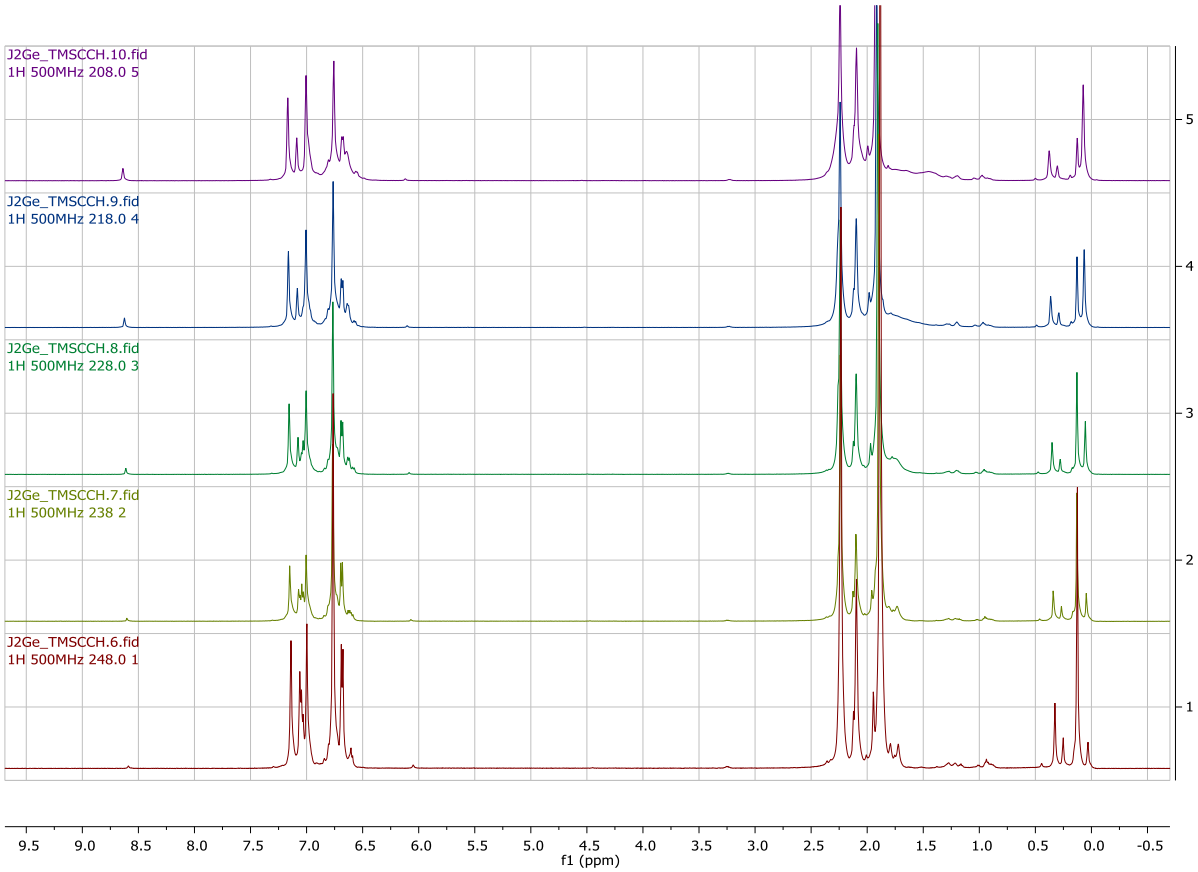

Uncomplexed $Ge(Ar^{Me6})_2$ signals appear at 1.95 and 2.3ppm

Variable temperature ^{1}H NMR spectroscopy and Van't Hoff analysis of **1c**

The integral for the signal atoms of the, o-Me of $Ge(Ar^{Me6})_2$, terminal methyl groups for trimethylsilylacetylene and compound **1c** were used for the determination of the equilibrium constant for the conversion of the germylene with trimethylacetylene to give the germirene.

T	$Ge(Ar^{Me6})_2$	Me_3SiCCH	complex	
248	24	4.96	0.58	Intensity
238	11.79	2.22	0.59	
228	10.92	1.49	1.16	
218	10.16	1.44	1.91	
208	9.3	0.96	2.69	

T	$Ge(Ar^{Me6})_2$	Me_3SiCCH	complex	Scale to number of Hydrogens
318.9	1	0.551111111	0.064444444	
308	0.49125	0.37	0.098333333	
294.9	0.455	0.248333333	0.193333333	
283.9	0.423333333	0.24	0.318333333	
276	0.3875	0.16	0.448333333	

T	$Ge(Ar^{Me6})_2$	Me_3SiCCH	complex	
318.9	0.00002287	1.26039E-05	1.47384E-06	mol
308	1.12349E-05	8.4619E-06	2.24888E-06	
294.9	1.04059E-05	5.67938E-06	4.42153E-06	
283.9	9.68163E-06	5.4888E-06	7.28028E-06	
276	8.86213E-06	3.6592E-06	1.02534E-05	

T	$Ge(Ar^{Me6})_2$	Me_3SiCCH	complex	Concentration Volume
318.9	0.04574	0.025207822	0.002947689	5.00E-04
308	0.022469775	0.0169238	0.004497767	
294.9	0.0208117	0.011358767	0.008843067	
283.9	0.019363267	0.0109776	0.014560567	
276	0.01772425	0.0073184	0.020506767	

van't Hoff analysis of Figure AVI9.

T	Keq	lnK	1/T
248	2.56	0.938	0.0040
238	11.828	2.47	0.0042
228	37.40	3.62	0.004386
218	68.50	4.226	0.004587
208	158.1	5.063	0.0048

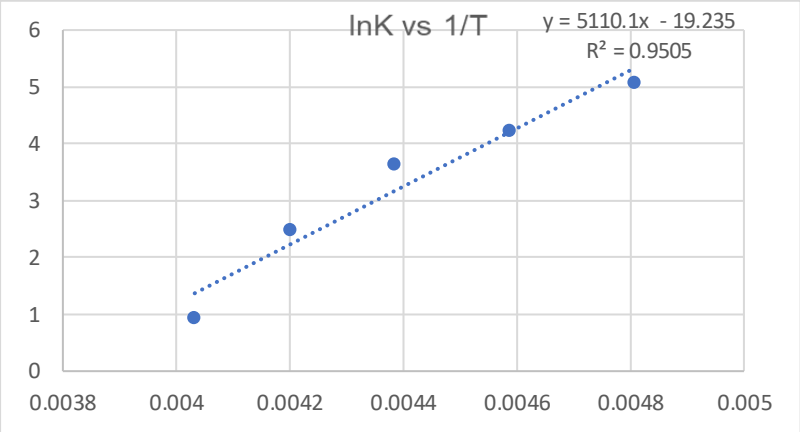

ΔH_{assn}= -42.485 kJ mol^{-1}

ΔS_{assn}= -159.9 J $K^{-1}mol^{-1}$

ΔG_{assn}(298K)= 5.165 kJ

ΔG_{assn}(248K, observed)= -2.83 kJ mol^{-1}

Estimate of Error: The uncertainty in the integration was estimated to be 5%. The VT apparatus indicated an uncertainty in the temperature of 1°C. The concentration is accurate ca. 5% and 2% for Tetrylene and trimethylsilylacetylene.

Table AVI1. Selected X-ray Crystallographic Data for **1a** and **1d**

Compound	**1a**	**1d**
Formula weight, $gmol^{-1}$	$C_{53.88}H_{59.82}$ Ge I0.02	$C_{56}H_{56}$ Ge
T (K) / *l* (Å)	90(2) K / 0.71073 Å	90(2)K/ 0.71073
Crystal system	Triclinic	Triclinic
Space group / *Z*	P-1	P-1
a, Å	9.9517(3) Å	11.139(2) Å
b, Å	12.4503(4) Å	12.049(2) Å
c, Å	17.3364(5) Å	18.956(4) Å
α, °	95.6342(13)°	78.079(2)°
β, °	90.0826(13)°	73.863(2)°
γ, °	96.1859(12)°	65.561(2)°
V, $Å^3$	2125.03(11) $Å^3$	2212.6(8) $Å^3$
ρ, mg m^{-3}	1.223Mg/m^3	1.203 Mg/m^3
Abs. coeff., mm^{-1}	0.771 mm^{-1}	0.728 mm^{-1}
F(000)	832.3	848
Crystal size, mm^3	0.450 x 0.290 x 0.102 mm^3	0.836 x 0.771 x 0.703 mm^3
θ range, °	1.653 to 27.639°	1.867 to 27.693°
Reflns collected	17801	20139
Ind. reflns	9459	10243
R(int)	0.0329	0.0194
Obs. reflns [$I > 2\sigma(I)$]	7610	9710
Completeness to 2θ	97.2%	99.8%
Goodness-of-fit F^2	1.048	1.051
Final *R* [$I > 2\sigma(I)$]	R1 = 0.0435 wR2 = 0.1010	R1 = 0.0311 wR2 = 0.0821
R (all data)	R1 = 0.0590 wR2 = 0.1095	R1 = 0.0329 wR2 = 0.0835

Images and Videos:

Figure AVI10. Dissolving **1d** in toluene.

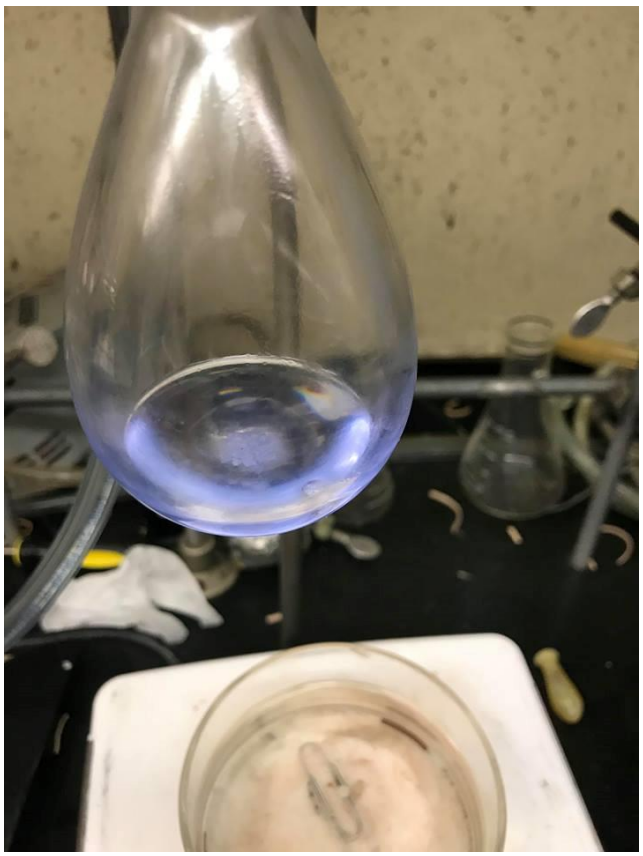

A video recording of the reversible reaction between $Ge(Ar^{Me6})_2$ with 3-hexyne

https://youtu.be/7SUWaJVadTU

Appendix VII

Supporting Information for Chapter 8: Catalytic Dehydrocoupling of Amines and Boranes by an Incipient Tin(II) Hydride

Crystal Structure of $\{Ar^{iPr_4}SnOMe\}_2$ (**2**).

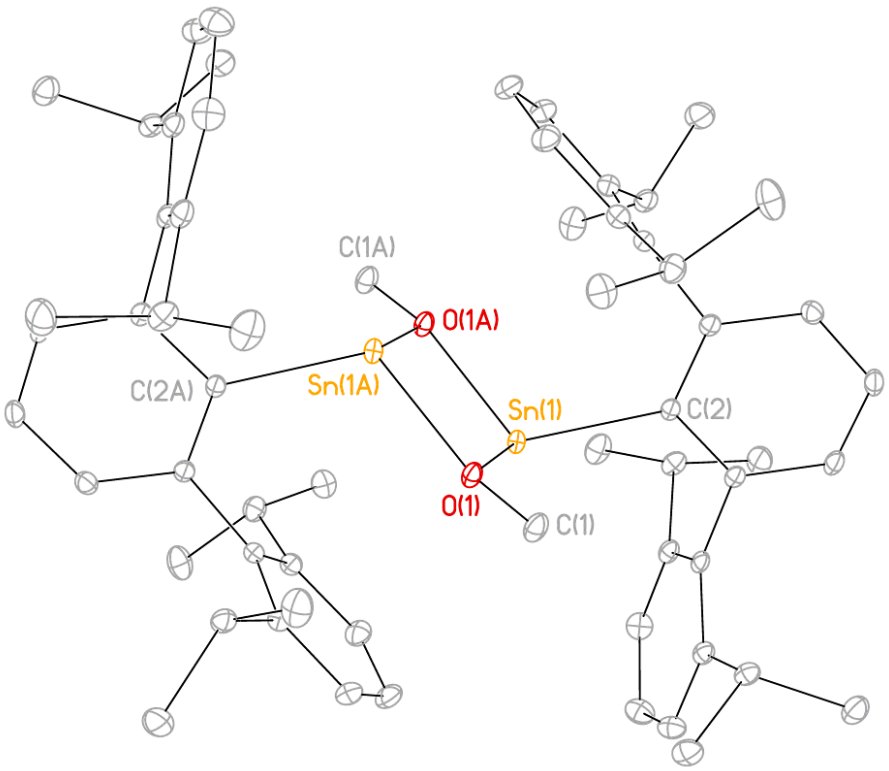

Figure AVII1. Thermal ellipsoid (30%) plot of **2**. Hydrogen atoms are not shown for clarity. Selected bond lengths (Å) and angles (deg): Sn(1)-O(1) 2.1379(11), Sn(1)-O(1A) 2.2081(10), O(1)-C(1) 1.4268(17), Sn(1)-C(2) 2.2720(14), Sn(1)-O(1)-Sn(1A) 108.33(4), O(1)-Sn(1)-O(1A) 71.67(4), O(1)-Sn(1)-C(2) 94.14(4).

Table AVII1. Crystal Data and Refinement Summary for **2**.

Identifier	JE81
Formula	$C_{62}H_{80}O_2Sn_2$
fw (g mol^{-1})	1094.64
Crystal system	monoclinic
Space group	$P2_1/n$
a (Å)	13.542(3)
b (Å)	13.931(3)
c (Å)	14.562(3)
α (°)	90
β (°)	97.201(3)
γ (°)	90
V (Å^3)	2725.6(10)
Z	2
Radiation	MoKα (λ = 0.71073)
T (K)	90.15
cryst. size (mm)	0.311 x 0.310 x 0.128
F(000)	1136.0
ρ_{calc} (g cm^{-3})	1.334
μ (mm^{-1})	0.957
$2\theta_{max}$ (°)	3.872 to 55.09
reflns. collected	36174
unique reflns.	6261
R_{int}	0.0236
reflns. [I>2σ(I)]	5778
R_1 [I>2σ(I)]	0.0179
wR_2 (all data)	0.0488
GoF (F^2)	1.045

Figure AVII2. ^{1}H NMR Spectra of 1.

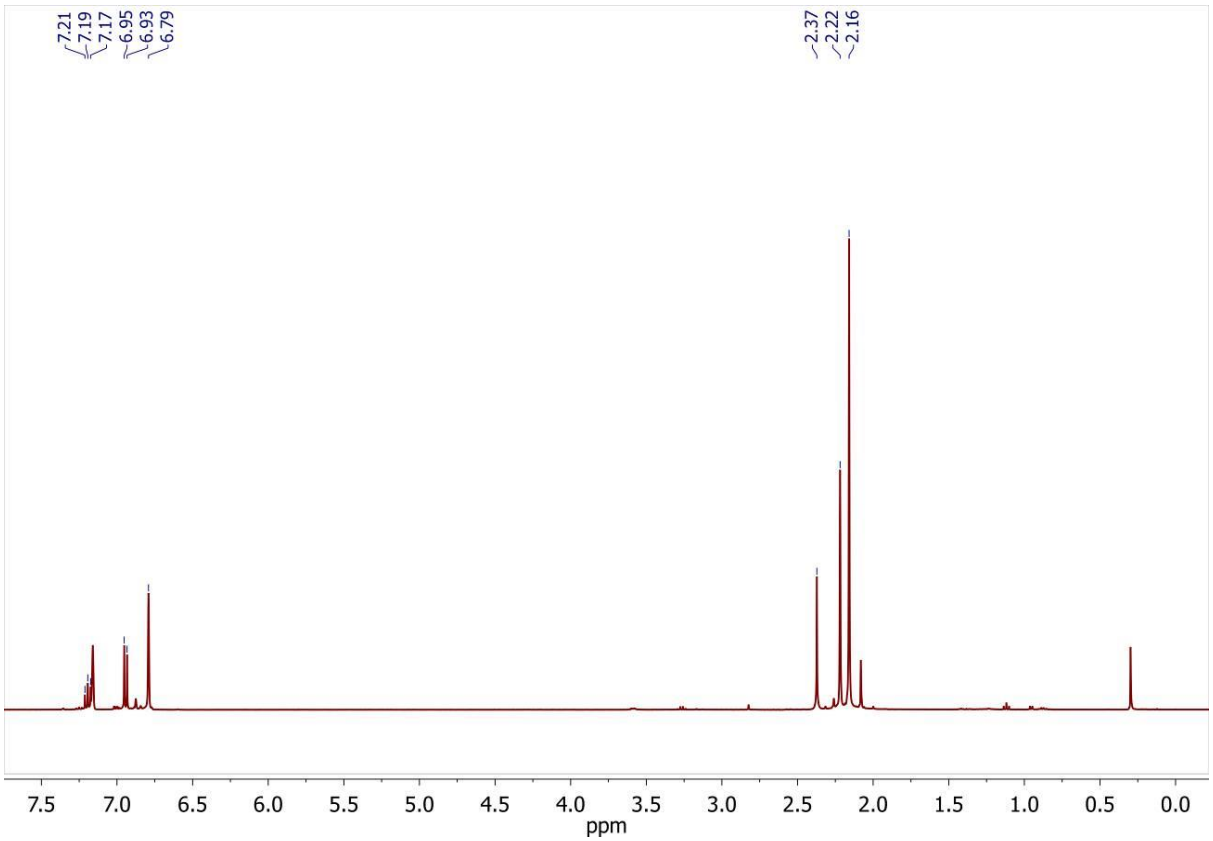

Figure AVII3. ^{1}H NMR Spectra of 2.

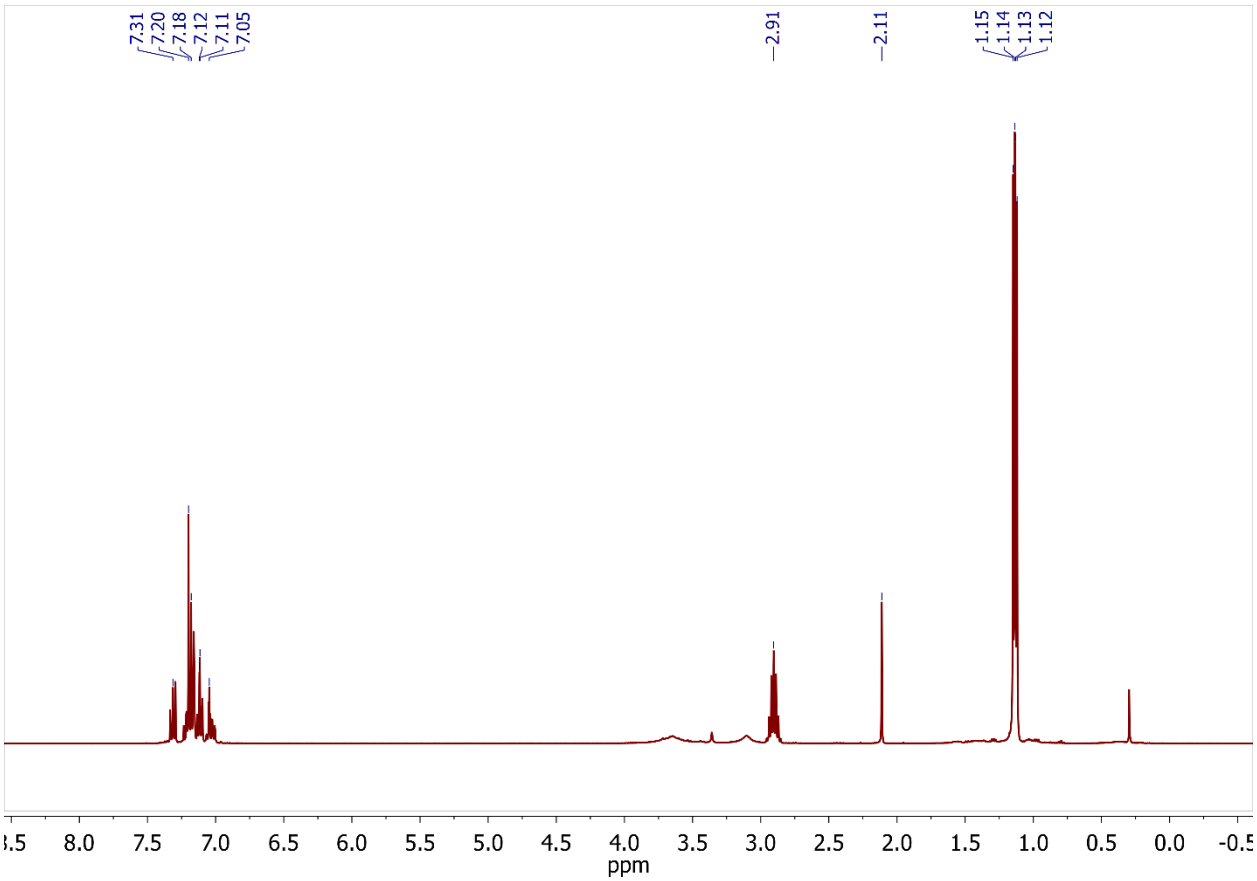

^{1}H NMR (400 MHz, C_6D_6, 25 ºC, ppm): 1.13 (m, 24H, CH($C\mathbf{H}_3$)$_2$), 2.11 (s, 6H, OMe), 2.91 (sept, 4H, $C\mathbf{H}$(CH_3)$_2$), 7.05 (m, 2H), 7.12 (m, 4H), 7.19 (d, 8H, *m*-C_6H_3), 7.31 (t, 4H, *p*-C_6H_3).

Figure AVII4. ^{13}C NMR Spectrum of 2. Small hexane impurity.

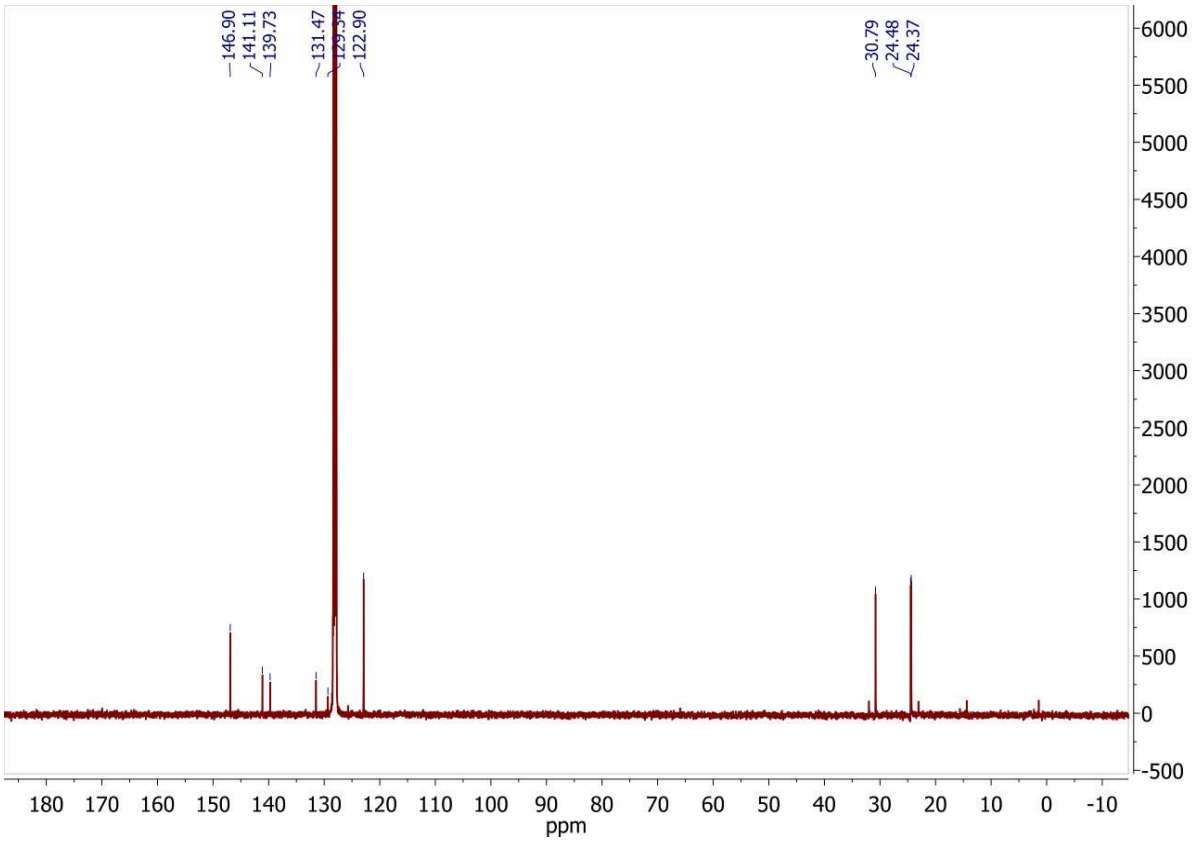

$^{13}C\{^{1}H\}$ NMR (126MHz, C_6D_6, 25° C, ppm): 24.37, 24.48, 30.79, 122.90, 129.34, 131.47, 139.73, 141.11, 146.90.

Figure AVII5. IR Spectrum of 2

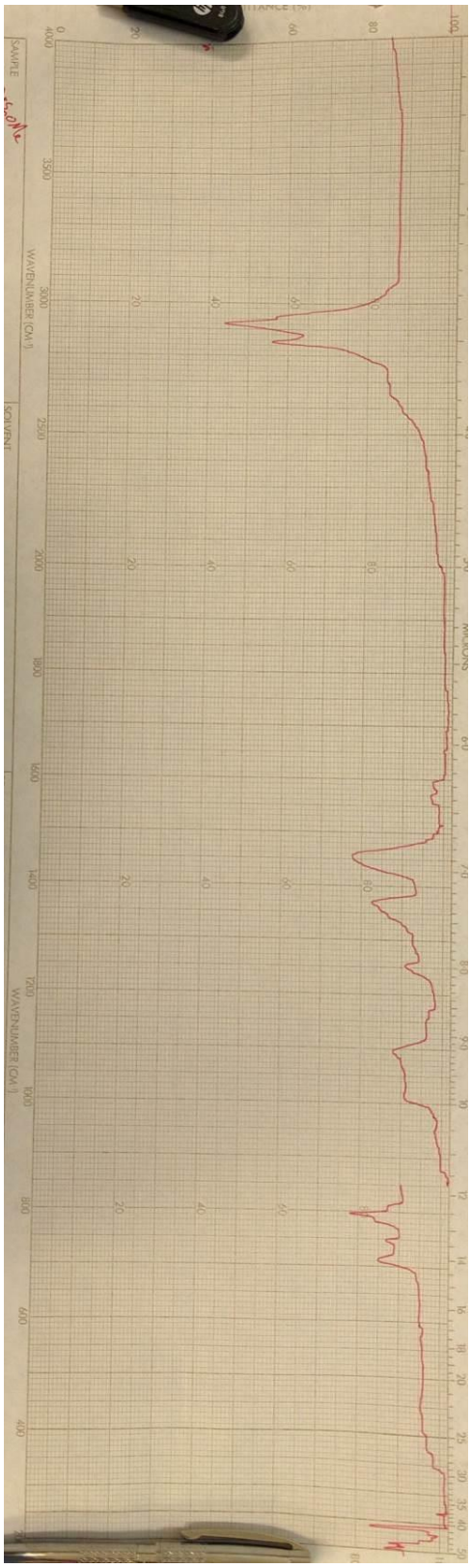

Figure AVII6. UV-Vis Spectrum of 2.

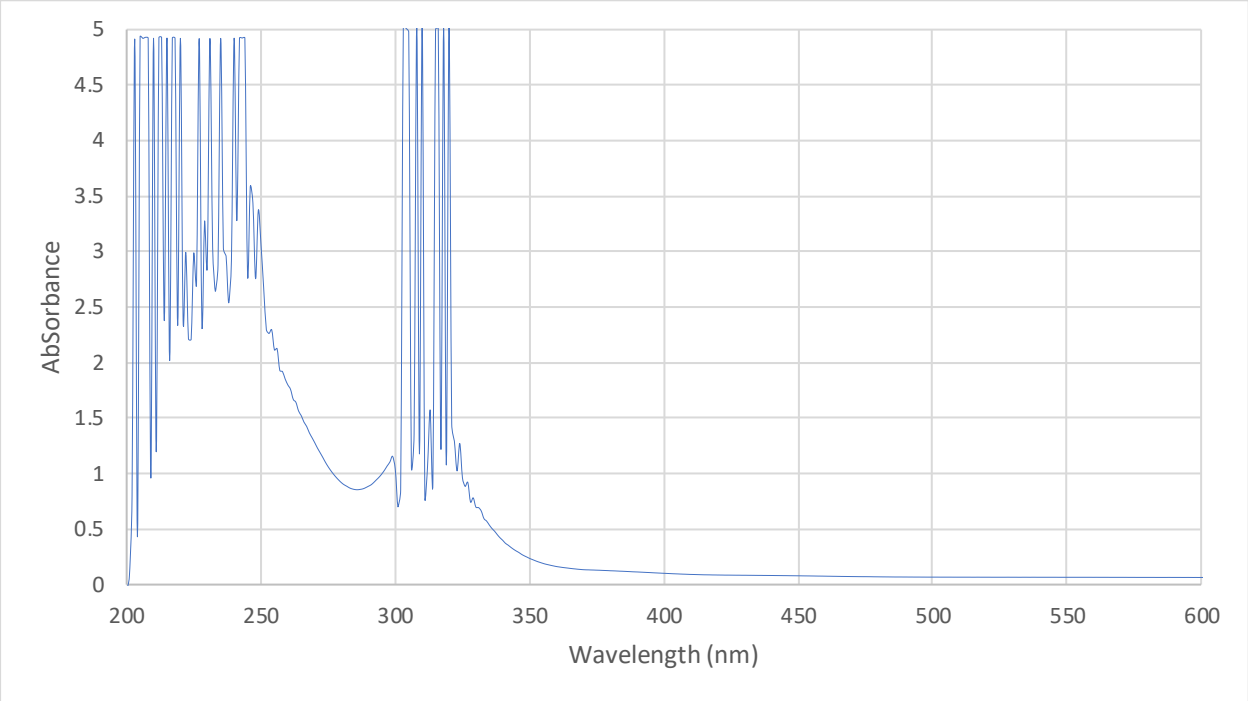

Figure AVII7. ^{1}H NMR Spectra of 3. Some residual toluene.

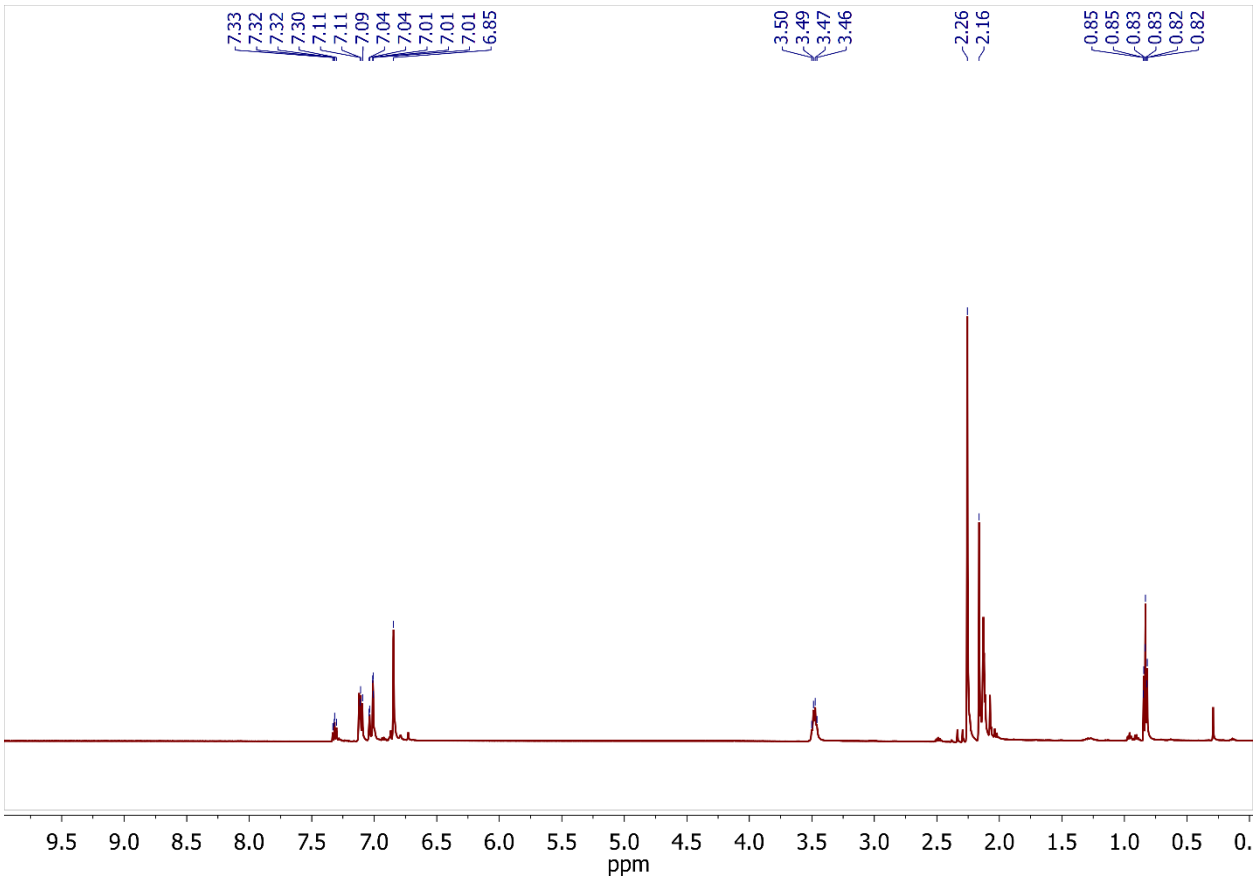

^{1}H NMR (400 MHz, C_6D_6, 25 ºC, ppm): 0.81 (t, J_{HH} = 7.0 Hz, 12H, $NCH_2C\mathbf{H}_3$), 2.12 (s, 12H, *p*-Me), 2.27 (s, 24H, *o*-Me), 3.47 (m, 8H, $NC\mathbf{H}_2CH_3$), 6.84 (s, 8H, $C_6\mathbf{H}_2$), 7.12 (d, J_{HH} = 7.5 Hz, 4H, *m*-C_6H_3), 7.31 (t, J_{HH} = 7.5 Hz, 2H, *p*-C_6H_3)

Figure AVII8. ^{13}C NMR Spectrum of 3.

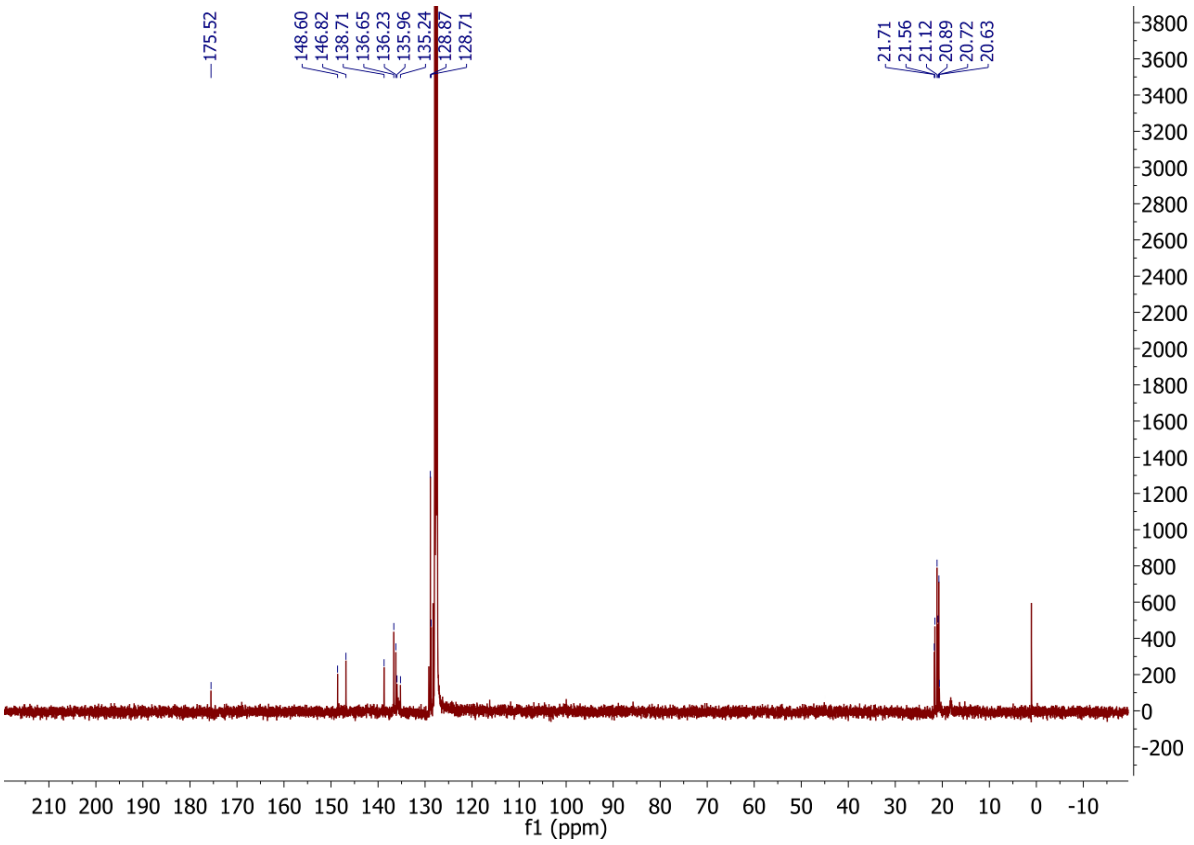

$^{13}C\{^{1}H\}$ NMR (126MHz, C_6D_6, 25° C, ppm): 20.63, 20.72, 20.89, 21.12, 21.56, 21.71, 128.71, 128.87, 135.24, 135.96, 136.23, 136.65, 138.71, 146.82, 148.60, 175.52.

Figure AVII9. ^{119}Sn Spectrum of 3.

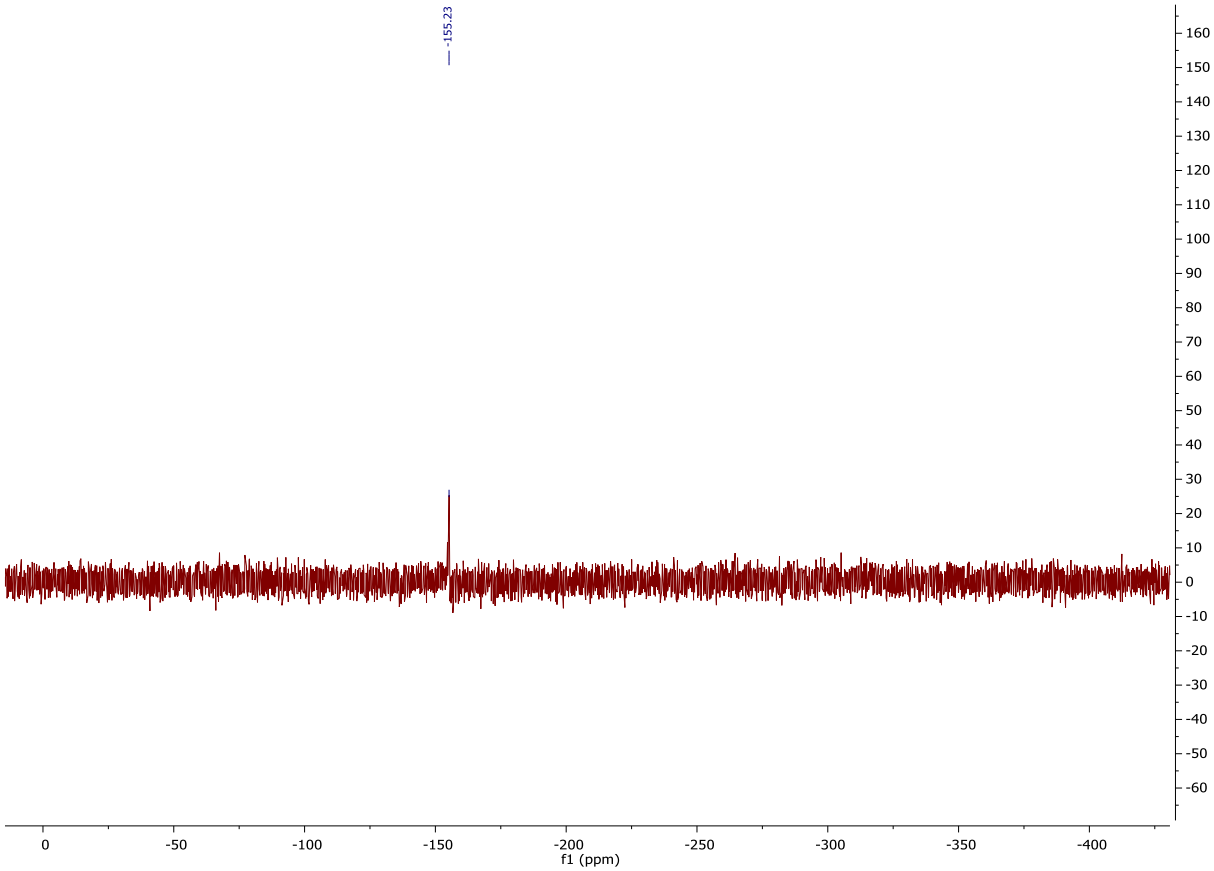

^{119}Sn{^{1}H} NMR (186.36 MHz, C_6D_6, 25 °C): −155.23 ppm.

Figure AVII10. IR Spectrum of 3.

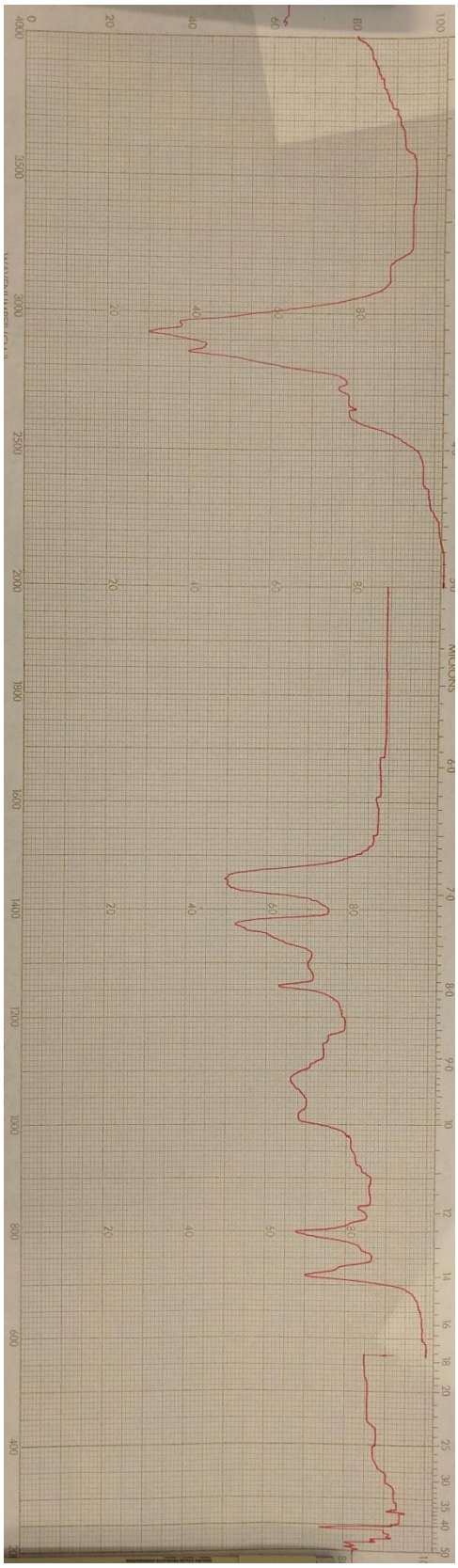

Figure AVII11. UV-Vis Spectrum of 3.

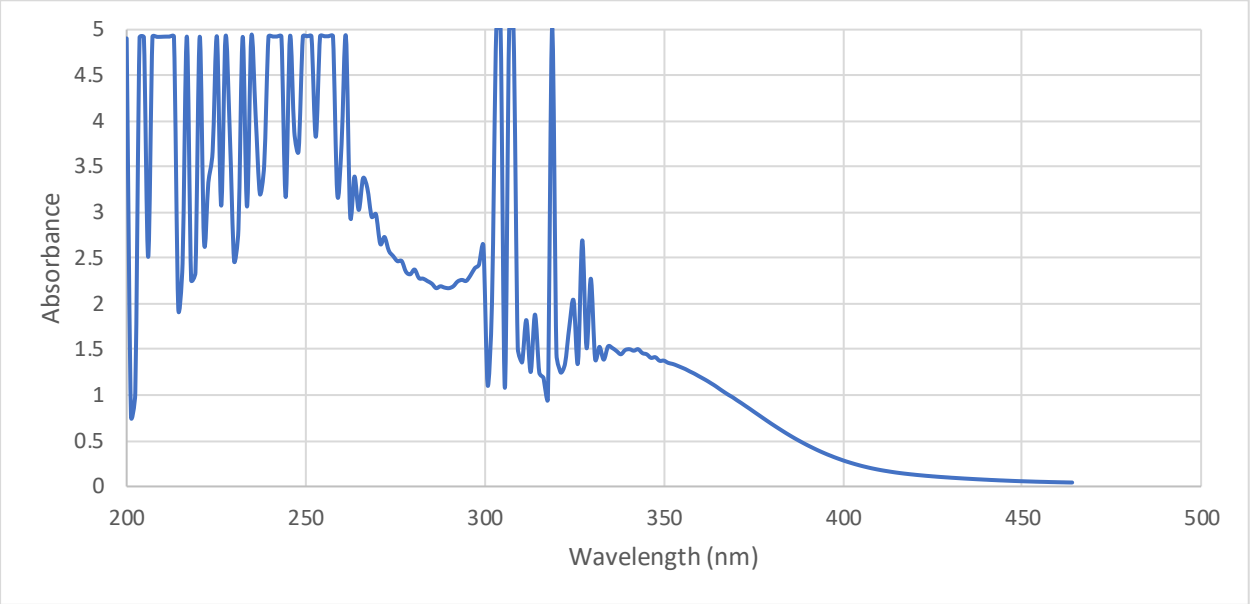

Figure AVII12. ^{1}H Spectrum of 4.

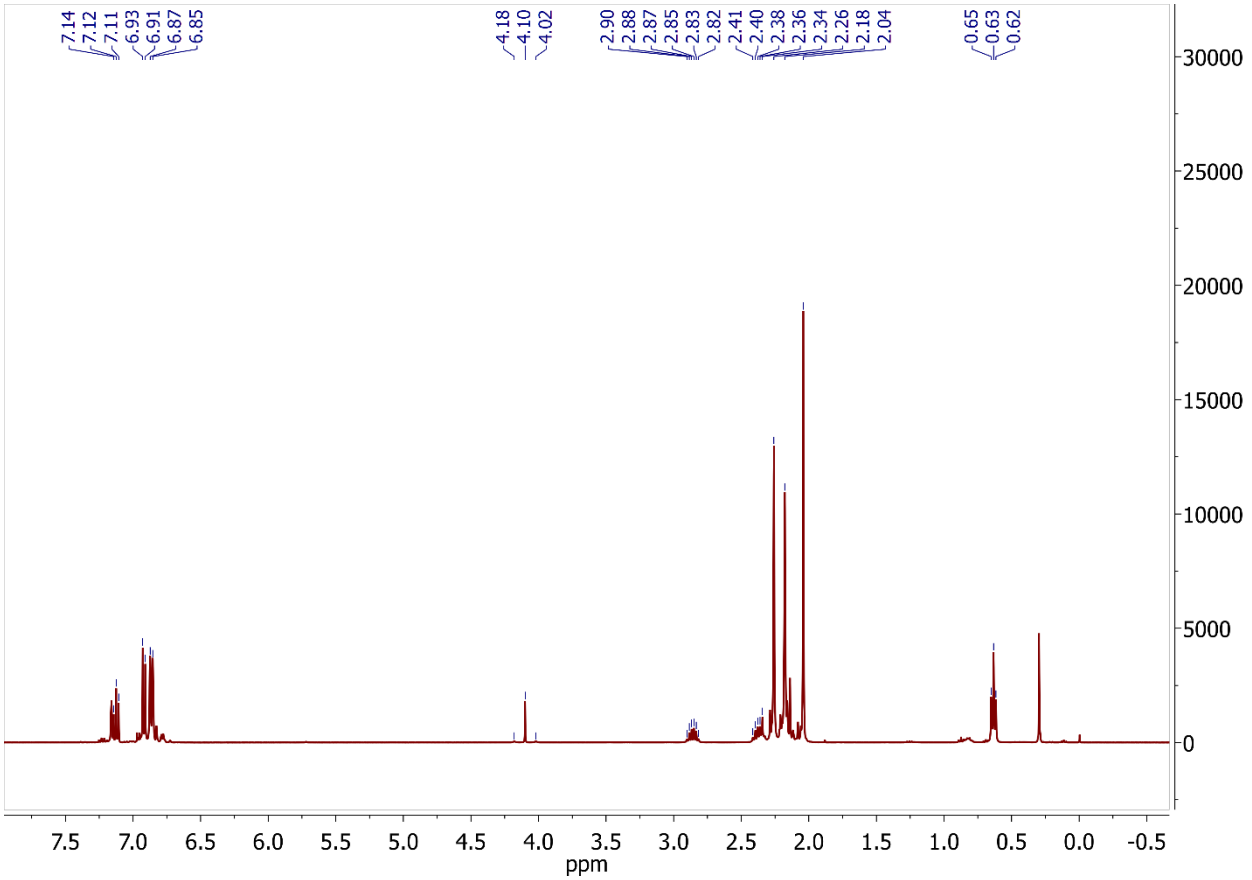

^{1}H NMR (400 MHz, C_6D_6, 25 ºC, ppm): 0.63 (t, J_{HH} = 7.0 Hz, 6H, $NCH_2C\mathbf{H}_3$), 2.04 (s, 12H, *p*-Me), 2.18 (s, 12H, *o*-Me), 2.26 (s, 12H, *o*-Me), 2.34 (dq, J_{HH} = 13.5/6.7 Hz, 1H, $NC\mathbf{H}_2CH_3$), 2.86 (dq, J_{HH} = 13.5/6.7 Hz, 1H, $NC\mathbf{H}_2CH_3$), 4.10 (s, 1H, Sn**H**Sn, ^{119}Sn satellites $J_{H^{119}Sn}$ = 64 Hz), 6.85 (s, 4H, *m*-C_6H_2), 6.87 (s, 4H, *m*-C_6H_2), 6.92 (d, J_{HH} = 7.5 Hz, 4H, *m*-C_6H_3), 7.12 (t, J_{HH} = 7.5 Hz, 2H, *p*-C_6H_3).

Figure AVII13. ^{13}C Spectrum of 4.

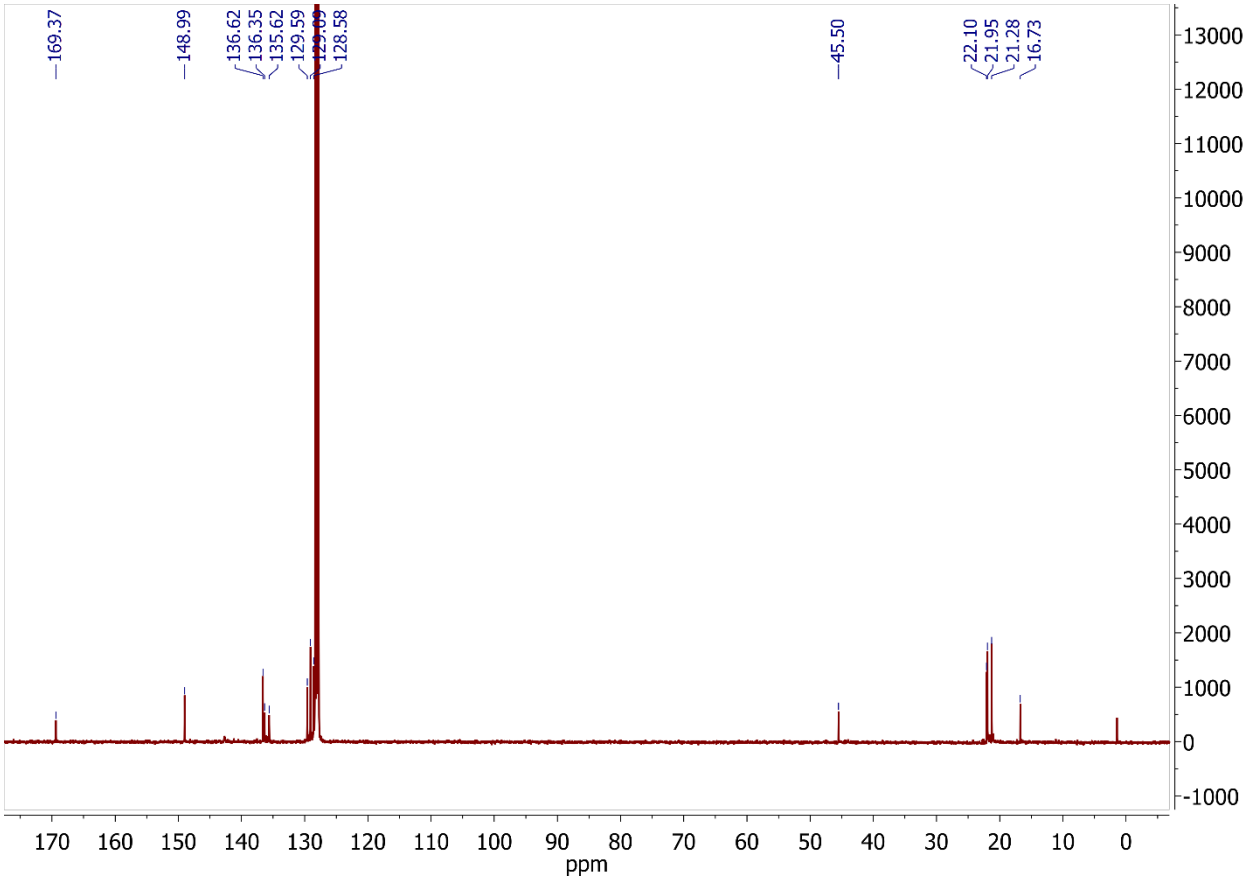

$^{13}C\{^{1}H\}$ NMR (126MHz, C_6D_6, 25° C, ppm): 16.73 ($NCH_2C\mathbf{H}_3$), 21.28 (*p*-Me), 21.95 (*o*-Me), 22.10 (*o*-Me), 45.50 ($NC\mathbf{H}_2CH_3$), 128.58, 129.09, 129.59, 135.62, 136.35, 136.62, 148.99, 169.37.

Figure AVII14. ^{119}Sn Spectrum of 4.

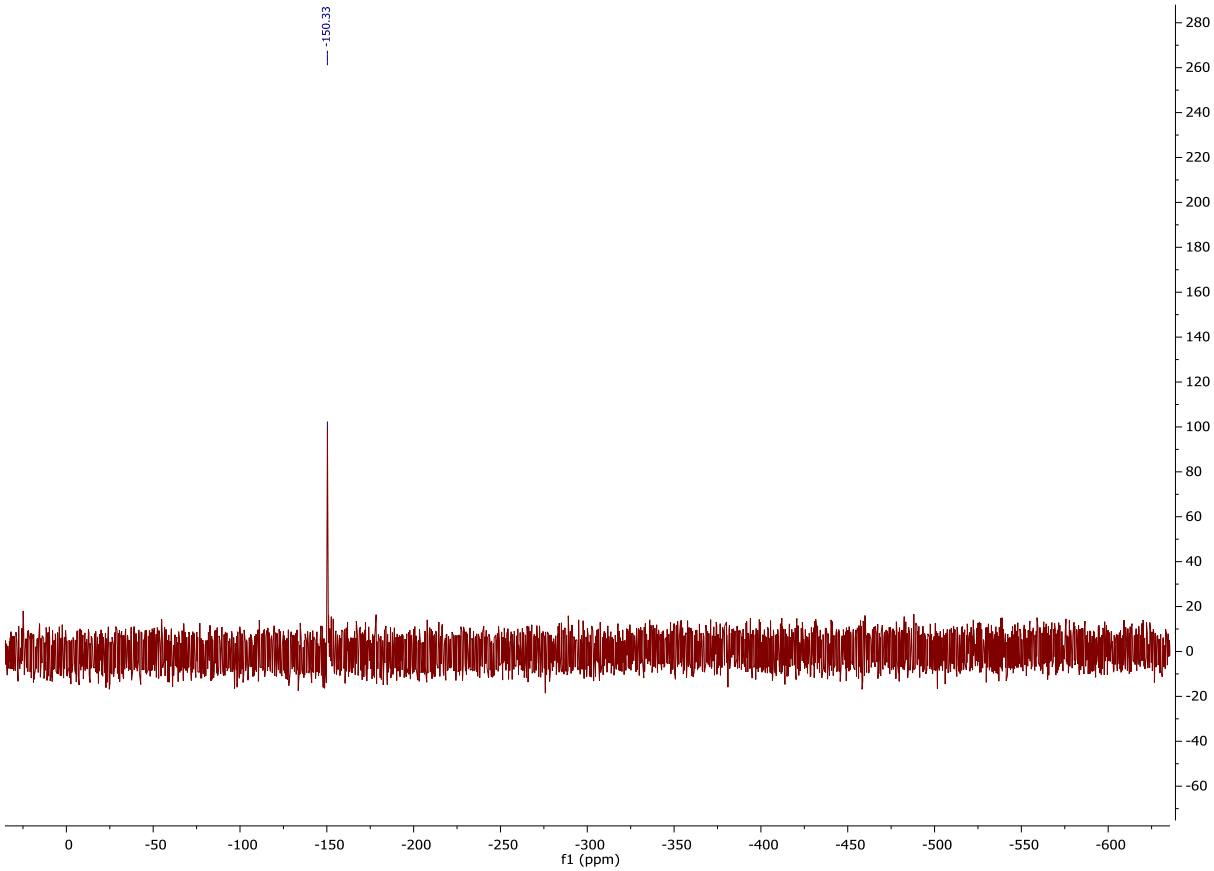

^{119}Sn{^{1}H} NMR (186.36 MHz, C_6D_6, 25 °C): −150.33 ppm.

Figure AVII15. IR of 4.

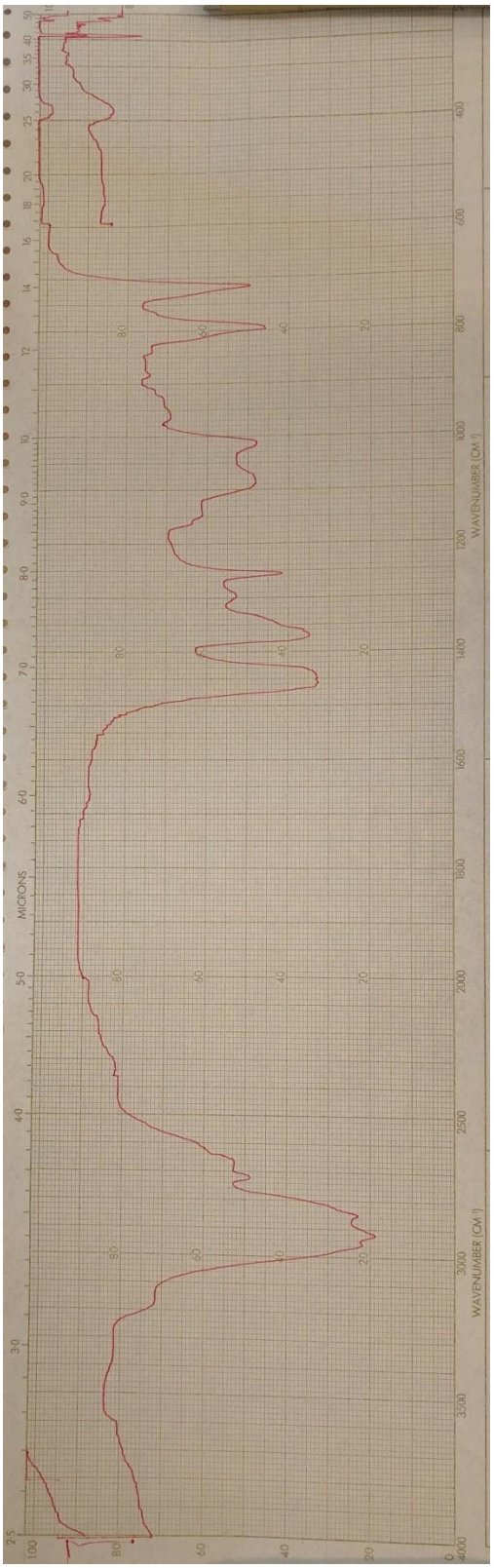

Figure AVII16. UV-Vis of 4.

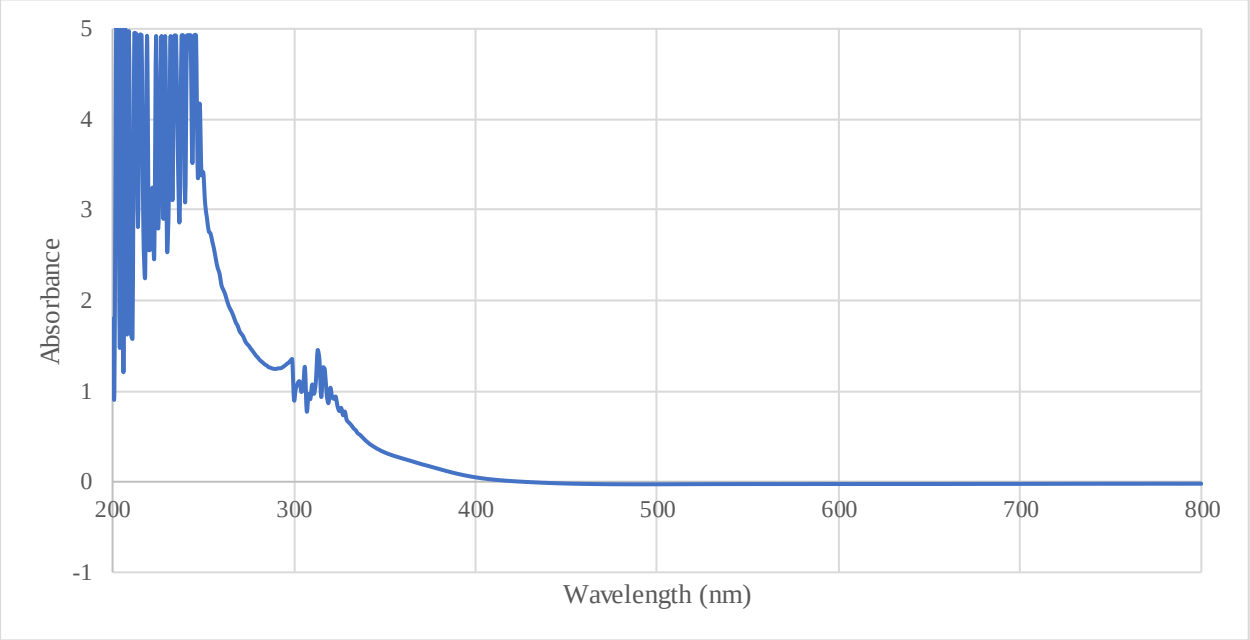

Initial Investigation into Catalytic Activity.

To test if $\{Ar^{Me}{}_6SnH\}_4$ was able to catalyze the dehydrocoupling of Et_2NH and HBPin, **1** (0.047 g, 0.0515 mmol) was first reacted with HBPin in an NMR scale experiment to synthesize $\{Ar^{Me}{}_6SnH\}_4$, which was confirmed by its ^1H NMR spectrum. An excess of Et_2NH and HBPin was then added, but no reaction was found to occur over 48 hours and the ^1H NMR resonances of $\{Ar^{Me}{}_6SnH\}_4$ were still readily visible. This same method was used in an initial testing of the catalytic activity of $\{Ar^{iPr}{}_4Sn(\mu\text{-}H)\}_2$ towards Et_2NH and HBPin, which also gave no dehydrocoupled product. This was eventually found to be due to the narrower scope of the $Ar^{iPr}{}_4Sn$ pre-catalyst species. The addition of HBPin to a mixture of aniline and $\{Ar^{iPr}{}_4Sn(\mu\text{-}H)\}_2$ resulted in the production of PhN(H)BPin.

Catalytic NMR Experiments.

Standard solutions of **1** and **2** were made and used throughout all catalytic experiments. Pinacolborane and all amines were distilled prior to use. All substance were added directly to a Youngs tap NMR tube under an inert atmosphere, which were then inverted repeated to ensure a homogeneous solution. All liquids and the stock solutions of **1** and **2** were measured with Eppendorf pipettes. Aminoboranes presented in Table were identified by comparison to published data and their ^1H NMR spectra are shown below. Novel compounds were characterized by ^1H, ^{11}B and ^{13}C NMR and are also presented below.

sBuNH$_2$:HBPin: ^1H NMR (400 MHz, C_6D_6, 25 ºC, ppm): 0.85 (t, 3H, CH_2CH_3), 0.96 (d, 3H, $CHCH_3$), 1.14 (s, 12H, Pin)), 1.27 (m, 1H, C(**H**)HCH_3), 1.90 (s, 1H, NH), 3.23 (m, 1H, C(**H**)HCH_3). ^{11}B NMR (128.26 MHz, C_6D_6, 25 ºC, ppm): 24.55 (sBuNH**B**Pin). $^{13}C\{^1H\}$ NMR (126MHz, C_6D_6, 25° C, ppm): 10.56 (CH_2**C**H_3), 23.97 (CH**C**H_3), 24.38 (Me-Pin), 24.49 (Me-Pin), 32.76 (**C**H_2CH_3), 47.90 (**C**H), 48.36 (**C**H), 81.32 (Pin).

4-fluoroaniline:HBPin: ^1H NMR (400 MHz, C_6D_6, 25 ºC, ppm): 0.84 (s, 12H, Pin), 4.04 (s, 1H, NH), 6.53 (t, 2H, *o*-C_6H_4), 6.60 (t, 2H, *m*-C_6H_4). ^{11}B NMR (128.26 MHz, C_6D_6, 25 ºC, ppm): 24.07 (4-fluoroaniline**B**Pin) $^{13}C\{^1H\}$ NMR (126MHz, C_6D_6, 25° C, ppm): 24.52 (Me-Pin), 83.26 (Pin), 116.46, 120.38, 135.49, 146.12 (Ar).

4-Chloroaniline:HBPin: ^1H NMR (400 MHz, C_6D_6, 25 ºC, ppm): 1.05 (s, 12H, Pin), 4.27 (s, 1H, NH), 6.80 (d, 2H, *o*-C_6H_4), 7.05 (d, 2H, *m*-C_6H_4). ^{11}B NMR (128.26 MHz, C_6D_6, 25 ºC, ppm): 24.05 (4-chloroaniline**B**Pin) $^{13}C\{^1H\}$ NMR (126MHz, C_6D_6, 25° C, ppm): 24.66 (Me-Pin), 82.89 (Pin), 116.11, 119.28, 129.17, 129.30 (Ar).

4-bromoaniline:HBPin: ^1H NMR (400 MHz, C_6D_6, 25 ºC, ppm): 1.05 (s, 12H, Pin), 4.26 (s, 1H, NH), 6.75 (d, 2H, *o*-C_6H_4), 7.19 (d, 2H, *m*-C_6H_4). ^{11}B NMR (128.26 MHz, C_6D_6, 25 ºC, ppm): 24.03 (4-bromoaniline**B**Pin) $^{13}C\{^1H\}$ NMR (126MHz, C_6D_6, 25° C, ppm): 24.66 (me-Pin), 82.91 (Pin), 116.38, 119.29, 129.16, 128.32 (Ar).

4-ethylaniline:HBPin: ^{1}H NMR (400 MHz, C_6D_6, 25 ºC, ppm): 1.04 (t, 3H, $CH_2C\mathbf{H}_3$), 1.10 (s, 12H, Pin) 2.42 (q, 2H, $C\mathbf{H}_2CH_3$), 6.98 (d, 2H, *o*-C_6H_4), 7.07 (d, 2H, *m*-C_6H_4). ^{11}B NMR (128.26 MHz, C_6D_6, 25 ºC, ppm): 24.22 (4-ethylaniline**B**Pin) ^{13}C{^{1}H} NMR (126MHz, C_6D_6, 25° C, ppm): 15.88 ($CH_2\mathbf{C}H_3$), 24.35 (Me-Pin), 28.13 ($\mathbf{C}H_2CH_3$), 82.24 (Pin), 114.97, 117.80, 128.24, 128.42 (Ar).

3,5-dichloroaniline:HBPin: ^{1}H NMR (400 MHz, C_6D_6, 25 ºC, ppm): 0.99 (s, 12H, Pin), 4.26 (s, 1H, NH), 6.84 (s, 1H, *p*-C_6H_3), 6.85 (s, 2H, *o*-C_6H_3). ^{11}B NMR (128.26 MHz, C_6D_6, 25 ºC, ppm): 23.88 (3,5-dichloroaniline**B**Pin) ^{13}C{^{1}H} NMR (126MHz, C_6D_6, 25° C, ppm): 24.52 (Me-Pin), 83.26 (Pin), 116.46, 120.38, 135.49, 146.12 (Ar).

NH_2BPin: ^{1}H NMR (400 MHz, C_6D_6, 25 ºC, ppm): 0.13 (NH_3), 1.07 (s, 12H, H_2NB**Pin**), 2.60 (s, 2H, $\mathbf{H}_2$NBPin). ^{11}B NMR (128.26 MHz, C_6D_6, 25 ºC, ppm) 25.05 (NH_2**B**Pin) ^{13}C{^{1}H} NMR (126MHz, C_6D_6, 25° C, ppm): 24.58 (Me-Pin), 81.66 (Pin).

PinNH_2:HBPin. Excess HBPin: ^{1}H NMR (400 MHz, C_6D_6, 25 ºC, ppm): 0.99 (HBPin), 1.05 (HN{B**Pin**}$_2$), 3.33 (**H**N{BPin}$_2$). ^{11}B NMR (128.26 MHz, C_6D_6, 25 ºC, ppm) 25.60 (NH_2**B**Pin) ^{13}C{^{1}H} NMR (126MHz, C_6D_6, 25° C, ppm): 24.76, 24.66 (**Me**-Pin), 82.93, 82.47 (Pin).

Figure AVII17. ^{1}H NMR, Table 1, Entry 1: *n*BuNH$_2$:HBPin. 10% excess HBPin

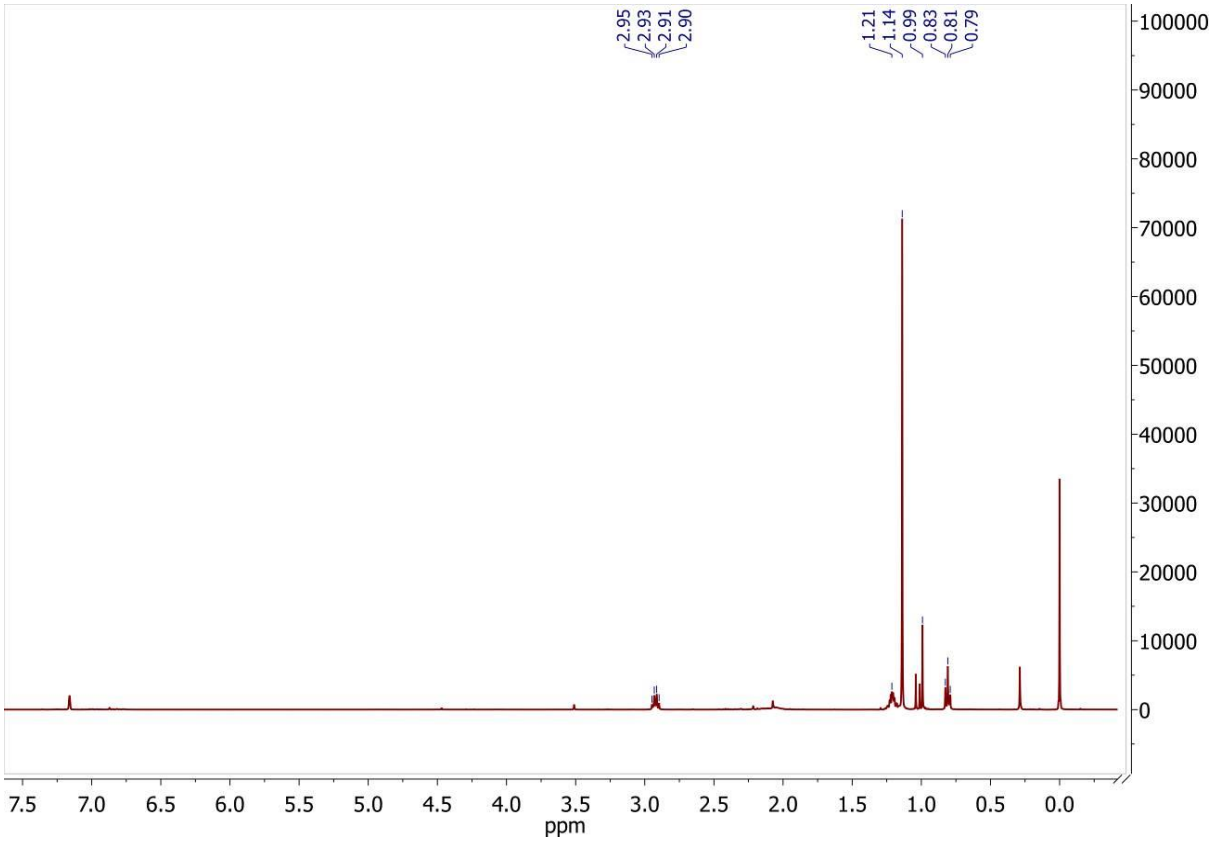

Figure AVII18. ^{11}B NMR, Table 1, Entry 1: *n*BuNH$_2$:HBPin. 10% excess HBPin.

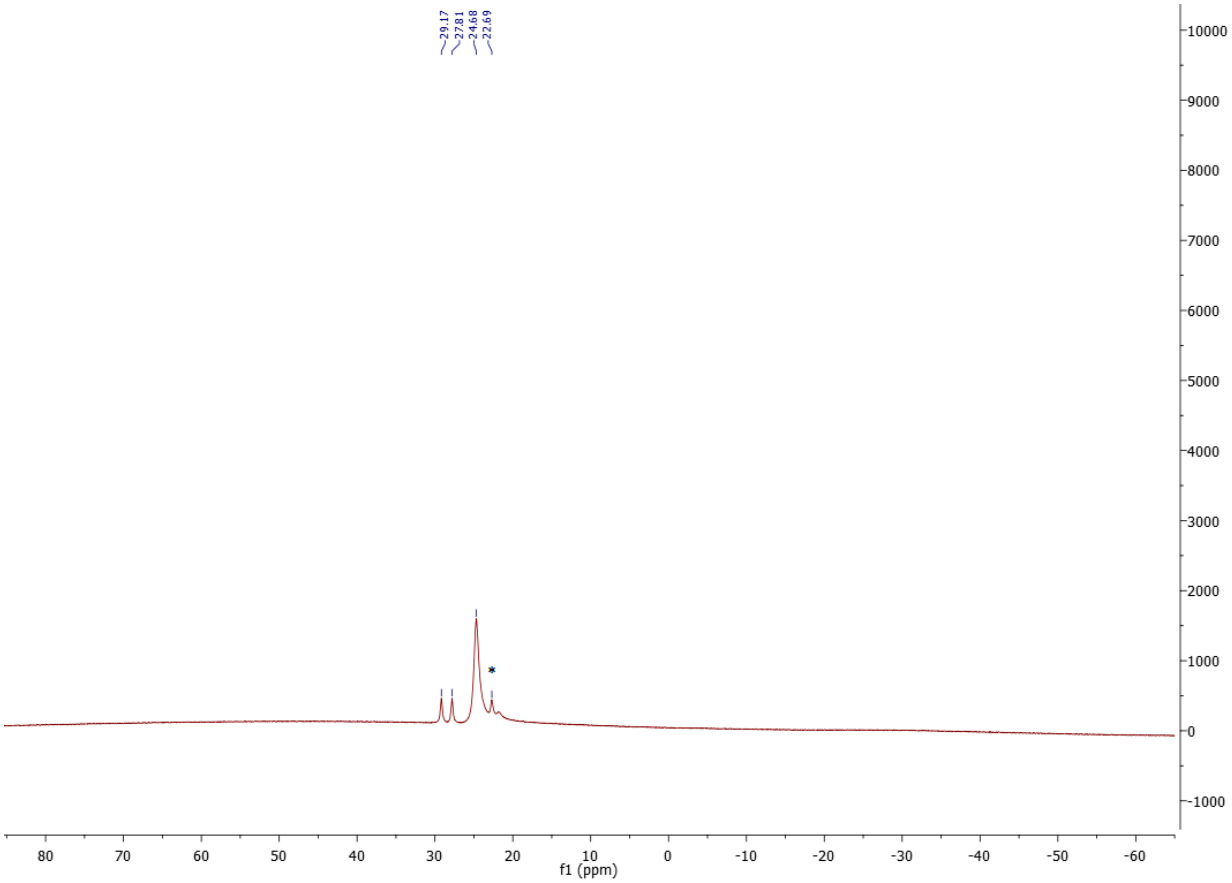

* PinBOBPin

Figure AVII19. ^{1}H NMR, Table 1, Entry 2: *s*BuNH$_2$:HBPin.

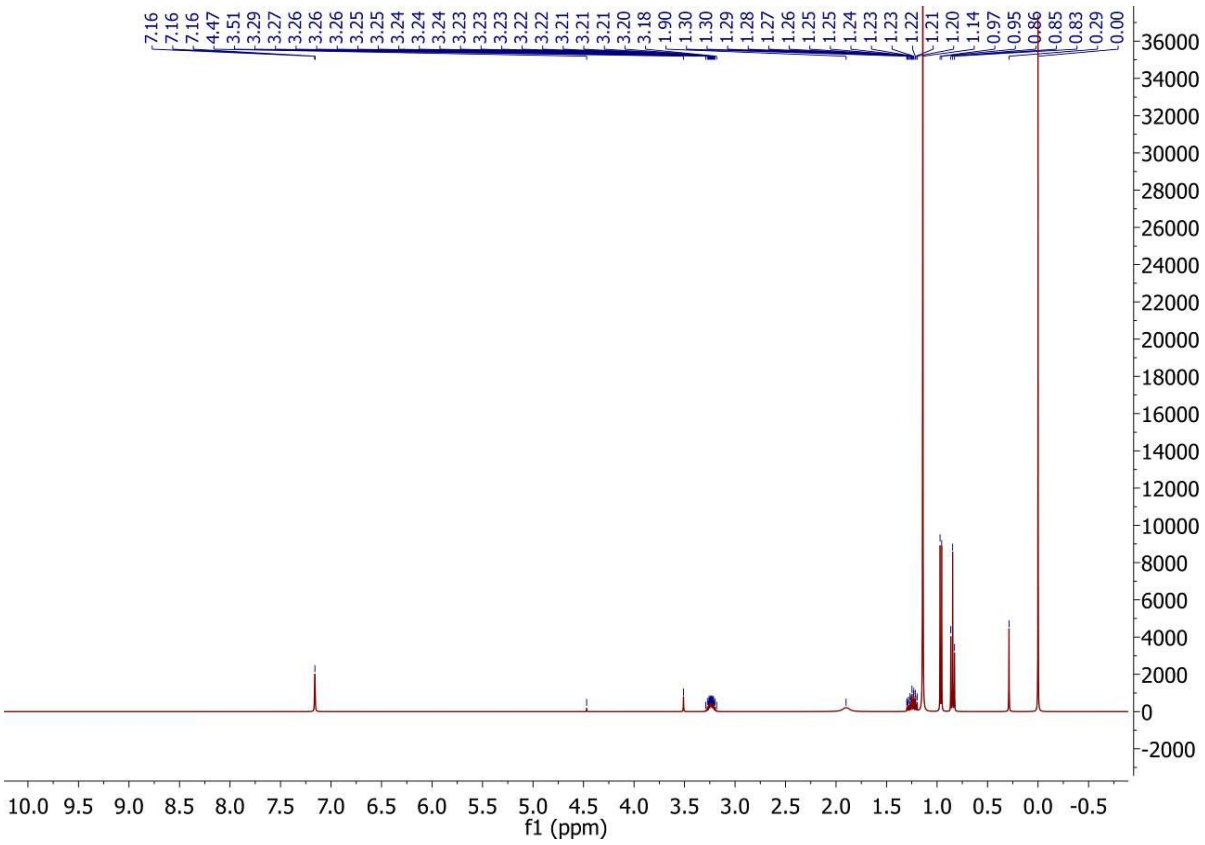

Figure AVII20. ^{11}B NMR, Table 1, Entry 2: *s*BuNH$_2$:HBPin.

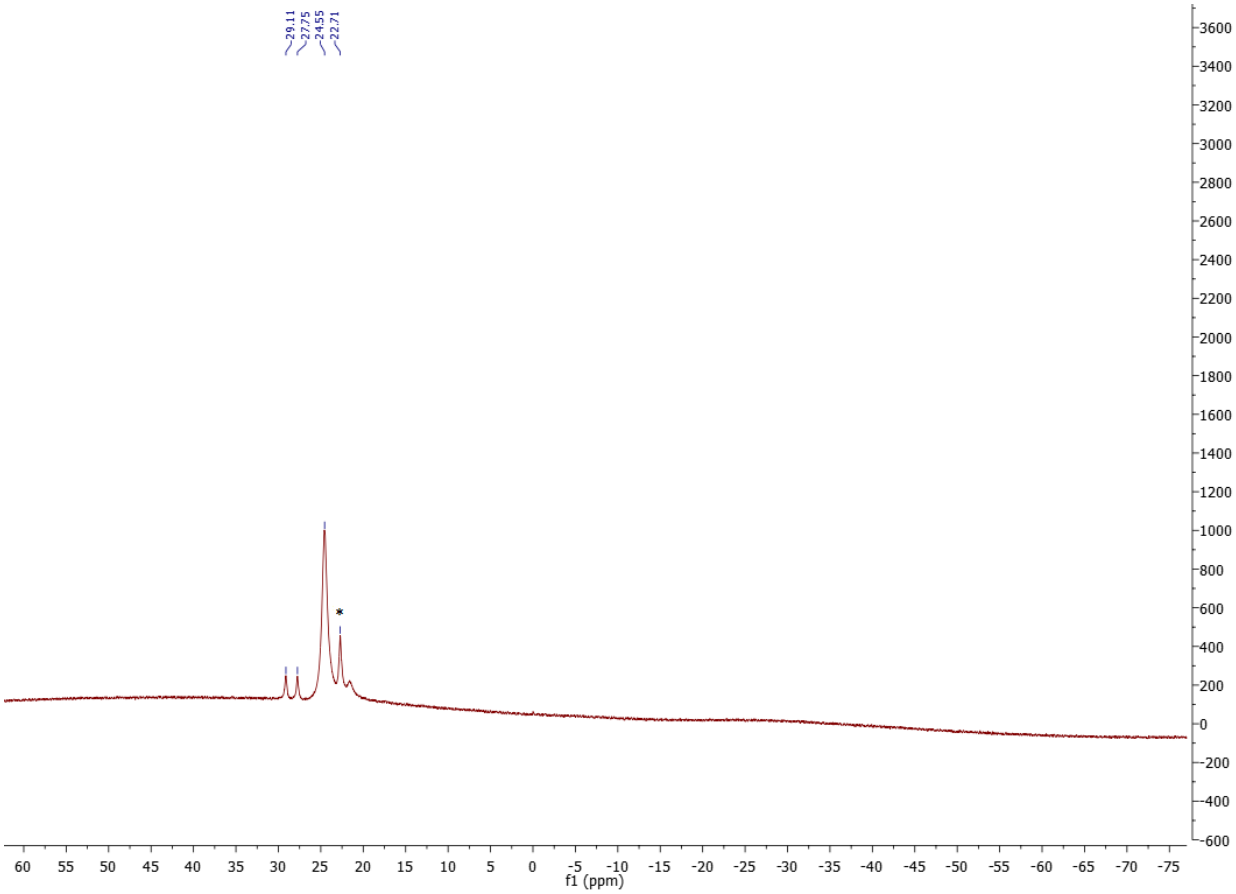

* PinBOBPin

Figure AVII21. ^{13}C NMR, Table 1, Entry 2: *s*BuNH$_2$:HBPin.

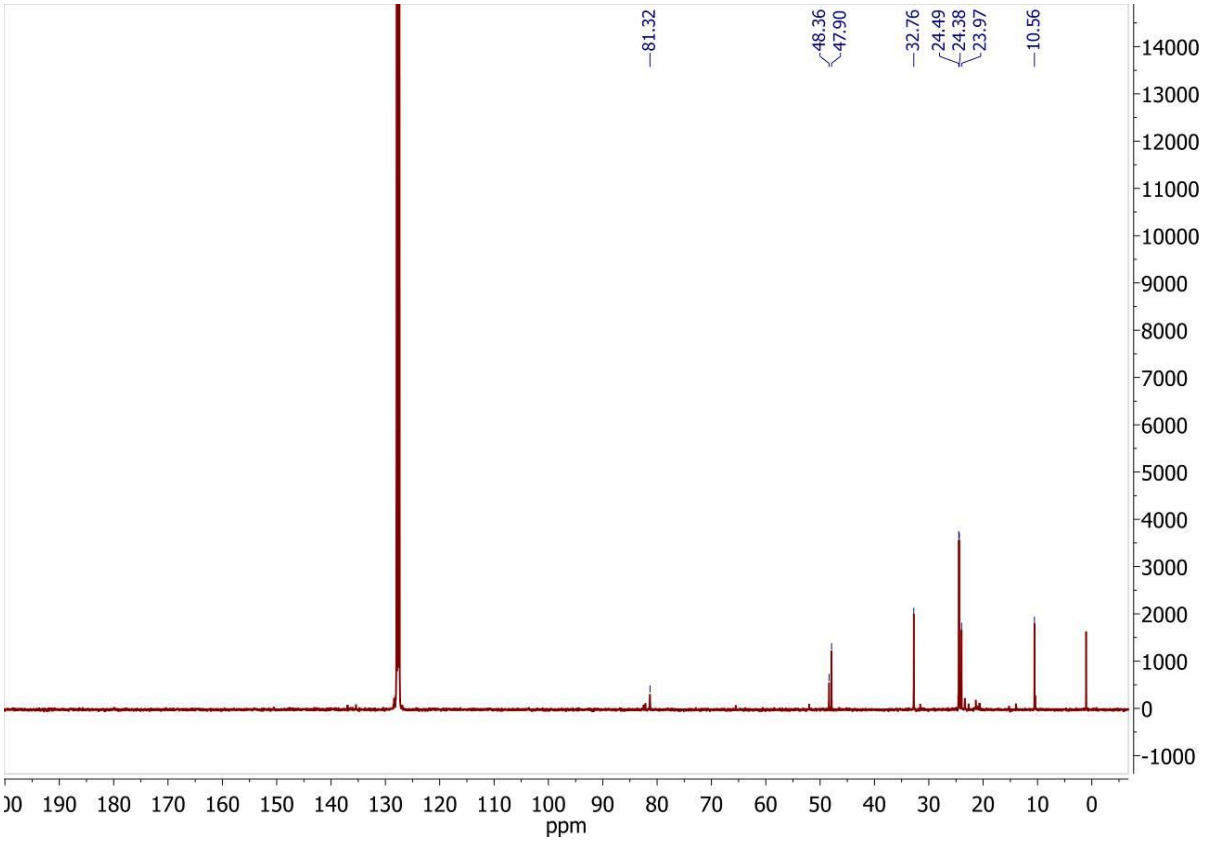

Figure AVII22. ^{1}H NMR, Table 1, Entry 3: $PhNH_2$:HBPin.

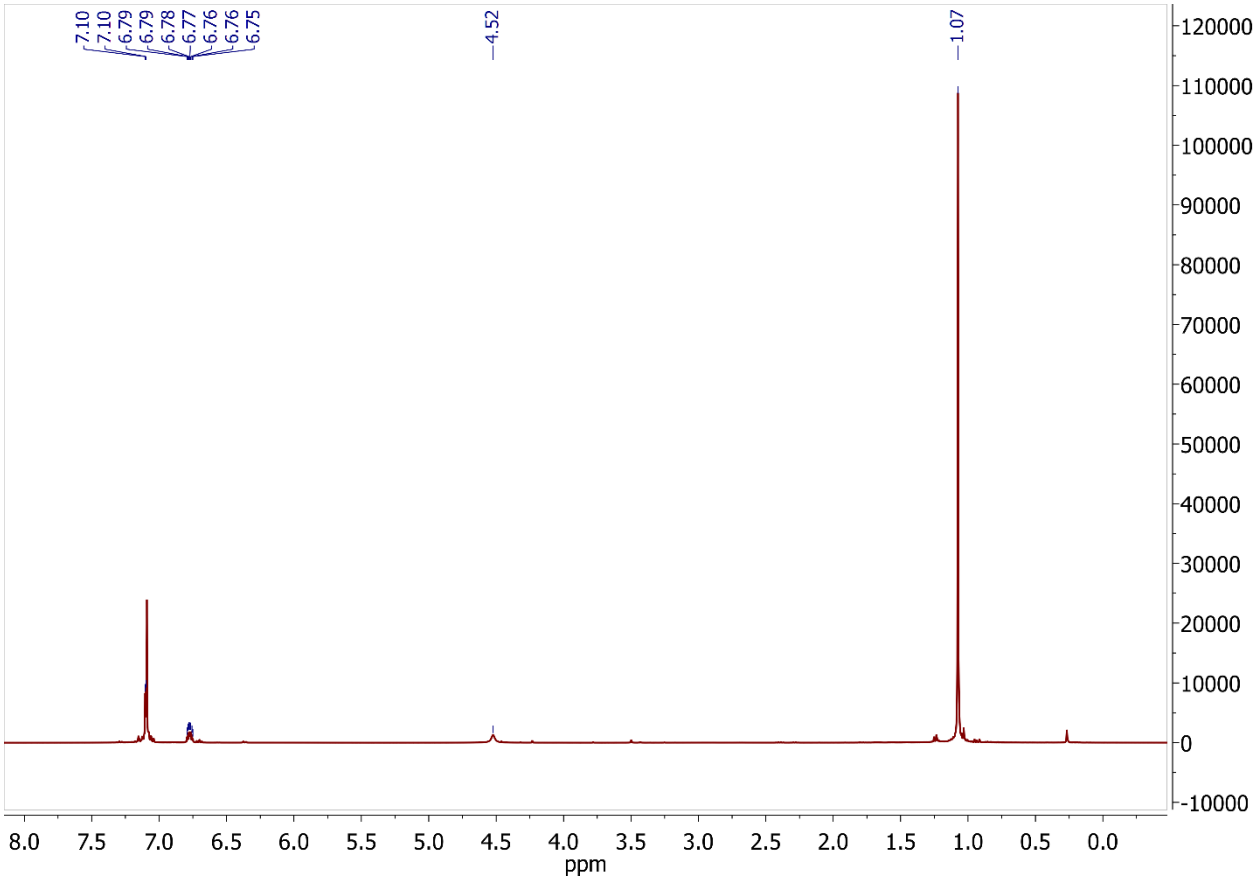

Figure AVII23. ^{11}B NMR, Table 1, Entry 3: $PhNH_2$:HBPin.

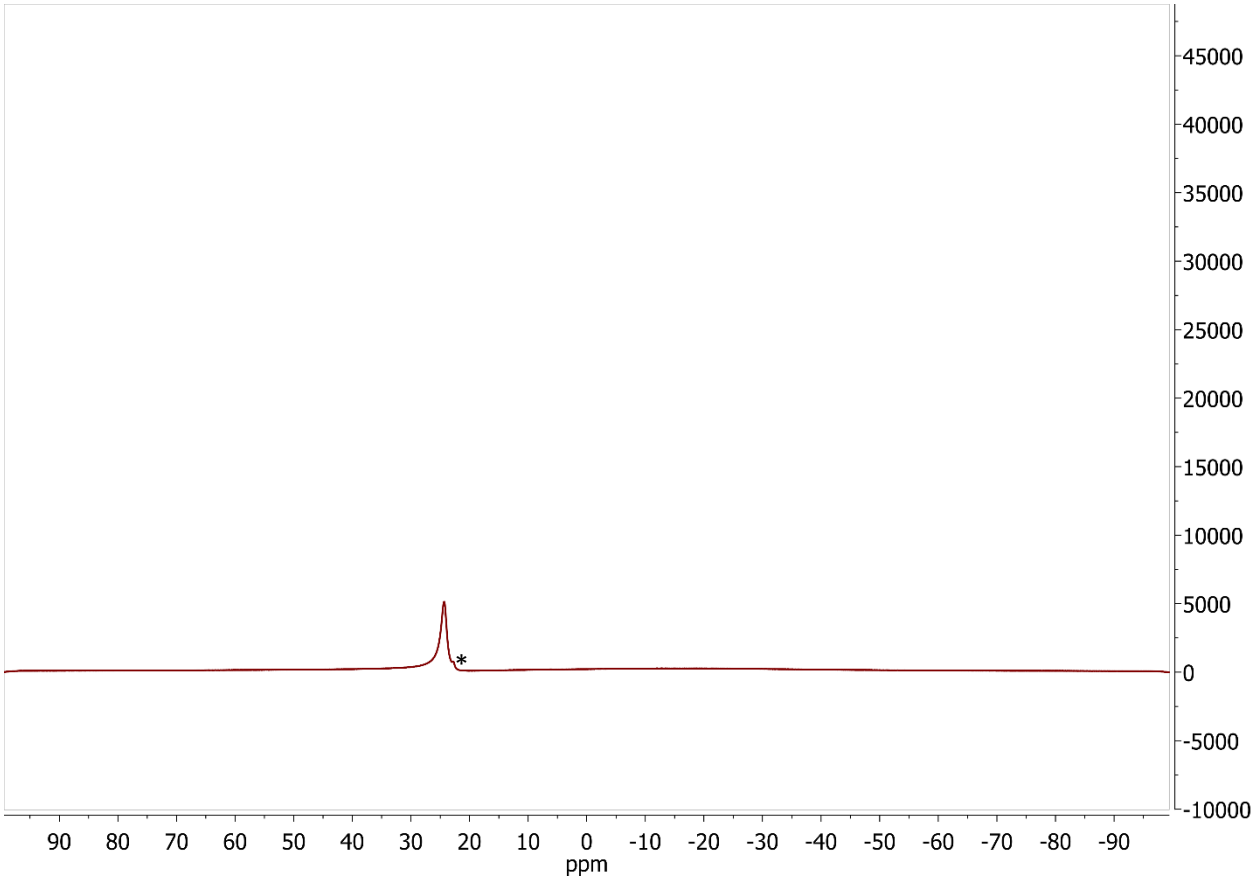

* PinBOBPin

Figure AVII24. ^{1}H NMR, Table 1, Entry 4: 4-fluoroaniline:HBPin.

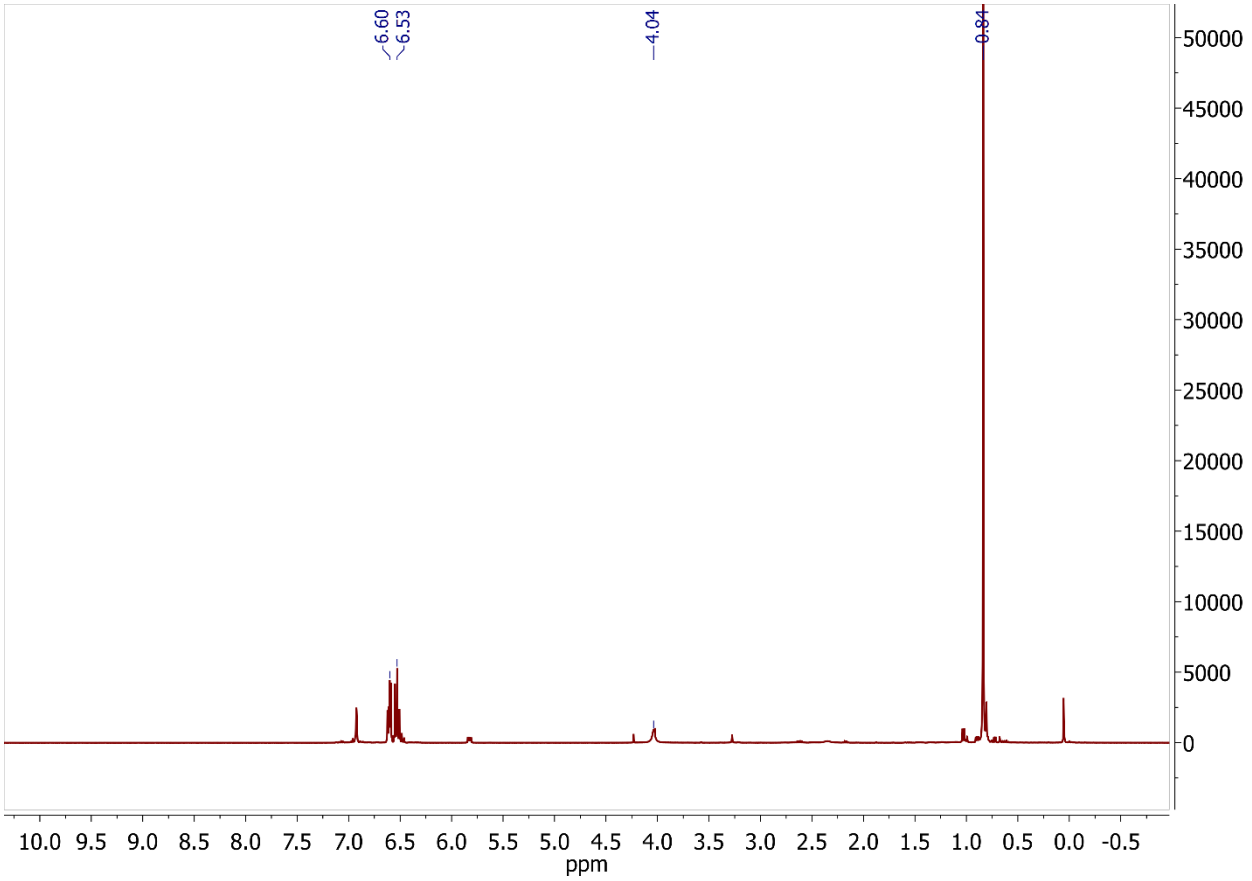

Figure AVII25. ^{13}C NMR, Table 1, Entry 4: 4-fluoroaniline:HBPin.

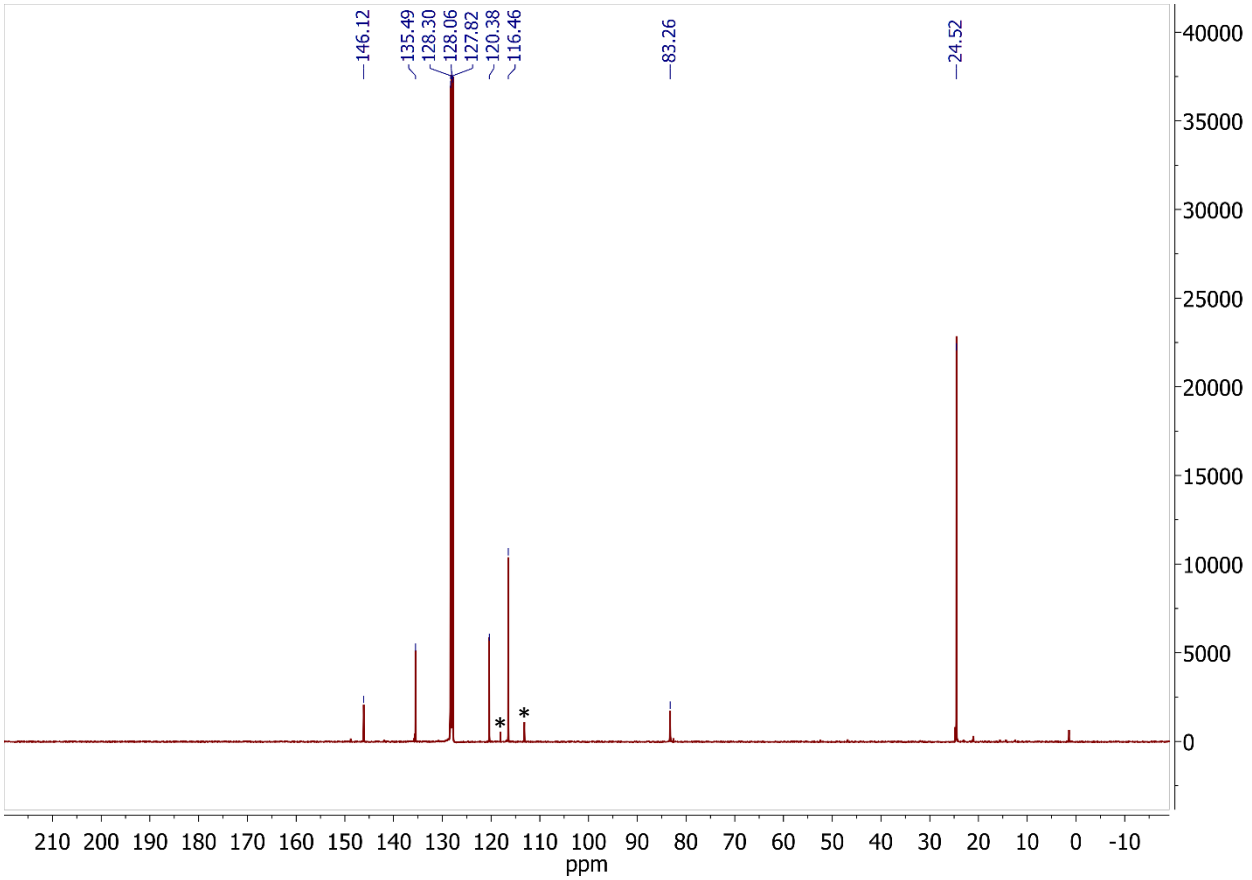

* slight excess of 4-fluoroaniline

Figure AVII26. ^{11}B NMR, Table 1, Entry 4: 4-fluoroaniline:HBPin.

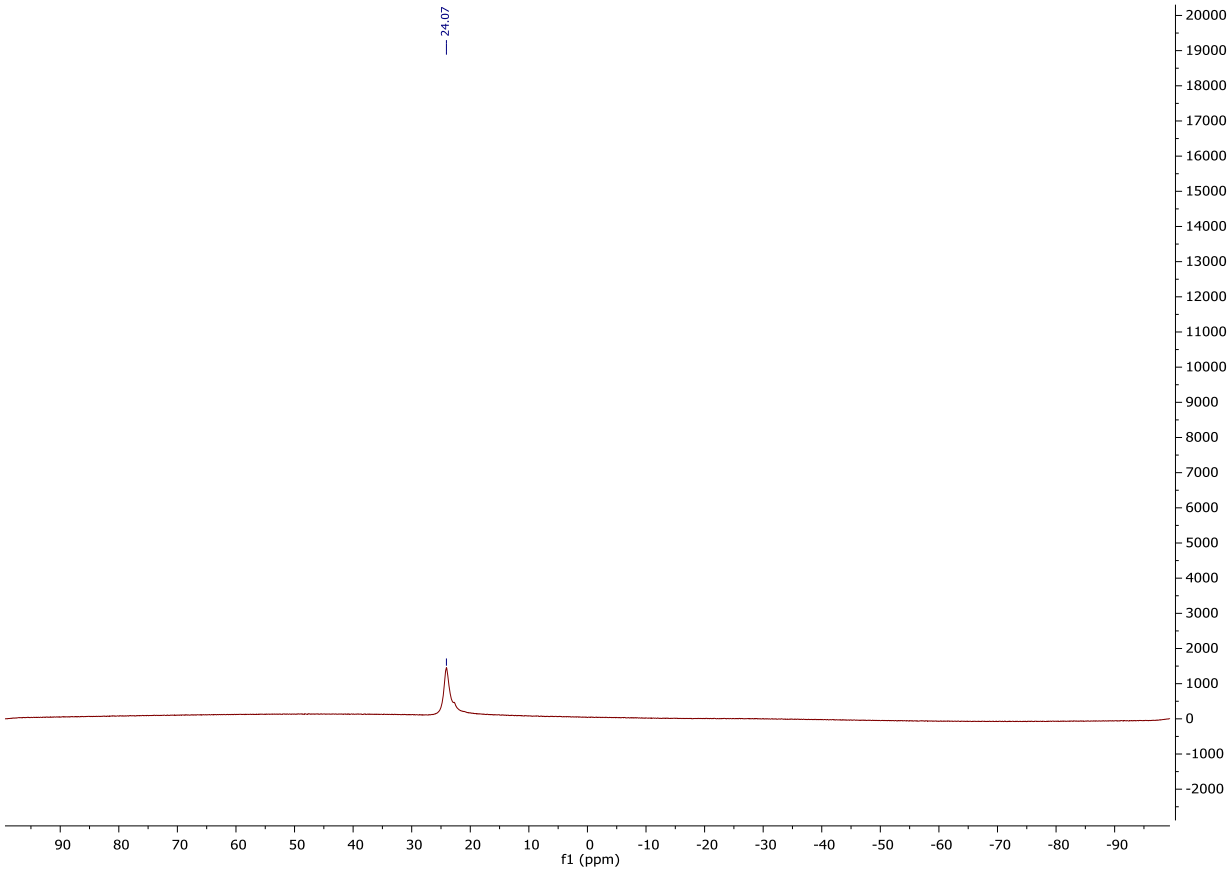

Figure AVII27. ^{1}H NMR, Table 1, Entry 5: 4-Chloroaniline:HBPin.

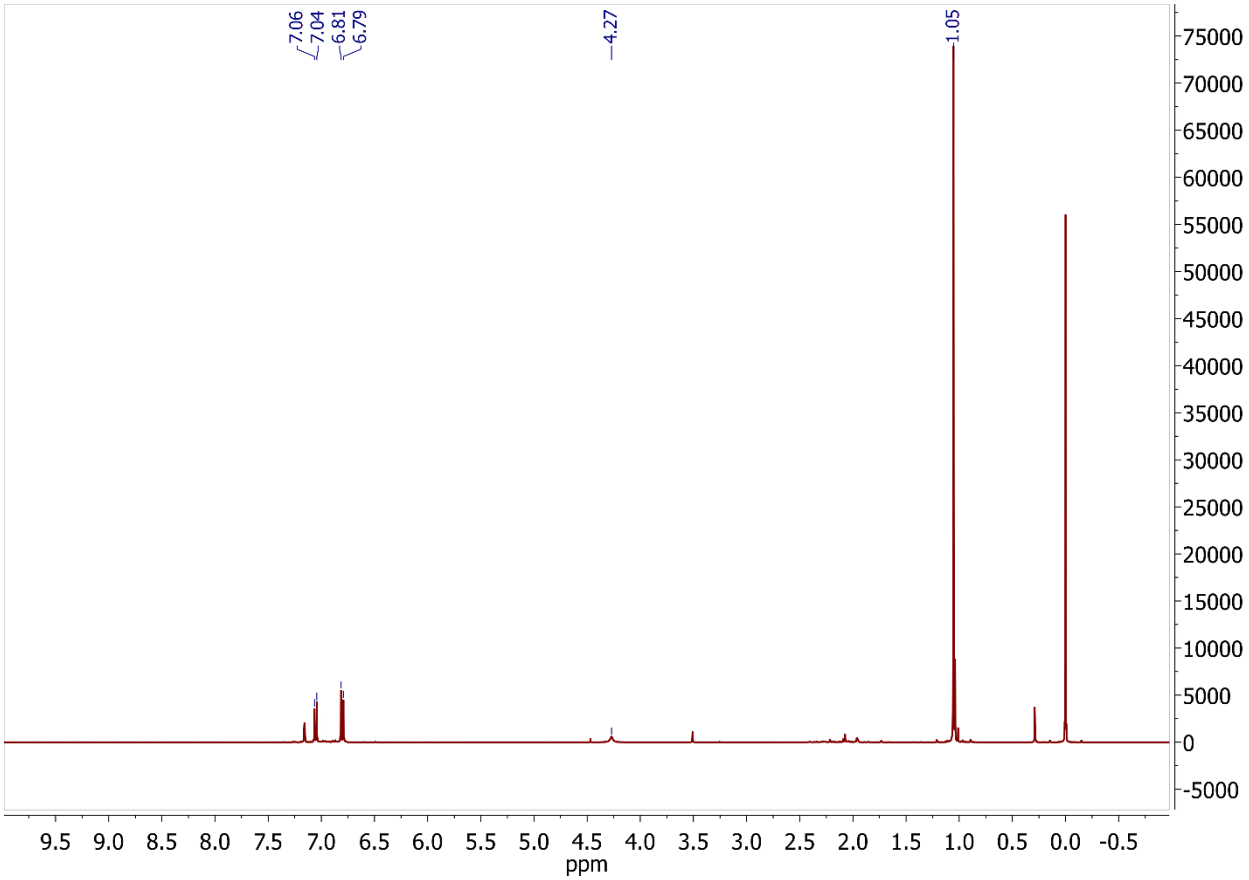

Figure AVII28. ^{13}C NMR, Table 1, Entry 5: 4-Chloroaniline:HBPin.

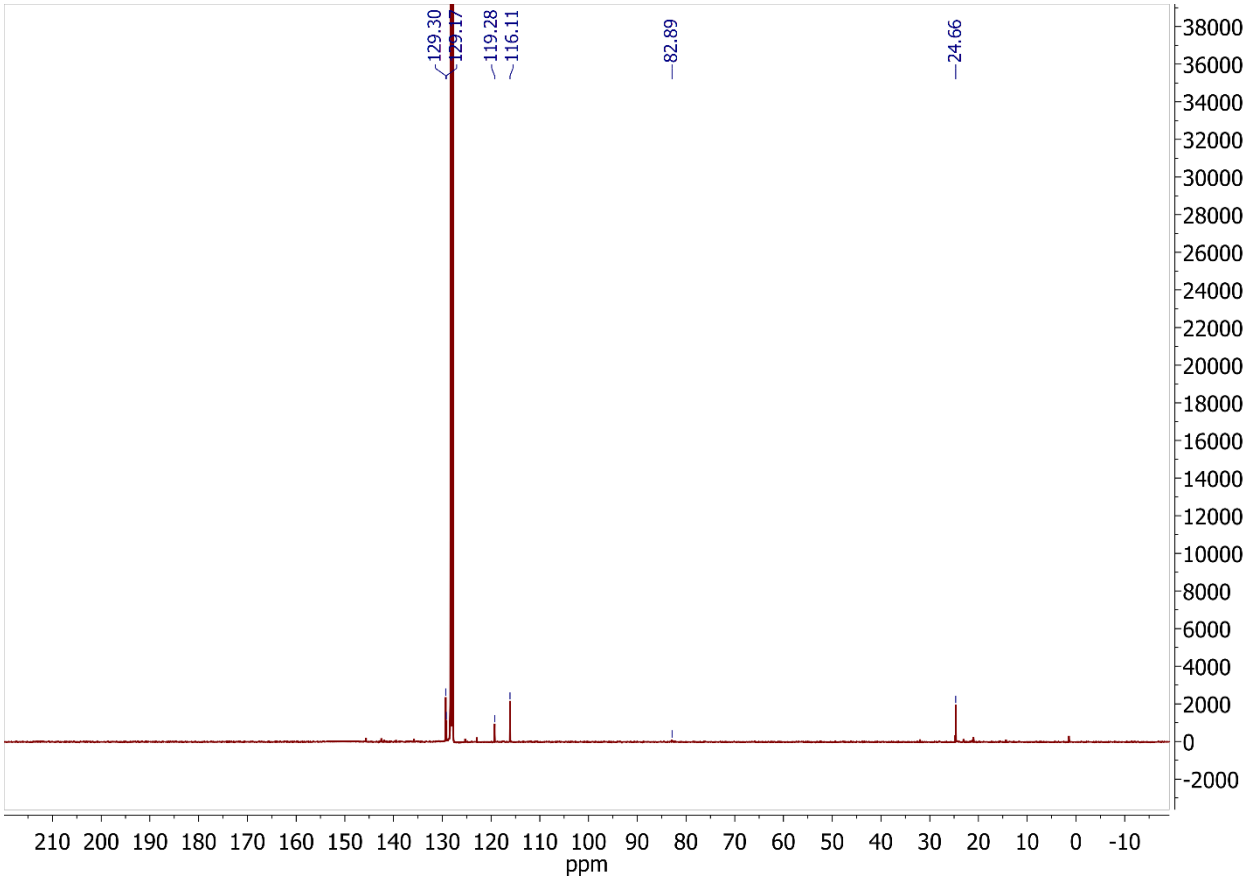

Figure AVII29. ^{11}B NMR, Table 1, Entry 5: 4-Chloroaniline:HBPin.

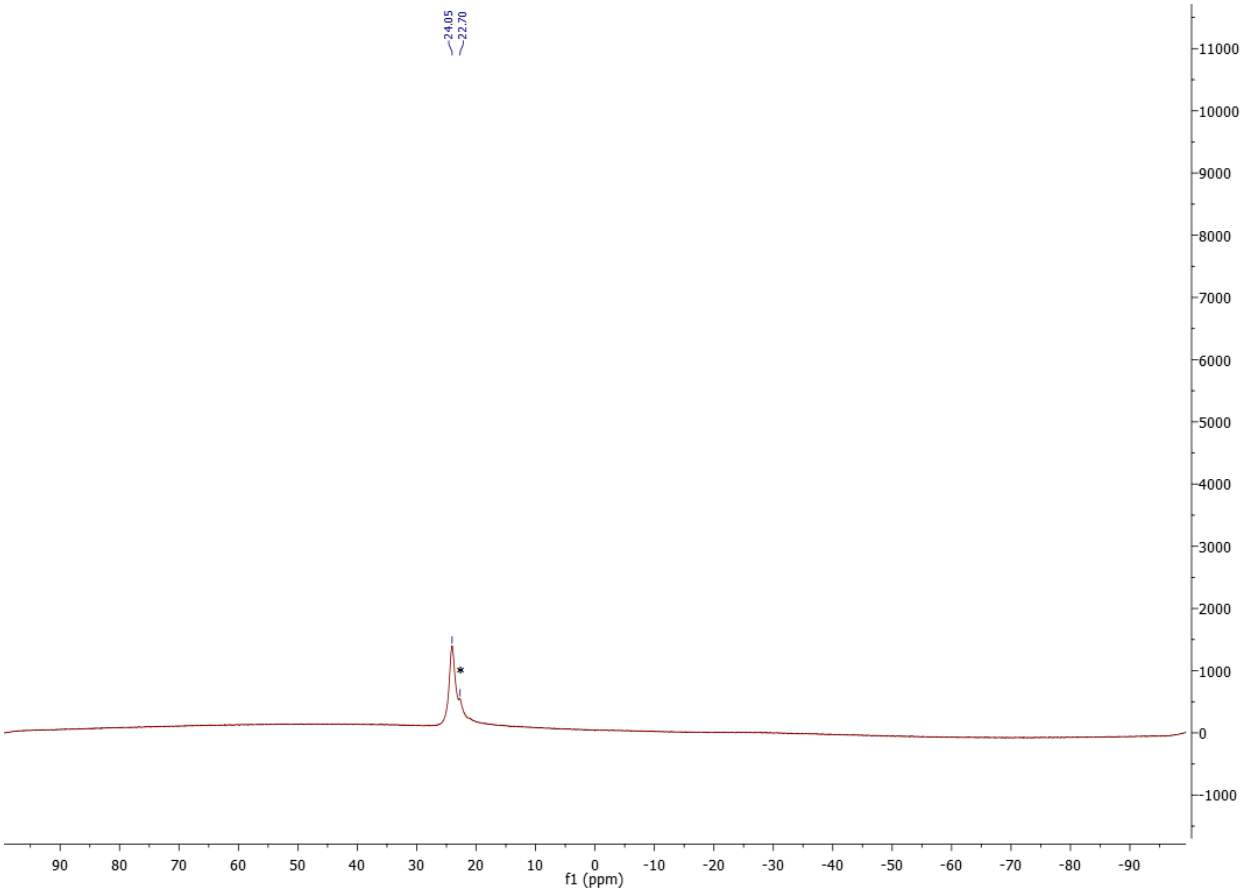

* PinBOBPin

Figure AVII30. ^{1}H NMR, Table 1, Entry 6: 4-bromoaniline:HBPin.

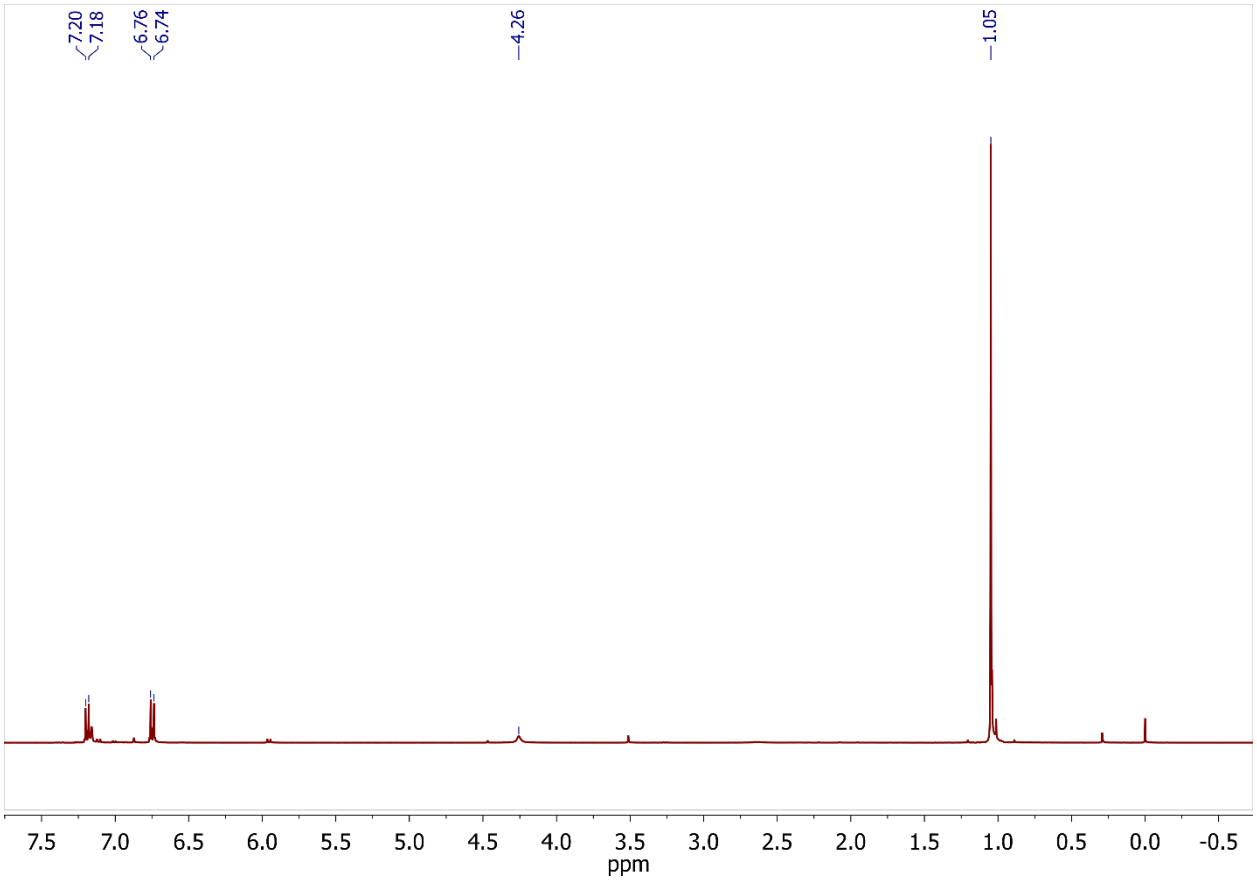

Figure AVII31. ^{13}C NMR, Table 1, Entry 6: 4-bromoaniline:HBPin.

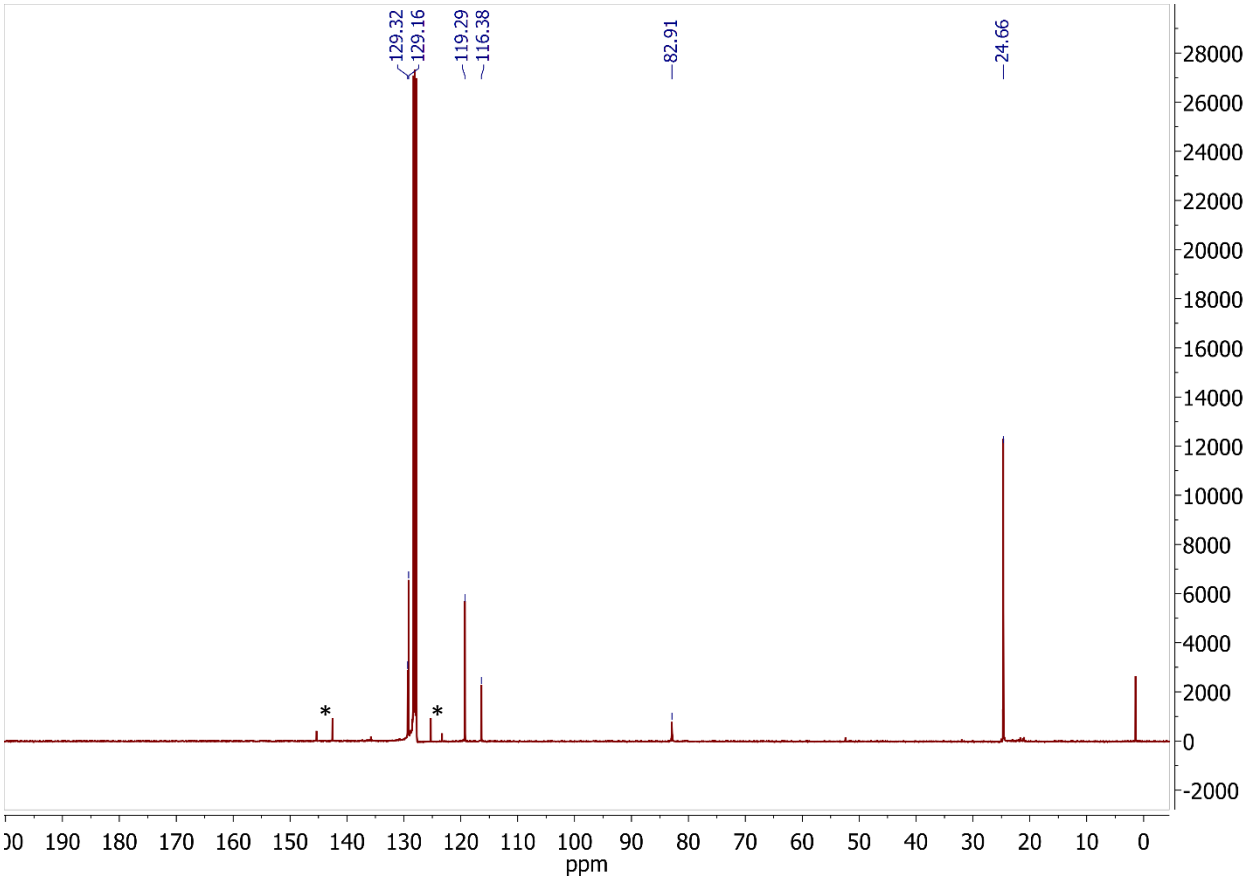

* Excess 4-bromoaniline

Figure AVII32. ^{11}B NMR, Table 1, Entry 6: 4-bromoaniline:HBPin.

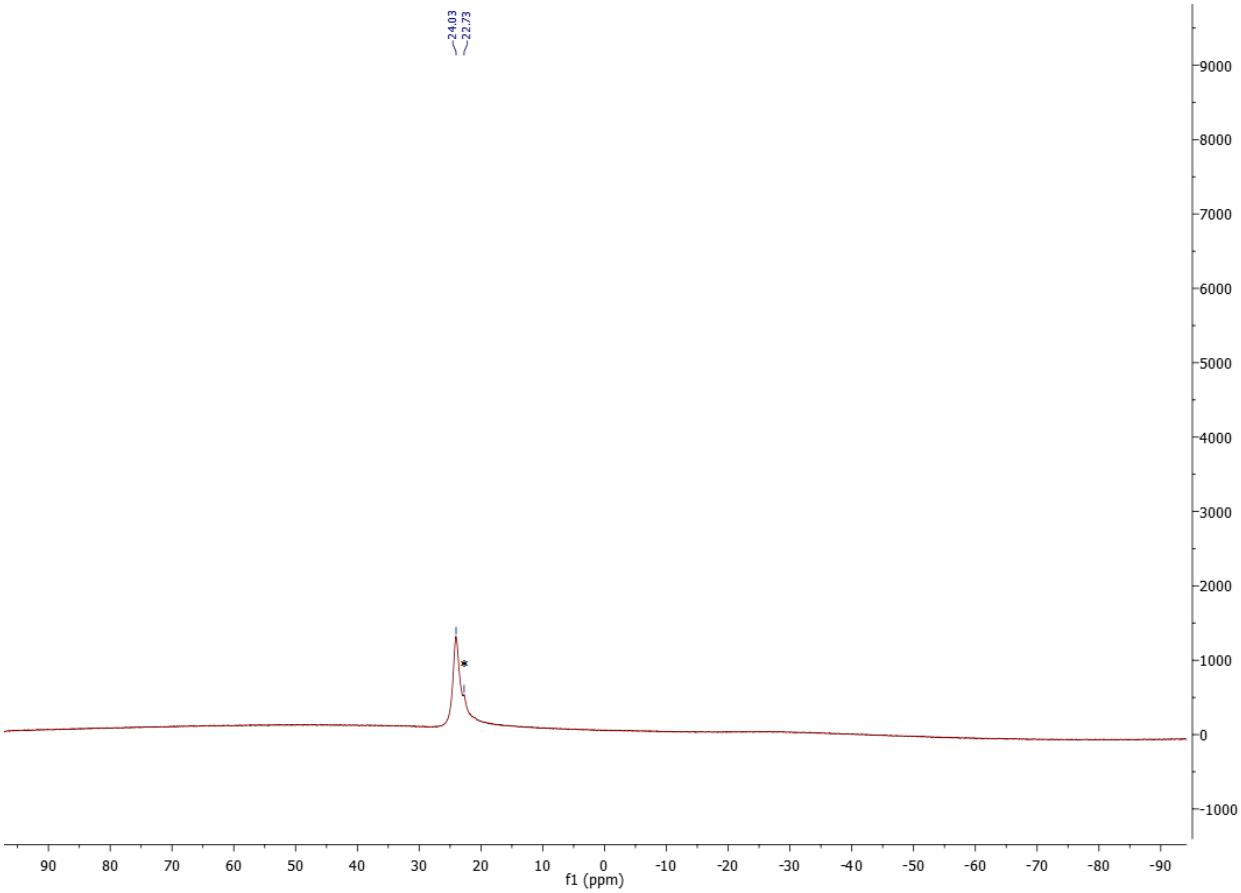

* PinBOBPin

Figure AVII33. ^{1}H NMR, Table 1, Entry 7: 4-ethylaniline:HBPin.

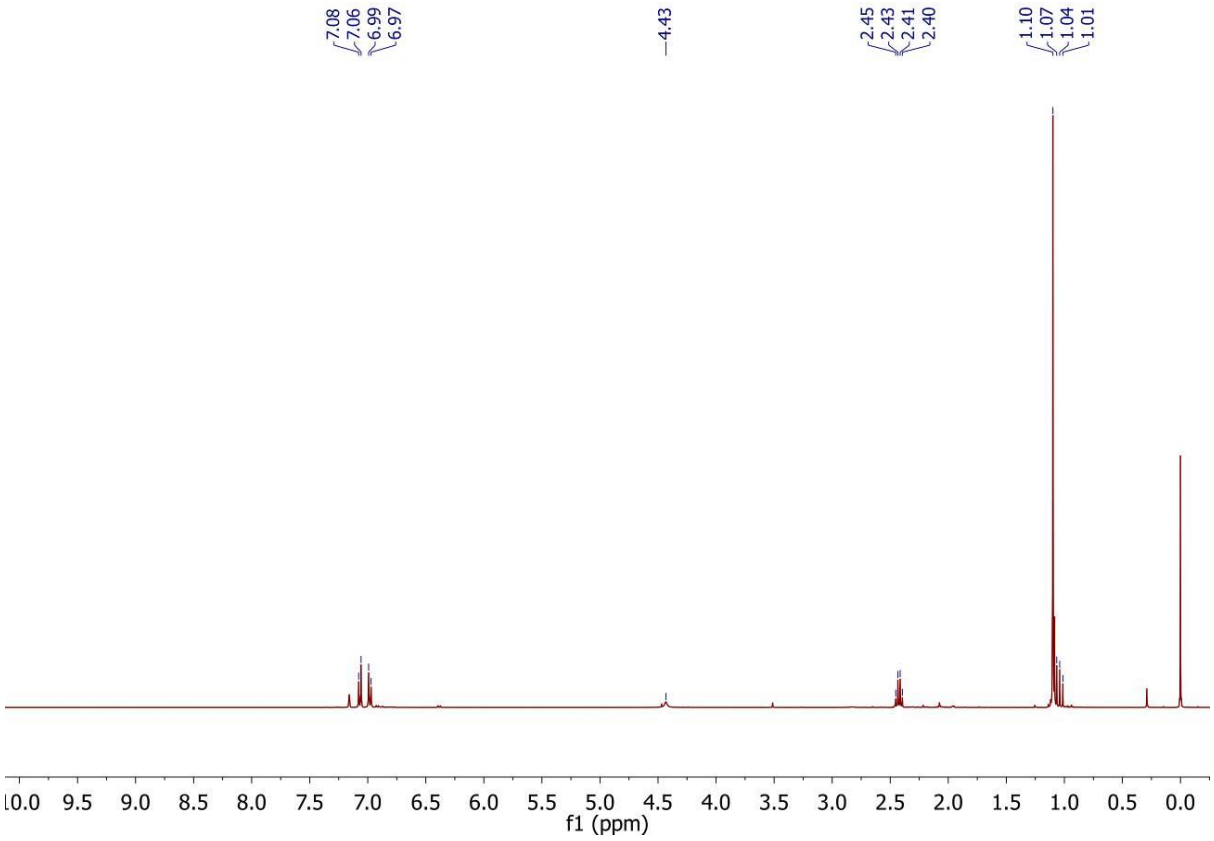

Figure AVII34. ^{13}C NMR, Table 1, Entry 7: 4-ethylaniline:HBPin.

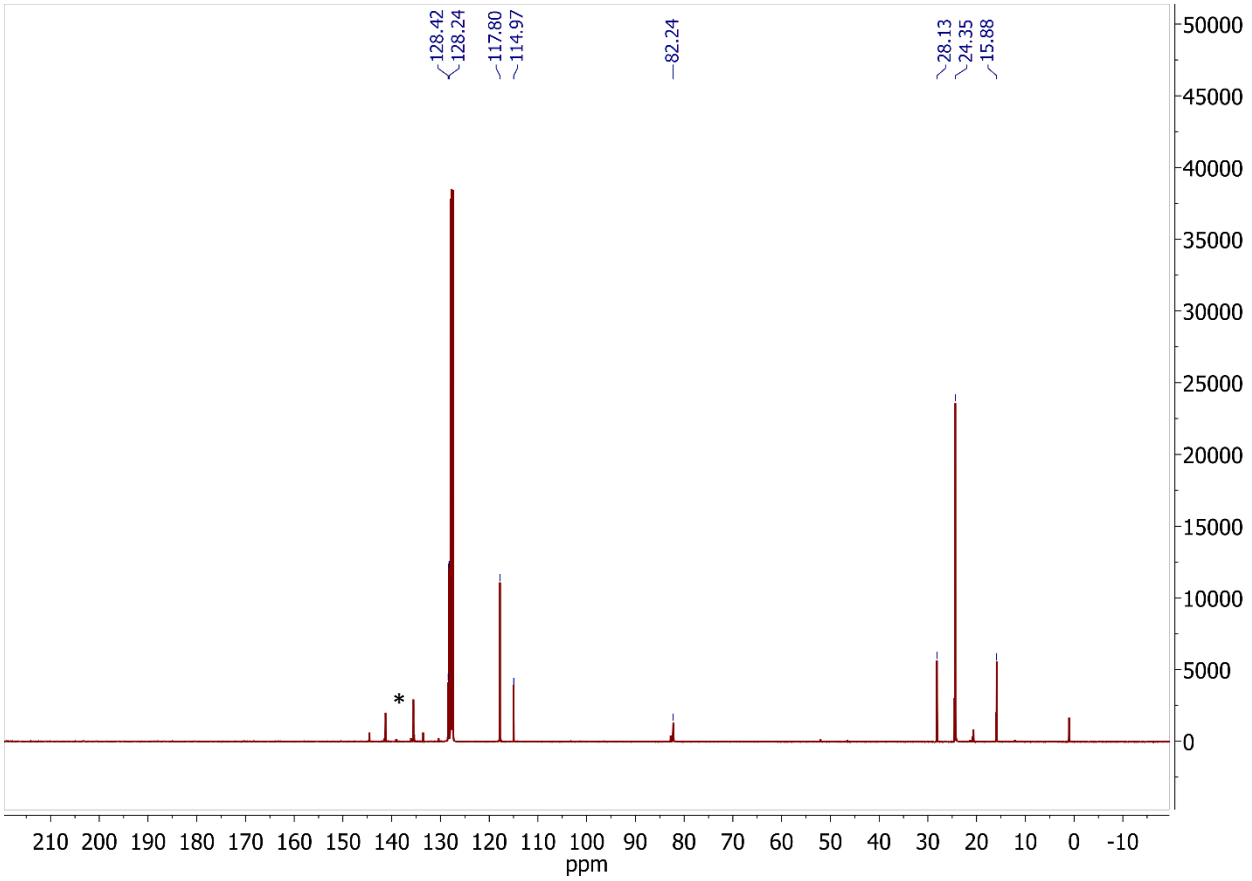

* Excess 4-ethylaniline

Figure AVII35. ^{11}B NMR, Table 1, Entry 7: 4-ethylaniline:HBPin.

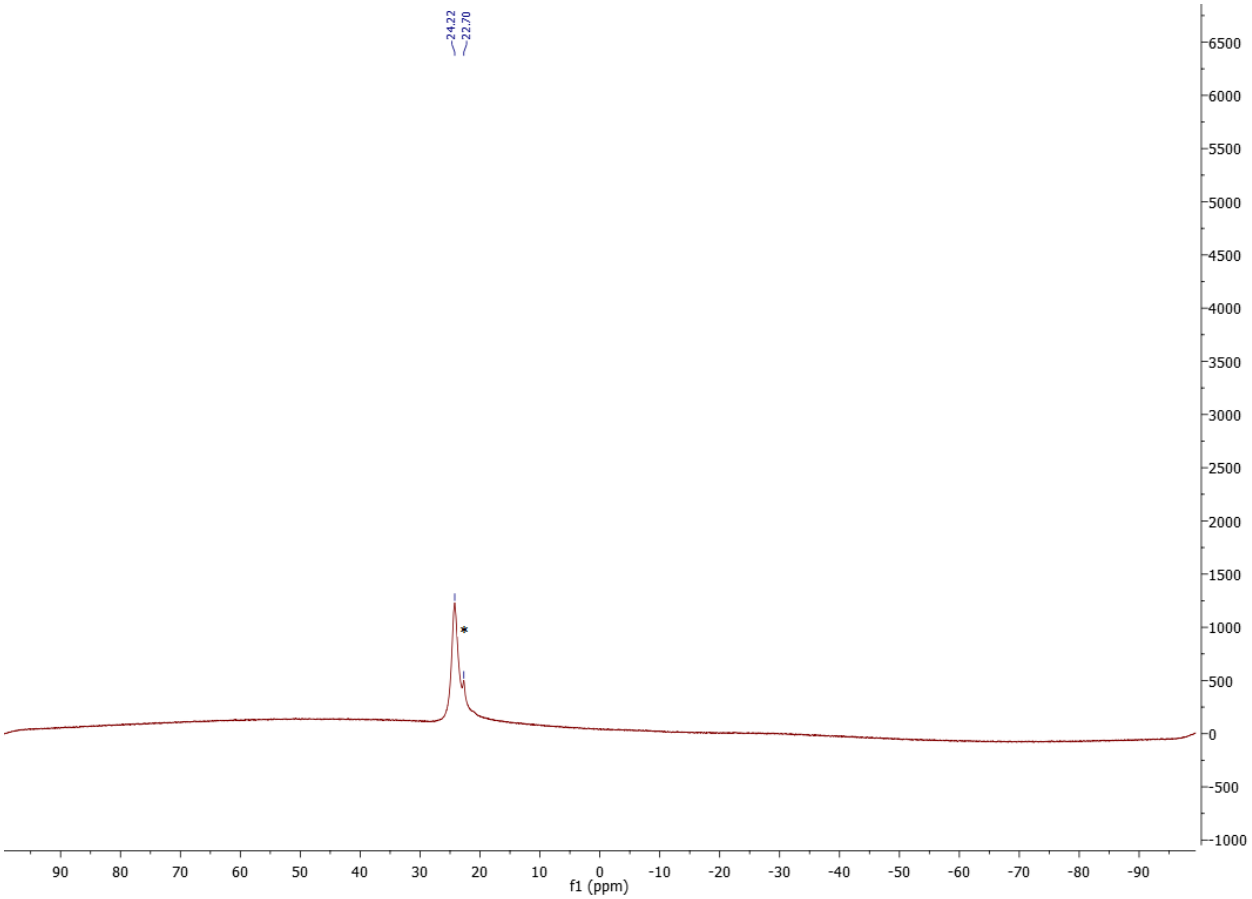

* PinBOBPin

Figure AVII36. ^{1}H NMR, Table 1, Entry 8: 2,6-diisopropylaniline:HBPin.

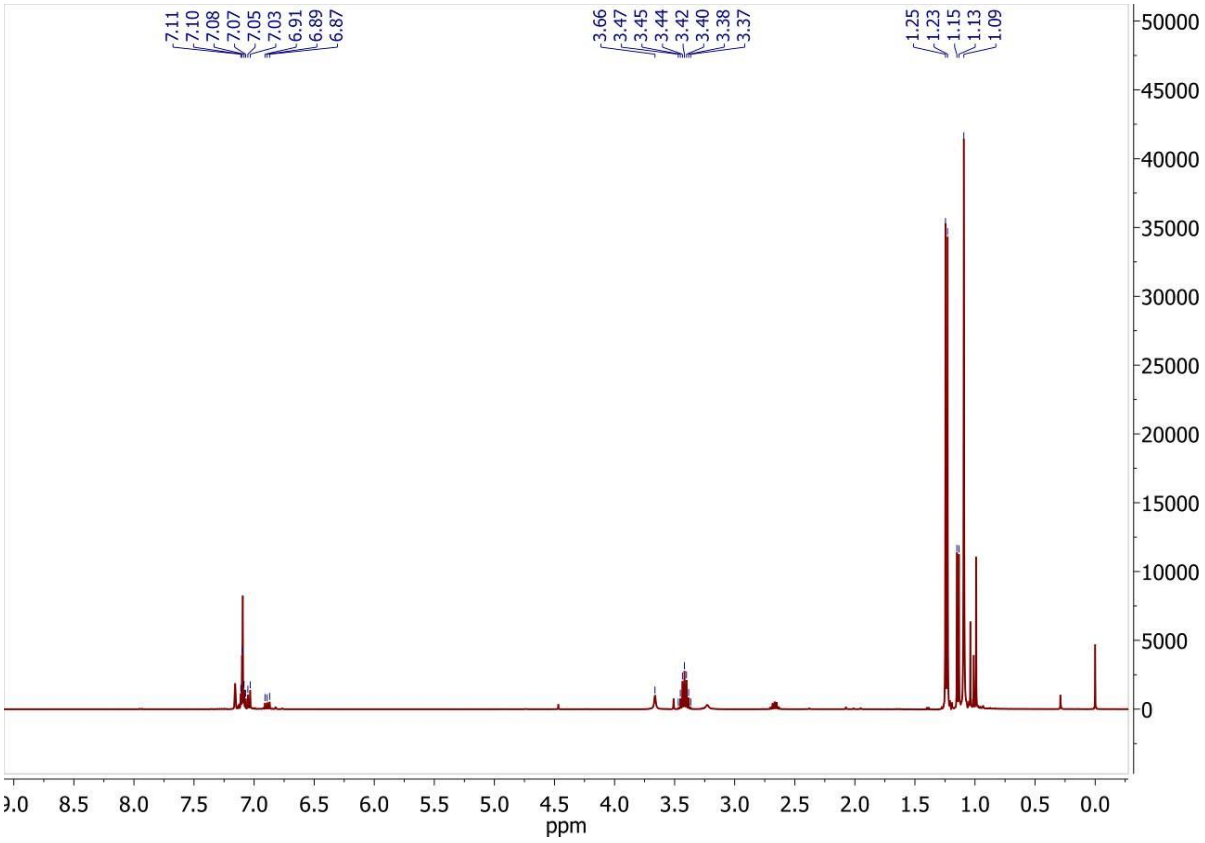

Figure AVII37. ^{11}B NMR, Table 1, Entry 8: 2,6-diisopropylaniline:HBPin.

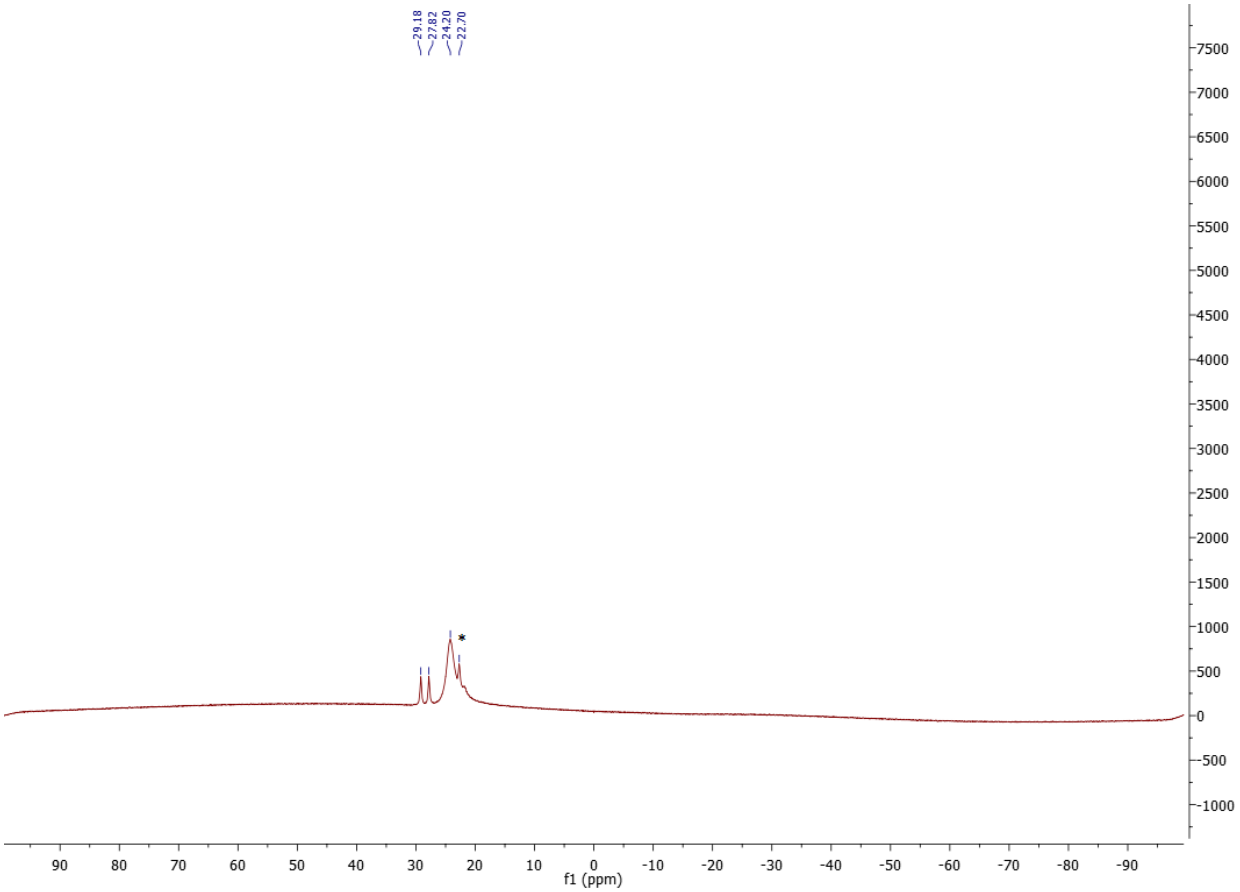

* PinBOBPin

Figure AVII38. ^{1}H NMR, Table 1, Entry 9: 3,5-dichloroaniline:HBPin.

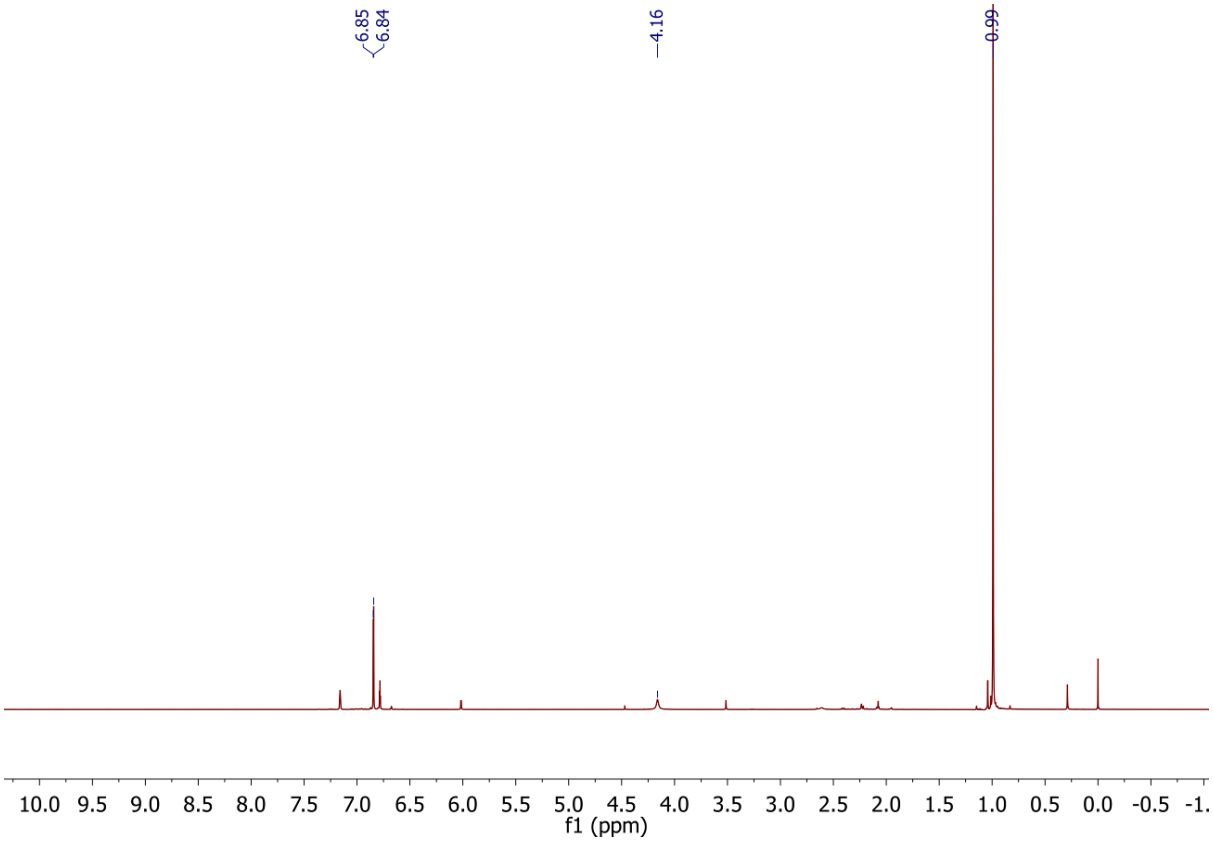

Figure AVII39. ^{13}C NMR, Table 1, Entry 9: 3,5-dichloroaniline:HBPin.

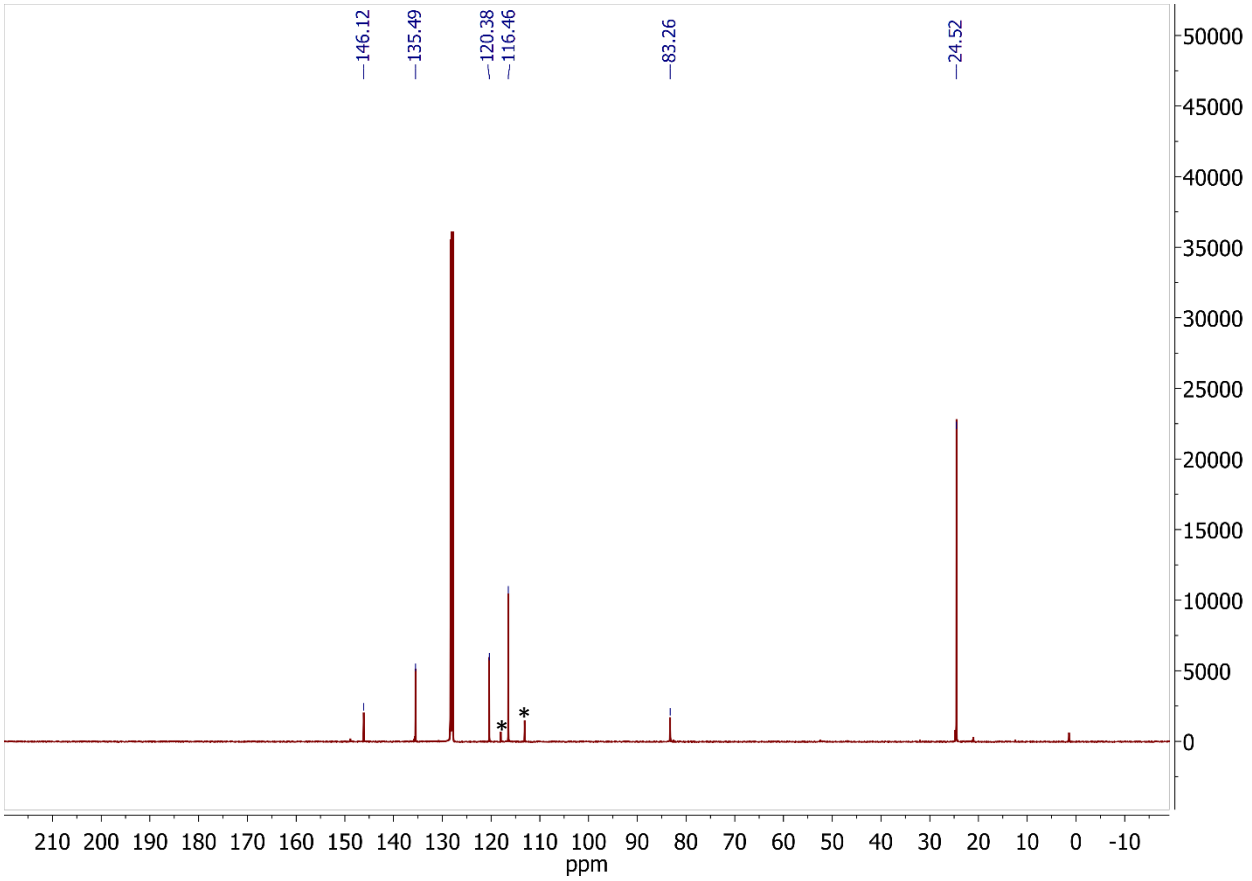

* Excess 3,5-dichloroaniline

Figure AVII40. ^{11}B NMR, Table 1, Entry 9: 3,5-dichloroaniline:HBPin.

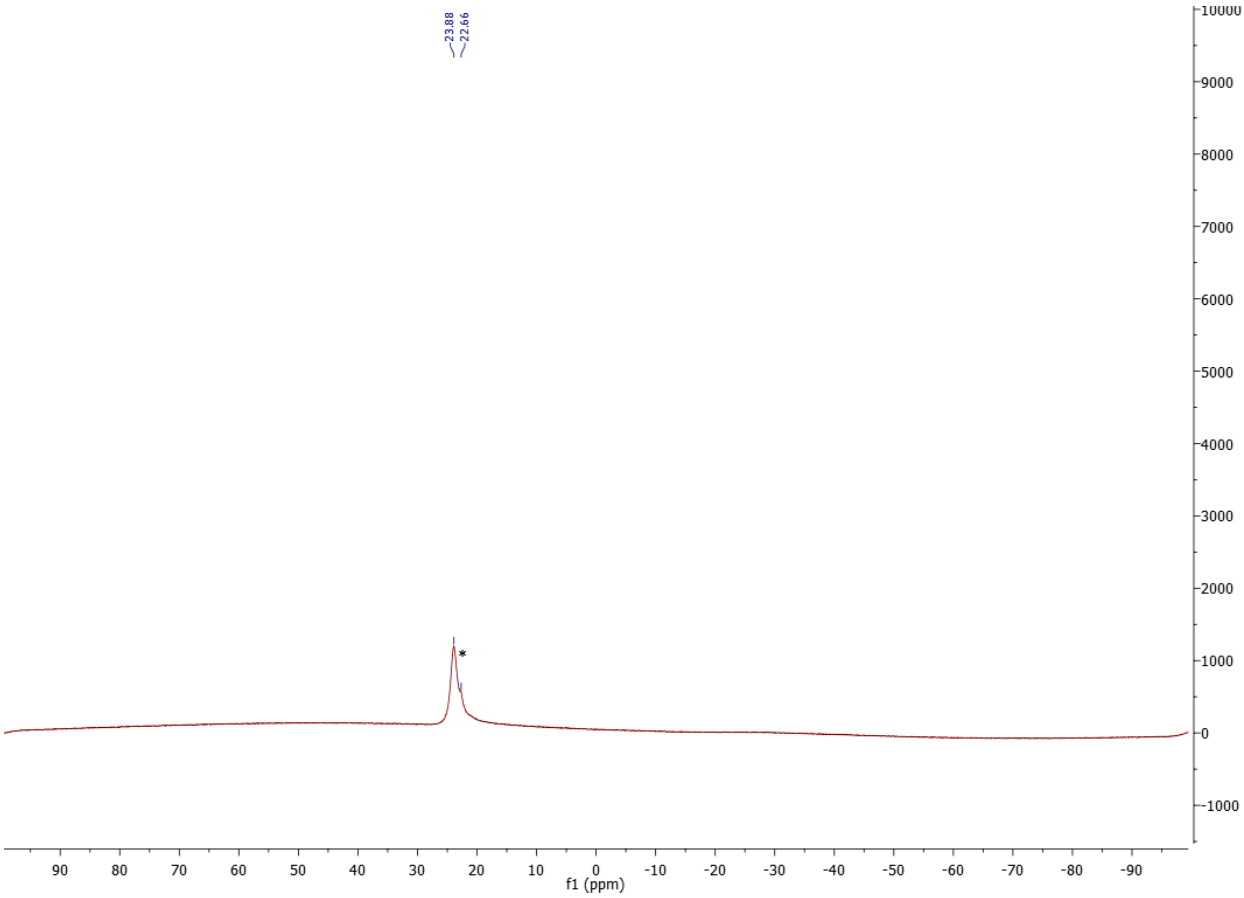

* PinBOBPin

Figure AVII41. ^{1}H NMR, Table 1, Entry 10: Et_2NH:HBPin.

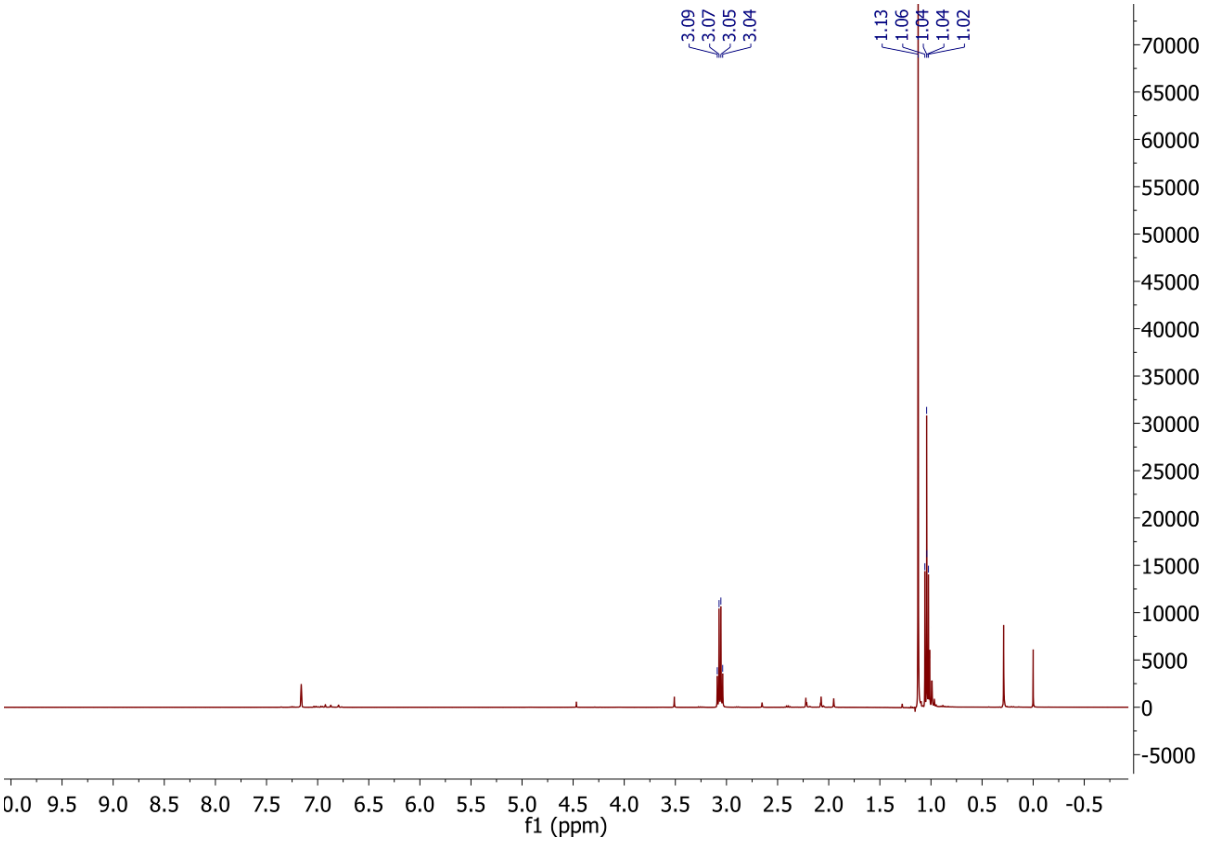

Figure AVII42. ^{11}B NMR, Table 1, Entry 10: Et_2NH:HBPin.

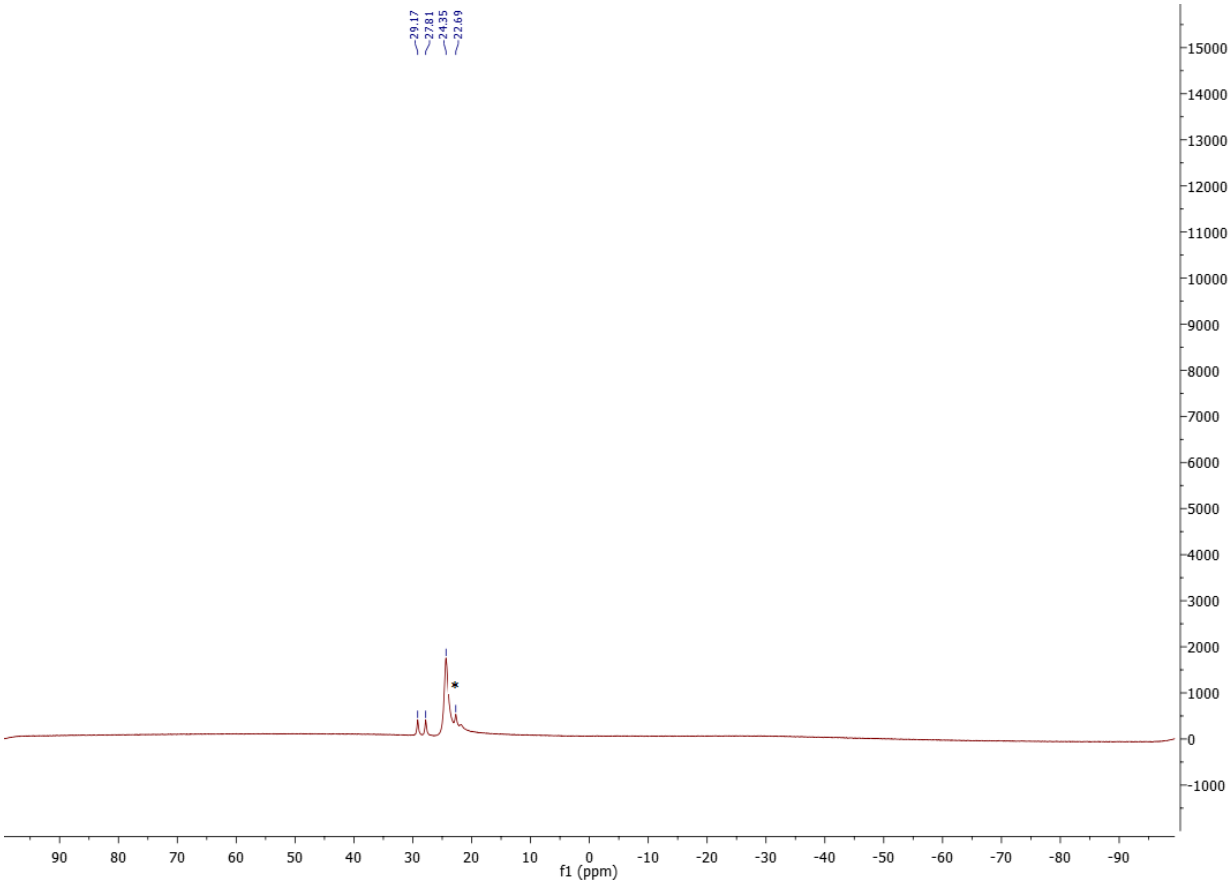

* PinBOBPin

Figure AVII43. ^{1}H NMR, Table 1, Entry 11: *i*Pr$_2$NH:HBPin.

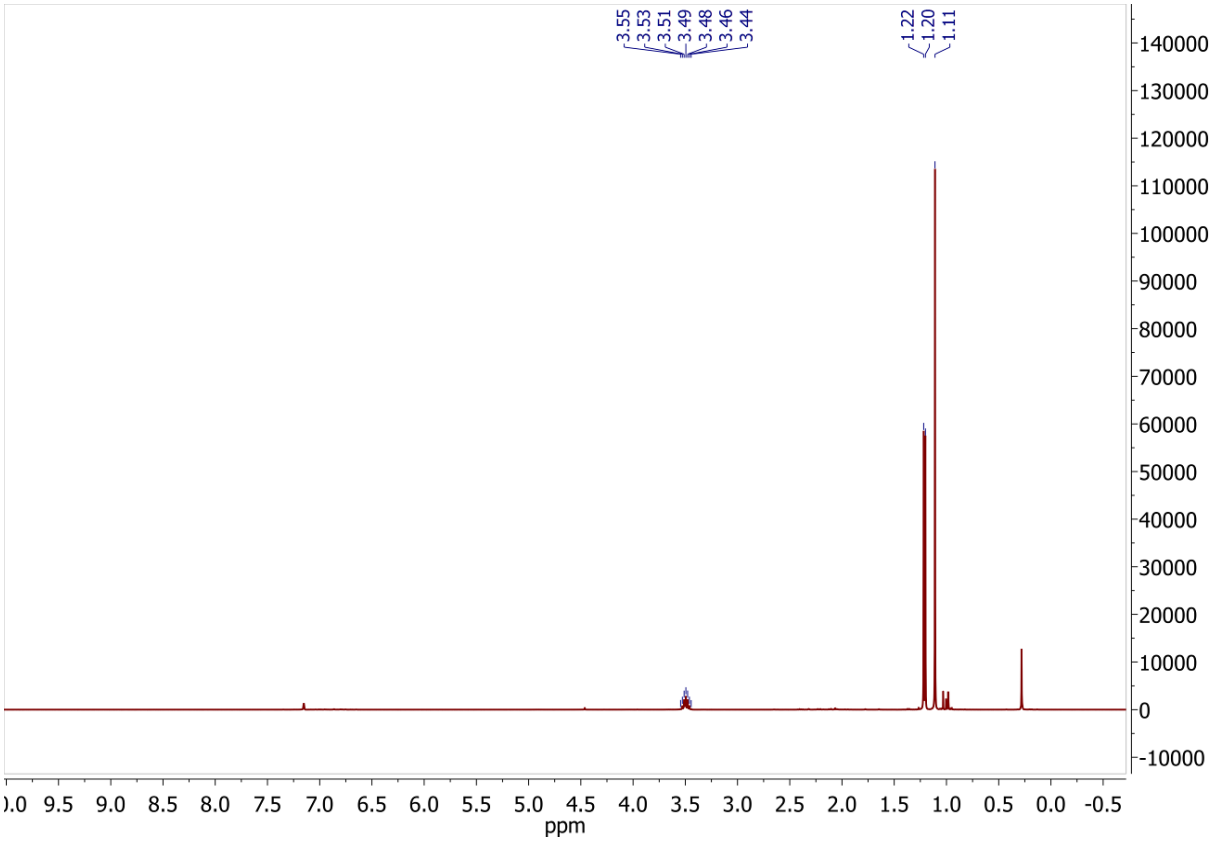

Figure AVII44. ^{11}B NMR, Table 1, Entry 11: *i*Pr_2NH:HBPin.

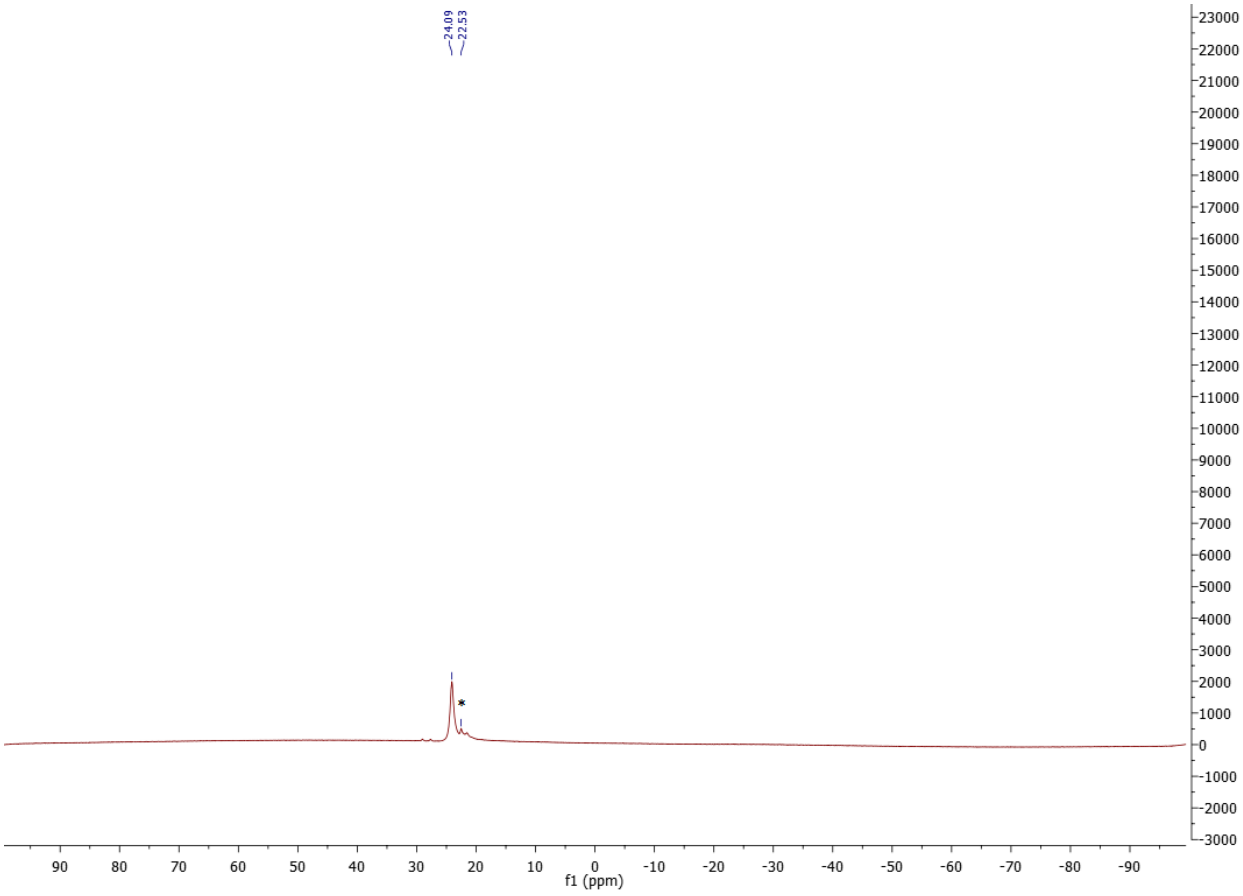

* PinBOBPin

Figure AVII45. ^{1}H NMR, Table 1, Entry 12: Cy_2NH:HBPin.

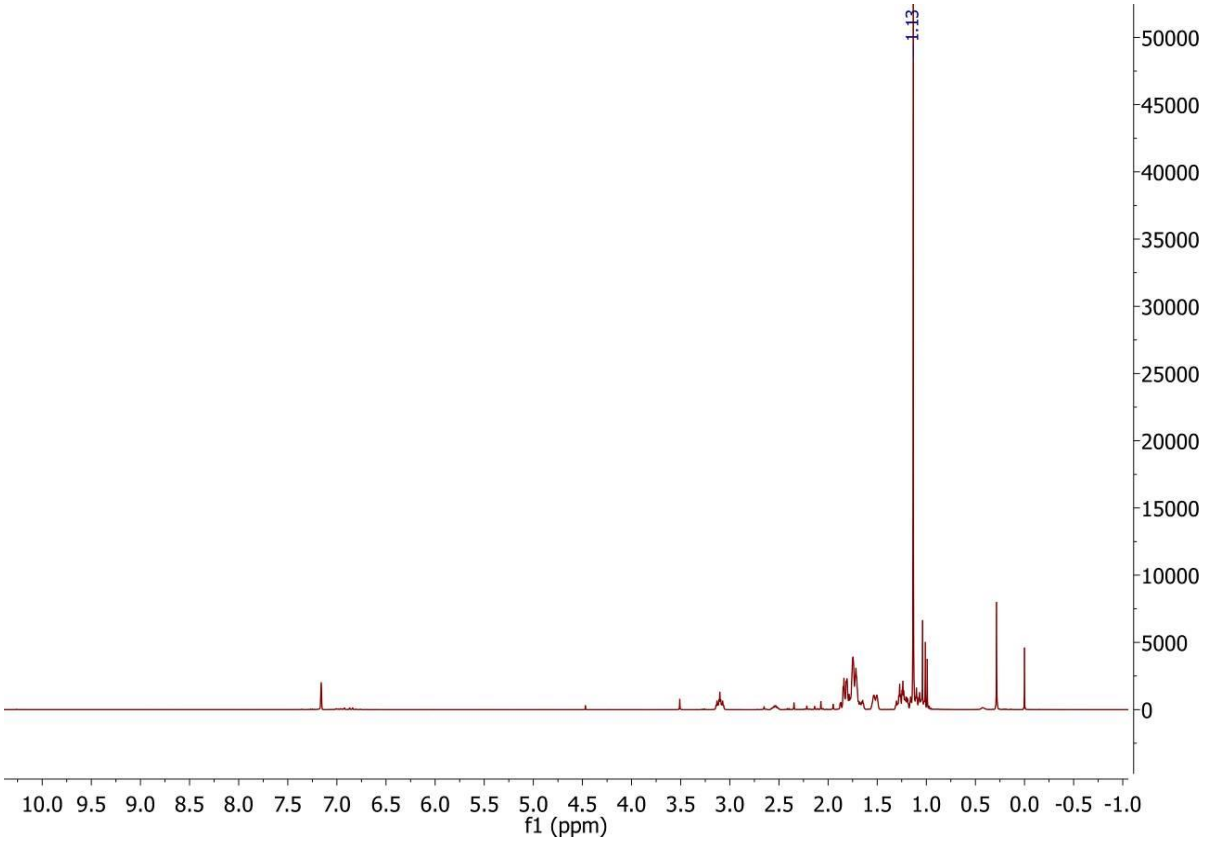

Figure AVII46. ^{11}B NMR, Table 1, Entry 12: Cy_2NH:HBPin.

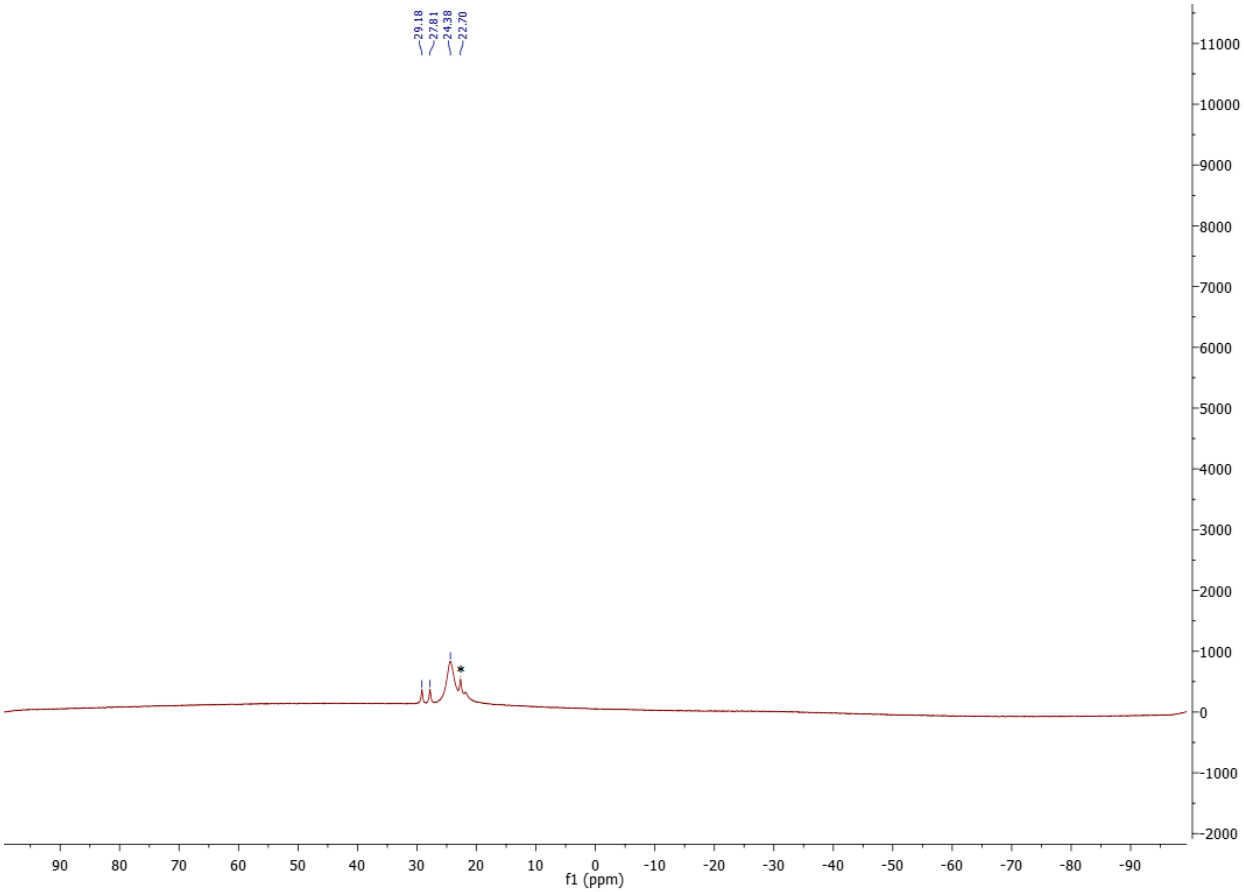

* PinBOBPin

Figure AVII47. ^{1}H NMR, Table 1, Entry 13: Ph_2NH:HBPin.

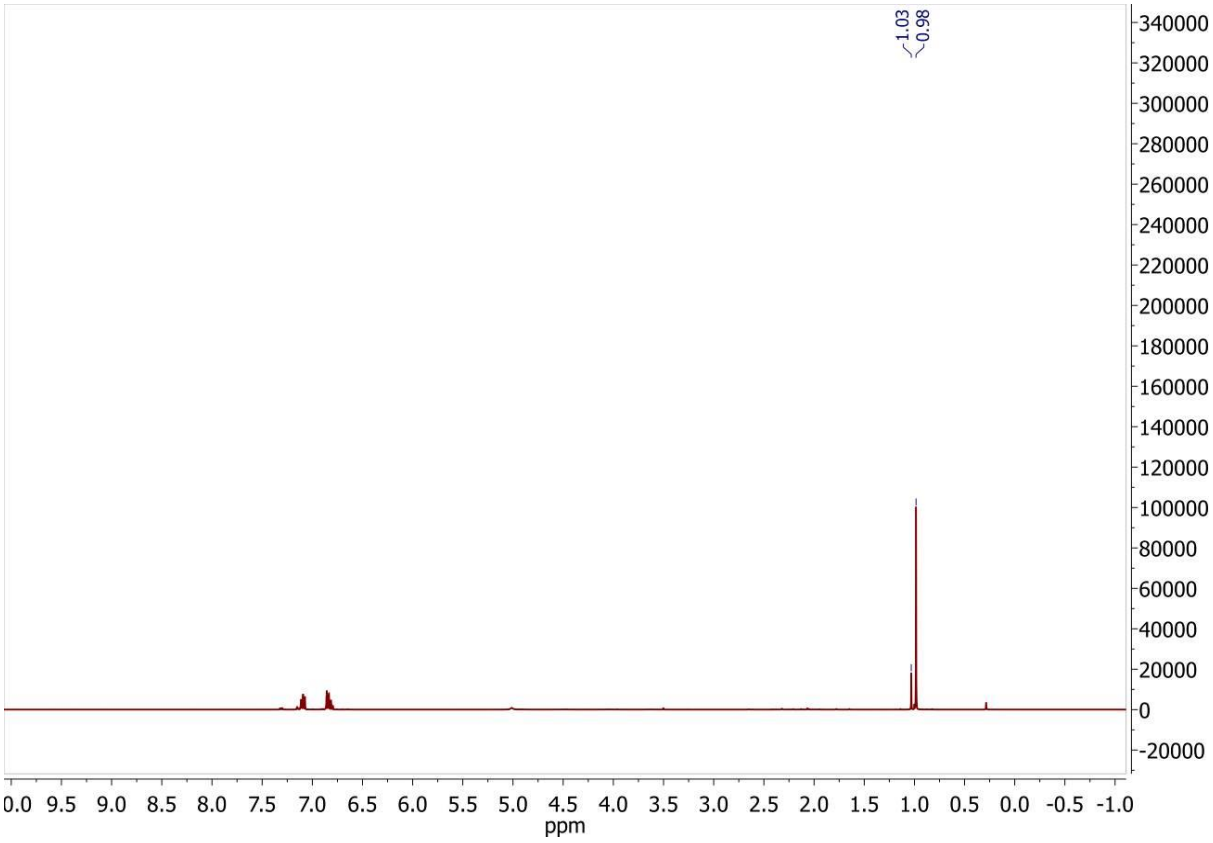

Figure AVII48. ^{11}B NMR, Table 1, Entry 13: Ph_2NH:HBPin.

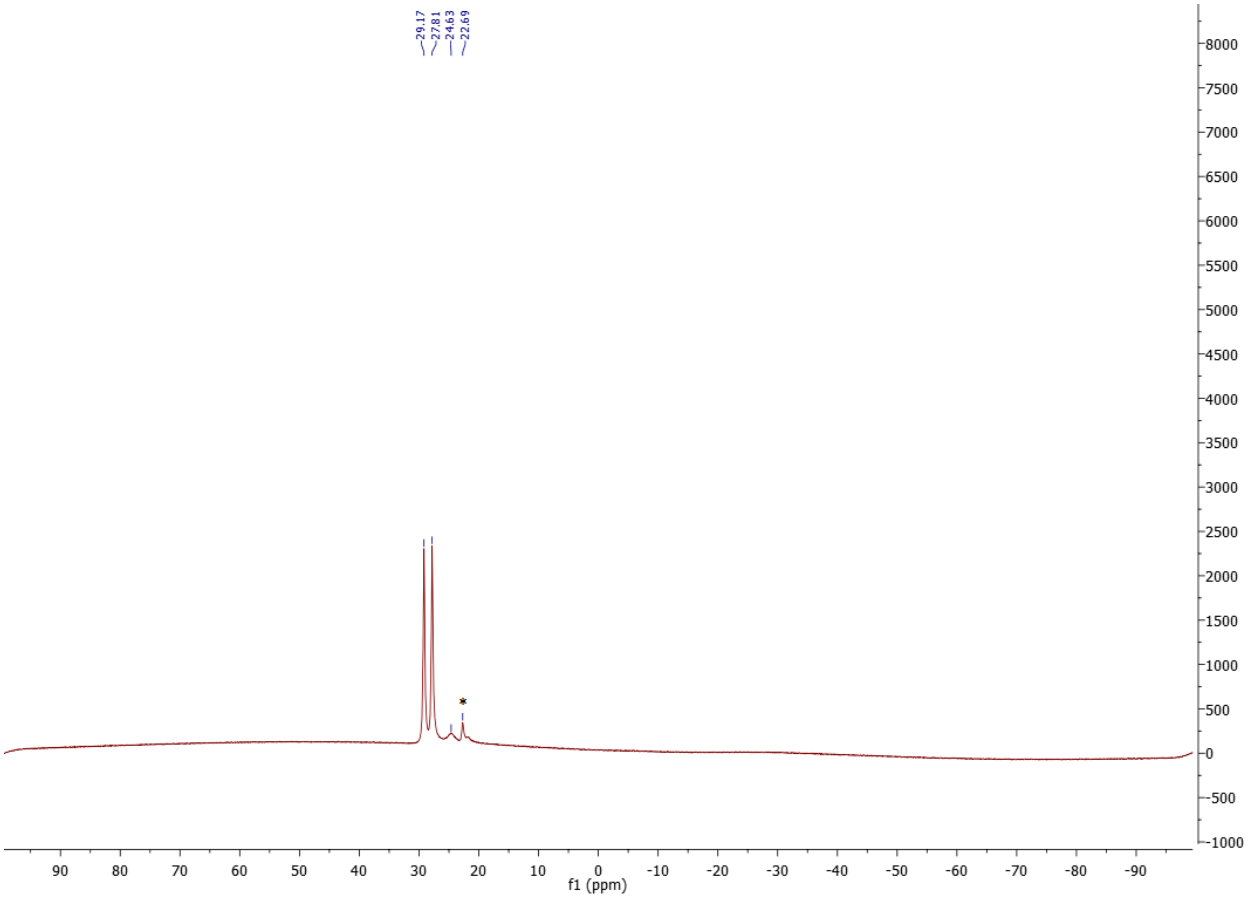

* PinBOBPin

Figure AVII49. ^{1}H NMR, Table 1, Entry 15: NH_3:HBPin. Excess NH_3.

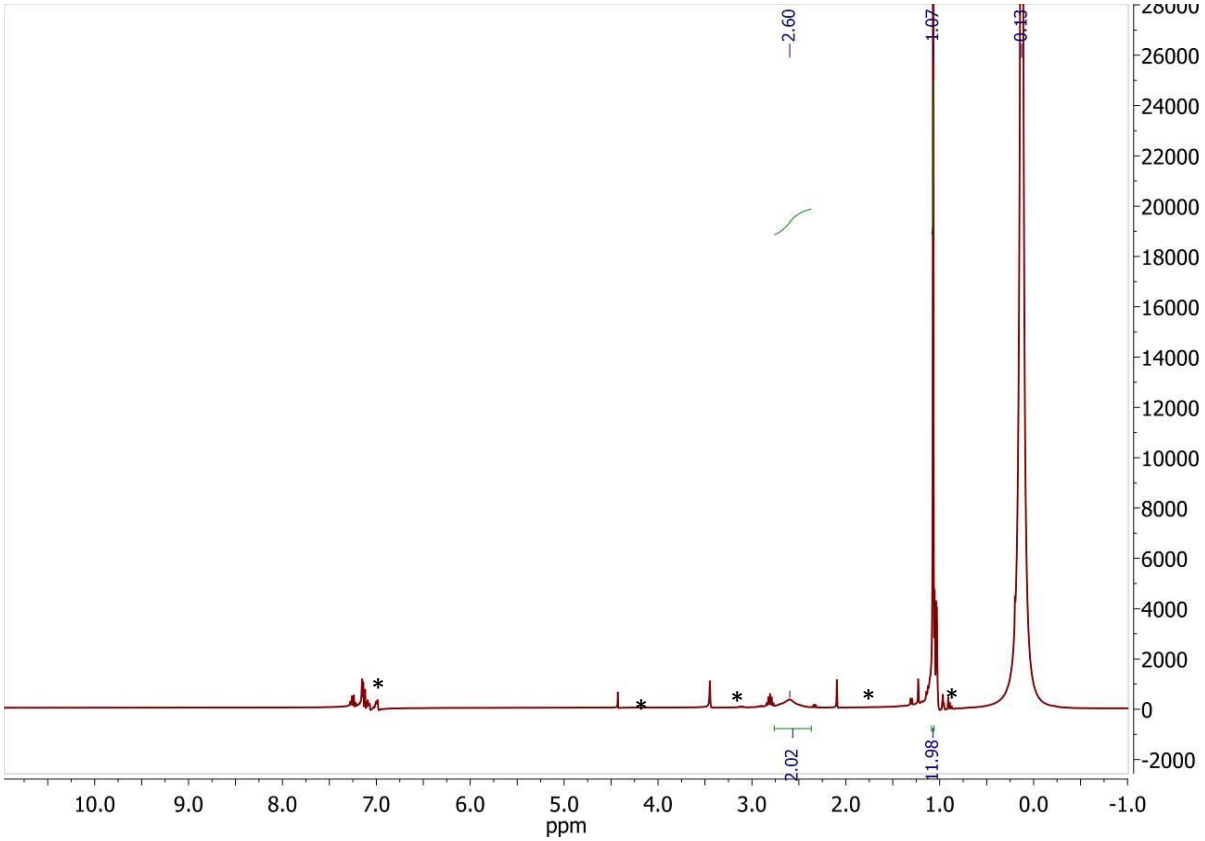

* $\{JSnH\}_4$

Figure AVII50. ^{13}C NMR, Table 1, Entry 15: NH_3:HBPin.

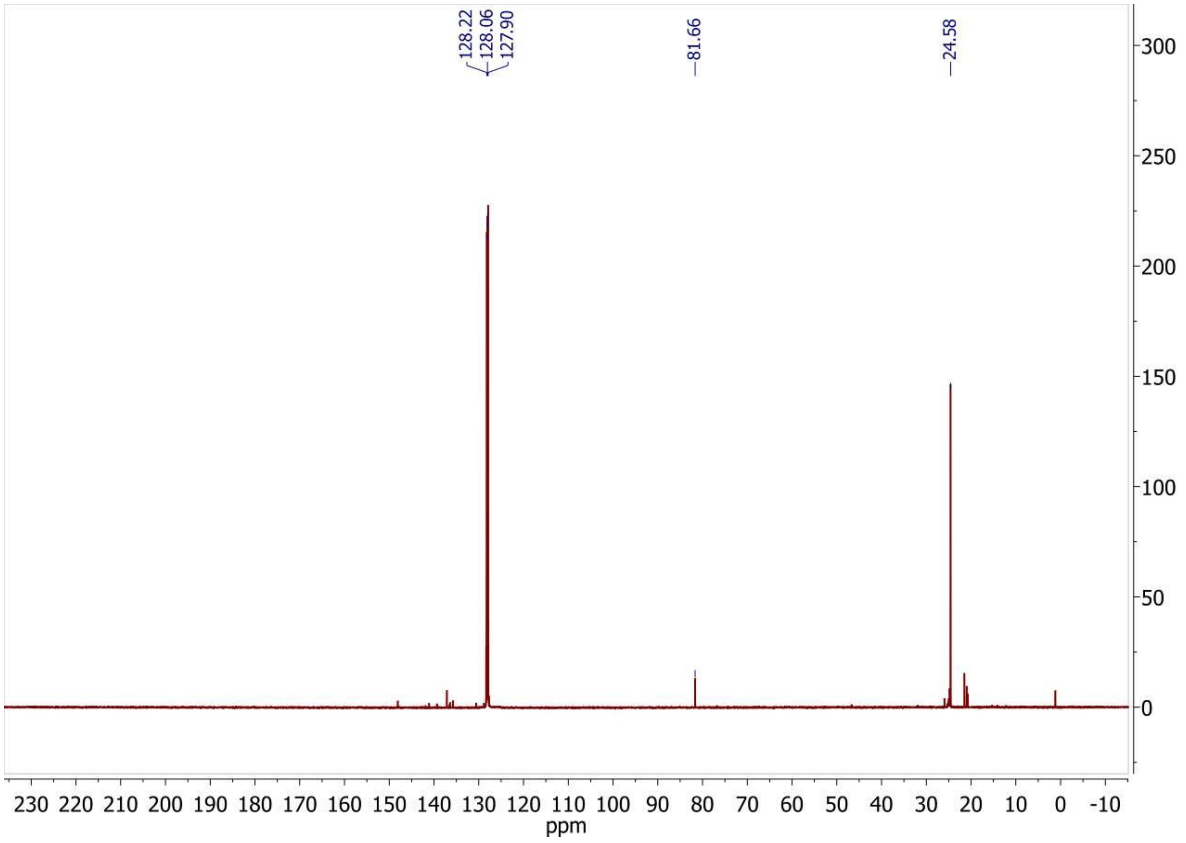

Figure AVII51. ^{11}B NMR, Table 1, Entry 15: NH_3:HBPin.

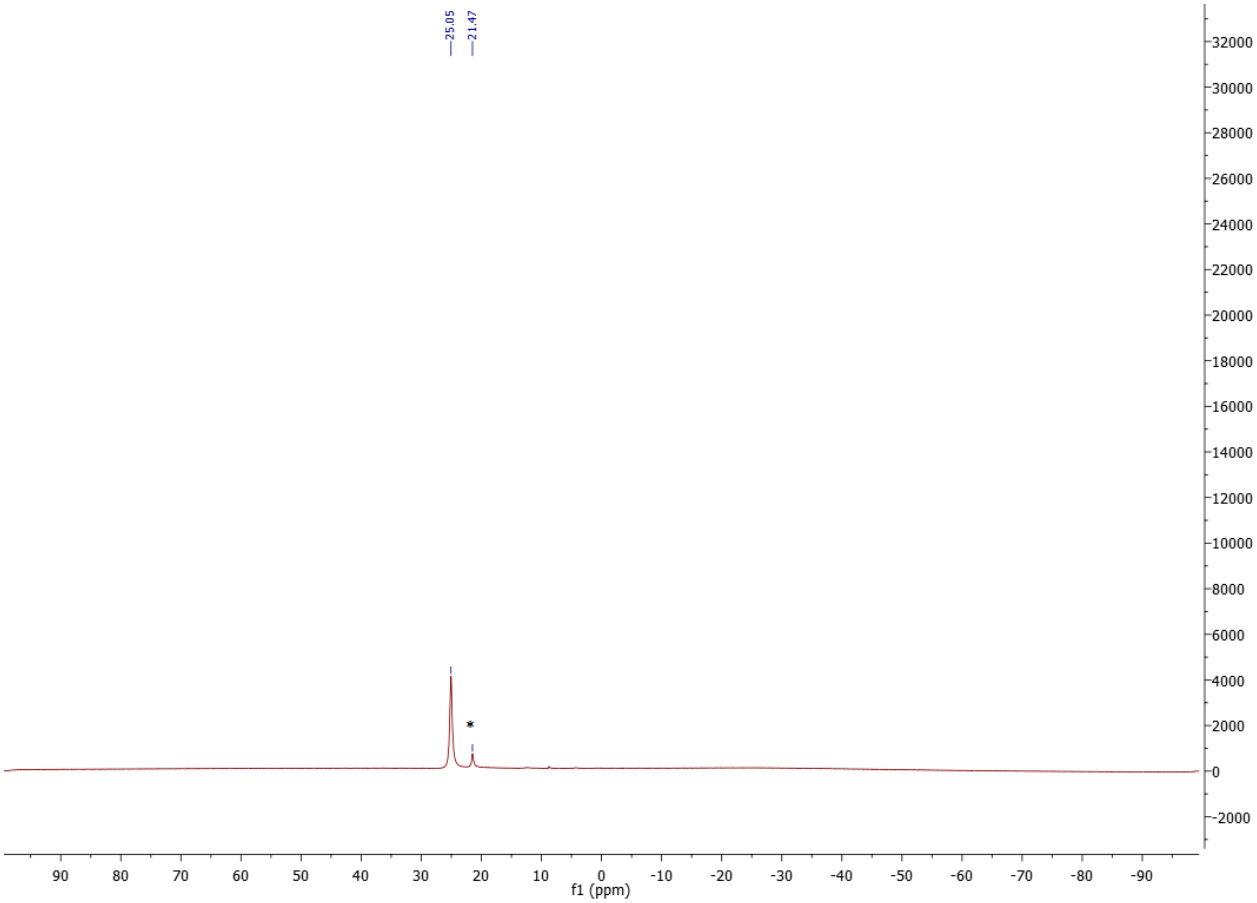

* PinBOBPin

Figure AVII52. ^{1}H NMR, Table 1, Entry 16: PinNH_2:HBPin. Excess HBPin.

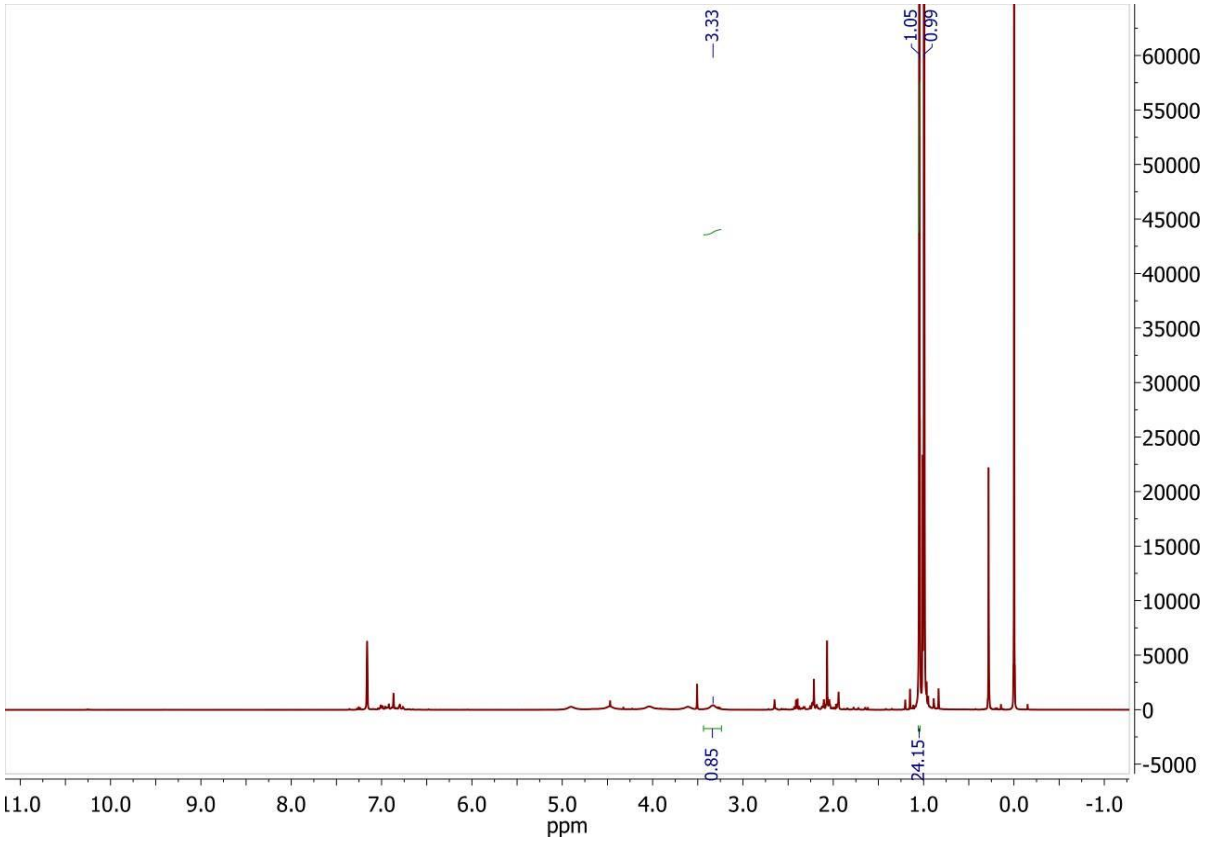

Figure AVII53. ^{11}B NMR, Table 1, Entry 16: PinNH_2:HBPin. Excess HBPin.

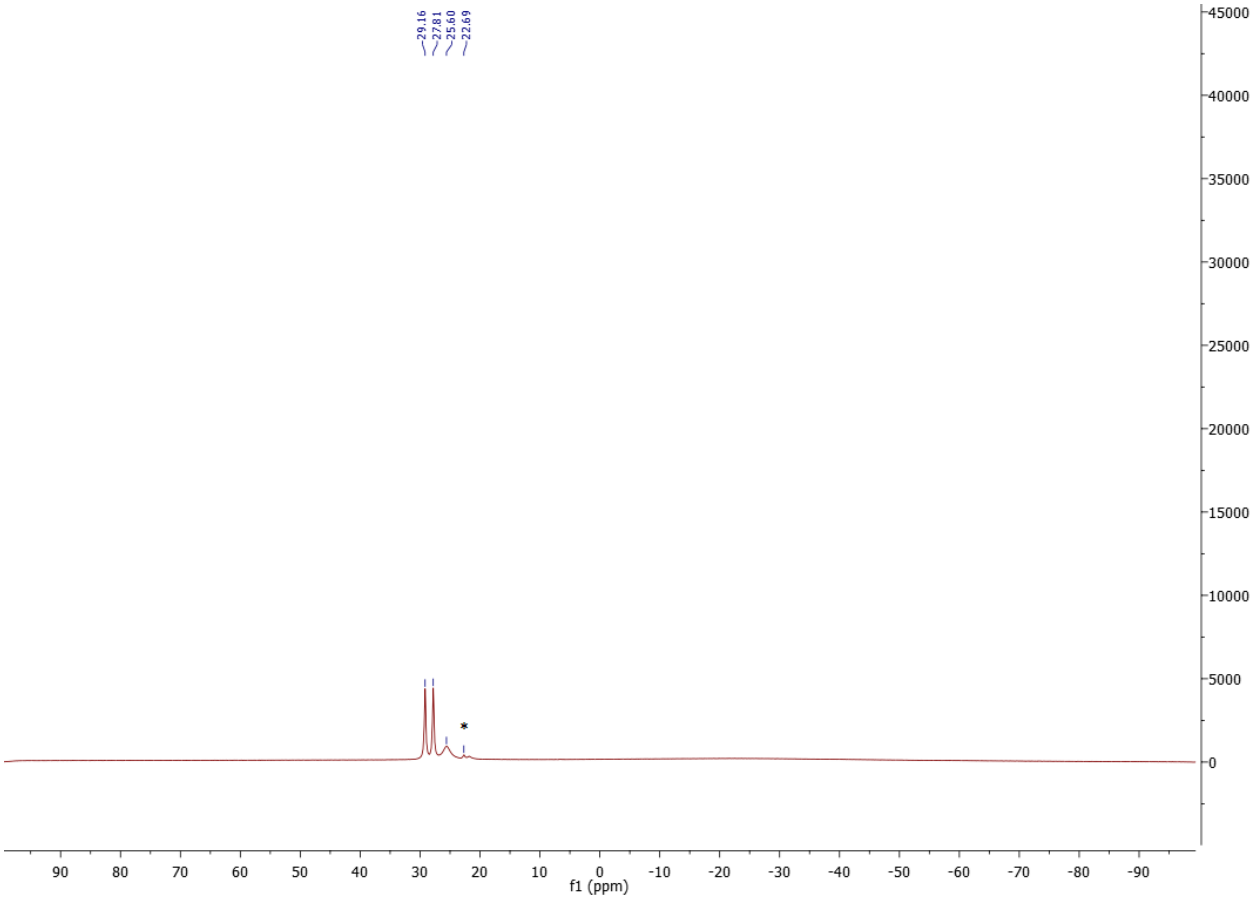

* PinBOBPin

Figure AVII54. ^{13}C NMR, Table 1, Entry 16: PinNH_2:HBPin.

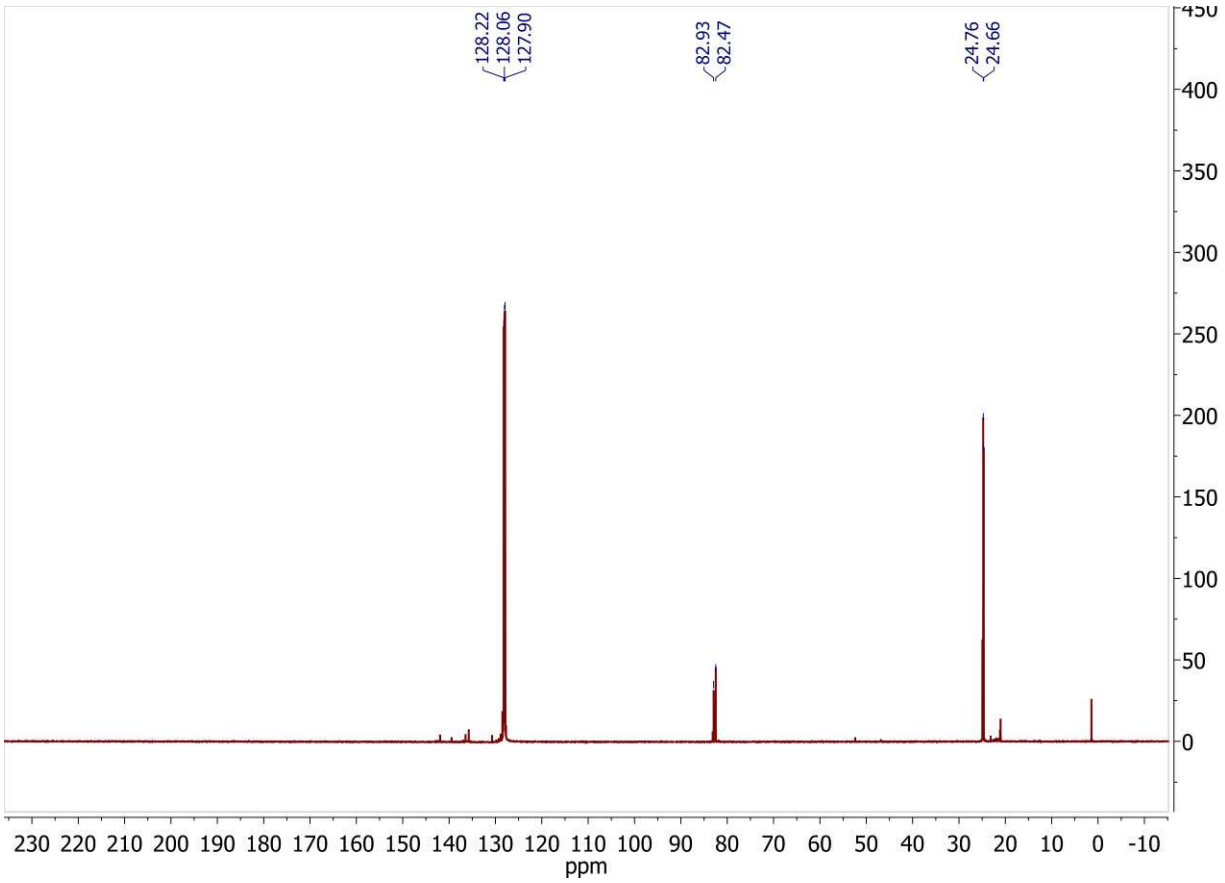

Appendix VIII

Supporting Information for Chapter 9: N-N Double Bond Cleavage and Azobenzene Rearrangement with C-C Bond Formation Induced by a Germylene

Figure AVIII1. ^{1}H NMR Spectrum of **1a** (400 MHz, C_6D_6, 298K)

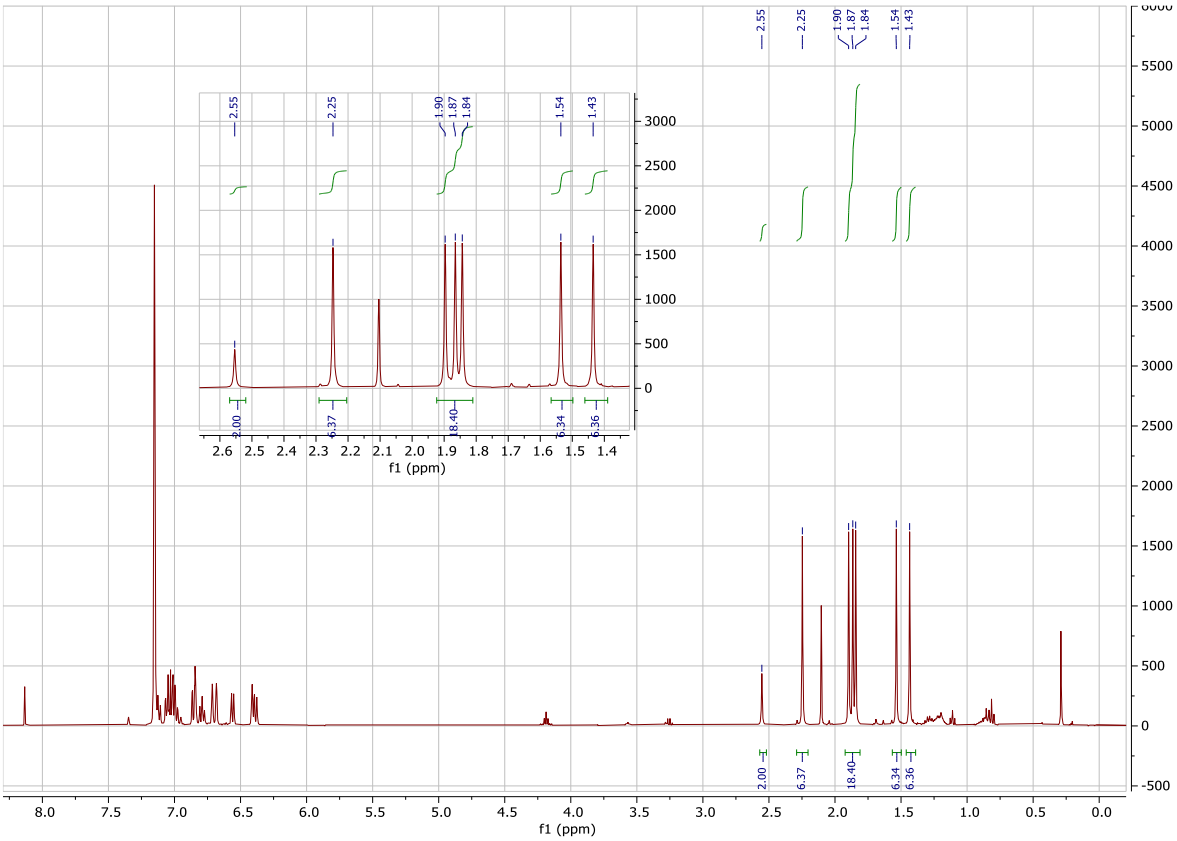

*2.1ppm residual toluene from single crystal.

Figure AVIII2. $^{13}C\{^{1}H\}$ NMR Spectrum of **1b** (126 MHz, C_6D_6, 298K)

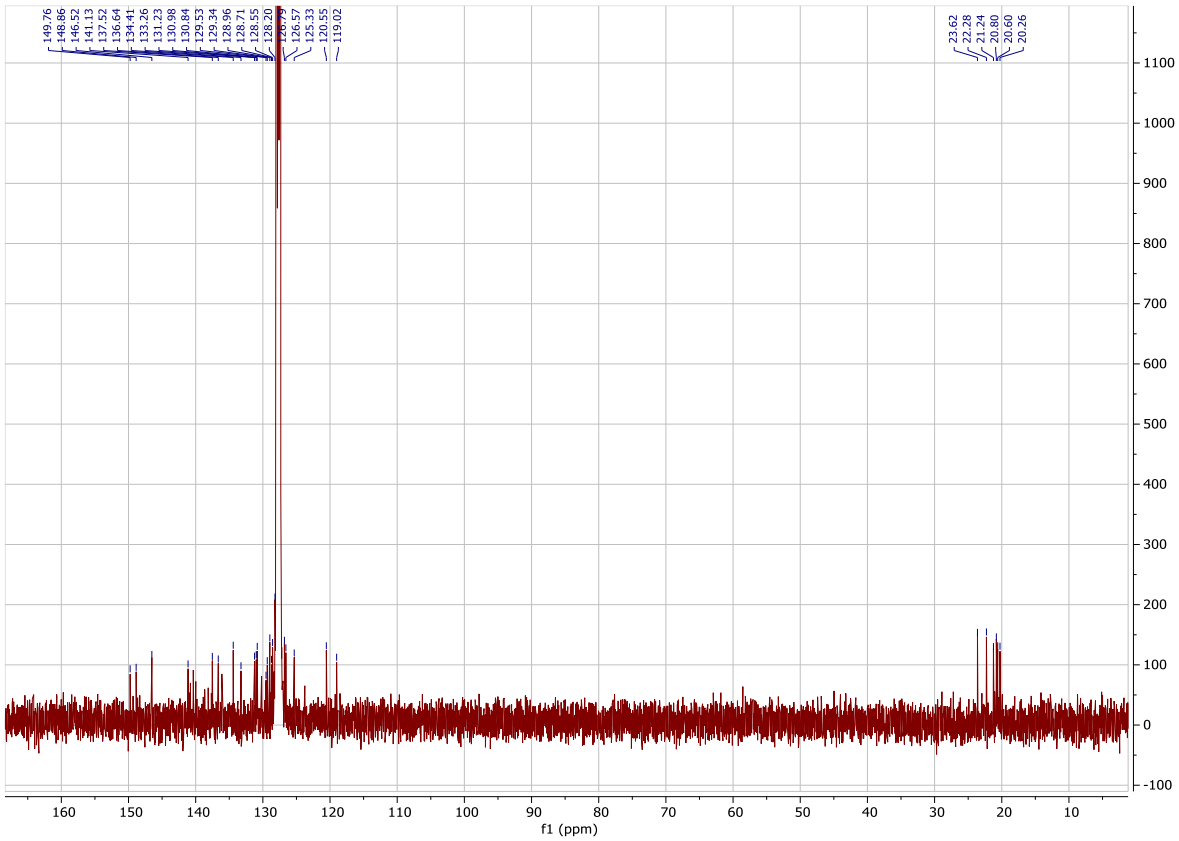

Figure AVIII3. ^{1}H NMR Spectrum of **1b** (400 MHz, C_6D_6, 298K)

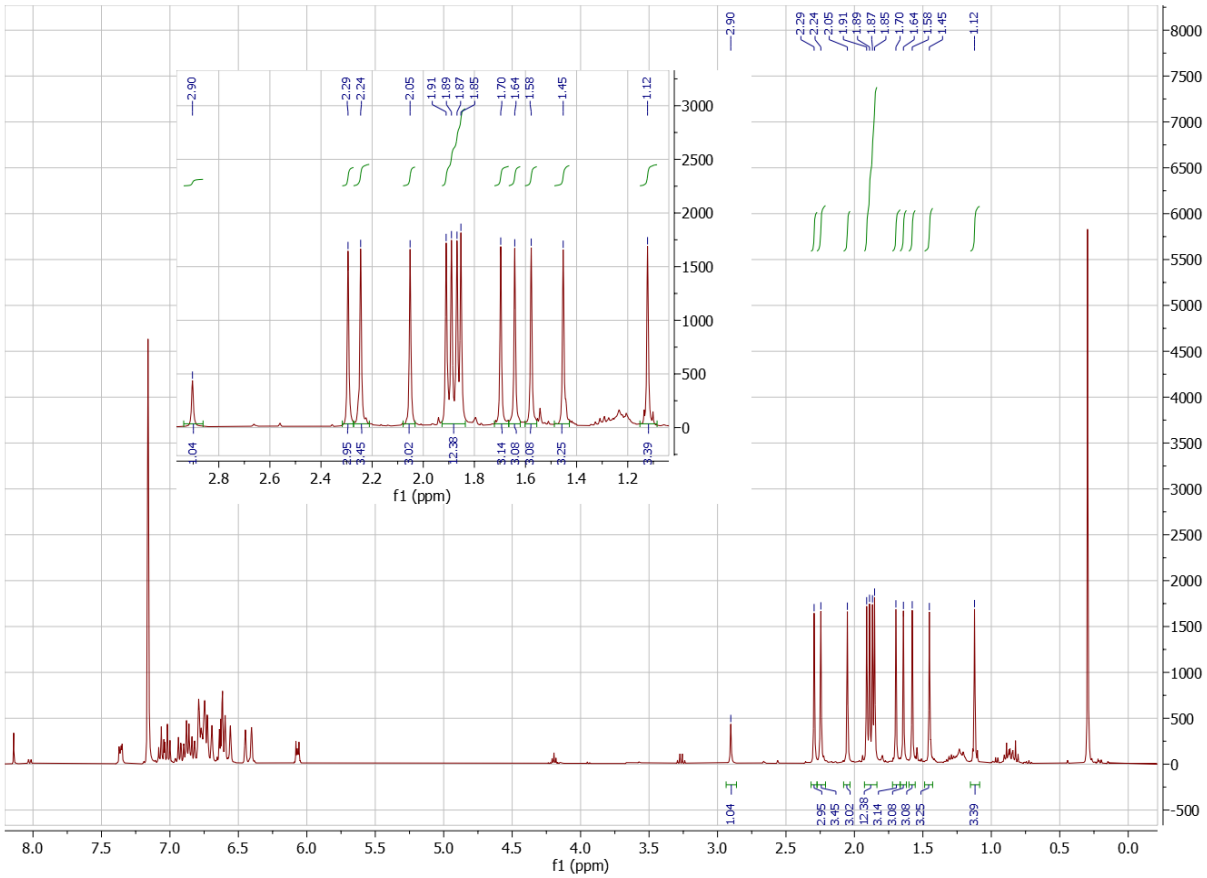

Figure AVIII4. $^{13}C\{^{1}H\}$ NMR Spectrum of **1b** (126 MHz, C_6D_6, 298K)

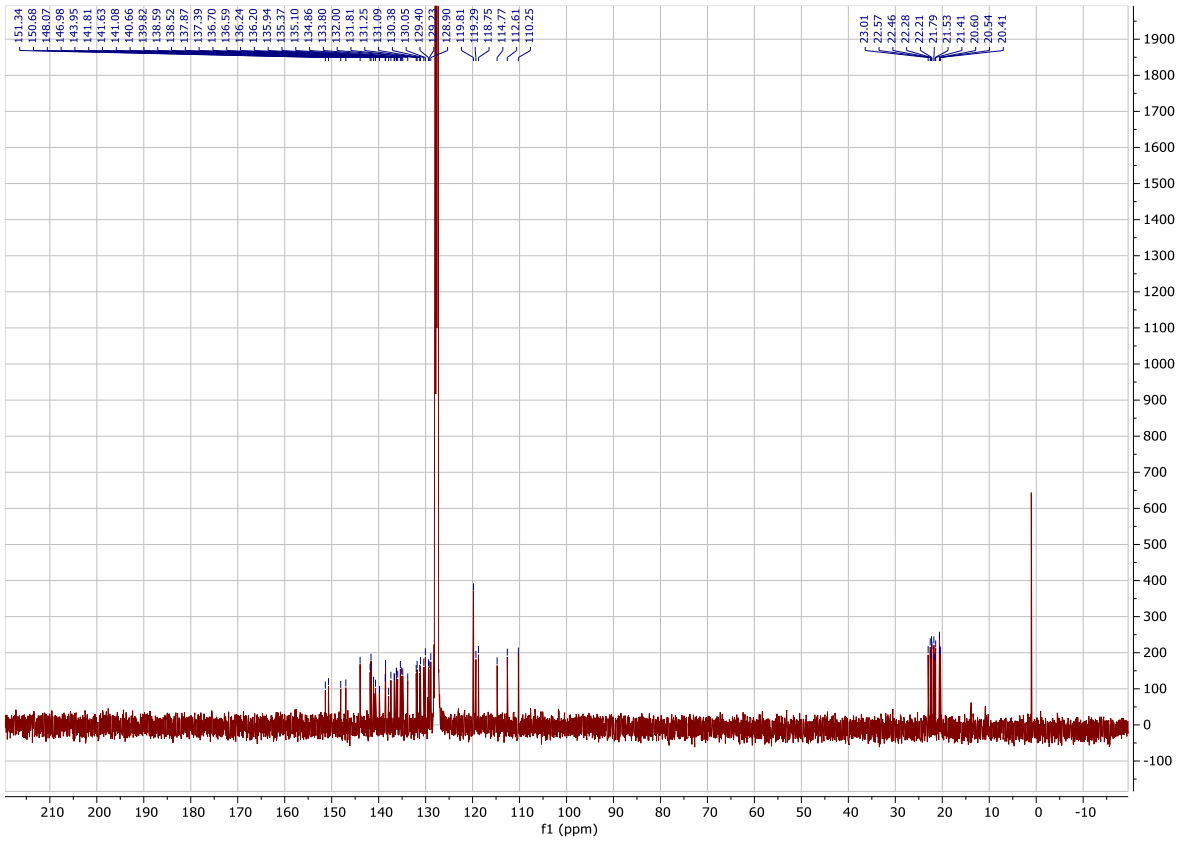

Figure AVIII5 ^{1}H NMR Spectrum of the Reaction of $Ge(Ar^{Me6})_2$ with Azobenzene (400 MHz, C_6D_6, 298K)

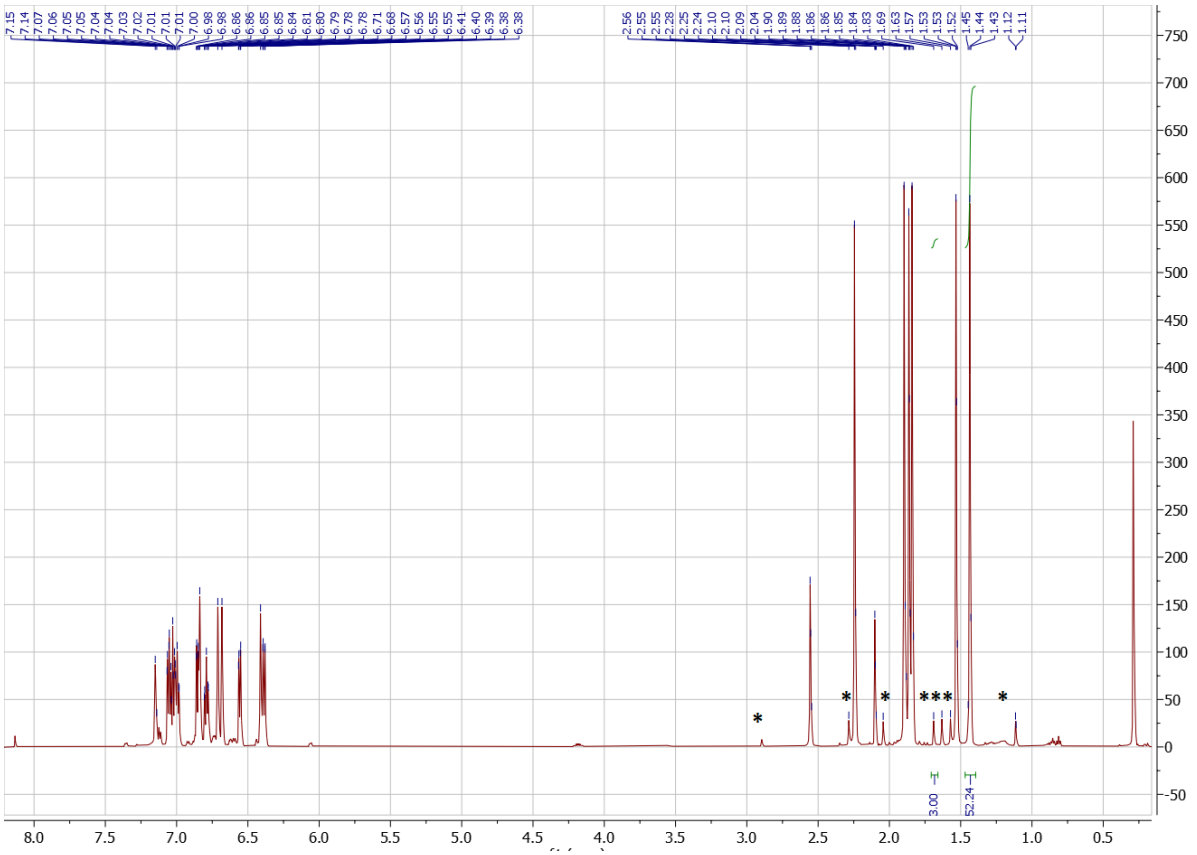

*= **1b**

1a:1b has a ratio of 8:1

Figure AVIII6. ^{1}H NMR Spectrum of a product of the decomposition of $Ge(Ar^{Me6})_2$ (400 MHz, C_6D_6, 298K)

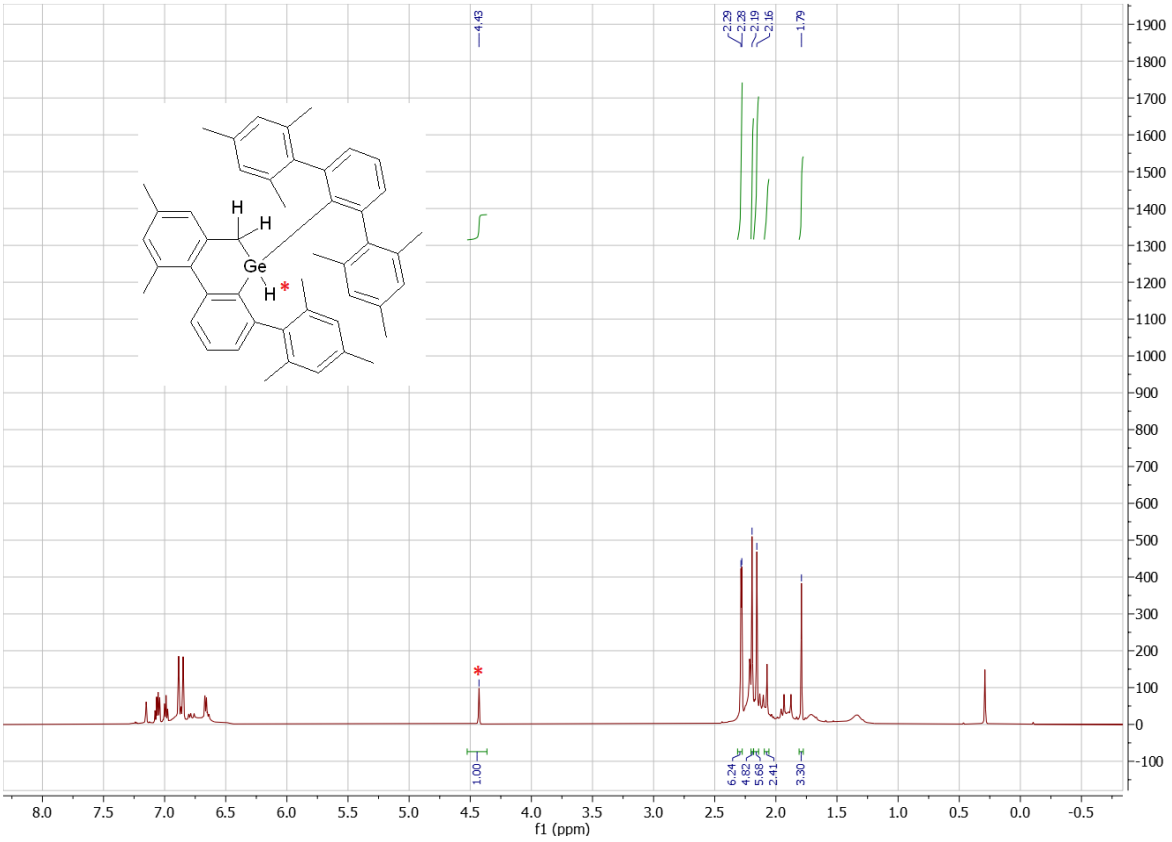

Figure AVIII7. Illustration of the structure of **1a** and **1b** co-crystallized with ether.

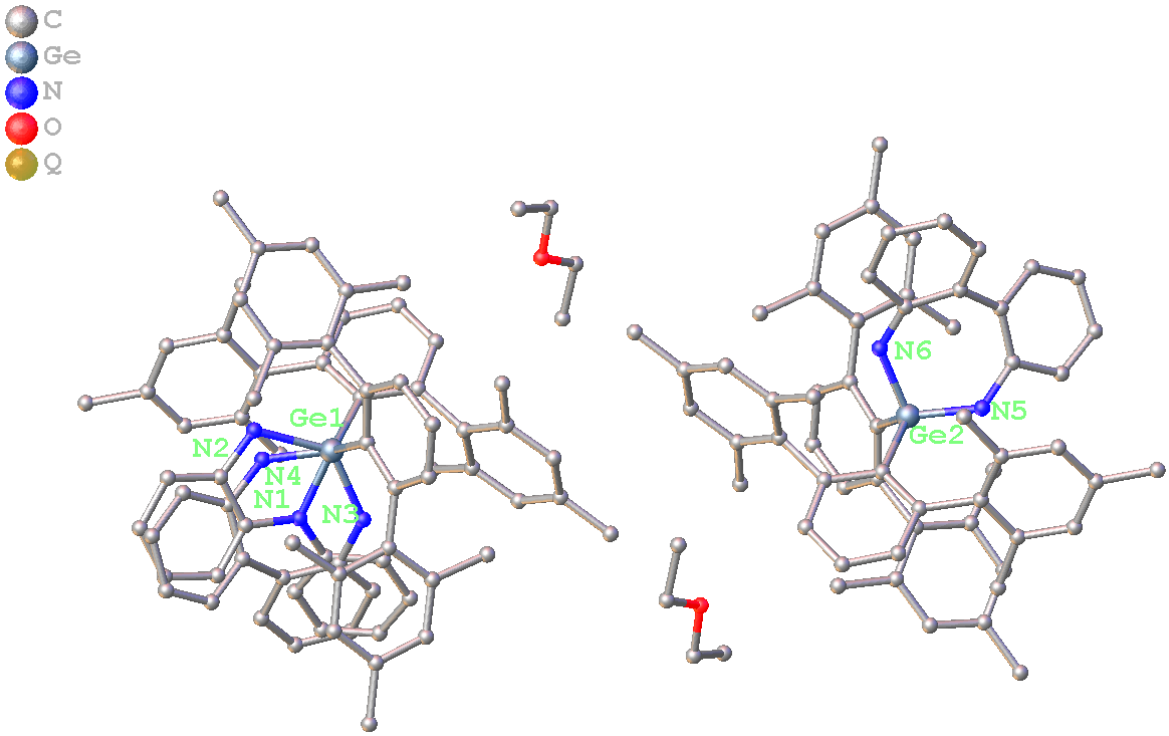

The molecule appears to be in the space group P1 because only one of the molecules is disordered with two different ligands and is also racemically twinned about 10% of the time.

Figure AVIII8. Illustration of product of the decomposition of $Ge(Ar^{Me6})_2$

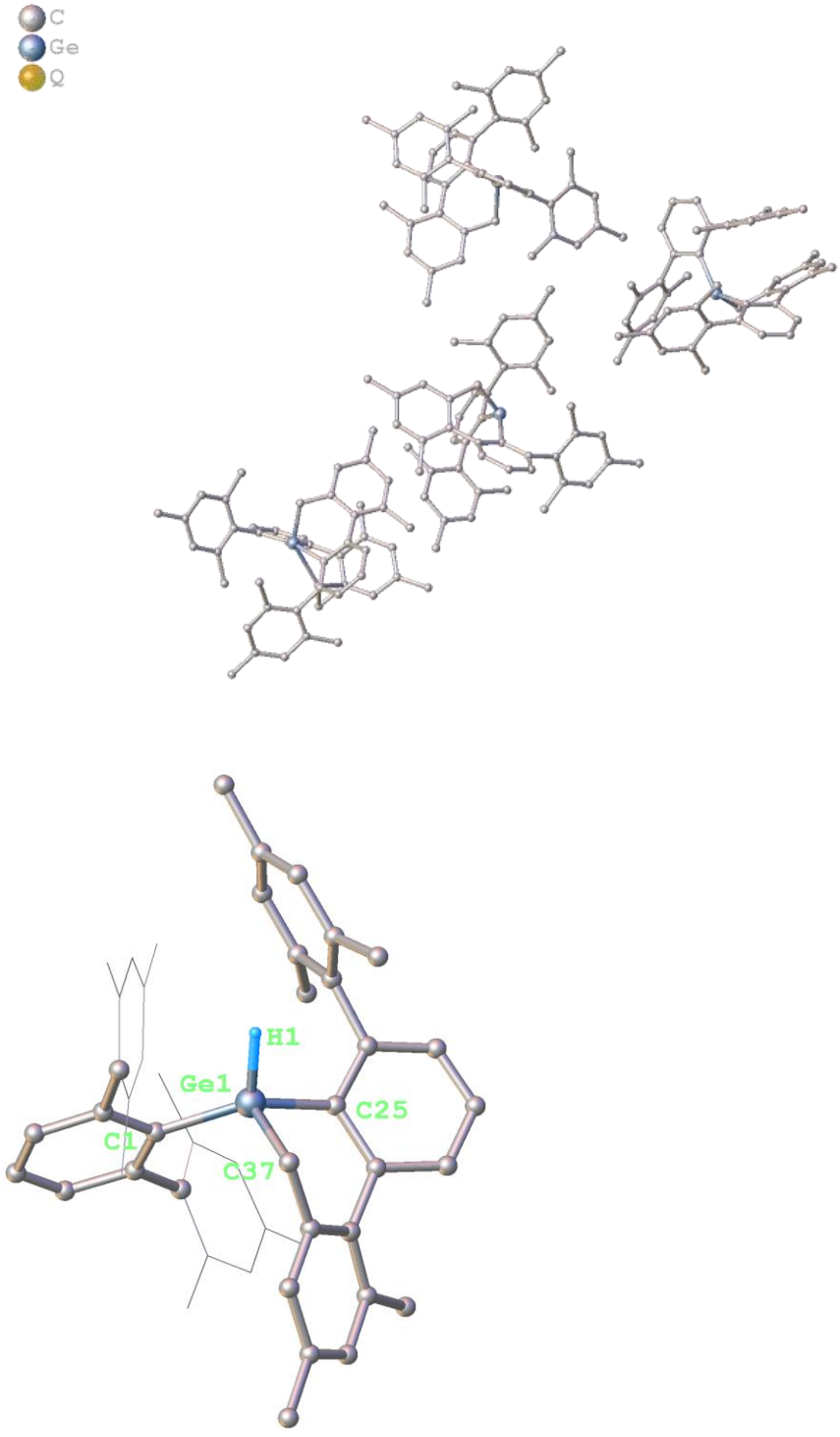

A detailed discussion of bond lengths and angles of this structure is not included due to the poor quality of the obtained crystals. Nevertheless, the connectivity could be easily established.

Table AVIII1. Selected X-ray Crystallographic Data for **1a** and **1b**

Compound	**1a**	**1b**
Formula weight, $gmol^{-1}$	C67 H68 Ge N2	C120 H120 Ge2 N4
T (K) / *l* (Å)	190(2) K/0.71073 Å	90(2) K/0.71073 Å
Crystal system	Monoclinic	Monoclinic
Space group / *Z*	$P2_1/c$	$P2_1/c$
a, Å	20.4815(6) Å	23.9089(7) Å
b, Å	12.2472(3) Å	18.9706(6) Å
c, Å	21.1132(5) Å	20.9483(6) Å
α, °	90°	90°
β, °	93.8024(11)°.	92.5214(18)°.
γ, °	90°	90°
V, $Å^3$	5284.4(2) $Å^3$	9492.2(5) $Å^3$
ρ, mg m^{-3}	1.224 Mg/m^3	1.234 Mg/m^3
Abs. coeff., mm^{-1}	0.623 mm^{-1}	0.687 mm^{-1}
F(000)	2064	3728
Crystal size, mm^3	0.366 x 0.320 x 0.279 mm^3	0.763 x 0.317 x 0.276 mm^3
θ range, °	2.137 to 30.528°.	1.659 to 27.503°.
Reflns collected	53524	73508
Ind. reflns	16137	21762
R(int)	0.0192	0.0504
Obs. reflns [$I > 2\sigma(I)$]	13713	14870
Completeness to 2θ	99.9%	100.0 %
Goodness-of-fit F^2	1.035	1.013
Final *R* [$I > 2\sigma(I)$]	R1 = 0.0318, wR2 = 0.0851	R1 = 0.0461, wR2 = 0.1042
R (all data)	R1 = 0.0397, wR2 = 0.0886	R1 = 0.0800, wR2 = 0.1185